INFORMATION TO USERS

This material was produced from a microfilm copy of the original document. While the most advanced technological means to photograph and reproduce this document have been used, the quality is heavily dependent upon the quality of the original submitted.

The following explanation of techniques is provided to help you understand markings or patterns which may appear on this reproduction.

1. The sign or "target" for pages apparently lacking from the document photographed is "Missing Page(s)". If it was possible to obtain the missing page(s) or section, they are spliced into the film along with adjacent pages. This may have necessitated cutting thru an image and duplicating adjacent pages to insure you complete continuity.

2. When an image on the film is obliterated with a large round black mark, it is an indication that the photographer suspected that the copy may have moved during exposure and thus cause a blurred image. You will find a good image of the page in the adjacent frame.

3. When a map, drawing or chart, etc., was part of the material being photographed the photographer followed a definite method in "sectioning" the material. It is customary to begin photoing at the upper left hand corner of a large sheet and to continue photoing from left to right in equal sections with a small overlap. If necessary, sectioning is continued again — beginning below the first row and continuing on until complete.

4. The majority of users indicate that the textual content is of greatest value, however, a somewhat higher quality reproduction could be made from "photographs" if essential to the understanding of the dissertation. Silver prints of "photographs" may be ordered at additional charge by writing the Order Department, giving the catalog number, title, author and specific pages you wish reproduced.

5. PLEASE NOTE: Some pages may have indistinct print. Filmed as received.

Xerox University Microfilms
300 North Zeeb Road
Ann Arbor, Michigan 48106

75-29,169

ALLENDER, James Harry, 1948-
NUMERICAL SIMULATION OF CIRCULATION AND ADVECTION-DIFFUSION PROCESSES IN SAGINAW BAY, MICHIGAN.

The University of Michigan, Ph.D., 1975
Oceanography

Xerox University Microfilms, Ann Arbor, Michigan 48106

THIS DISSERTATION HAS BEEN MICROFILMED EXACTLY AS RECEIVED.

NUMERICAL SIMULATION OF CIRCULATION AND ADVECTION-DIFFUSION PROCESSES IN SAGINAW BAY, MICHIGAN

by

James Harry Allender

A dissertation submitted in partial fulfillment
of the requirements for the degree of

Doctor of Philosophy
(Oceanic Science)
in The University of Michigan
1975

Doctoral Committee:

Assistant Professor Albert W. Green, Chairman
Professor Stanley Jacobs
Professor Wilfred Kaplan
Assistant Professor Philip A. Meyers
Associate Professor Edward C. Monahan

ACKNOWLEDGEMENTS

The author is especially grateful to his long time advisor, Dr. Albert Green, whose continued interest and keen insights have added significantly to this work. Dr. Stanley Jacobs is thanked for his guidance and scrutiny regarding the methodology used in this research. Dr. Phillip Meyers is thanked for improving the presentation of this research effort. Dr. Edward Monahan made unpublished observational data from Saginaw Bay readily available, and is thanked for his helpful advice. The author is also appreciative of many illuminating discussions with Dr. Wilfred Kaplan, who gave freely of his time.

Dr. Frank Rose, professor of physics at the University of Michigan at Flint, contributed greatly toward the systematic improvement of this manuscript. Dr. Rose is thanked for his many literary suggestions and perceptive remarks.

Mr. Paul Liu of NOAA, Ann Arbor, is thanked for obtaining water level records collected by U.S. Lake Survey.

Drs. Gary Goldman, Thomas Kaye, and Joseph Maresca, and Mr. William Tucker are thanked for their continued input and patient interaction.

Mrs. Judith Tucker, Miss Karen Webb, and Miss Pamella DeSmit are thanked for their patience in typing the manuscript.

Acknowledgement is made to the National Center for Atmospheric Research, which is supported by the National Science Foundation, for computer time used in this research.

The University of Michigan Sea Grant program has supported this work.

Finally, the author is most grateful to his loving wife, Mary, whose continued encouragement has contributed immeasureably toward the completion of this research.

TABLE OF CONTENTS

LIST OF FIGURES	vi
LIST OF TABLES	ix
LIST OF APPENDICES	xi
I. INTRODUCTION	1
II. DIFFERENTIAL EQUATIONS AND BOUNDARY CONDITIONS	9
A. Flow equations	9
1. Derivation	9
2. Analytical aspects	13
B. Advection-diffusion equation	21
1. Derivation	21
2. Analytical aspects	23
III. EXTERNAL FORCING, FORMULATION OF STRESS TERMS, AND APPROXIMATION OF DIFFUSION COEFFICIENTS	26
A. Surface stress	26
1. Parametric expressions	26
2. Method for generating the forcing function	28
B. Bottom stress	30
C. Boundary stress	31
1. Effects of inaccurate data	31
2. Method for generating the forcing function	32
D. Diffusion coefficients	47
IV. FORMULATION OF THE NUMERICAL METHOD	52
A. Finite difference method	52
B. Properties of the method	60

V. DISCUSSION OF NUMERICAL EXPERIMENTS 69

A. Effects of temporal and spatial step size 70

B. Results of steady forcing 72

C. Effects of bottom friction 77

D. System hysteresis 80

E. Effects of diffusion coefficients 93

F. Long-term simulations 98

VI. CONCLUDING REMARKS 130

APPENDIX 132

REFERENCES 167

LIST OF FIGURES

1. Simplified chart of Saginaw Bay 3
2. Idealized bay sketch showing "talweg" 14
3. Sketch showing water level gauge locations 37
4. Harrisville power spectrum (60 lags) 38
5. Harrisville power spectrum (199 lags) 39
6. Harbor Beach spectrum (60 lags) 38
7. Port Au Gres spectrum (60 lags) 40
8. Port Au Gres spectrum (199 lags) 40
9. Essexville spectrum (60 lags) 41
10. Essexville spectrum (199 lags) 41
11. Coherence square, Harrisville and Port Au Gres 42
12. Coherence square, Harrisville and Port Au Gres 43
13. Power spectrum of current meter speed record 44
14. Spatial disposition of variables 56
15. Shoreline stepping pattern 56
16. Average transport plot, over 70 hr, 8 km model 71
17. Transport plot, t = 10 hr, southwest wind, 12 kt 73
18. Transport plot, t = 10 hr, southeast wind, 12 kt 74
19. Transport plot, t = 10 hr, northwest wind, 12 kt 75
20. Transport plot, t = 10 hr, northeast wind, 12 kt 76
21. Transport plot, t = 4 hr, 1.6hr seiche forcing 78
22. Transport plot, t = 4 hr, 3.3hr seiche forcing 79
23. Transport plot, t = 112 hr, realistic forcing, κ=.02 81
24. Transport plot, t = 112 hr, realistic forcing, κ=.03 82

25. Transport plot, t = 112 hr, realistic forcing, κ=.04 83

26. Transport plot, t = 204 hr, realistic forcing 85

27. Concentration contour plot, t = 204 hr, realistic forcing 86

28. Transport plot, t = 204 hr, realistic forcing, started from rest at t = 180 hr 87

29. Concentration contour plot, t = 204 hr, realistic forcing, started from rest at t = 180 hr 88

30. Transport plot, t = 360 hr, realistic forcing 89

31. Concentration contour plot, t = 360 hr, realistic forcing 90

32. Transport plot, t= 360 hr, realistic forcing restarted from perturbed initial conditions at t= 180 hr. 91

33. Concentration contour plot, t = 360 hr, realistic forcing, restarted from perturbed initial conditions at t = 180 hr 92

34. Concentration contour plot, t = 96 hr, steady forcing, constant diffusion, $10^4 cm^2/sec$. 94

35. Concentration contour plot, t = 96 hr, realistic forcing, diffusion = U*L, ($5(10^5) cm^2/sec$) 99

36. Concentration contour plot t = 96 hr, realistic forcing, diffusion = U*L*f(gradC), (artificial diffusion) 100

37.-50. Transport and contour plots at selected times during a 720 hr realistic simulation 103

51. Wind speed history previous to release from set-up seen in figure 40 117

52. Wind direction history to accompany figure 51 117
53. Average transport plot 1 hr - 360 hr (from realistic simulation depicted in figures 37-50) 118
54. Average transport plot, 360 hr - 720 hr, (from realistic simulation depicted in figures 37-50) 119
55. Quasi-steady-state circulation produced by mean wind, 1-15 August, 1973 (compare Figures 17 and 53). 120

LIST OF TABLES

1. Longitudinal seiche periods of Lake Huron, Lake Michigan, and Saginaw Bay (Rockwell, 1966) 35
2. Summary of estimates of constants of proportionality relating the mean wind to amplitude of seiche modes at boundary of model adjoining Lake Huron 48
3. Arithmetic mean transport (U component) in m^2/sec, columns 2-14, for the period 16-31 August 1973. (+U is toward 214° magnetic.) 122
4. Arithmetic mean transport (U component) in m^2/sec, columns 15-27, for the period 16-31 August 1973. (+U is toward 214° magnetic.) 123
5. Arithmetic mean transport (V component) in m^2/sec, columns 2-14, for the period 16-31 August 1973. (+V is toward 124° magnetic.) 124
6. Arithmetic mean transport (V component) in m^2/sec, columns 15-27, for the period 16-31 August 1973. (+V is toward 124° magnetic.) 125
7. Surface height (ζ) in m for t = 60 hr, columns 2-14, from simulation which began 1 August 1973. 126
8. Surface height (ζ) in m for t = 60 hr, columns 15-27, from simulation which began 1 August 1973. 127
9. Chlorine concentration in ppm/100 for t = 60 hr, columns 2-14, from simulation which began 1 August 1973. 128

10. Chlorine concentration in ppm/100 for t = 60 hr, columns 15-27, from simulation which began 1 August 1973. 129

LIST OF APPENDICES

A. Stability analysis for flow equations 132

B. Graphical presentation of additional spectral results 135

C. Graphical presentation of further numerical simulations 142

ABSTRACT

NUMERICAL SIMULATION OF CIRCULATION AND ADVECTION-DIFFUSION PROCESSES IN SAGINAW BAY, MICHIGAN

by

James H. Allender

Chairman: Albert W. Green

A finite difference method was used to solve the linear, barotropic equations for two dimensional motion. This integration was coupled with a finite difference method of solving a vertically integrated advection-diffusion equation for any conservative substance in dilute concentration, such as chlorine. The numerical methods used, which are forms of alternating direction implicit methods of integration, were applied to Saginaw Bay, Michigan. Interpolated time histories of wind records provided surface stress data. The result of numerous spectral analyses of water level records were used in a novel procedure to infer time-dependent boundary data. These carefully processed wind and boundary data were intended to simulate actual meteorological conditions. Diffusion coefficients were formulated so that they were functions of the transport variables which depend on space and time. A large number of computer simulations have been made using a wide variety of steady and realistic forcing conditions; some simulations extended over periods as great as one month of real time. The results of these

fine-mesh, extended computer runs strongly suggest that the numerical methods and their concomitant boundary conditions represent well-posed problems. A representative portion of the results of the computer simulations are shown graphically. Several features of the predictions of the model have been corroborated by observational data. Net flow often opposes the wind direction in the connecting channel between the inner and outer bays. Only relatively weak circulations develop in the southwest corner of the bay. A lakeward boundary current often exists along the southeast shore as a result of the predominant southwest winds. Chlorinity distributions often respond to advection induced by the mean forcing by moving lakeward along the southeast shore. The concentration of chlorine can increase sharply in the southwest corner of the bay under certain meteorological conditions. Strong external forcing changes a given chlorinity distribution markedly in a time period of one or two days. Prior to this study such behavior has been difficult to anticipate a priori. The techniques utilized are appropriate for certain other estuarine situations, and the insights developed during this research regarding processes in Saginaw Bay should aid in the understanding of and perhaps in the anticipation of the dynamical responses of other similar bodies.

I. Introduction

The object of this study was to simulate circulation and advection-diffusion processes in Saginaw Bay, Michigan for time periods of the order of one month. The governing equations for the nearly homogeneous body being modeled here are the linear barotropic equations for flow on a rotating tangent plane and an advection-diffusion equation for a substance in dilute concentration in a well-mixed medium. These equations were integrated numerically to obtain time-space-dependent solutions for fluid flow and chlorine concentration.

Previous studies of this type have been applied to storm surges at sea and in harbors. A noteworthy exception is the study of Grand Traverse Bay, Michigan, by Smith (1973). The present study is the first time these equations have been applied to a body of water of this size and type. Five unique aspects of this work are noted. First, the computational procedures used allow fine-mesh simulation of circulation and advection-diffusion processes over a relatively long period of time. Second, before this study, little attention had been given to large freshwater bays, whose shallow depths allow large stresses to be exerted on the water column, and to which the barotropic equations may be applied with reasonable validity. Third, special attention was given to the open-

mouth boundary condition. Recent theoretical studies of non-physical boundaries in geophysical fluid dynamics problems, for example, Sundstrom (1973), Elvius and Sundstrom (1973), and Davies (1973), show that lateral boundary conditions are an important consideration. This is especially true when there are important effects other than tidal forcing. Fourth, special consideration was given to the formulation of expressions to represent sub-grid scale processes in the advection-diffusion problem. Finally, an extensive measurement program is now being conducted by the National Oceanic and Atmospheric Administration (NOAA) in Saginaw Bay; the preliminary results of that program have already corroborated several of the results given by the present simulations.

Saginaw Bay provides an ideal environment in which to apply the barotropic equations. It is situated at 44° North latitude and adjoins Lake Huron's western shore (see figure 1). A freshwater bay of this size (30km x 70km) has not been modeled in such detail previously. The average depth of Saginaw Bay is 8 meters, and no sill separates it from Lake Huron. Unlike a salt water estuary tidal forcing and salt budgets play no important role. However, wind and seiche forcing are important in determining the dynamics of the bay, and so they must be specified carefully if a realistic simulation is to be produced. As in many other such areas industrial concerns

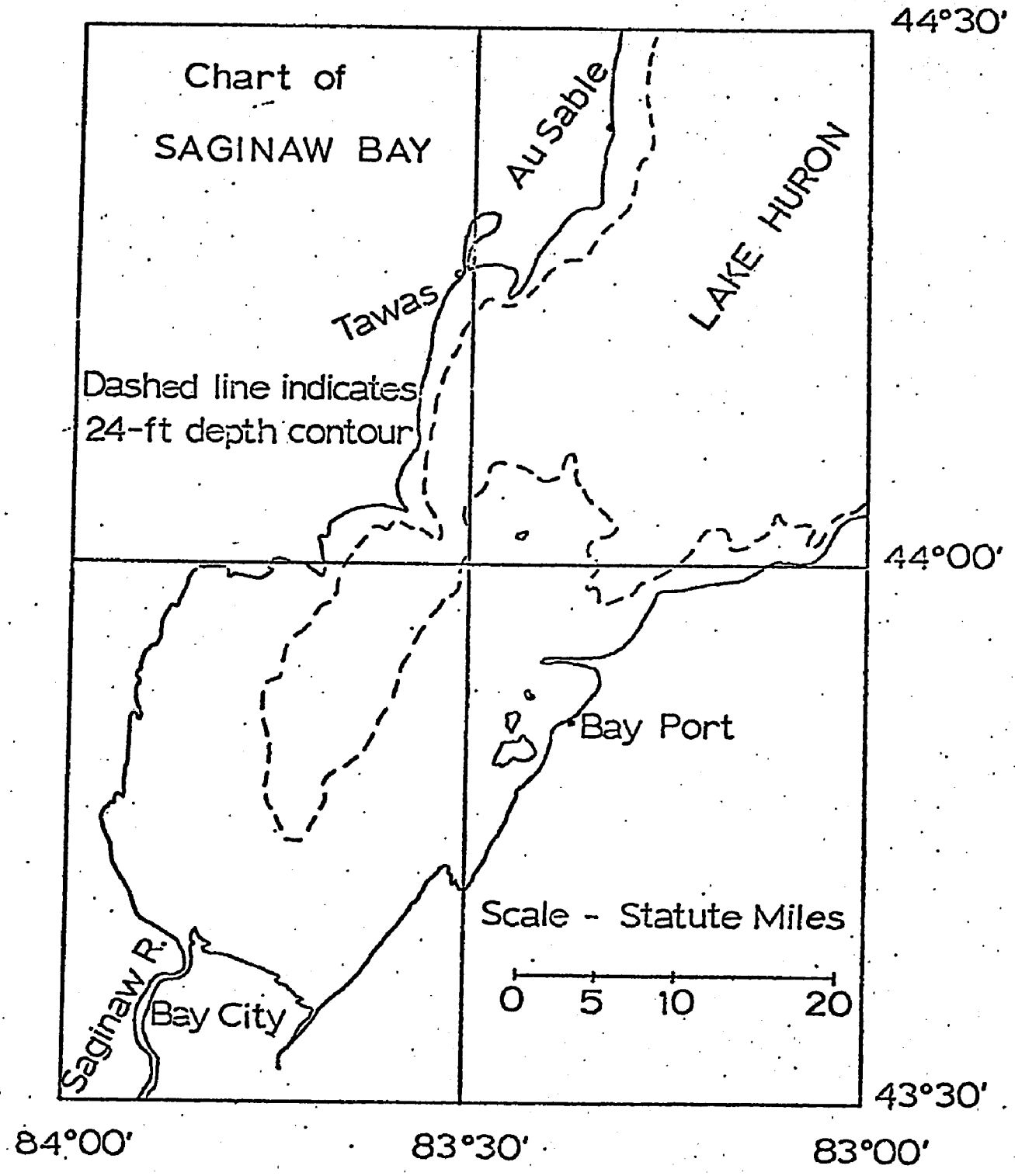

Chart of
SAGINAW BAY
Au Sable
LAKE HURON
Tawas
Dashed line indicates
24-ft depth contour
44°30'
44°00'
43°30'
Bay Port
Scale - Statute Miles
0 5 10 20
Saginaw R.
Bay City
84°00'
83°30'
83°00'

Figure 1.

have outlets on the water. The extraneous substances introduced are dispersed by eddy diffusion and advection.. For some substances biological interaction may be important. In Saginaw Bay chlorinity distributions have been measured by Dow Chemical Company for many years, and may be compared with numerically simulated chlorinity distributions.

Motions in Saginaw Bay are of the order of hours to days. Typical wind durations are 8 hours or less, and wind stresses are typically .5 dyne/cm^2 at 10 meters height. Atmospheric pressure differences over the bay are generally negligible because of its small horizontal dimensions. The exterior seiche periods (Lake Huron) range from 6.6 hr to 2.25 hr for the first five modes of longitudinal free oscillation. Field measurements, even during August, show that the seasonal thermocline is weak and is often within one meter of the bottom in 10 meters of water. This suggests strong mixing, resulting in a largely homothermal fluid. The fundamental frequency and the next two harmonics of the bay itself have the periods 10.00 hr, 3.33 hr, and 2.31 hr. The seiche amplitudes at the lakeward truncation of the model are less than one centimeter, and have been estimated in a manner to be described subsequently. Typical fluid velocities are the order of 10 cm/sec. The bay is often nearly at rest. Both flow patterns and matter distributions show

strong orographic effects which were difficult to understand prior to this research.

With the availability of computers in the late 1950's modeling of wind-driven currents and seiche motions in bays and lakes became possible. Surges on the North Sea were predicted by Hansen (1956, 1962). In the early work the equations of motion were integrated over cross sections perpendicular to an axis of the body, resulting in a one-dimensional calculation. Later Hansen developed a two-dimensional scheme. Computational methods accounting for variable cross section have been used, for example in Lake Michigan (Defant, 1953: Mortimer, 1965), and Lake Erie, (Platzman and Rao, 1964) and for all the Great Lakes (Rockwell, 1966). The last study was especially useful in this research.

The first real breakthrough in two dimensional numerical calculations came in 1950 as a result of work by Charney and his co-workers at Princeton (Charney, Fjorfort, and vonNeumann, 1950). They solved a finite difference approximation for the barotropic vorticity equation to produce a 24 hour forecast of the 500 mb pressure field over the United States. Development of more sophisticated models for atmospheric problems has proceeded rapidly in the past two decades.

To some extent the development of oceanographic models has lagged behind meteorology in this area. Initially,

at least, this was due to the greater social impetus for weather prediction. Because of growing interest in seas and lakes and their interaction with the atmosphere, hydrodynamical modeling research has become important and significant advances have also been made in this area. Platzman (1958), assuming hydrostatic pressure and constant density, developed a finite difference approximation to the vertically integrated barotropic equations. The equations were linearized and the horizontal viscous terms were dropped. (Hereafter, these equations will be referred to as simply the barotropic equations.) Platzman used this method, neglecting the coriolis term, to compute currents and water heights for the southern end of Lake Michigan for a storm surge which occurred on June 26, 1954. Fischer (1959) devised a simplified finite difference scheme, which has been widely used with various modifications, and applied it to the North Sea. Miyazaki, Ueno, and Unoki (1961, 1962) in Japan used Hansen's scheme for the barotropic equations and simulated typhoon surges which have occurred in that area in the past several decades. Welander (1961) wrote an extensive review summarizing progress in numerical storm surge prediction to that date. Most of these methods are of an explicit nature and have been used to simulate motion over relatively short periods of time (i.e., for up to a few hours).

Harris and Jelansnianski (1964) of the U.S. Weather Bureau reviewed the numerical considerations involved in various finite difference methods for the linear barotropic equations. They pointed out that the depth-averaged velocity would undergo greater variations due to changes in bottom topography than the transport (horizontal velocity integrated over the depth of the fluid), a finding applicable to this work.

Leendertse (1967) has used an alternating direction implicit (ADI) scheme, which is stable for any time step, to calculate tide-forced oscillations in the Haringvliet estuary of the Rhine River in Holland. Leendertse (1970) has also extended his work to water quality simulation in estuaries, notably Jamaica Bay, New York. The advection-diffusion in Leendertse's work was also solved by an ADI technique. Alternating direction implicit techniques) introduced by way of companion papers by Peaceman and Rachford (1955), and Douglas (1955), have not been widely applied in geophysical hydrodynamics.

The following Great Lakes area models are also noteworthy, Simons has used essentially Platzman's scheme for the varotropic equations to compute wind-driven circulation in Lake Ontario, (Simons, 1971a,b; Simons and Jordan, 1972). Nonlinear and horizontal viscous terms were included. Simons (1971b, 1972) computed flow in Lake Ontario using a four layer rigid lid model. Steady-

state two-dimensional models have been presented by Gedney and Lick (1970, 1971) for Lake Erie and by Murty and Rao (1970) for all the Great Lakes.

Although a large amount of literature exists on oceanographic modeling, the references given here are limited to those having special relevance to the present research. Among the most comprehensive models developed to date are the two-dimensional, two-layered, steady state models by Lee and Liggett (1970), the two dimensional models by Veronis (1966), three dimensional transient models by Bryan and Cox (1967, 1968a,b), the model of Crowley (1968), and the global ocean-atmosphere model by Manabe, Bryan, and Spelman (1975).

II. Differential equations and boundary conditions

A. Flow equations

1. Derivation

The balance of accelerations to be considered first are the Navier-Stokes equations for incompressible flow on a rotating tangent plane. Through a scaling analysis, it will be shown that the linear, barotropic equations are well-suited to the geophysical fluid dynamics problem at hand. The equations are

$$\frac{\partial \vec{u}}{\partial t} + (\vec{u}\cdot\nabla)\vec{u} + f\hat{k}\times\vec{u} = -1/\rho\nabla P + \nu_h\nabla^2\vec{u} + \nu_v\frac{\partial^2\vec{u}}{\partial z^2} - g\hat{k} \qquad (2.1)$$

$$\nabla\cdot\vec{u} = 0 \qquad (2.2)$$

In (2.1) and (2.2) the +x axis points eastward, the +y points northward, and the +z axis vertically upward; $\vec{u}=(u,v,w)$ are the components of fluid flow in the x,y,z directions, respec. z=0 is taken at the level of the undisturbed free surface; f is the Coriolis parameter, $f=2\Omega\sin\phi$, where $\Omega=2\pi/24$ radians per hour and ϕ is the latitude; $\hat{k}$ is a unit vector directed upward and perpendicular to the undisturbed free surface; ρ is the density; p is the pressure; t is time; $g=9.81$ m/sec^2; ν_h and ν_v are horizontal and vertical eddy viscosity coefficients, respectively. In addition to these equations of mass and momentum conservation one must apply free surface and

bottom boundary conditions. Continuity at the free surface requires that

$$w = \frac{\partial \zeta}{\partial t} + u\frac{\partial \zeta}{\partial x} + v\frac{\partial \zeta}{\partial y} \qquad (2.3)$$

for $z = \zeta(x,y,t)$.

The bottom boundary condition is

$$w + u\frac{\partial H}{\partial x} + v\frac{\partial H}{\partial y} = 0 \qquad (2.4)$$

for $z = -H(x,y)$, where $H(x,y)$ is the depth of the bottom. Suitable shoreline boundary conditions are that $\vec{u}\cdot\hat{n}=0$ at solid boundaries, and $\vec{u}\cdot\hat{n}$ or ζ specified at open boundaries.

Equation (2.1) will now be transformed to a non-dimensional form appropriate for Saginaw Bay. Define $p \equiv p^{atm} - pgz + P$ and at $z=\zeta$, take $p=p^{atm}$=constant. Let L,D, T,U represent characteristic length, depth, time, and speed scales, respec. The continuity equation requires that $W \simeq \frac{UD}{L}$. Further, assume that the local acceleration and pressure gradient term balance, so that $\frac{\partial u}{\partial t} \simeq \frac{1}{\rho}\frac{\partial p}{\partial x}$, which implies that $p \simeq \frac{\rho LU}{T}$. Let h represent the scale height for surface gravity waves, so that $\zeta \simeq h$. Then, $w \simeq \frac{\partial \zeta}{\partial t} \simeq \frac{h}{T}$, which implies that $U \simeq \frac{Lh}{DT}$. The pressure becomes $p = \frac{\rho L^2 h}{DT^2}$. From the upper boundary condition $\frac{\rho gh}{p} = 0(1) = T^2/(L^2/gD)$, which shows that the scaling is internally consistent. Substituting into 1), (all variables are now non-dimensional), the result is

$$\frac{\partial}{\partial t}(u,v) + h/D\left(u\frac{\partial}{\partial x} + v\frac{\partial}{\partial y} + w\frac{\partial}{\partial z}\right)(u,v) + fT(-v,u) \qquad (2.5)$$

$$\doteq -\left(\frac{\partial P}{\partial x}, \frac{\partial P}{\partial y}\right) + \nu_h/L(gD)^{\frac{1}{2}}\left(\frac{\partial^2}{\partial x^2} + \frac{\partial^2}{\partial y^2}\right)(u,v) + \nu_v L/D^2(gD)^{\frac{1}{2}}\frac{\partial^2}{\partial z^2}(u,v)$$

$$(D/L)^2\frac{\partial w}{\partial t} + (D/L)^2(h/D)\left(u\frac{\partial w}{\partial x} + v\frac{\partial w}{\partial y} + w\frac{\partial w}{\partial z}\right) = -\frac{\partial P}{\partial z} \qquad (2.6)$$
$$+ \nu_h D(gD)^{1/2}/gL^3\left(\frac{\partial^2}{\partial x^2} + \frac{\partial^2}{\partial y^2}\right)w + \nu_v(gD)^{1/2}/gLD\frac{\partial^2}{\partial z^2}w$$

Now let h=10cm, D=8m , L=70km, $\nu_h=10^6 cm^2/sec$, $\nu_v=10^2 cm^2/sec$, and $f=10^{-4}sec^{-1}$. Then the quantities multiplying the dimensionless terms have the following magnitudes:

$h/D \simeq 1.3(10^{-2})$, $\nu_h/L(gD)^{1/2} \simeq 1.6(10^{-4})$,
$\nu_v L/D(gD)^{1/2} \simeq 1.3(10^{-1})$, $fT \simeq 9.0(10^{-1})$,
$(D/L)^2 \simeq 1.3(10^{-8})$, $h/D(D/L)^2 \simeq 1.7(10^{-10})$,
$\nu_h D(gD)^{1/2}/gL^3 \simeq 1.9(10^{-12})$, $\nu_v(gD)^{1/2}/gLD \simeq 1.2(10^{-8})$

The local acceleration and pressure gradient terms are seen to be about two orders of mangitude larger than the non-linear terms. The dominant terms exceed horizontal friction by about four orders of magnitude, and vertical friction by about one order, but the latter must be retained to allow for surface stress. Bottom friction has been shown to be of importance through numerical experiments. It affects mainly the magnitude of computed transport, without creating marked changes in the flow pattern. The apparent importance of the coriolis term is reduced by topographic effects over much of the bay. In the vertical momentum equation, the hydrostatic

approximation is clearly justified.

Therefore the following approximate equations are valid:

$$\frac{\partial}{\partial t}(u,v) + f(-v,u) = -g(\frac{\partial \zeta}{\partial x},\frac{\partial \zeta}{\partial y}) + \nu_z \frac{\partial^2}{\partial z^2}(u,v) \qquad (2.7)$$

$$\frac{\partial u}{\partial x} + \frac{\partial v}{\partial y} + \frac{\partial w}{\partial z} = 0 \qquad (2.8)$$

$$\frac{\partial P}{\partial z} = 0 \qquad (2.9)$$

To obtain the final form of the shallow water wave equations (2.7) and (2.8) are vertically integrated over the depth of water column. After operating on (2.7) and (2.8) by integrating: $\int_{-H}^{\zeta} [\ ]dz$, and by using (2.3) and (2.4) and by applying Leibnitz's rule for integrals, the resulting equations are

$$\frac{\partial \vec{U}}{\partial t} + f\hat{k}\times\vec{U} = -gH\nabla_H\zeta + 1/\rho(\vec{\tau}_w - \vec{\tau}_B) \qquad (2.10)$$

$$\frac{\partial \zeta}{\partial t} + \nabla_H \cdot \vec{U} = 0 \qquad (2.11)$$

where $(U,V) = \int_{-H}^{\zeta}(u,v)dz$ is the horizontal transport vector, $\nabla_H = (\frac{\partial}{\partial x},\frac{\partial}{\partial y})$ and τ_w and τ_B are surface and bottom stress, respectively. Equation (2.10) states that momentum is added to the system through the surface stress, dissipated by the bottom stress, and the adjustment of the mass field is between net flow and the resulting surface height gradients, and conversely. As indicated, the flow pattern is modified slightly by the earth's rotation.

Equation (2.11) indicates that the fluid is horizontally non-divergent, except for changes in the water level due to surface gravity waves.

2. Analytical aspects of the flow equations

Insight regarding the transport equation may be gained by forming a vorticity balance from (2.10). By applying the curl operator, and defining the vorticity, $\vec{\omega} = \nabla \times \vec{U}$, the result is

$$\frac{\partial \vec{\omega}}{\partial t} = -g(\nabla_H \times \nabla_H \zeta) - \nabla \times (\kappa \vec{U}/H) + 1/\rho \; \nabla \times \vec{\tau}_w \qquad (2.12)$$

where the bottom stress has been assumed proportional to the transport ($\vec{\tau}_B = \rho\kappa \frac{\vec{U}}{H}$). From (2.12) one sees that vorticity may be pumped into the system through the curl of the wind stress, and added or removed through the gradients in surface height elevation and bottom topography. The bottom stress term plays a dissipative role as before. Vorticity dynamics in large lakes have been discussed by Csanady (1973). As an example consider a basin closed at one end, deeper in the center than at the sides with a "set-up" toward the windward boundary, (see figure 2). (A set-up is a state in which there is a non-trivial surface height gradient along a major axis of the body.) Assuming spatial independence for the wind stress for simplicity, the gradients of surface height and bottom topography couple to produce opposing gyral

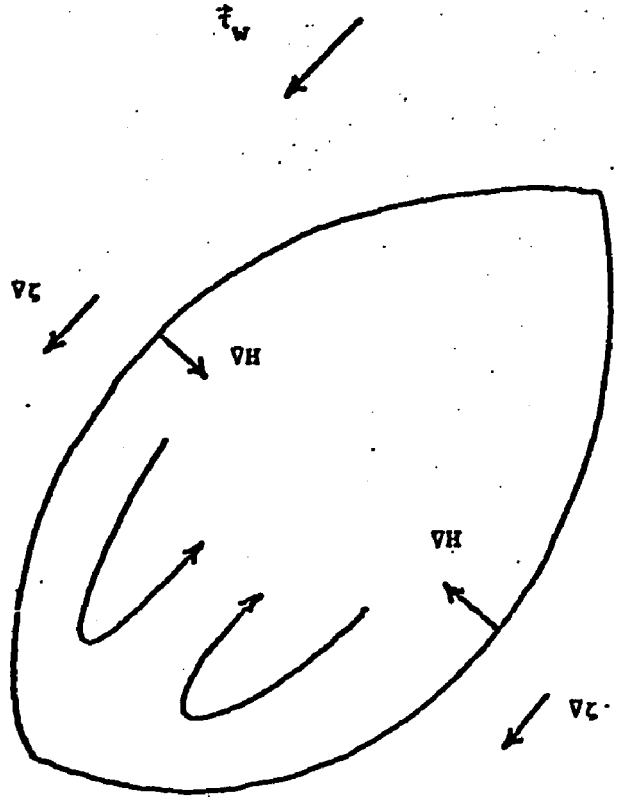


Figure 2. Idealized basin showing "Talweg", as discussed by Csanady(1973).

motions with a return flow in the center, referred to by Csanady as the "talweg". Such effects have been seen in numerical experiments under steady forcing conditions. There are shortcomings to such arguments, however, since the reasoning is essentially inapplicable if the stress vector is not aligned with the axis of the water body. Further, the motion will always be made more complex by the unsteady nature of the external forcing.

Further insight regarding the hydrodynamics of the bay may be gained by considering various simple solutions of the flow equations. First, consider the one-dimensional problem

$$\frac{\partial U}{\partial t} = -gH\frac{\partial \zeta}{\partial x} \tag{2.13}$$

$$\frac{\partial \zeta}{\partial t} = -\frac{\partial U}{\partial x} \tag{2.14}$$

subject to boundary conditions,

$U(0,t) = 0$

$\zeta(L,t) = a_f \cos\omega_f t$

where a_f is the amplitude of the forcing and ω_f is the forcing frequency. A solution for the surface height is

$$\zeta(x,t) = a_f \cos(\omega_f t)\cos(\omega_f x/(gH)^{1/2})/\cos(\omega_f L/(gH)^{1/2}) \tag{2.15}$$

which predicts the familiar phenomenon of amplification of surface height at the bay head. Note that the solution fails for resonant modes, a consequence of neglecting friction.

Consider next the transient solution of the one dimensional, damped, unforced problem, H=constant,

$$\frac{\partial U}{\partial t} + 2\kappa U/H = -gH\frac{\partial \zeta}{\partial x} \tag{2.16}$$

$$\frac{\partial \zeta}{\partial t} + \frac{\partial U}{\partial x} = 0 \tag{2.17}$$

subject to $U(0,t) = 0$, $\zeta(L,t) = 0$. Cross-differentiating and adding (2.16) and (2.17), the result is

$$\frac{\partial^2 U}{\partial t^2} + 2\kappa/H\frac{\partial U}{\partial t} - gH\frac{\partial^2 U}{\partial x^2} = 0 \tag{2.18}$$

Equation (2.18) is formally similar to the classical wave equation for damped vibrations. The transient solution is

$$U(x,t) = \sum_0^\infty \beta_n \exp(-\kappa t/H)\left[\sin(\omega_n t+\delta_n)\sin(n\pi x/2L)\right] \tag{2.19}$$

where $\omega_d = \left(gH\left(\frac{n\pi}{2L}\right)^2 - \left(\frac{\kappa}{H}\right)^2\right)^{1/2}$, δ_n, β_n are to be determined from initial conditions. Thus, the response of the system to given initial conditions will be an infinite number of modal oscillations which decay with time. The fundamental mode has 1/4 wavelength within the bay, the first harmonic has 3/4 wavelength within the bay, etc., in a manner ana-

lagous to the pressure solutions for an organ pipe open at only one end.

Finally, consider whether the following two dimensional damped problem is well-posed:

$$\frac{\partial U}{\partial t} + 2\kappa U/H + gH\frac{\partial \zeta}{\partial x} = \tau(x) \qquad (2.20)$$

$$\frac{\partial V}{\partial t} + 2\kappa U/H + gH\frac{\partial \zeta}{\partial y} = \tau(y) \qquad (2.21)$$

$$\frac{\partial \zeta}{\partial t} + \frac{\partial U}{\partial x} + \frac{\partial V}{\partial y} = 0 \qquad (2.22)$$

on the rectangular region x=0, x=L, y=0, y=b, where H, the depth, is again taken as a constant. Equations (2.20)-(2.22) are to be solved subject to the conditions that

$$\frac{\partial \zeta}{\partial x}(0,y,t) = \frac{\partial \zeta}{\partial y}(x,0,t) = \frac{\partial \zeta}{\partial y}(x,b,t) = 0, \quad \zeta(L,y,t) = F(y,t)$$

The first three conditions imply no normal flow, and the last condition specifies the surface height variation along the "open boundary" as a function of time. As before one may generate an equation formally similar to the classical wave equation,

$$\frac{\partial^2 \zeta}{\partial t^2} + 2\kappa/H\frac{\partial \zeta}{\partial t} - gHV_H^2\zeta = -\left(\frac{\partial \tau}{\partial x}(x) + \frac{\partial \tau}{\partial y}(y)\right) \qquad (2.23)$$

The solution to the homogeneous problem may be generalized from the one dimensional case, or see, e.g., Kaplan, (1952)

p. 655, or Lamb (1932) p. 282. the solution is

$$\zeta(x,y,t) = \sum_{1}^{\infty}\sum_{1}^{\infty} \exp(-\kappa t/H) C_{mn} \cos(n\pi x/2L)\cos(m\pi y/b) \sin(\lambda_{mn} t+\varepsilon_n) \quad (2.24)$$

where $\lambda_{mn}=[gH((\frac{m\pi}{b})^2 + (\frac{n\pi}{2L})^2 - (\frac{\kappa}{H})^2]^{1/2}$, and C_{mn}, ε_n are determined from initial conditions. To solve for the response to the problem with non-homogeneous boundary conditions and zero right-hand side, a new problem having homogeneous boundary conditions, but a non-homogeneous right-hand side, is constructed, see, e.g., Kaplan (1952) or Courant and Hilbert (1953). In particular one seeks a function $f(x,y,t)$ that satisfies the boundary conditions, but is otherwise arbitrary. One then writes the identity

$$\frac{\partial^2 f}{\partial t^2} + 2\kappa/H\frac{\partial f}{\partial t} - gH\nabla_H^2 f = F_1(x,y,t) \quad (2.25)$$

where $F_1(x,y,t)$ is the function which results when $f(x,y,t)$ is substituted directly into (2.23). Now let $\zeta^*(x,y,t) = \zeta(x,y,t)-f(x,y,t)$. Then

$$\frac{\partial^2 \zeta^*}{\partial t^2} + 2\kappa/H\frac{\partial \zeta^*}{\partial t} - gH\nabla_H^2\zeta^* = -(\frac{\partial \tau}{\partial x} + \frac{\partial \tau}{\partial y}) - F_1(x,y,t) \equiv F^* \quad (2.26)$$

subject to $\frac{\partial \zeta}{\partial x}(0,y,t)=\frac{\partial \zeta}{\partial x}(L,y,t)=\frac{\partial \zeta}{\partial y}(x,0,t)=\frac{\partial \zeta}{\partial y}(x,b,t)=0$

is the problem to be solved.

In principle one may solve (2.26) by using the method of variation of parameters. This would appear to be possible if F* may be represented as a Fourier series, in x and y. This can be done provided that F* may be extended to form a periodic function and that it is piecewise continous. The resulting solution has the form

$$\zeta^*(x,y,t) = \sum_{n} \sum_{m} \exp(-\kappa t/H)\cos(n\pi x/2L)\cos(m\pi y/b) \qquad (2.27)$$
$$\left[\int_0^t F^*_{mn}(s)\cos\lambda_{mn}s\, ds - \int_0^t F^*_{mn}(s)\sin\lambda_{mn}s\, ds\right]$$

where the $F^*_{mn}(t)$ are the Fourier coefficients of the double Fourier series in x and y for the function F*. Thus, one sees that the system's response has an infinite number of oscillatory modes, the amplitudes of which depend upon the Fourier components of the applied forcing. In order to find the Fourier series for F* the wind stress and open boundary forcing functions must have at least two continuous time derivatives. This remark will be amplified later in the discussion of data preparation for the numerical model.

Next, consider the energy in the system, and how it is changed by non-homogeneous boundary conditions. If the wind stress and coriolis terms are ignored for the moment, and equation (2.10), the momentum equation, is premultiplied by U, the result is

$$1/2\frac{\partial}{\partial t}|\vec{U}|^2 + gH\nabla\zeta\cdot\vec{U} + \kappa|\vec{U}|^2 = 0 \qquad (2.28)$$

From (2.11), the continuity equation, after multiplying by ζ and rearranging,

$$1/2\ \frac{\partial}{\partial t}\zeta^2 = -[\nabla\cdot(\zeta\vec{U}) - \nabla\zeta\cdot\vec{U}] \qquad (2.29)$$

Now, let R denote the region occupied by the bay, and let Γ be the segment of the lateral boundary which adjoins Lake Huron. After integrating equation (2.29) over the region R, and using the divergence theorem and equation (2.28), the result is

$$1/2\ \frac{\partial}{\partial t}\iint_R \zeta^2 dR = -\int U_{normal}\zeta d\Gamma \qquad (2.30)$$

$$- 1/gH\iint_R (\frac{\partial}{\partial t}|\vec{U}|^2 + \kappa/H|\vec{U}|^2)dR$$

Integrating (2.30) from 0 to t gives

$$1/2\iint_R (|\vec{U}|^2+\zeta^2)dR = -\int U_{normal}\zeta d\Gamma \qquad (2.31)$$

$$+ \iint(\zeta_0^2 + |\vec{U}_0|^2/gH - \kappa|\vec{U}|^2/gH^2)dR$$

where $\zeta_0, \vec{U}_0$ are the initial data, and F(x,y,t) is the time dependent height function along the open boundary which forces the system. Equation (2.33) states that the time rate of change of kinetic and potential energy in the system is balanced by the effects of energy in the initial state, the dissipative effects, and input by way of height excursions along the open boundary. By ignoring other forcing, it is found that a positive height excursion will give $U<0$, i.e., into the region, and result in

an increase in the total energy of the system. A negative excursion has the opposite effect.

B. Advection-diffusion equation

1. Derivation

The budget of mass fluxes to be considered is one determined by eddy diffusion, advective processes, and reaction with the surroundings. Following Neumann and Pierson (1966) one may write

$$\frac{\partial c}{\partial t} + \nabla \cdot (c\vec{u}) - \frac{\partial}{\partial x}\left(D_x \frac{\partial c}{\partial x}\right) - \frac{\partial}{\partial y}\left(D_y \frac{\partial c}{\partial y}\right) - \frac{\partial}{\partial z}\left(D_z \frac{\partial c}{\partial z}\right) + R_c = S \quad (2.32)$$

In (2.32) the +x axis points eastward, the +y axis points northward, and the +z axis vertically upward, and perpendicular to the undisturbed free surface; $\vec{u}=(u,v,w)$ are the components of flow in the x,y,z, directions, respectively; C is a non-conservative property associated with the fluid, e.g., the concentration of a reactive species in dilute solution; S is a source function for property C, R_c is a reaction term for species C; D_x, D_y, and D_z are eddy diffusion coefficients. Equation (2.32) indicates that the net concentration of C in a fixed infinitesimal volume element is changed, in the presence of currents through advection, and is further modified by the diffusion processes, and finally, is changed by the presence of sources or sinks of material.

Since observational data strongly suggest that the bay is well-mixed, and since the flow equations have been vertically integrated, it is desirable to operate on (2.32) with $\int_H^\zeta [\ ]dz$. Using Leibnitz rule for integrals, and grouping appropriate terms, the result is

$$\begin{aligned}
&(c[w - (\frac{\partial \zeta}{\partial t} + u\frac{\partial \zeta}{\partial x} + v\frac{\partial \zeta}{\partial y})])\Big|_\zeta \qquad (2.33)\\
&+ [c(w + u\frac{\partial H}{\partial x} + v\frac{\partial H}{\partial y})]\Big|_{-H} + [D_x\frac{\partial c}{\partial x}\Big|_\zeta \frac{\partial \zeta}{\partial x} + D_y\frac{\partial c}{\partial y}\Big|_\zeta \frac{\partial \zeta}{\partial y}]\\
&- [D_x\frac{\partial c}{\partial x}\Big|_{-H} \frac{\partial(-H)}{\partial x} + D_y\frac{\partial c}{\partial y}\Big|_{-H} \frac{\partial(-H)}{\partial y}] + \frac{\partial}{\partial t}\int_{-H}^{\zeta} c\,dz + \frac{\partial}{\partial x}\int_{-H}^{\zeta} cu\,dz\\
&+ \frac{\partial}{\partial y}\int_{-H}^{\zeta} cv\,dz - (\frac{\partial}{\partial x}\int_{-H}^{\zeta} D_x\frac{\partial c}{\partial x}dz + \frac{\partial}{\partial y}\int_{-H}^{\zeta} D_y\frac{\partial c}{\partial y}dz\\
&+ \int_{-H}^{\zeta} \frac{\partial}{\partial z}D_z\frac{\partial c}{\partial z}dz) + \int_{-H}^{\zeta} (R_c - S)dz = 0
\end{aligned}$$

The first and second terms in (2.33) vanish due to the free surface and bottom boundary conditions, as applied to the flow equations previously. The third and fourth terms vanish because the concentration flux cannot be directed out of the free surface or into the bottom, respectively. Finally, assuming $C \neq C(Z)$,

$$\frac{\partial Hc}{\partial t} + \nabla_H\cdot(c\vec{U}) - \frac{\partial}{\partial x}(HD_x\frac{\partial c}{\partial x}) - \frac{\partial}{\partial y}(HD_y\frac{\partial c}{\partial y}) = H(S - \int_{-H}^{\zeta} R_c\,dz) \qquad (2.34)$$

where $\vec{U} = H\vec{u}$ as before. Let $\hat{n}$ be a unit vector normal to the bay's shoreline and Γ be the line segment which artificially divides Lake Huron from the Saginaw Bay, thus truncating the model. Then, the boundary conditions to be employed are that $\nabla C\cdot\hat{n} = 0$ and $C(x,y,t)$ is is given along Γ for all time.

In the numerical model which follows, only non-reactive species will be considered due to the lack of data for non-conservative substances. Thus, the right hand side of (2.34) reduces to HS.

2. Analytical aspects of the advection-diffusion equation

It is instructive to present solutions for certain simplified advection-diffusion problems. For example, consider a situation in homogeneous turbulence where the concentration is a function of x and t only:

$$\frac{\partial c}{\partial t} + u\frac{\partial c}{\partial x} = \frac{\partial}{\partial x}\left(D\frac{\partial c}{\partial x}\right) \qquad (2.35)$$

where u (mean speed) and D are constants. As an initial condition choose $C(x,o) = 0$, and as boundary conditions take $C(o,t) = C_o$, $C(\infty,t) = 0$. The solution of equation (2.35), given in Ogata and Banks (1961), is

$$c/c_0 = 1/2\ \exp(ux/D)\,\mathrm{erfc}[(x+ut)/2(Dt)^{1/2}] + 1/2\ \mathrm{erfc}[(x-ut)/2(Dt)^{1/2}] \qquad (2.36)$$

where the coerror function $\mathrm{erfc}(\gamma) = 1-\mathrm{erf}(\gamma)$ and the error function $\mathrm{erf}(\gamma) = \frac{2}{\sqrt{\pi}}\int_0^{\gamma} e^{-\eta^2} d\eta$. Note that the mean point on the concentration curve $(C - C_o/2)$ moves at speed u, and that as $t\to\infty$, the steady-state solution for u positive is $C/C_o = 1$ for all x, since $\mathrm{erfc}(-\infty) = 2$ and $\mathrm{erfc}(+\infty) = 0$. For U negative, the steady-state solution is an exponential curve,

$$c/c_0 = \exp(-ux/D) \qquad (2.37)$$

This distribution represents a balance between the diffusive flux in the direction of decreasing concentration (+x) and the advective flux in the -x direction.

As a further example consider the solution of (2.35) when the initial condition is a finite source at x=0 and t=0, viz., $C(x,o) = 0, t \geq 0$. Since $\int_{-\infty}^{\infty} C_o\, \delta(x)dx = C_o$., $C(\pm\infty,t) = 0$; the concentration is given by

$$c = c_0/(4\pi Dt)^{1/2}\exp[-(x-ut)^2/4Dt] \qquad (2.38)$$

(Taylor, 1954). The material moves downstream and spreads as a symmetrical Gaussian curve whose peak moves at speed u. As $t\to\infty$, $C\to 0$ for all x. For additional comments see, e.g., Ippen (1966).

As with the flow equations the magnitudes of terms in the advection-diffusion relation can be displayed through a scaling analysis. Define characteristic quantities so that

$$t=Tt^*,\ U=u_oH_oU^*,\ (X,Y)=L(X^*,Y^*),\ D_x=\mathring{D}_xD^*_x,\ Dy=\mathring{D}_yD^*_y,$$

$$\text{and } H=H_oH^*_o,$$

where all starred variables are O(1). By normalizing the concentration, the result is, after omitting the asterisks (all variables being non-dimensional),

$$\frac{\partial Hc}{\partial t} + u_0/L\ \nabla_H\cdot(c\vec{U}) - \mathring{D}_xT/L^2\frac{\partial}{\partial x}(HD_x\frac{\partial c}{\partial x}) - \mathring{D}_yT/L^2\frac{\partial}{\partial y}(HD_y\frac{\partial c}{\partial y}) = 0 \qquad (2.39)$$

Source and sink terms have been temporarily omitted. If $T = L/u_o$, usually referred to as a residence time, then (2.39) becomes

$$\frac{\partial Hc}{\partial t} + \nabla_H \cdot (c\vec{U}) - 1/R_x \frac{\partial}{\partial x}(HD_x \frac{\partial c}{\partial x}) - 1/R_y \frac{\partial}{\partial y}(HD_y \frac{\partial c}{\partial y}) = 0 \quad (2.40)$$

where $R_x = \frac{u_o L}{\tilde{D}_x}$, $R_y = \frac{u_o L}{\tilde{D}_y}$ are non-dimensional parameters comparing the inertial and diffusive effects.

Perusal of Dow Chemical Company's chlorinity data indicates that the concentration changes by an appreciable fraction of itself in about 20 km, i.e., L≈20 km. Available current meter data (Monahan, 1974) suggests that u_o should be at least 5 cm/sec. Various investigators have measured diffusivities in the Great Lakes region, e.g., Hamblin (1971) and Csanady (1963) in Lake Ontario and Ahrnsbrak and Ragotzkie (1970) in Green Bay, Wisconsin. These studies indicate that eddy diffusion coefficients are probably not greater than order 10^6 in shallow lakes and bays subject to strong forcing. Combining the characteristic values just given, one finds R_x, R_y are $0(10^1)$. The smallness of the diffusive terms is fortunate, since suitable data is lacking for the reliable estimation of the diffusion coefficients.

Analytical implications of the relative magnitudes of the terms in (2.40) should not be overlooked. Ignoring surface gravity waves, equation (2.40) becomes $\partial c/\partial t + \vec{U}/H \cdot \nabla C = 0$, if R_x and R_y are infinite. This implies that

concentration within a given fluid element is conserved along particle paths, and specification of C during outflow conditions might lead to violation of this conservative property. This situation is formally similar to the vorticity streamline equations for inviscid flow as discussed by Charney et al. (1950). Further, if R_x, R_y are small but non-zero, (2.40) exemplifies a classic singular perturbation problem, and one might therefore expect a boundary layer phenomenon.

III. External forcing, formulation of stress terms and approximation of diffusion coefficients

A. Surface stress

1. Parametric expressions

Realistic simulation of physical processes in Saginaw Bay requires careful specification of external forcing. The dominant mechanism of forcing is through surface stress. The only other significant, but much less powerful, forcing mechanism is the seiche motion of Lake Huron.

The wind stress at the free surface can be expressed in terms of the wind at ten meters height by the widely used relation

$$\vec{\tau}_w = \rho_{air} C_D \bar{u}_{10}^2 \hat{u}_{10} \qquad (3.1)$$

where ρ_{air} is the density of air, C_D is a drag coefficient, $\bar{u}_{10}$ is the mean wind at ten meters above the surface, and

$\hat{u}_{10}$ is a unit vector in the direction of the mean wind. C_D must be chosen from empirical data, and unfortunately is strongly affected by thermal atmospheric stability.

Deacon and Webb (1962) have summarized the methods for estimating surface drag and discussed the usefulness of introducing the drag coefficient. Essentially, two methods have been used. The so-called profile method claims that the mean wind above the surface is given by $\bar{u} = (u_*/k) \ln (Z/Z_o)$ where k is von Karman's constant, Z_o is a roughness parameter, and u_* is the friction velocity, $u_* = (\tau/\rho)^{1/2}$, $\tau = -\rho\overline{u'w'}$ where u', w' are the horizontal and vertical wind component deviations from the temporal mean.

The eddy correlation technique seems preferable since it deals directly with terms involved in the averaged momentum equations, i.e., the Reynold's stresses. Davidson (1970) using hot-wire anemometry, made such turbulence measurements on Lake Michigan, and calculated C_D for various atmospheric conditions. He obtained C_D = (2.5 to 6.4) x 10^{-3} for speeds ($\bar{u}_{10}$) in the range (3.9 to 6.6) m/sec. for unstable atmospheres, (-0.5° C/15 m), C_D = (.9 to 1.5) x 10^{-3} for speeds ($\bar{u}_{10}$) in the range (7 to 7.5) m/sec. for neutral atmospheres, and C_D = (1.2 to 2.5) x 10^{-3} for speeds ($\bar{u}_{10}$) in the range (5.1 to 5.7) m/sec. for stable atmospheres, (1.0° C/15m). These values are in general somewhat higher than those predicted by the profile method.

A value of $C_D = 2.6 \times 10^{-3}$ was chosen for this work. This choice is by no means completely satisfactory, but is believed to be reasonable. The wind speed data were to be multiplied by empirical correction factors depending upon atmospheric stability, as given by Richards et. al. (1966). However, the necessary data do not exist for Saginaw Bay to the author's knowledge.

2. Method for generating the forcing function

Wind data for the Saginaw Bay area were available from two different stations. One site was the Saginaw Tri-city Airport, located some twenty miles inland from the bay, and the other was Wirtsmuth Air Force Base, located about ten miles north of the bay and slightly inland from Lake Huron. It was assumed that usual atmospheric phenomenon would have a spatial scale significantly greater than the distance between the two stations. Further, perusal of the Wirtsmuth reocrd indicates that it is not dominated by lake effects, and therefore an arithmetic average of the hourly values of wind speed and direction was sought. To provide for automatic averaging, a computer code was constructed which forms the arithmetic average of the two speed records by computing $\overline{u}_{10_i} = (\overline{u1}_{10_i} + \overline{u2}_{10_i})/2$, $i = 1$, no. of hours. To average the directions, $\overline{\theta}1$ and $\overline{\theta}2$, the same program then tests each pair of direction values to determine the quadrant in which each value is found. This was done by using six

separate tests each involving four inequalities. For example, if sin $(\overline{\theta 1})>0$, sin $(\overline{\theta 2})<0$, cos $(\overline{\theta 1})>0$, cos $(\overline{\theta 2})>0$, then $\overline{\theta 1}$ is in the 1st quadrant, $\overline{\theta 2}$ is in the 4th quadrant, and the azimuth 0,360° lies between them. The average azimuth for this pair was computed as $\overline{\theta}_i = \overline{\theta 1}_i + (360° - (\overline{\theta 2}_i - \overline{\theta 1}_i))/2$. Whenever the smaller angle between the two points is less than 180° and does not include 0,360°, the averaging used was $\overline{\theta_i} = (\overline{\theta 1}_i + \overline{\theta 2}_i)/2$. Finally, the program generated an indicator function which switches from 1 to -1 and vice-versa on each crossing through 0,360°.

A value for the wind stress remains to be determined at each time step. To accomplish this interpolation, splines under tension were used to generate smooth curves conforming to the averaged hourly data. The speed vector caused no difficulty, but for the direction vector additional logic was required in the event that the azimuth crossed 0,360°, in which case linear interpolation was used. The indicator function mentioned above was used to control this logic. A desirable consequence of employing splines under tension is that the resultant function has two continuous derivatives. Analytically, as was seen previously, this differentiability would appear to be a requisite for obtaining a solution, unless generalized function theory is used. Numerically, the spline interpolation produced forcing data which were much less noisy than would have resulted from linear interpolation. The interpolated stress vectors were stored

for subsequent use with the computational model described below.

B. Bottom stress

A suitable approximation also had to be chosen for the bottom stress. Methods of expressing this term as a function of the transport $\vec{U}$ and other known variables are given in Bowden (1953), Groen and Groves (1960), and Welander (1961). The basic rationale for most parametric expressions is that essentially the same relation holds as for the wind stress, i.e.,

$$\vec{\tau}_B = \rho C'_D |\vec{u}_B|^2 \hat{u}_B \qquad (3.2)$$

where C'_D is a drag coefficient, $\vec{u}_B$ is the horizontal component of velocity at the outer edge of the boundary layer, and $\hat{u}_B$ is a unit vector in the $\vec{u}_B$ direction. To give the bottom stress in terms of the transport, assume that the previous relation may be approximated as $\vec{\tau}_B = \rho\kappa\vec{U}/H$. To determine an appropriate value for κ, available water level records (from the Lake Survey Office, NOAA, Detroit) and a current meter record (Monahan, 1974), were studied in conjunction with the contemporary wind records. On numerous occasions an oscillatory release from "set-up" is apparent in the bay. If it is assumed that the amplitude of the wave disturbance decays at a given location according to $\zeta = \zeta_0(x,y)e^{-\kappa t/2H}$, the e-folding time for that event can be assessed from the data. Several such estimates were made;

they yielded an average decay time $T \approx 10$ hr . The multiplication of $1/T$ by twice the average depth of the bay (8m), gives $\kappa \approx .04$ cm/sec.

More elaborate formulations for the bottom stress certainly have been used. For example, Leendertse (1967) has introduced so-called Chezy coefficients, K_1 (X,Y) and K_2 (X,Y), which are varied to produce the best fit of the solution to observational data when they are employed in the following parametric expression for stress:

$$\vec{\tau}_B = \rho(U^2 + V^2)^{1/2}/H \; (U/K_1, V/K_2) \qquad (3.3)$$

Unfortunately, insufficient observational data are available to allow introduction of such parameters. Thus, it is necessary to determine the system's sensitivity to changes in frictional drag by numerical experiments. This work is summarized below in the chapter entitled "Description of Numerical Experiments".

C. Boundary Data

1. Effects of inaccurate data

A procedure must be outlined for determining the boundary forcing. The intent is to simulate the rest of the fluid surroundings for the bay, and to avoid interfering with the way in which the bay interacts with that surrounding. Elvius and Sundstrom (1973) have discussed the effects of inaccurate boundary data on the solution of the non-linear shallow water wave equations near the outflow boundary. Errors in the boundary values can result in the growth of

error waves which propagate into the region of interest. This difficulty also occurs for the linear shallow water equations (2.10-2.11). The advection-diffusion equation (2.34) is subject to deleterious boundary influences in at least two ways: 1) it depends on a possibly erroneous boundary condition for the concentration at the outflow boundary; 2) it is coupled to the possibly erroneous flow field through the advection term.

While such error growth may be inconsequential for simulation over a short period, it seems quite relevant for this work. Thus, it is highly desirable to provide accurate boundary data having at least two relatively noise-free, continuous derivatives. (Recall from the previous section that the analytical solution for $\vec{U}$ required that the boundary function be twice differentiable.) Specification of the open boundary concentration is also required as a function of time as noted earlier when the problem was posed. The difficulties peculiar to dealing with this condition are largely numerical, and therefore are discussed in Chapter IV.

2. Method for generating the forcing function

Saginaw Bay is forced through the open boundary by seiche motion in Lake Huron. The response of the bay to this forcing can be studied quantitatively through the techniques of time series analysis. Let X and Y be random variables describing a stationary random process. Let the

autocorrelation function of X be given by

$$R_X(\tau) = \lim_{\tau \to \infty} \int_0^{\tau} x(t)\ x(t+\tau)\ d\tau \qquad (3.4)$$

Similarly, the cross-correlation of X and Y is

$$R_{xy}(\tau) = \lim_{\tau \to \infty} \int_0^{\tau} x(t)\ y(t+\tau)\ d\tau \qquad (3.5)$$

The power spectral density (or simply power spectrum) of X can be shown to be the Fourier transform of the autocorrelation function, viz.,

$$G_x(f) = 2 \int_{-\infty}^{\infty} R_x(\tau)\ \exp(-i\omega\tau)\ d\tau \qquad (3.6)$$

Similarly, the cross-spectrum of X and Y is

$$G_{xy}(f) = 2 \int_{-\infty}^{\infty} R_{xy}(\tau)\ \exp(-i\omega\tau)\ d\tau \qquad (3.7)$$

Finally, the coherence function, γ, of X and Y can be indicated by

$$\gamma^2_{xy}(f) = |G_{xy}(f)|^2 / [G_x(f) G_y(f)] \qquad (3.8)$$

Further discussion of these concepts may be found, for example, in Blackman and Tukey (1958), Bendat and Piersol (1966), and Enochson and Otnes (1968).

Water level records from within and outside of the bay were obtained from the Lake Survey Office, NOAA, Detroit. Figure 3 shows the locations of gauges. These time series were then analyzed using the Blackman-Tukey method (with a Hamming window) to generate estimates of

power spectral densities. Figures 4 through 12 show representative results of the computations. To utilize existing computer software, record length was limited to approximately 80 hr, i.e., approximately 1000 data points or less. When 60 lags, (in effect, 60 estimates of the power spectrum), are used as in Figure 4, peaks tend to be broad, and sometimes not well-defined. When 199 lags are used as in Figure 5, spectral content is much better resolved, but the statistical variability of the estimates is much greater. Thus, a kind of uncertainty principle operates which demands a trade-off between resolving peaks and calculating amplitudes, provided that the number of data points is fixed.

The complexity of oscillatory motions in the bodies under consideration is obvious from the figures. Table 1 shows the calculated periods of free oscillations of Lake Michigan, Lake Huron, and Saginaw Bay (Rockwell, 1966). In view of Rockwell's results, the Harrisville spectra, Figures 4 and 5, would thus appear to show activity at the 1st, 3rd, and 5th longitudinal modes of Lake Huron, as well as some modes which appear to be associated with Lake Michigan's motion. Simple calculations strongly suggest that the 1.6 hr and 1.1 hr peaks are transverse modes of Lake Huron. The Harbor Beach spectrum, Figure 6, shows marked similarities to Harrisville, as expected. The Port AuGres spectra, Figures 7 and 8, consistently show activity at approximately 3.0 hr and 1.8 hr. The majority of

Mode	Lake Michigan	Lake Huron	Saginaw Bay
1	8.83	6.49	10.00
2	4.37	4.57	3.33
3	3.54	3.13	2.31
4	2.86	2.60	
5	2.39	2.24	

Table 1. Summary of longitudinal free oscillations of Lake Michigan, Lake Huron, and Saginaw Bay, (Straits of Mackinac open), (Rockwell, 1966).

Essexville spectra, e.g., Figures 9 and 10, show broad peaks centered about 2.6 to 4.3 hr. When resolved by increasing the number of lags, these peaks show evidence of oscillations near 3.3 hr and 2.15 hr. As seen from Figures 11 and 12, certain periods of oscillation are highly coherent when signals from within and outside of the bay are compared. Portions of a current meter record (Monahan, 1974) were also analyzed. Figure 13 shows a strong excitation of the bay's 2nd mode during a period of high winds over the bay and the lake.

Based upon the results just discussed as well as additional time series analyses, many of which may be found in Appendix B, the following generalizations can be made: 1) motions having periods of less than two hours are strongly damped in the inner bay; 2) the motion of the bay is clearly influenced by seiching of Lake Huron; 3) oscillatory motion in the outer and inner bays often can be quite different; 4) the periods of frequently observed modes having the greatest amplitudes, (excluding very low frequency activity), are approximately 3.3 hr and 1.8 hr. Thus, a minimum subset of the motion of Lake Huron has been found which must be introduced as boundary data in order to simulate circulation processes in Saginaw Bay. These analyses neither exhaust nor elucidate all possibilities but appear to be sensible choices based upon existing data.

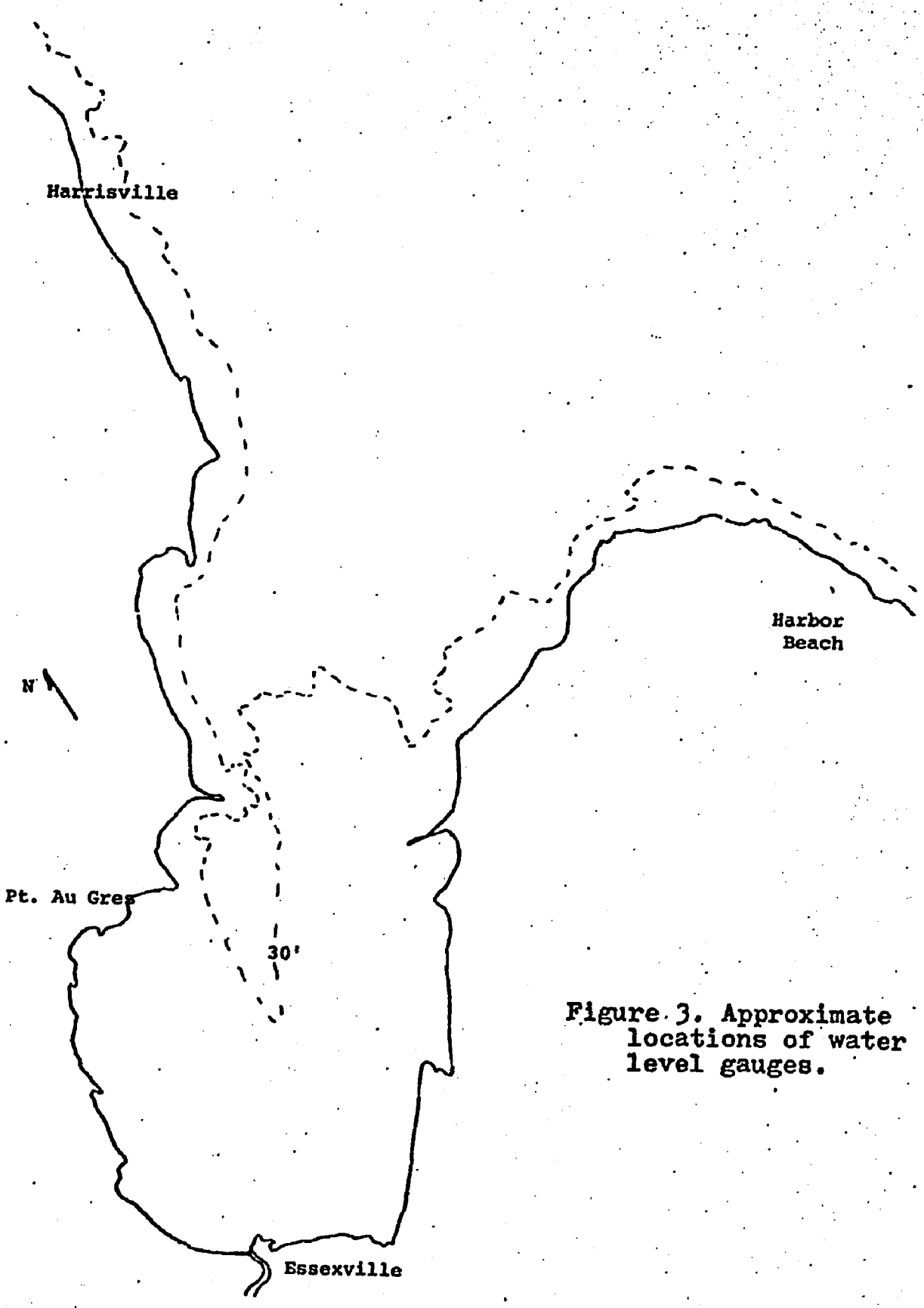


Figure 3. Approximate locations of water level gauges.

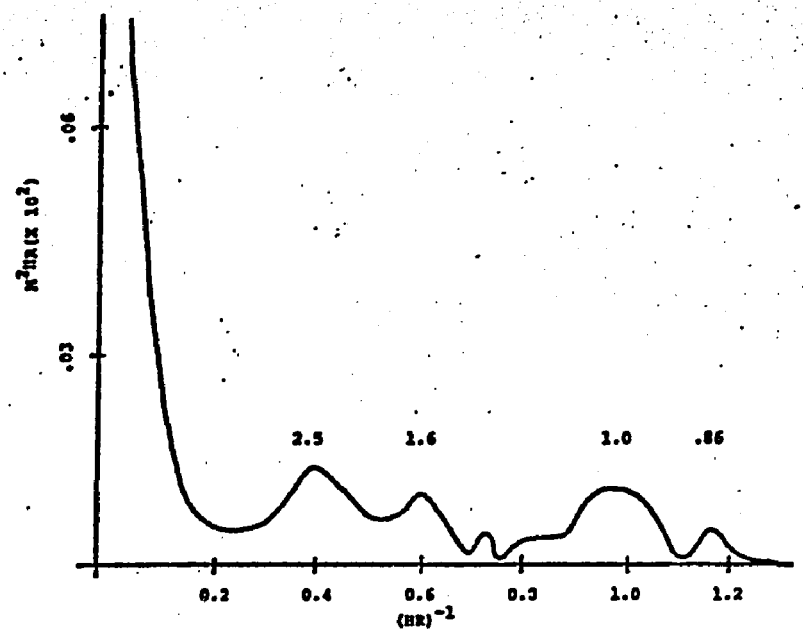


Figure 4. Estimate of power spectral density near Harrisville; duration=64hrs., lags=60, periods in hrs. are noted near each peak.

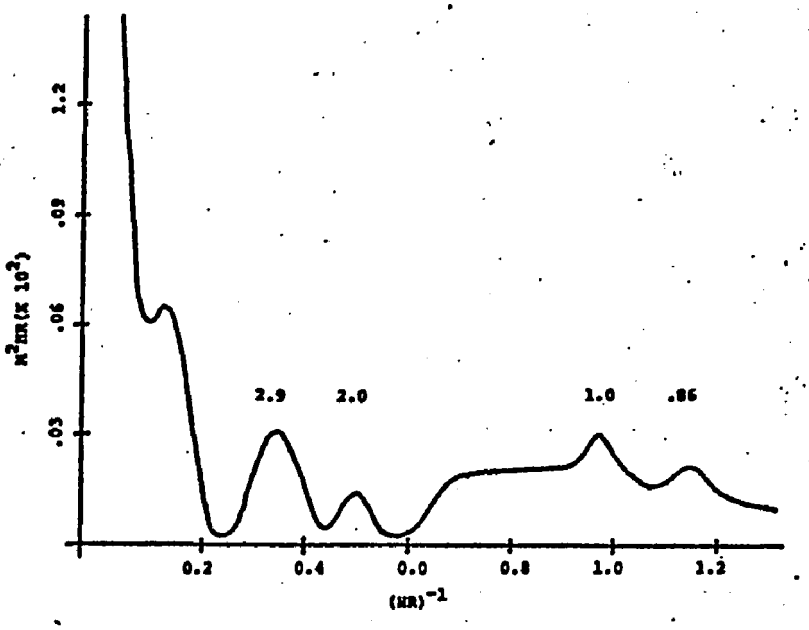


Figure 6. Estimate of power spectral density near Harbor Beach; duration=64hrs., lags=60, periods in hrs. are noted near each peak.

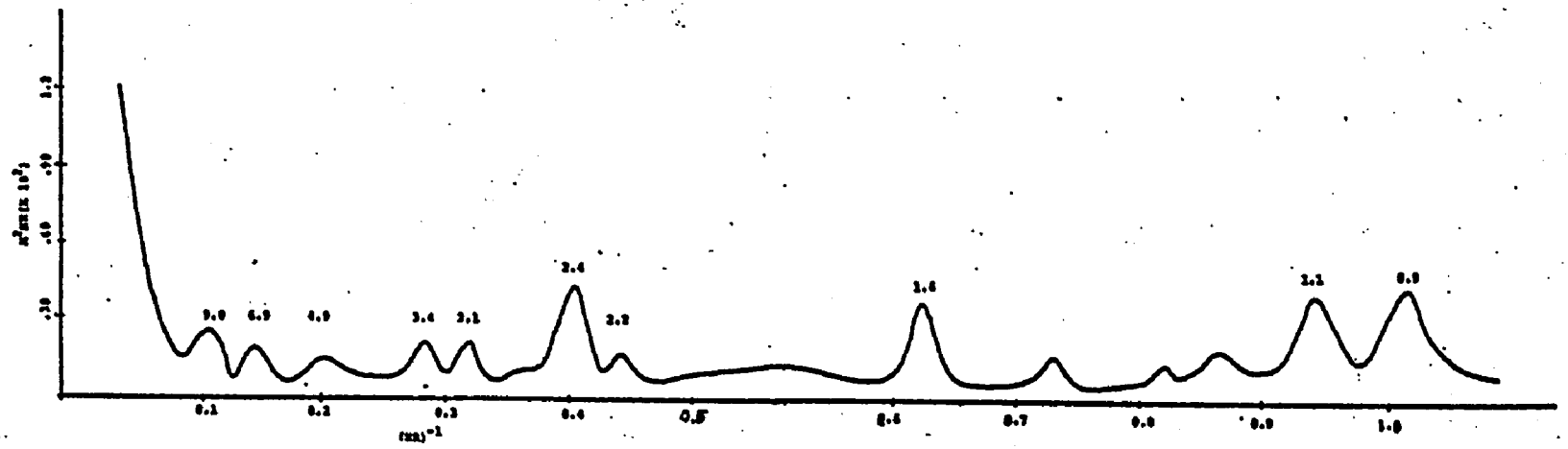


Figure 5. Estimate of power spectral density near Harrisville; duration=64hrs., lags=199, periods in hrs. are noted near each peak.

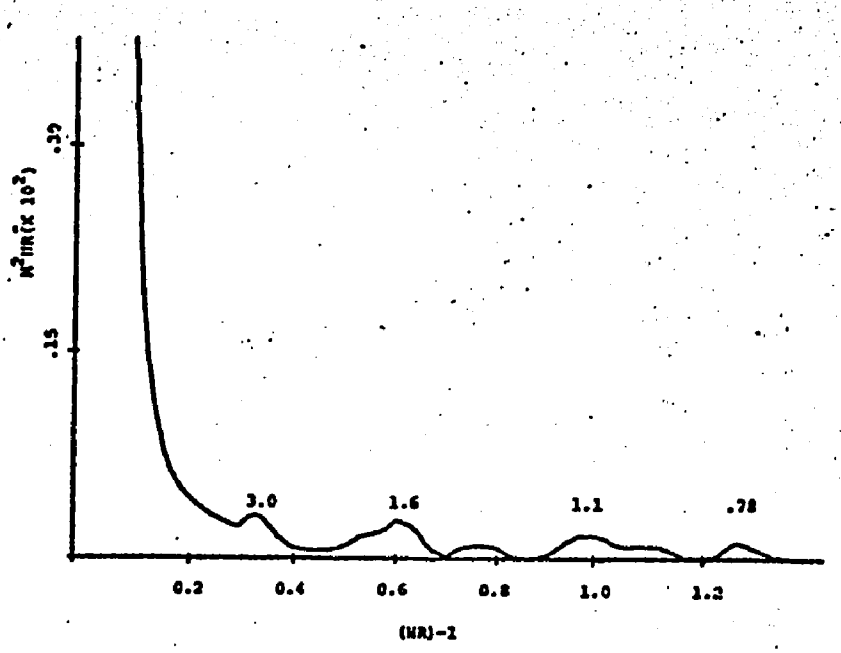


Figure 7. Estimate of power spectral density near Port AuGres; duration=64hrs., lags=60, periods in hrs. are noted near each peak.

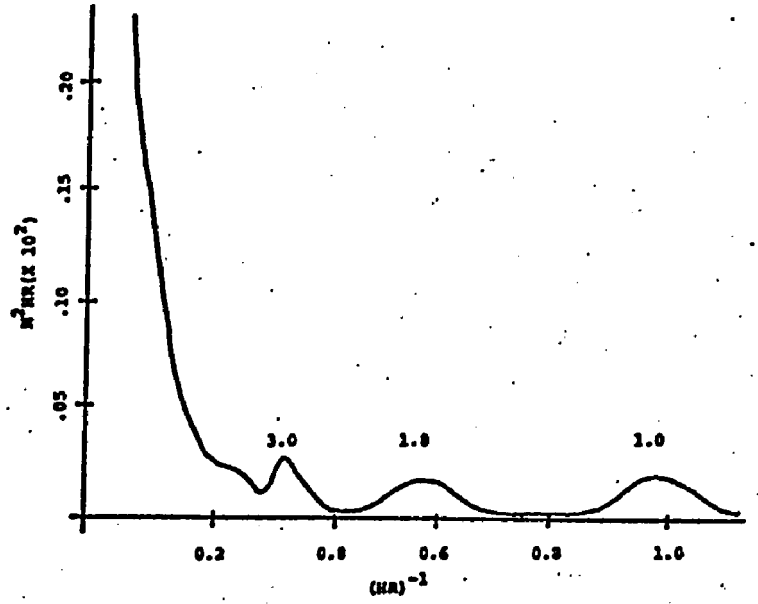


Figure 8. Estimate of power spectral density near Port AuGres; duration=84hrs., lags=199, periods in hrs. are noted near each peak.

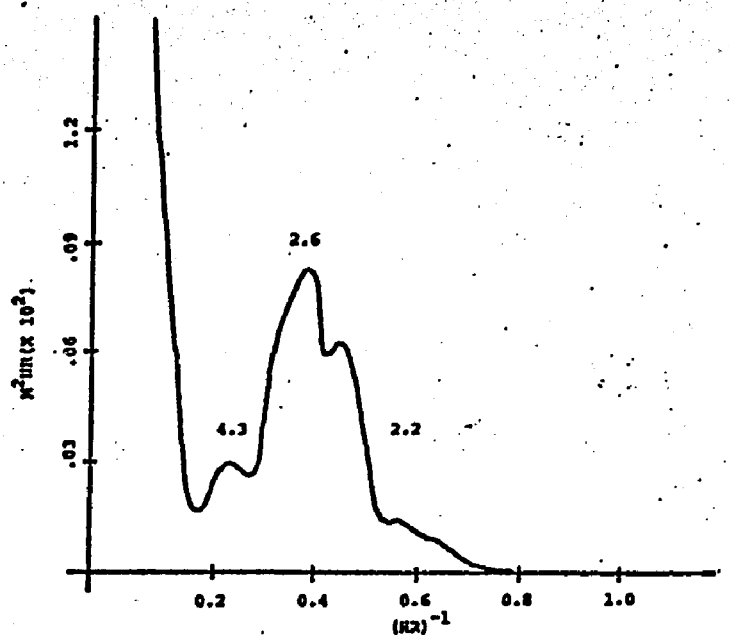


Figure 9. Estimate of power spectral density near Essexville; duration=64hrs., lags=60, periods in hrs. are noted near each peak.

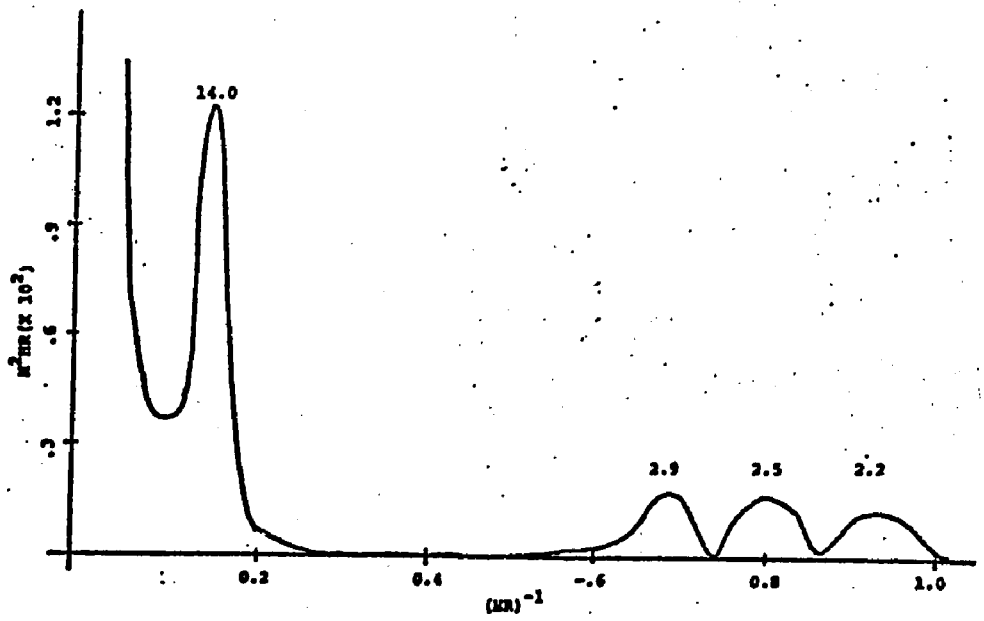


Figure 10. Estimate of power spectral density near Essexville; duration=64hrs., lags=199, periods in hrs. are noted near eavh peak.

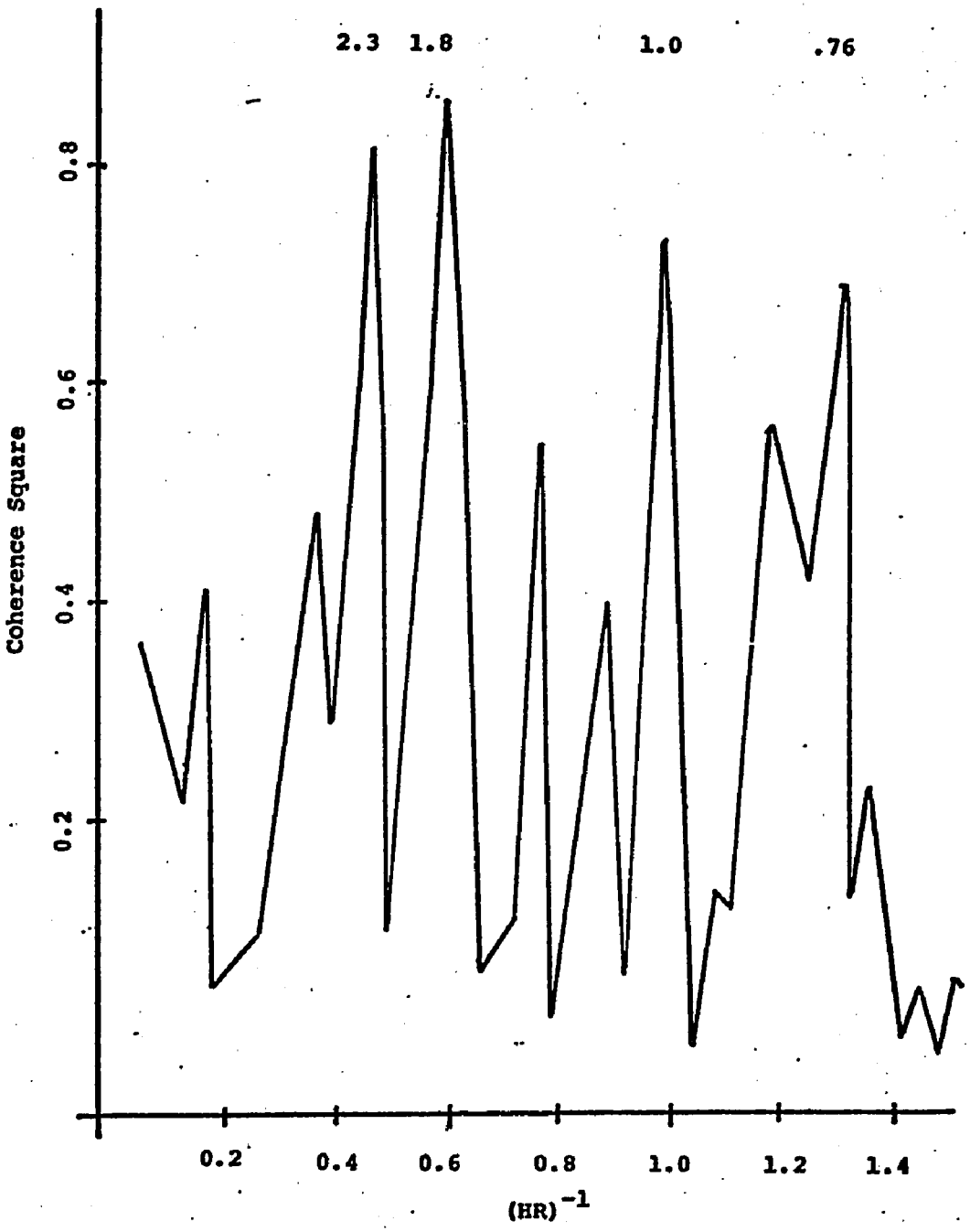


Figure 11. Estimate of coherence square, Harrisville-Port AuGres; duration=64hrs., lags=60, periods in hrs. are noted near each peak.

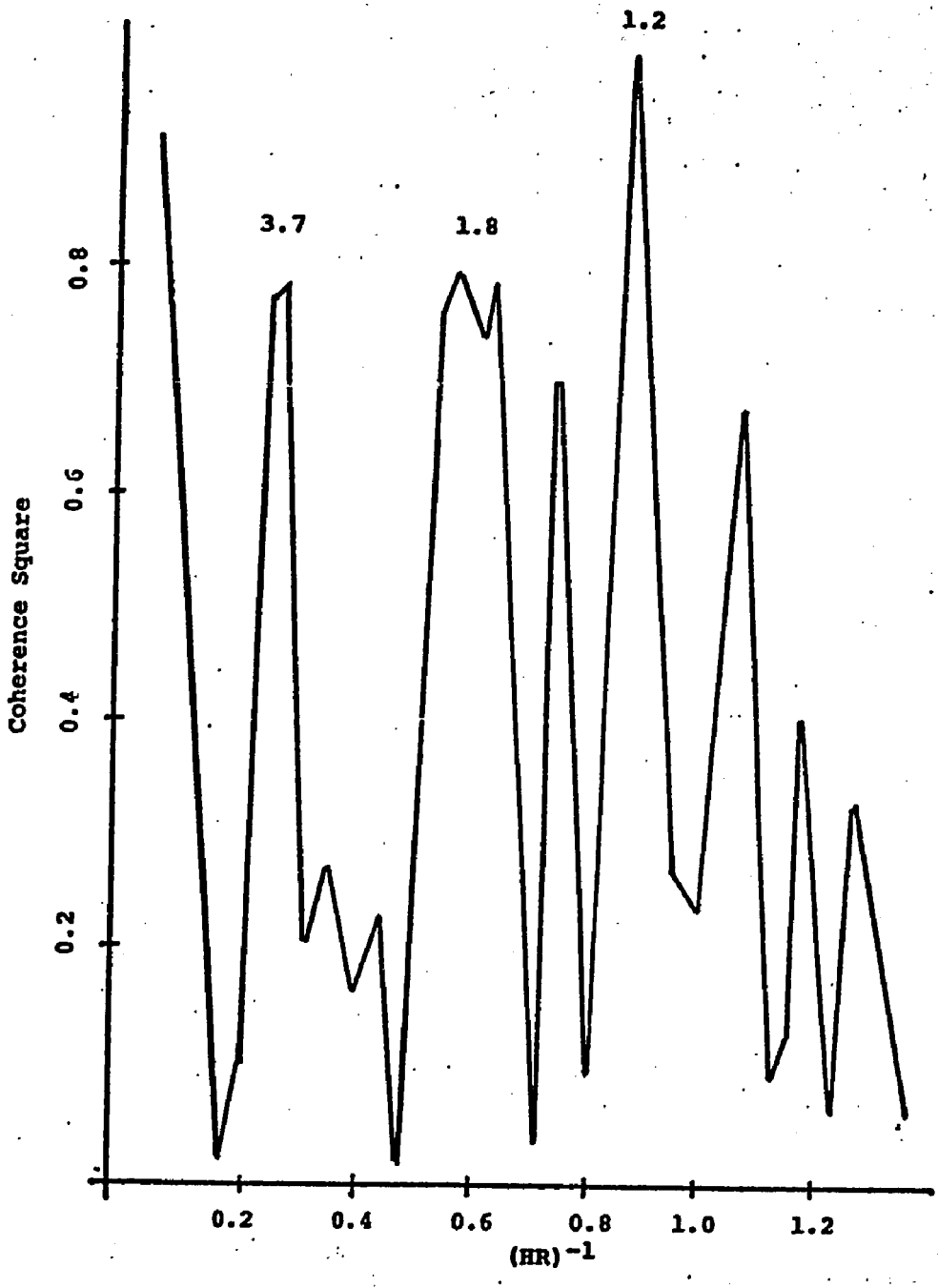


Figure 12. Estimate of coherence square, Harrisville-Port AuGres; duration=64hrs., lags=60, periods in hrs. are noted near each peak.

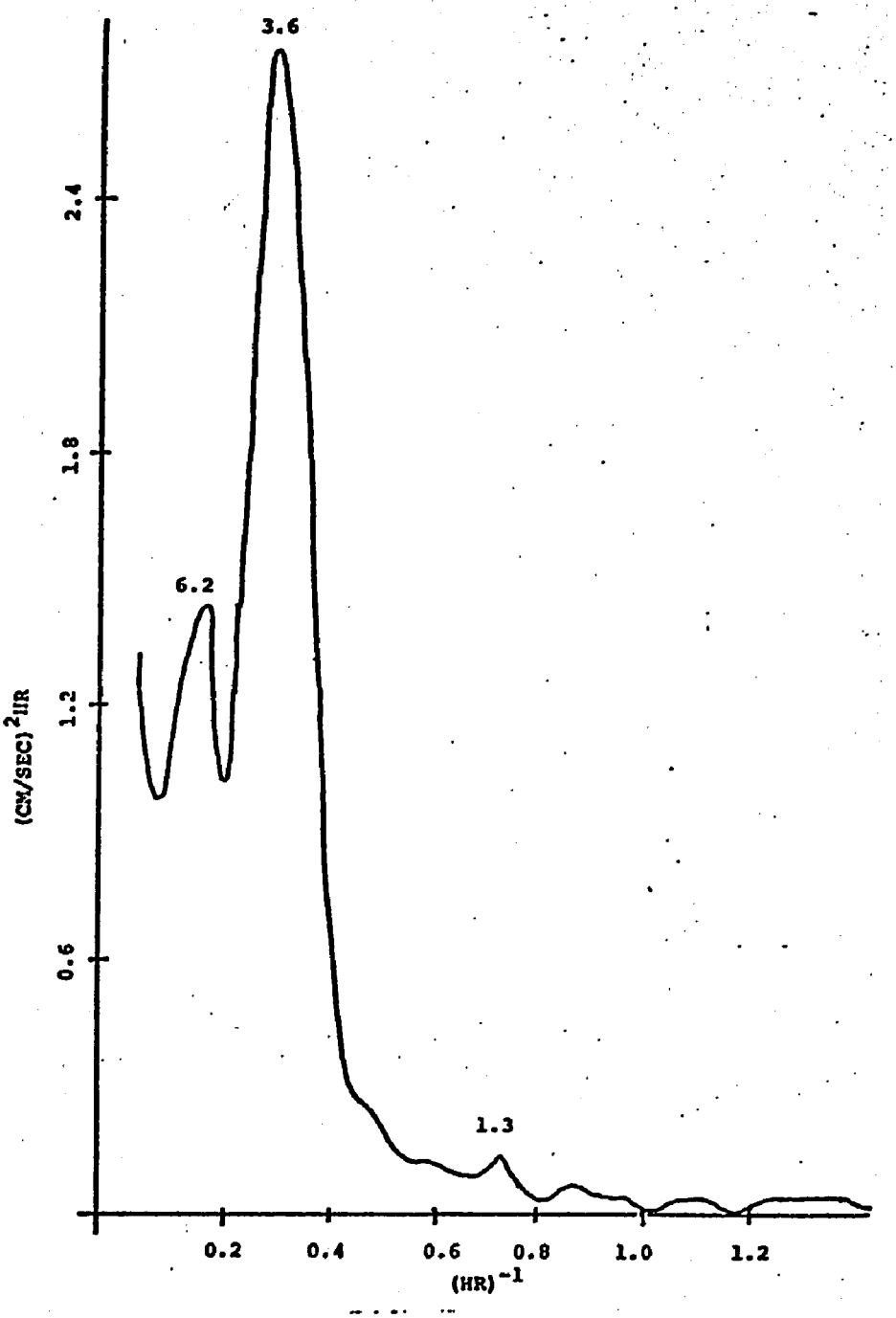


Figure 13. Estimate of power spectral density near Lookout Point (current meter data); duration=67hrs., lags=60, periods in hrs. are noted near each peak.

The rms displacement of the signal within a given frequency band over the duration of a series can be calculated from a given spectrum using simple graphical integration. If frequency bands centered about the model frequencies are chosen, the amplitudes, A_i, thus obtained are proportional to the energies of corresponding modes of the system. Assume that the scale of meteorological systems is large compared to Saginaw Bay and Lake Huron. Then the wind produces seiche motion in Lake Huron which forces Saginaw Bay, and, of course, produces the so-called wind-driven circulation of the bay itself. The amplitude of seiching in the bay now can be related to the mean wind, $(\bar{u},\bar{v})$. (The overbar denotes time averaging over a period which is large compared with time scales of the turbulent components simulated by the eddy diffusion concept.) To see this, consider two components of the stress tensor describing the force exerted on the surface of water by the wind;

$$\tau_{xz} + \tau_{yz} = \mu_T[(\frac{\partial \bar{u}}{\partial z} + \frac{\partial \bar{w}}{\partial x})\hat{i} + (\frac{\partial \bar{v}}{\partial z} + \frac{\partial \bar{w}}{\partial y})\hat{j}] \qquad (3.9)$$

where the first subscript indicates the direction in which the force is acting, the second subscript gives the direction normal to the plane in which the stress is acting, and μ_T is an eddy viscosity coefficient. Assuming the first term of each of the tensor components dominates, and operating with $(\bar{u},\bar{v})\cdot$ to obtain a quantity proportional to energy, the

result is

$$\Phi_i \propto \mu_T[\bar{u}\frac{\partial \bar{u}}{\partial z} + \bar{v}\frac{\partial \bar{v}}{\partial z}] \tag{3.10}$$

where Φ_i is the flux of energy into the i^{th} mode due to wind stress. Substituting the previously chosen parametric expression for the stress, and integrating to obtain the energy introduced into the system over an interval from t_o to t, the result is

$$\Phi_i|_{t_0}^{t} = K_i \int_{t_0}^{t} |\bar{u}|^3 \, dt' \tag{3.11}$$

where the K_i are merely constants of proportionality; $|\bar{u}|$ is the magnitude of the mean horizontal wind. By viewing the bay as an ensemble of simple harmonic oscillators, (3.11) can be written

$$1/2\, A_i^2 = K_i \int_{t_0}^{t} |\bar{u}|^3 \, dt' \tag{3.12}$$

where A_i are the amplitudes which exist during the time interval t_o to t. Through knowledge of the surface height profiles along the longitudinal axis of the bay for its various modes (Rockwell, 1966), the amplitudes at the open boundary can be related to the amplitudes at Port AuGres. These amplitude ratios have been included in the K_i.

The mean square displacements for the 3.3 hr and 1.8 hr oscillations at Port AuGres were calculated from spectral densities for five different time series. Then,

from (3.12), estimates of the constants of proportionality were found and are given in Table 2.

To obtain each hourly value of boundary data, the mean wind speed was averaged over the previous six hours, (slightly less than the response time of the bay); this value was then substituted into equation (3.12) to determine values for the A_i. These hourly values of boundary data for the two modes being considered were then fitted to a smooth curve using splines under tension. Values of the height excursions for each time step were then readily available, and were stored for use with the computational model.

D. Diffusion Coefficients

From data showing the distribution of chloride ions within the bay, it appears that the advective field dominates dispersion processes in the bay. However, introduction of space and time-dependent eddy diffusion coefficients would seem to be a requisite for fine-mesh simulation of concentration patterns. By viewing the system as a turbulent medium it could be supposed that eddies having different length scales affect various parts of the medium simultaneously, or perhaps that eddies having similar length scales have different effects due to the spatially dependent flow pattern. Since the aim was to construct parametric expressions for sub-grid scale processes, it was presumed that the latter of these hypotheses should form the basis for construction of the diffusion coefficients.

Spectral data begin	k_1 (1.8 hr. osc.)	k_2 (3.3 hr. osc.)
22 September 73	$2.6(10^{-6})$	$7.8(10^{-6})$
1 October 73	$5.0(10^{-6})$	$1.1(10^{-5})$
25 September 73	$1.7(10^{-6})$	$2.0(10^{-6})$
7 October 73	$0.4(10^{-6})$	$4.3(10^{-6})$

$k_{1\ avg} = 2.4(10^{-6})$; $k_{2\ avg} = 6.3(10^{-6})$

Table 2. Summary of analysis performed to determine empirical constants of proportionality, k_i. These constants relate energy input over given time interval to integral of cube of mean wind over that time interval.

It is believed that Kolmogoroff's hypotheses may be applied with some validity for two-dimensional eddies in natural waters with horizontal dimensions ranging from meters to kilometers, see, e.g. (Bowden, 1972). In particular, it is assumed that horizontal diffusion is governed by inertial sub-range eddies to which Kolmogoroff's second similarity hypothesis may be applied. In essence the inertial sub-range represents a region in wave number space where essentially only energy transferral is occurring. It connects the low wave number part of the spectrum to the high wave number part, where viscous effects finally dissipate the kinetic energy of turbulent motions. According to the second hypothesis, at sufficiently high wave numbers the spectrum of turbulence depends only upon the rate of kinetic energy decay per unit mass, ε, and the kinematic viscosity, $\nu = \mu/\rho$. In the sub-range the spectral intensity, $E(k)$, as a function of wave number, k, should be given by $E(k) \propto \varepsilon^{2/3} k^{-5/3}$.

Kolmogoroff's theories were developed for three dimensions. Recent theoretical work (Kraichnan, 1967) has shown that restriction to two dimensions adds another important constraint, at least for inviscid motion. In addition to the inertial range for kinetic energy the fluid should exhibit an inertial range for mean square vorticity, or enstrophy. It is suggested by Kraichnan that these two ranges could coexist, transferral of kinetic energy being

toward zero wave number according to the familiar -5/3 law and transfer of enstrophy being upward toward the dissipation range, according to a -3 law. However, transferral of energy in the -5/3 range to longer wavelength cannot exist as a quasi-steady state. It is conjectured that after energy reaches down to the lowest mode, some modification of the -5/3 range is required, starting at the bottom and working upward, as in the normal cascading process conceived in three dimensions.

In any case it was presumed that useful estimates of eddy diffusion coefficients in two-dimensional situations could be found in the following manner. According to the similarity hypotheses presented originally by Kolmogoroff, a coefficient of horizontal eddy diffusion can be given as $D \alpha \varepsilon^{1/3} L^{4/3}$, where L is the mean separation of water particles subject to diffusion. The so-called Richardson 4/3 law as just given is discussed in recent work by Bowden (1972). Observational evidence in support of the -5/3 law is also summarized therein. Presuming that eddies lose energy at a rate dependent upon their length scale, i.e. $\varepsilon \simeq u^2/(u/L)$, the diffusion law becomes $D \simeq uL$.

To find an appropriate length scale, L, the Kolmogoroff length scale, L_K, was introduced. The upper limit of the dissipation range was thus conceived to have a length $L_K = (\nu^3 L_{char}/u^3)^{1/4}$, where L_{char} is thought of as a large length scale in some sense. Values of eddy viscosity of the order

of 10^5 have been used by Simons (1971, 1972) in Lake Ontario. The smallest wave which can be resolved by the finite difference method (to be discussed in the next chapter) is 4km. Finally, a typical fluid speed, as indicated by available current meter data (Monahan, 1974) is 10 cm/sec. Using these estimates for the parameters involved in the Kolmogoroff length scale, and assuming that turbulent fluctuations can be typically as much as 50 percent of the mean, the result is $L \simeq 500$ m. It should be noted that an order of magnitude increase in ν, the most uncertain quantity in the above, leads to a length scale only about 2-1/2 times as large as that just given. Within the framework of the computational algorithm the diffusion coefficients were computed as

$$D_x = U(x,y,t)L/H(x,y) \quad \text{and} \quad D_y = V(x,y,t)L/H(x,y)$$

Finally, to summarize the preceeding sections, parametric expressions for the surface and bottom stress have been chosen, and the processing of wind data has been described. Results of spectral analyses have been shown, which give insights into Saginaw Bay's motion. Important forced modes identified by these spectral analyses, have been coupled in a mathematical way with the wind data, leading to the generation of a time-dependent boundary forcing function. Lastly, a method has been described whereby time and space dependent diffusion coefficients were found.

IV. Formulation of the numerical method

A. Finite difference method

To fulfill the ultimate goal of this work, approximate solutions to the circulation and advection-diffusion problems, as posed above, had to be found. Clearly, if real topography and shoreline configuration were to be used, a numerical method of some sort was necessary. Numerous considerations enter into the selection of a computational framework to solve a given initial-boundary value problem. Necessary forethoughts include the availability of computer hardware and funding, the resolution in space and time needed to elucidate physical processes in the problem at hand, and the accuracy of the approximate solutions over the long and short term as affected by the discrete representation of the continuum equations.

For clarity the equations which were solved numerically are stated here as well as in Chapter II. The flow equations are

$$\frac{\partial \vec{U}}{\partial t} + f\hat{k}\times\vec{U} + \kappa\vec{U}/H = -gH\nabla_H\zeta + 1/\rho\ \vec{\tau}_w \qquad (4.1)$$

$$\frac{\partial \zeta}{\partial t} + \nabla_H\cdot\vec{U} = 0 \qquad (4.2)$$

subject to the conditions that $\vec{U}\cdot\hat{n} = 0$ at solid boundaries and $\zeta(x,y,t)$ is specified along the open boundary. The advection-diffusion equation is

$$\frac{\partial Hc}{\partial t} + \nabla_H \cdot (c\vec{U}) - \frac{\partial}{\partial x}(HD_x \frac{\partial c}{\partial x}) - \frac{\partial}{\partial y}(HD_y \frac{\partial c}{\partial y}) = HS \qquad (4.3)$$

subject to the conditions that $\nabla C \cdot \hat{n} = 0$ at solid boundaries and $C(x,y,t)$ is specified along the open boundary.

The finite difference approximations chosen for this work were alternating direction implicit, ADI, procedures, and were originally introduced in companion papers by Peaceman and Rachford (1955) and Douglas and Gunn (1955). Also known as the method of variable direction (Kuskova, 1968) this method makes use of a splitting of the time step to obtain a multidimensional implicit system, the solution of which involves only the inversion of tridiagonal matrices. As in all finite difference approximations, a variable $f(x,y,t)$ becomes $f(x_i,y_j,t_k)$, where $x_i = i\Delta x, y_j = j\Delta y$, and $t_k = k\Delta t$. The ADI procedure is unconditionally stable in that perturbations introduced into the initial data amplify only to a bounded extent. Convergence of the method as applied to the diffusion equation was shown formally by Douglas (1957) for rectangular regions. (A convergent scheme is one in which all values of the finite difference solution approach the continuum solution as the mesh intervals Δt, Δx, Δy, approach zero.) The ADI technique has not been used (to this author's knowledge) to study estuarine dynamics, except by Leendertse (1967). References discussing the method include Richtmeyer and Morton (1967), and Roache (1972).

Since values of variables were sought only at discrete locations, a spatial arrangement of these variables had to be pre-determined. A space-staggered scheme was used here, in which transports and water levels were described at different grid points, as shown in Figure 14. Concentrations and surface heights were described at integer values of j and k. The U transport, the depths for U points, H_U, and the diffusion coefficients for the x direction, D_x, were given at integer and one half values of j and integer values of k. The V transport, the depths for V points, H_V, and the diffusion coefficients for the y direction, D_y, were given at integer values of j and integer and one half values of k. The shoreline was approximated using the usual stepping pattern, as depicted in Figure 15. Three index matrices, Nupt, Nvpt, Nzetap, were also pre-calculated and stored. The index numbers in each were positive for points within the computational field, negative for all points outside, and zero for points along the open boundary. The matrices were used to identify the shoreline in the logic of the computational algorithm, and are illustrated in Figure 15.

To facilitate presentation of the numerical method, the following notation is introduced, where ϕ represents an arbitrary dependent variable:

$$\phi^n_{jk} \equiv \phi(x_j, y_k, t_n),\ x_j = j\Delta x,\ y_k = k\Delta y,\ t_n = n\Delta t$$

$$\bar{\bar{\phi}}_{j,k} \equiv 1/4(\phi_{j-1/2,k-1/2} + \phi_{j-1/2,k+1/2} + \phi_{j+1/2,k+1/2} + \phi_{j+1/2,k-1/2})$$

$$\bar{\phi}^{y}_{j,k} \equiv 1/2(\phi_{j,k-1/2} + \phi_{j,k+1/2})$$

$$\bar{\phi}^{x}_{j,k} \equiv 1/2(\phi_{j-1/2,k} + \phi_{j+1/2,k}), \quad \delta_{1/2t}\phi \equiv 2/\Delta t(\phi^{n+1/2} - \phi^{n})$$

$$\delta_x\phi \equiv 1/\Delta x(\phi_{j+1/2,k} - \phi_{j-1/2,k}), \qquad \phi^{+}_{\text{at } n} \equiv \phi^{n+1/2}$$

$$\delta_y\phi \equiv 1/\Delta y(\phi_{j,k+1/2} - \phi_{j,k-1/2})$$

The finite difference approximations for the 1st half time step can then be written: (4.4)

$$\delta_{1/2t}U - f\bar{\bar{V}} + gH_U\delta_x\zeta^{+} - \tau^{+}_{w}(x) + \kappa U/H_U = 0, \text{ at } n,j+1/2,k$$

$$\delta_{1/2t}\zeta + \delta_x U^{+} + \delta_y V = 0, \text{ at } n,j,k \tag{4.5}$$

$$\delta_{1/2t}\ 1/4(\bar{H}^{x}_{U} + \bar{H}^{y}_{V})c + \delta_x(U\bar{c}^{x})^{+} + \delta_y(V\bar{c}^{y}) \tag{4.6}$$

$$-\delta_x(H_U D_x \delta_x c^{+}) - \delta_y(H_V D_y \delta_y c)$$

$$= 1/4\ (\bar{H}^{x}_{U} + \bar{H}^{y}_{V})S, \quad \text{at } n,j,k$$

The equations for the second half step are

$$\delta_{1/2t}V + f\bar{\bar{U}} + gH_V\delta_y\zeta^{+} - \tau^{+}_{w}(y) + \kappa V/H_V = 0, \quad \text{at } n+1/2,j,k+1/2 \tag{4.7}$$

$$\delta_{1/2t}\zeta + \delta_x U + \delta_y V^{+} = 0, \text{ at } n+1/2,j,k \tag{4.8}$$

$$\delta_{1/2t}\ 1/4(\bar{H}^{x}_{U} + \bar{H}^{y}_{V})c + \delta_x(U\bar{c}^{x}) + \delta_y(V\bar{c}^{y})^{+} \tag{4.9}$$

$$-\delta_x(H_U D_x \delta_x c) - \delta_y(H_V D_y \delta_y c^{+})$$

$$= 1/4(\bar{H}^{x}_{U} + \bar{H}^{y}_{V})S, \text{ at } n+1/2,j,k$$

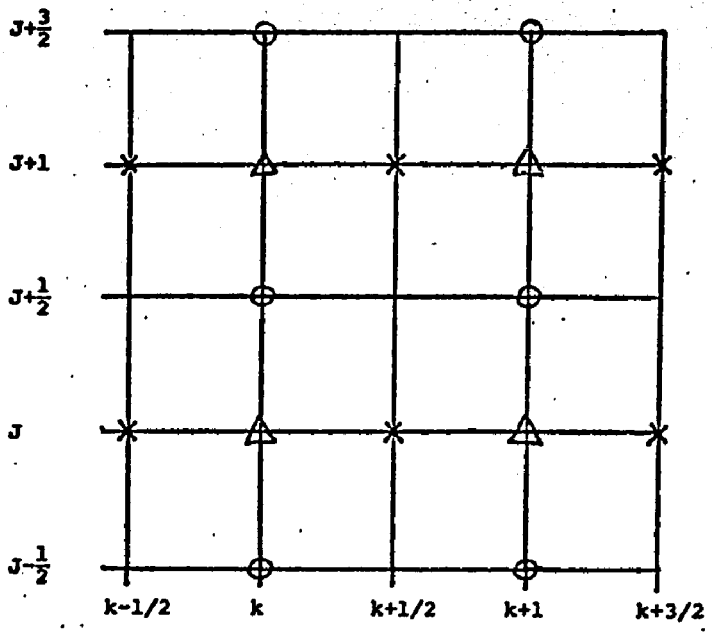


Figure 14. Spatial disposition of variables; grid legend:
O - U, H_U, D_x
X - V, H_V, D_y
Δ - ζ, C

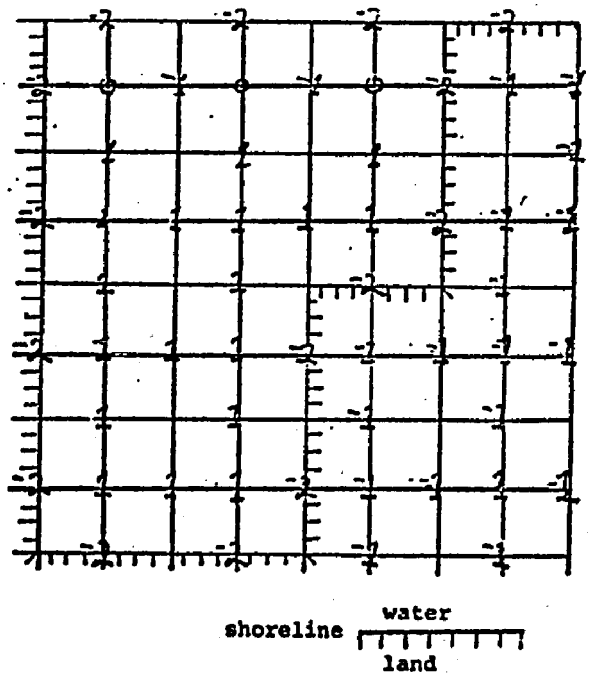


Figure 15. Shoreline stepping pattern, (simplified example).

Discrete forms of the boundary conditions given in Chapter II must now be given for (4.4) through (4.9). Let S be the set of all j,k grid points which fall inside the shoreline. Let $S_U(S_V)$ be the set of all grid pairs j+1/2,k (j,k+1/2) which fall upon segments of the shoreline parallel to the x(y) axis or are outside the shoreline. Define Γ to be the line segment dividing the bay from Lake Huron. Let S_Γ be the set of all j,k grid points along the open boundary which adjoins Lake Huron. Finally, for the substance under consideration define C_Γ to be the mean concentration in Lake Huron in the vicinity of the open boundary, and let J denote the subscript along Γ. The boundary conditions for equations (4.4), (4.5), (4.7), and (4.8) are then

$$U_{j+1/2,k} \equiv 0 \;\forall\; j+1/2,k \in S_U,\quad \zeta^n_{J,k} = F(t) \qquad j,k \in \Gamma \tag{4.10}$$

$$V_{j,k+1/2} \equiv 0 \;\forall\; j,k+1/2 \in S_V,\quad \zeta_{j,k} \equiv 0 \qquad j,k \notin S \tag{4.11}$$

The boundary conditions for equations (4.6) and (4.9) become

$$c_{j,k} \equiv 0 \;\forall\; j,k \notin S,\quad D_{x\ j+1/2,k} \equiv 0 \;\forall\; j+1/2,k \in S_U$$

$$D_{y\ j,k+1/2} \equiv 0 \;\forall\; j,k \in S_V, \text{ and for inflow, } U_{J,k} > 0,$$

$$c^{n+1/2} = c^n - 4\Delta t/(\bar{H}^x_U + \bar{H}^y_V)\,([\delta_x(Uc) - \delta_y(H_V D_y \delta_y c)]^n$$

$$-\delta_x(H_U D_x \delta_x c)^{n-1/2}), \text{ at } J,k \tag{4.12}$$

while for outflow along Γ, i.e., $U_{J,k}>0$

$$c^{n+1/2} = c^n + 1/4(c_\Gamma - c^n), \quad \text{at } J,k \tag{4.13}$$

The initial conditions for the problem (unless otherwise noted) were that $U = V = \zeta = 0$ everywhere, and the initial distribution of C was patterned after Dow Chemical Company chlorinity surveys. In the original data values of chlorinity in ppm were divided by 100, so that most computed values fell in the range 0.0 to 1.0. A distributed source function, S(j,k), was introduced near the outlet of the Saginaw River. Values of the transport in this same vicinity which represent the river inflow were also prescribed. The discharge rate was fixed at 95 m^3/sec, and the chlorine concentration in the incoming fluid was set at 280 ppm.

The first term in (4.6) and (4.9) uses four point depth averaging. Each concentration point, $C_{j,k}$, is in effect at the center of a square having a depth value specified on each corner. The averaging is performed so that the quantity being modeled is conserved. The two point depth averaging used in the advection terms in (4.6) and (4.9) represents a conservative differencing form as will be shown below.

The solutions for (4.4) - (4.9) are found by repeated inversion of tridiagonal matrices. For any line

k in the grid there are unknowns at only three points in the j direction in (4.4) - (4.5). For M points in the j direction there are 2M equations in 2M unknowns and there is a boundary condition at each end of the line. Solving this system on each line k gives $U^{n+1/2}, V^{n}\ \zeta^{n+1/2}$. The transport values are then used in (4.6) which advances the concentration solution from (c^{n} to $c^{n+1/2}$) by sweeping through the grid in the j direction in a manner analagous to that used to solve (4.4) and (4.5). During the second half time step unknowns exist at only three values of k along any given line j. Equations (4.7) and (4.8) are solved simultaneously for each k on each line j. This gives values for $U^{n+1/2}, V^{n+1}, \zeta^{n+1}$. The transport values are then used in (4.9) which advances the concentration solution from $C^{n+1/2}$ to C^{n+1} by sweeping through the grid in the k direction in a manner analagous to that used to solve (4.7) and (4.8). Further description of tridiagonal algorithms may be found in Richtmeyer and Morton (1967).

Application of ADI methods to irregular domains has sometimes been avoided due to the programming difficulties (Roache, 1972). In this research index matrices such as depicted in Figure 15 were used to control the calculations. Initially all variables were zero at all grid points. IF logic can be used subsequently so that no calculation for U or V is ever made along a solid boundary perpendicular to the x or y directions, respective-

ly. In this manner the boundary condition $\vec{U}\cdot\hat{n} = 0$ is satisfied. Further, if no calculation is made for U (V) at j,k, then $D_x (D_y)$ at that point remains equal to zero. So, the condition $\nabla C\cdot\hat{n} = 0$ at solid boundaries is met without difficulty.

B. Properties of the method

The open boundary concentration as given in (4.12) - (4.13) contains numerous subtleties. Physically, it is clear that the advection of material from within the computational field (outflow conditions) must affect the concentration along the open boundary. However, during inflow conditions it is reasonable to presume that the open boundary concentration will return to the mean lake value, C_T, unless, of course, C_J already equals C_T. Numerically, the method of treating the advection term in (4.12) is essentially upwind differencing, U_{J-1} being omitted since it is outside the model. This method was used to suppress wiggles (spatial oscillations in the solution) which could have arisen due to incorrect boundary data, or due to the preponderance of advective to diffusive effects near Γ, resulting in a quasi-boundary layer as discussed in conjunction with the scaling analysis in Chapter II. Wiggles have been wrongly associated with non-linearities or with linear instabilities in transient calculations. Such errors are merely the solution of the finite difference equations under certain circumstances which can

arise (Roache, 1972). Further discussion of this problem is given in the section "Effects of diffusion coefficients" in Chapter V. The x-diffusion term is taken at a lagged time level to prevent static instability, i.e., monotonic error growth, since the corrective displacement due to the second order term is applied at J+1 rather than J. While the stability of the total method would now appear to be limited by Courant number restrictions ($U\Delta t/H_U\Delta X \leq 1/2$) at the outflow boundary, there is apparently no restriction in conjunction with the ADI method as noted by Pao and Daugherty (1969). Upwind differencing and lagged time levels for second order terms are familiar techniques in meteorological endeavors, and are lucidly explained by Roache (1972) and Richtmeyer and Morton (1957).

The conservative properties of the grid point equations (or the lack thereof) should be recognized. Leendertse (1967) has shown that (4.4) and (4.7) conserve mass if an accounting is made for that which enters (or leaves) through the bounds over a time step. Momentum is also conserved for the linear equations, ignoring the earth's rotation, if an accounting is made for the impulses caused by the pressures at the boundaries and for the momentum which enters the flow through the boundaries into the field.

Similarly, it is possible to ascertain whether or not the advection-diffusion equation has been represented by a

conservative differencing technique. Focusing attention upon one line in the grid, and summing (4.5) over m from 1 to M, the result is

$$\sum_{1}^{M} (\bar{H}_U^x + \bar{H}_V^y) c_m^{n+1/2} = \sum_{1}^{M} (\bar{H}_U^x + \bar{H}_V^y) c_m^n \qquad (4.14)$$

$$+\Delta t/\Delta x [U_{1/2}(c_1+c_0)/2 - U_{M+1/2}(c_{M+1}+c_M)/2$$

$$+ H_{U\,M+1/2}\, D_{x\,M+1/2}\, (c_{M+1}-c_M)/\Delta x$$

$$- H_{U\,1/2}\, D_{x\,1/2}\, (c_1-c_0)/\Delta x]$$

Since $U_{M+1/2} = D_{X_{M+1/2}} \equiv 0$; i.e., the M+1/2 point is on the shoreline, the differencing is conservative provided that an accounting is made for matter exchange through the open boundary.

Next, note that the successive use of (4.5) and (4.8) results in spatial derivatives which are essentially centered in time or averaged over the iteration interval. Similarly, (4.6) and (4.9) result in time-centered differencing for the spatial terms. Substitution of Taylor's series expansions for all variables into the finite difference approximations results in an estimate for the truncation error inherent in the scheme. Retaining only lowest order terms, (4.4), (4.5), (4.7), and (4.8) yield solutions which are $0(\Delta t)$ for (U,V). Equations (4.6) and (4.9) formally yield $0(\Delta t^2)$, $0(\Delta X^2)$ and $0(\Delta y^2)$ accuracy. However, the advective field is not $0(\Delta t^2)$ as just indicated.

Such truncation error estimates provide a useful means of comparing numerical schemes, but do not necessarily imply the superiority of one technique over another. Accuracy may have to be sacrificed for computational speed or vice-versa. In fact, there are situations where apparently more accurate schemes have led to erroneous results, e.g., due to boundary influence (Roache, 1972).

Leendertse (1967) has presented a concise description of wave deformation (truncation error effects) for a scheme similar to (4.4), (4.5) and (4.7), (4.8). In synopsis, he defines the complex propagation factor as the ratio of the computed wave in amplitude and phase to the physical wave in amplitude and phase after a time interval in which the physical wave propagates over its wavelength. Graphical displays of this ratio are given as a function of the finite difference parameters. In this research a spatial step of 2 km was chosen, i.e., $\Delta X = \Delta y = \Delta S = 2000$ m. As recommended by Leendertse, a time step was selected so that $\Delta t/\Delta S (g H_{max})^{1/2} = 2$. Using these values his analyses indicate that the computational effects are much less than 1° phase retardation and 1% amplitude change after several hours for flow phenomena having spatial scales as small as 50 km. Since the meteorological forcing data used have significant lull periods, and since perusal of surface height data and current meter records indicates that the bay often returns to nearly quiescent

conditions, it is unlikely that long term simulation will suffer gross errors. A truncation error analysis has also been given for advection-diffusion equations similar to (4.6) and (4.9) by Leendertse (1970). Truncation error effects are small here, also, since the evolution of a given concentration pattern requires a time interval at least an order of magnitude longer than the solutions of typical flow processes observed. A longer time step might be considered for the advection-diffusion equation, thus requiring time-averaging of the flow fields. However, this leads to difficulties in the conservation of the substance being modeled.

Insight into the stability of the methods can be gained by following a Fourier expansion of a line of errors as time progresses. It is required that these errors, numerical or physical in nature, do not amplify in an unlimited manner. Using the technique introduced by von Neumann, see, e.g., Richtmeyer and Morton (1967), one term of the perturbations upon the solution for the flow equations is written as $\Delta\bar{U}(x,y,t) = \bar{U}^* e^{i\beta n\Delta t} e^{i(\sigma_1 j\Delta x+\sigma_2 k\Delta y)}$ where $\bar{U} = \begin{Bmatrix} U \\ V \\ \zeta \end{Bmatrix}$, β is a frequency, and σ_1, σ_2 are wave numbers. (Since a linear system is being investigated, only one term need be considered.) Letting $\bar{U}^n = \bar{U}^* e^{i\beta n\Delta t}$, the first operation, (4.4), (4.5), may be cast in the form $[A]\bar{U}^{n+1/2} = [B]\bar{U}^n$. The second operation, (4.7), (4.8), yields $[C]\bar{U}^{n+1} = [D]\bar{U}^n$. Combining, the result is $[D]^{-1}[C]\bar{U}^{n+1} = [A]^{-1}[B]\bar{U}^n$.

The eigenvalues, λ_i, of the scheme's amplification matrix can now be found from the determinant $|[A]^{-1}[B]-[D]^{-1}[C]\lambda| = 0$, where $\lambda = e^{i\beta n\Delta t}$. The necessary condition for stability proposed by von Neumann (for linear equations on a region of unbounded extent) states that the time step must be finite and for all wave numbers the eigenvalues of the amplification matrix must satisfy $|\lambda| \leq 1 + 0(\Delta t)$. Further, the fourth sufficient condition states that if the elements of the amplification matrix are bounded for finite time step and all wave numbers, and if all the eigenvalues of this matrix, with the possible exception of one which satisfies the necessary condition, are inside the unit circle, then the von Neumann condition is sufficient as well as necessary for stability. Thus, in principle, the analysis can be completed by finding the eigenvalues, λ_i. Since this can be a formidable task, methods have been developed to ascertain bounds for the eigenvalues. Following Leendertse (1967) it can be shown that all the eigenvalues for the method considered here are less than one and therefore unconditional stability is expected according to the fourth sufficient condition. The details of this analysis appear in Appendix A. It has often been acknowledged that the best stability analysis is one conducted through numerical experiment. Many different kinds of stability assessments are used, and many definitions of stability have been offered. The above discussion was presented because of its physical

relevance to the problem at hand and because the von Neumann analysis is viewed by many as the most dependable approach to assessing the unfortunately ill-defined concept of stability.

A detailed stability analysis of the advection-diffusion problem is not warranted. Equations (4.6) and (4.9) represent a straightforward application of the ADI method as has been used to solve the barotropic vorticity equation (see Roache, 1972). Stability analyses have appeared in previous works (see, e.g., Richtmeyer and Morton, 1967).

Unfortunately, the von Neumann analysis neglects boundary influence. Thus, it is not clear whether the given numerical schema and their concomitant boundary conditions represent well-posed problems in a numerical-analytical context. As indicated in Chapter I, current researchers are probing just such questions. Elvius and Sundstrom (1973) have shown primarily through proofs based on the energy method, that a semi-implicit representation of the linearized shallow-water wave equations, the primitive form of the barotropic forecast equations, leads to a well-posed problem numerically when coupled with either of the following two sets of conditions: 1) tangential velocity given at inflow points of the boundary, and normal velocity prescribed at all boundaries; 2) tangential velocity given

at inflow parts of the boundary, and the ingoing characteristic $\eta - \eta\vec{u}\cdot\hat{n}$ prescribed at all boundaries, where ζ is the geopotential. Davies (1973) has shown that a particular finite difference representation of the non-linear shallow water equations is well-posed when coupled with either of the following two sets of conditions: 1) normal velocity specified everywhere on the boundary, with the tangential velocity and height field given at inflow points; 2) a variable $\vec{u}\cdot\hat{n} - 2(gH)^{1/2}$ specified everywhere on the boundaries, and the tangential velocity given at inflow points. It should be remarked that the stability analyses given in the above two references are still not definitive, especially as regards the set 1) conditions in the first reference, and the set 2) conditions in the second reference. The energy methods used to investigate boundedness of solutions are not applicable to these sets of conditions. Elvius and Sundstrom therefore utilize a general method worked out by Kreiss (1971), but can find only necessary conditions for the two-dimensional case. Wurtele, Paegle, and Sielecki (1971) consider the use of open boundary conditions with the storm-surge equations. They discuss methods to prevent the reflection and/or re-reflection of gravity waves which have entered the system at open boundaries. The lateral conditions developed for the one-dimensional case are essentially linearized Riemann invariants, $U \pm \zeta(gH)^{1/2}$ (Garabedian, 1964). In the

two-dimensional case the quantities $(U^2+ V^2)^{1/2} \pm \zeta(gH)^{1/2}$ are given, assuming that the finite difference grid has a scale which is small compared to the radius of curvature of incoming wave fronts. Their work offers no proofs regarding boundedness of solutions. However, illuminating numerical experiments were performed.

Several observations may be made regarding these investigations. For the non-linear or linearized non-linear inviscid equations as studied in Davies (1973) and Elvius and Sundstrom (1973), tangential velocities along the inflow boundaries appear to be crucial. This would appear to be required because vorticity, ω, can be advected into the system. The accompanying vorticity balance can be written $\partial\omega/\partial t + J(\omega,\Psi) = 0$ where $J(\omega,\Psi)$ is the Jacobian operator, and Ψ is a stream function defined by $u = \frac{\partial\Psi}{\partial y}$, $U = \frac{-\partial\Psi}{\partial x}$. This relation states the well-known fact that in inviscid flow, vorticity is conserved along particle paths. The work of Wurtele et. al. (1971) is in accord with the discussion in the previous chapter. Therein it was pointed out that failure to simulate accurately the rest of the fluid surroundings admits to error growth originating near open boundaries.

It is this author's contention that the numerical flow equations and their boundary conditions as stated in this research represent a well-posed problem. Since the equations lack the advective property, specification

of the surface height at outflow parts of the boundary does not risk conservation of vorticity for the inviscid problem. Further, spurious wave disturbances emanating from the open boundary have never been detected in the numerical experiments. While this is no proof, it is true that no general theory yet exists for choosing numerical-analytical boundary conditions. In fact, Kasahara indicates in his perceptive foreword to GARP publ. no. 10 (Kreiss and Oliger, 1973) that case studies are needed in two-dimensional problems such as the shallow water equations to determine the adaquacy of a given scheme. Kreiss and Oliger in that treatise state that difference methods for irregular boundaries such as exist in this work must be examined by extensive numerical experiment, and that the researcher must continually question the physics of the results obtained.

The numerical advection-diffusion equation and its boundary conditions also appear to represent a well-posed problem based on the numerical solutions obtained. Error waves have never been observed near the open boundary. The results of the numerical experiments using the methods outlined above are discussed in the following chapter.

V. Discussion of numerical experiments

An extensive collection of numerical experiments have been conducted using the model described in the

preceding chapters. The first such experiments concerned a coarse grid model of Saginaw Bay. In this formulation a grid spacing of 8 km was chosen (i.e., $\Delta x = \Delta y = 8$ km) and numerous test runs were made to de-bug the computer programs. In addition to allowing relatively inexpensive development of a numerical code, useful results were obtained, especially as regards the bay's circulation. Figure 16 depicts the arithmetic mean of the transport field as given by the 8 km model over a period of approximately 70 hr. During this period a nodal condition was assumed at the mouth, and a real wind history provided surface stress. As will be seen below, the rudiments of the circulation pattern are very similar to those predicted by the fine grid model. However due to truncation error effects and the desire to produce detailed simulations over time periods as long as a month, the grid spacing to 2 km is absolutely necessary.

A. Effects of temporal and spatial step size

The sensitivity of a numerical method to changes in temporal and spatial step size sometimes can indicate stability of the method in a practical sense. The grid size in the 2 km model (hereafter the word model shall refer to the 2 km model) was changed to 1800 m and 2200 m and the iteration was carried out to about 1600 time steps (100 hr) in each case. The visual appearance of the transport and concentration patterns were largely

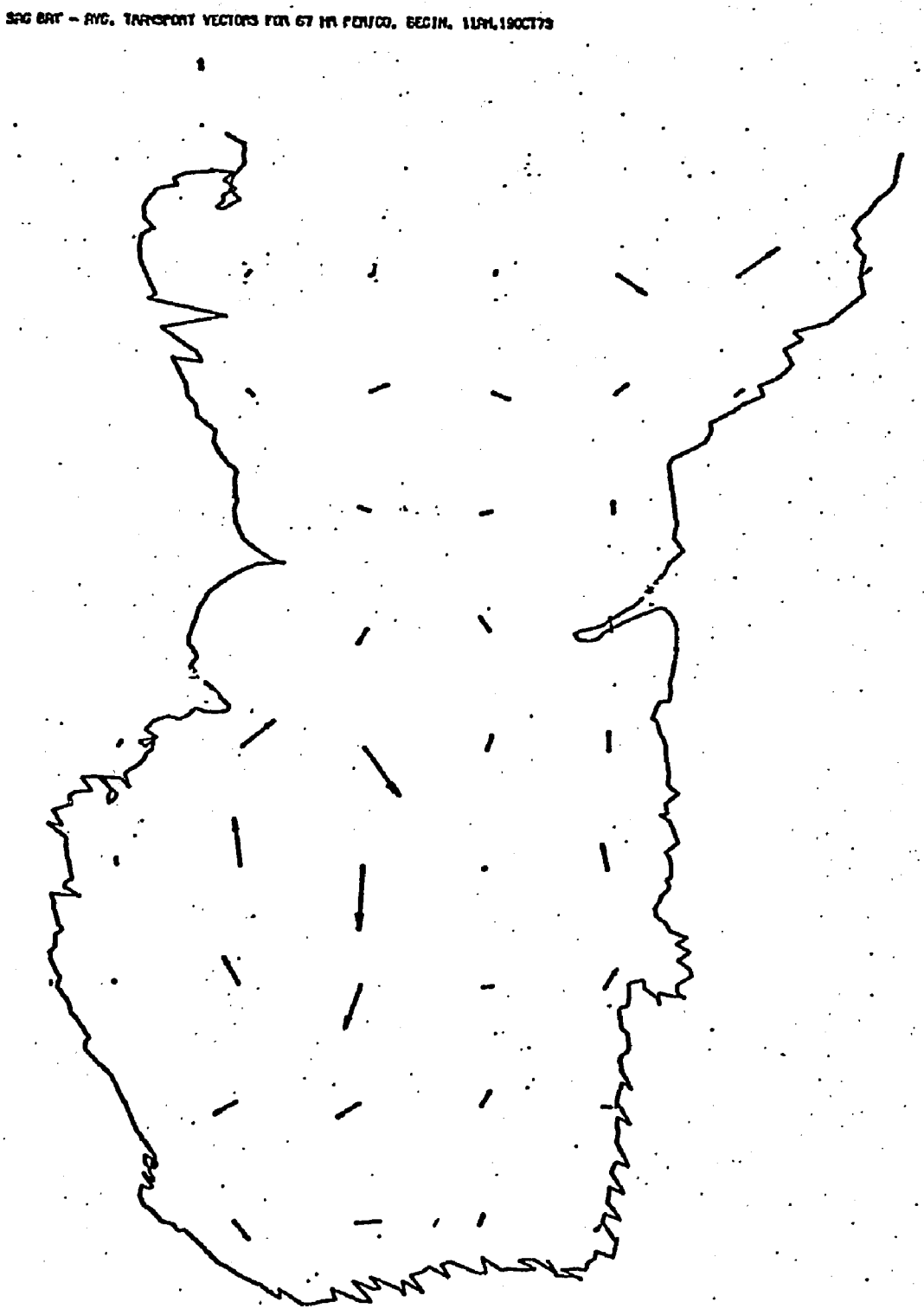


Figure 16.

Figure 16. Average transport vectors, 8 km model. Essence of pattern is similar to 2 km model(see Figs. 53-54).

indistinguishable from a similar run with the 2000 m grid spacing. Although certain understandable differences exist, it is clear that the scheme is not sensitive to small changes in the spatial differencing parameter. Depth variations appear to have minimal effect on scheme properties if $\Delta t/\Delta s (gH_{max})^{1/2} \approx 2$ (leendertse, 1970). Thus, for H_{max} = 30 m, Δt is chosen as .0625 hr. Comparison of model runs with Δt = .125 hr and Δt = .0625 hr indicated that the longer time step was unuseable, since computed fields of the unknowns differed by as much as 30 percent after 1600 steps. Comparison of model runs with Δt = .03125 hr and Δt = .0625 hr indicated that the shorter step was unnecessary since computed fields of the unknowns were essentially the same, even after 1600 steps.

B. Results of steady forcing

It is of interest to present the transport fields which were obtained under various steady, simplified forcing conditions. The general features of the circulation of the bay are clearly enunciated by these experiments. However, the magnitudes of the transport are significantly smaller than those resulting from realistic wind forcing. Figures 17-20 show the response to a steady 12 knot wind from each of the four quadrants with a nodal condition assumed at the mouth. Features of the circulation seen in the southwest wind case, Figure 17, appear repeatedly, especially in the average transport fields over many days.

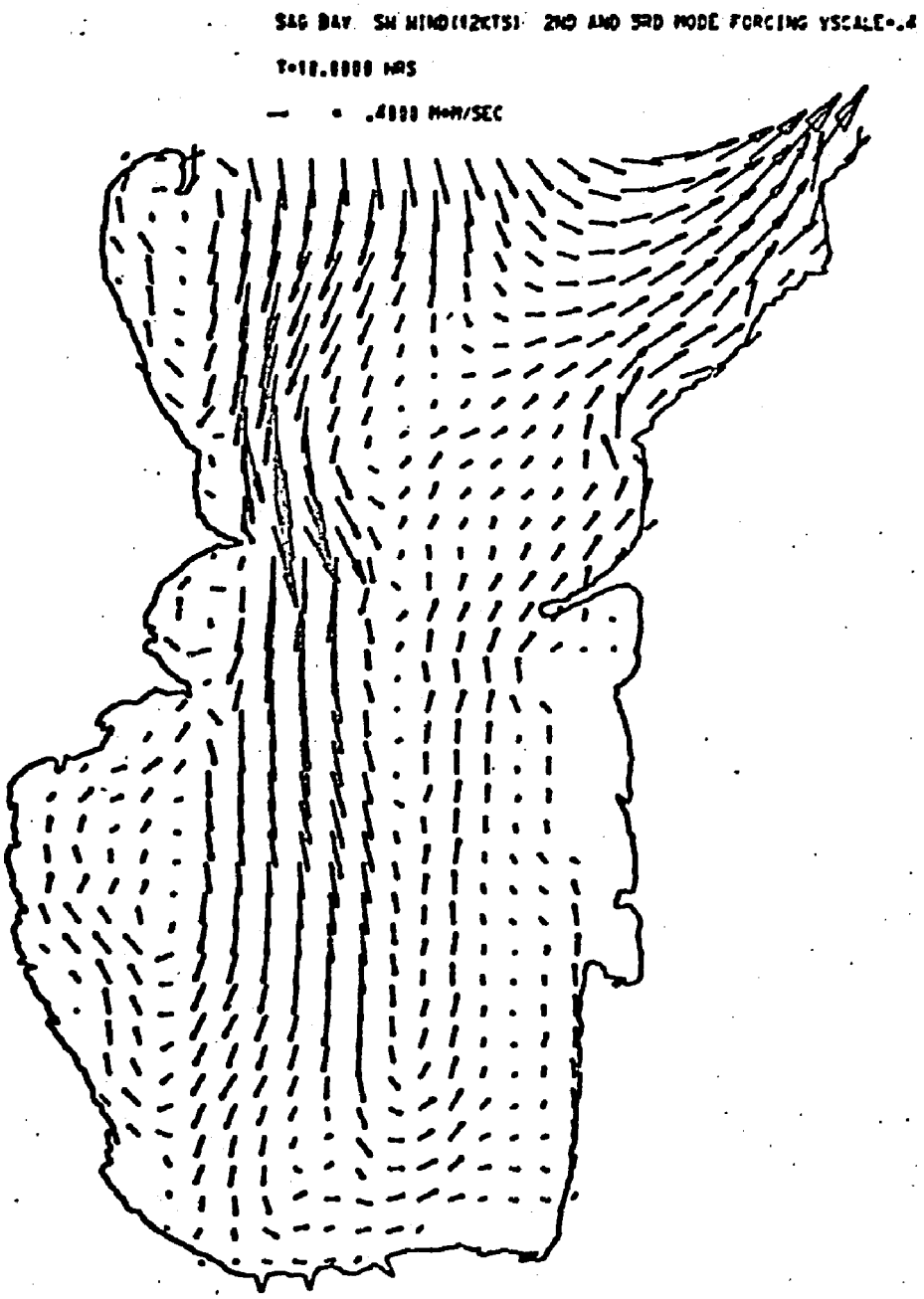


Figure 17. Response to southwest wind (12 kt), a pattern seen repeatedly.(Weak boundary forcing at 3.3 hr and 2.0 hr was also applied.)

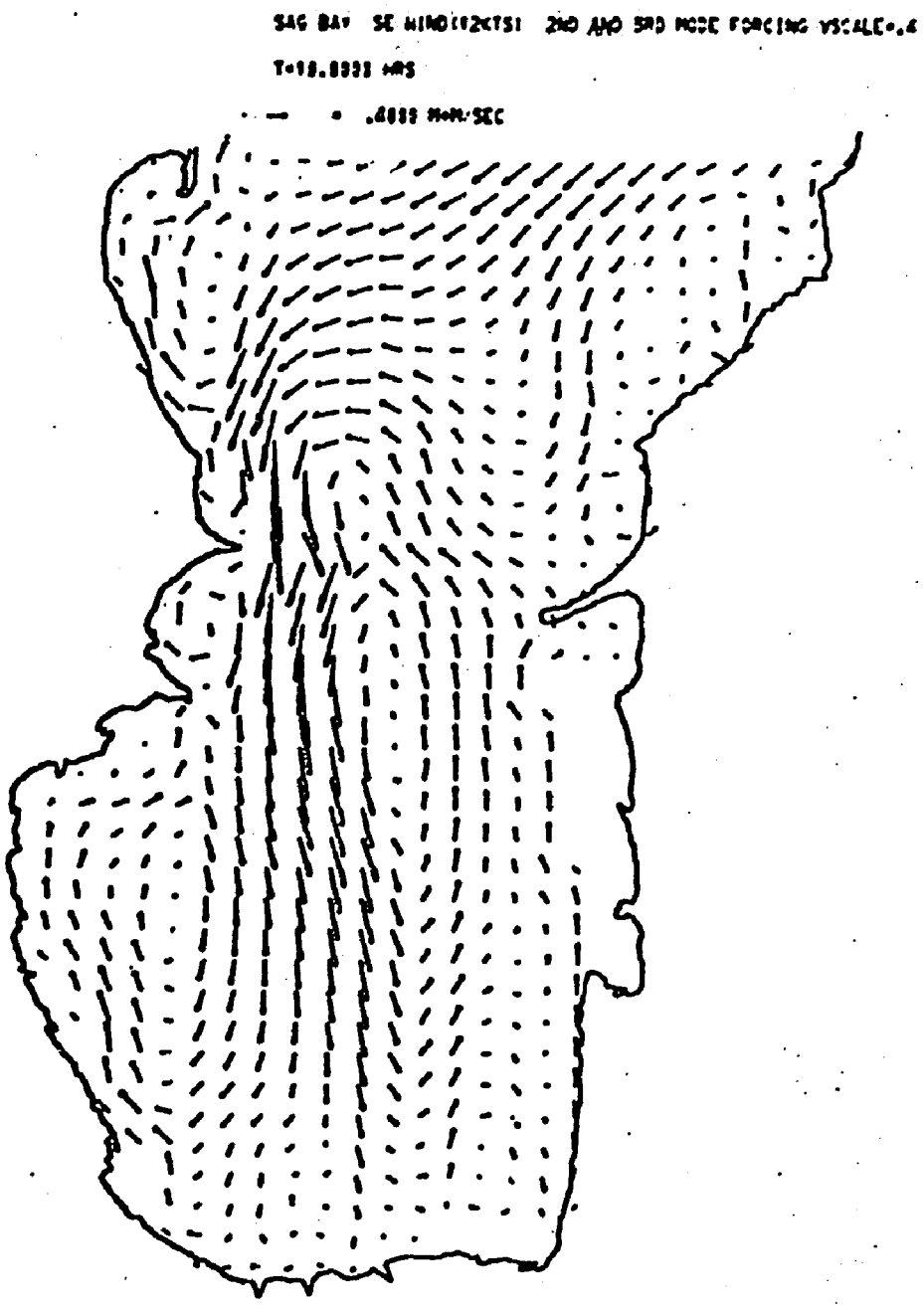


Figure 18. Response to southeast wind (12 kt) is 180 reversal from response to northwest wind (compare Fig. 19). (Weak boundary forcing at 3.3 hr and 2.0 hr was also applied.)

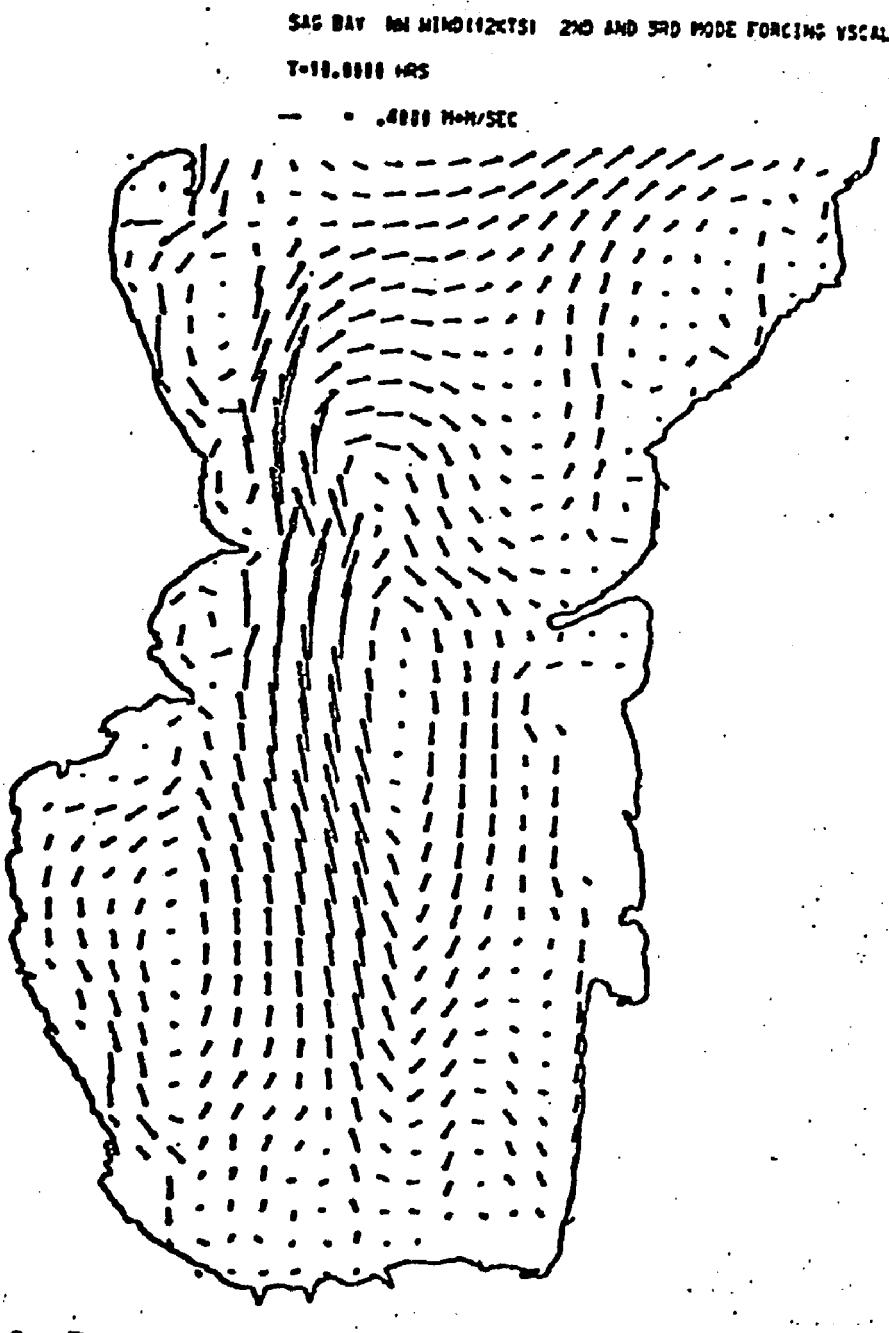


Figure 19. Response to northwest wind (compare Fig. 18) (Weak boundary forcing at 3.3 hr and 2.2 was also applied,)

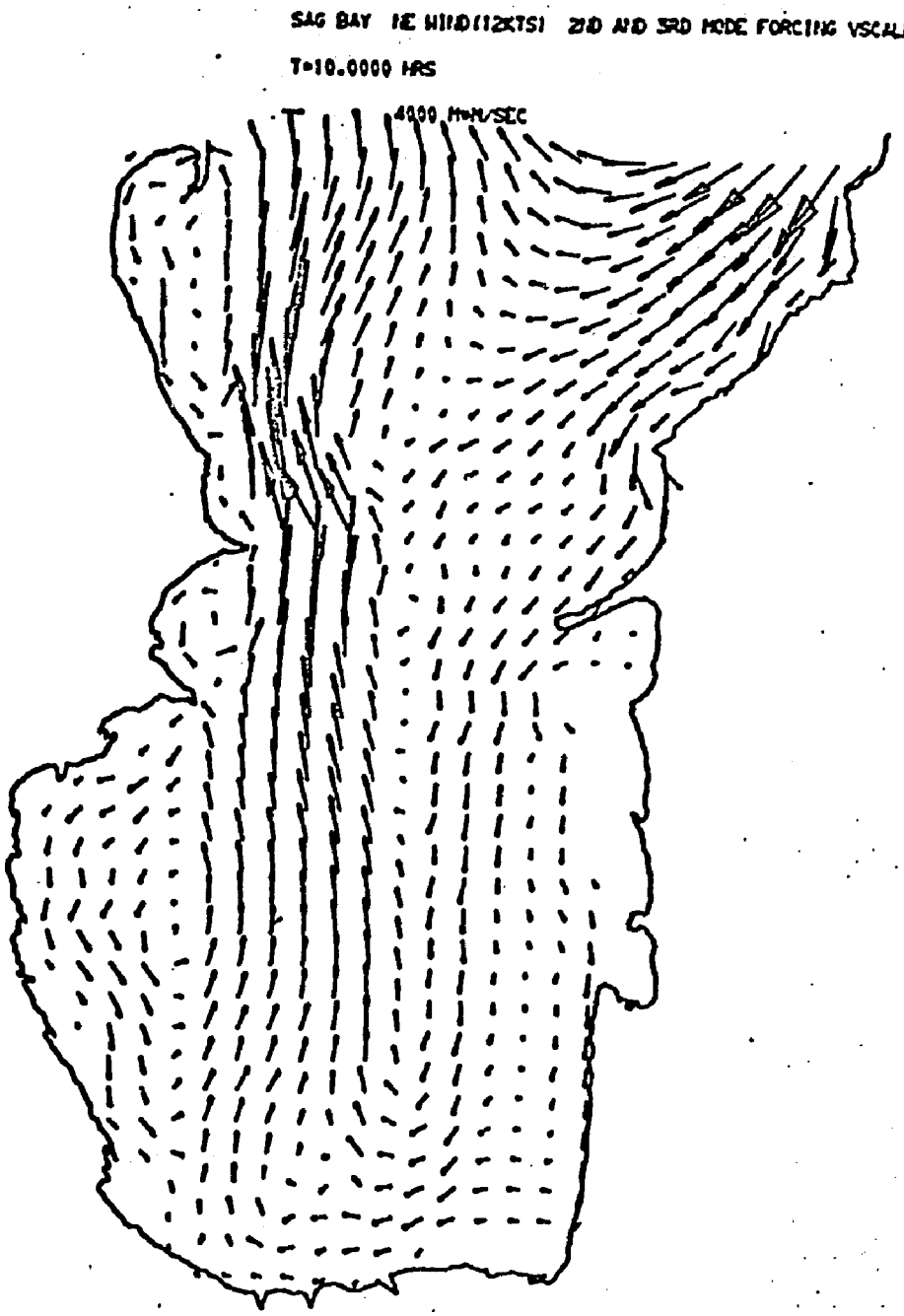


Figure 20. Response to northeast wind shows channel acting as release mechanism. (Weak boundary forcing at 3.3hr and 2.0hr was also applied.)

Figures 18 and 19 show that the responses to winds from southeasterly and northwesterly directions, respectively, are to a clear extent 180° reversals of one another. The fabled "noreaster", Figure 20, adds new features to the circulation pattern, however, as the bay's orientation lends itself to servere effects under this forcing.

The second kind of simplified forcing considered was oscillatory motion along the open boundary at 1.6 hr and 3.3 hr, no surface stress applied. Figures 21 and 22 show transport patterns which result from the use of these oscillatory boundary data. An antinode in the surface height can easily be inferred from the flow field seen in Figure 22. The position of this antinode is, in fact, in excellent agreement with one-dimensional predictions by Rockwell, (1966). This fact supports the use of Rockwell's work to infer the open boundary amplitudes from amplitudes near Port AuGres according to the procedure described in Chapter III. Having observed the responses to these simplified forcing conditions, it is easier to interpret the complicated responses arising under realistic forcing conditions.

C. Effects of bottom friction

Before proceeding to the discussion of output obtained under complicated forcing conditions, the effects of varying bottom friction should be displayed. As has been seen from the analytical solutions presented in

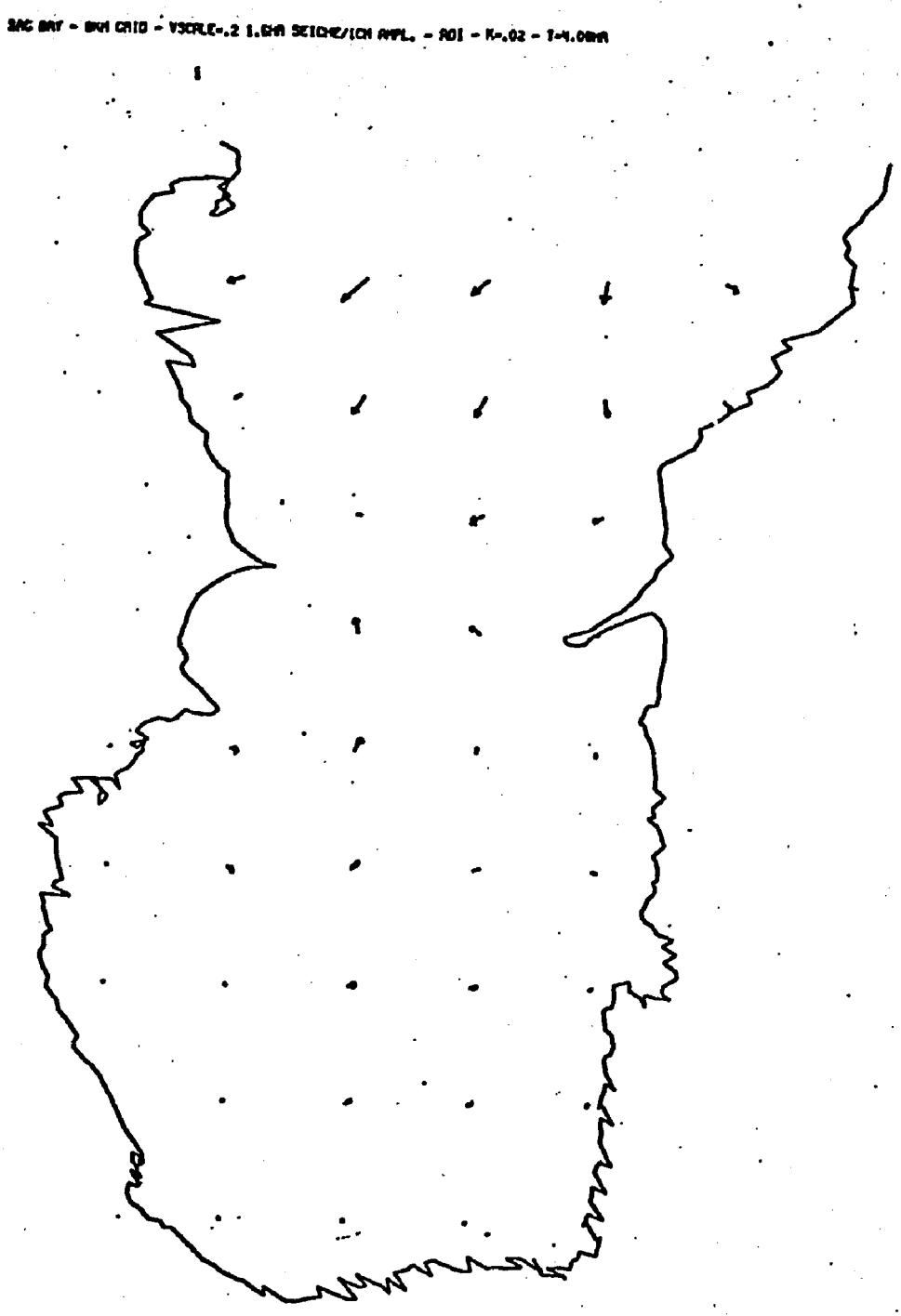


Figure 21. Response to 1.8 hr seiche forcing at 1 cm amplitude along open boundary. Only the outer bay is excited.

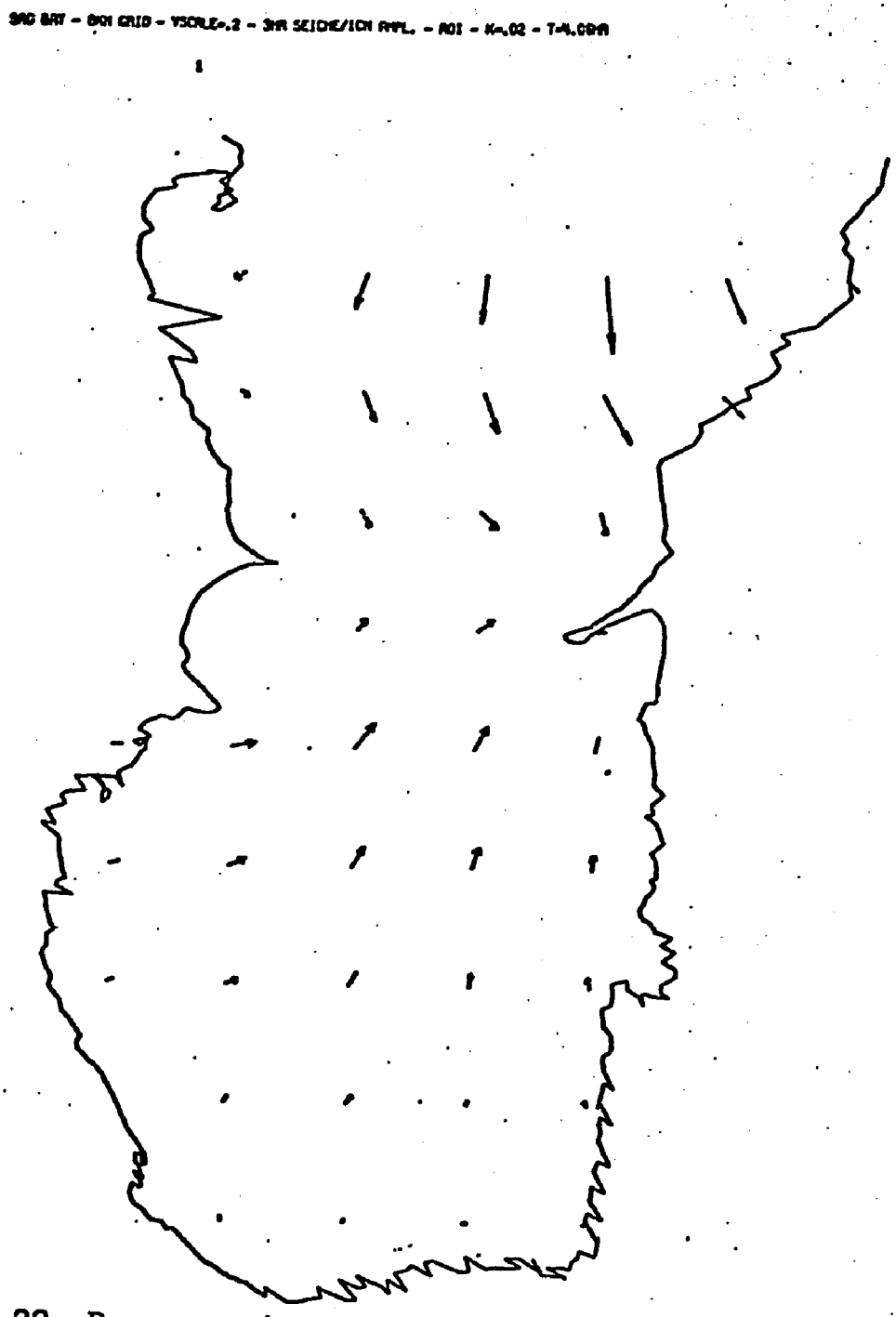


Figure 22. Response to 3.3 hr seiche forcing at 1 cm amplitude along open boundary. Antinode in surface height can be inferred.

Chapter II, one would not expect an order of magnitude change in the linearized friction parameter. Figures 23-24 confirm this remark, and show the effects of varying friction explicitly; the durations of these runs is conceived as a typical duration for significant surface stress on a usual day. It is evident that the general patterns in the bay are relatively unchanged by varying the dissipation. Changing κ from .02 cm/sec to .04 cm/sec leads to less than a 10 percent change in the magnitude of computed transports. Since the friction coefficient was estimated in as conscientious a manner as was possible, given the available data, it was felt that proceeding with complicated simulations was justified.

D. System hysteresis

It is instructive to consider experiments which test the memory of the system. This provides a further indirect assessment of possible cumulative errors. The model was started from rest and run to 180 hr using forcing data which began 1 August 1973. The initial conditions and source function were as described in Chapter IV. This calculation was then restarted and carried out to 360 hr. Figures 26 and 27 represent the flow and concentration patterns, respectively, which arose after 204 hr. To test the effects of initial conditions, these graphs may be compared to Figures 28 and 29, which represent the solutions of the equations as before, but starting at t = 180 hr

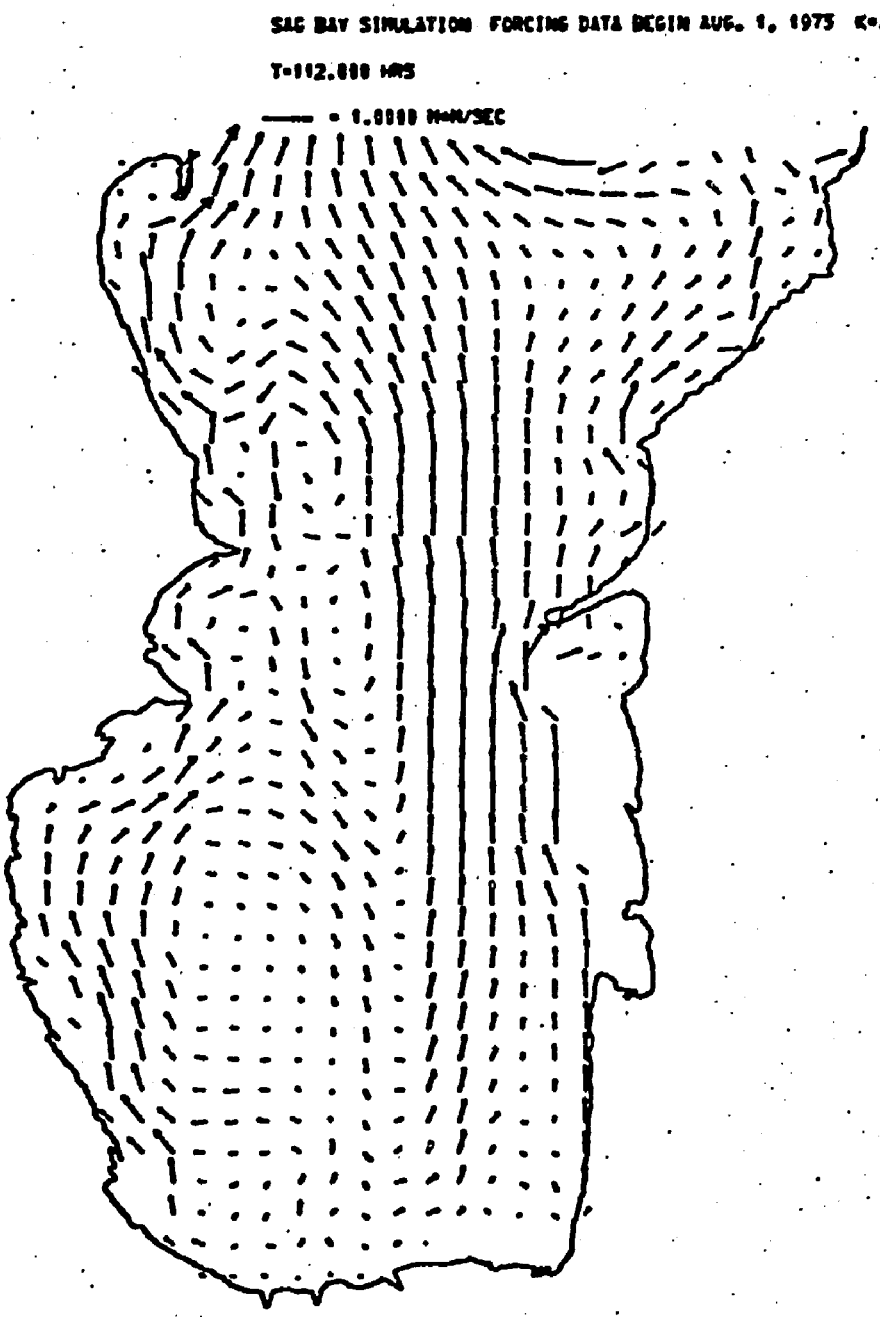


Figure 23. Circulation from realistic simulation.Friction parameter is .02cm/sec (Compare Figs.24-25).

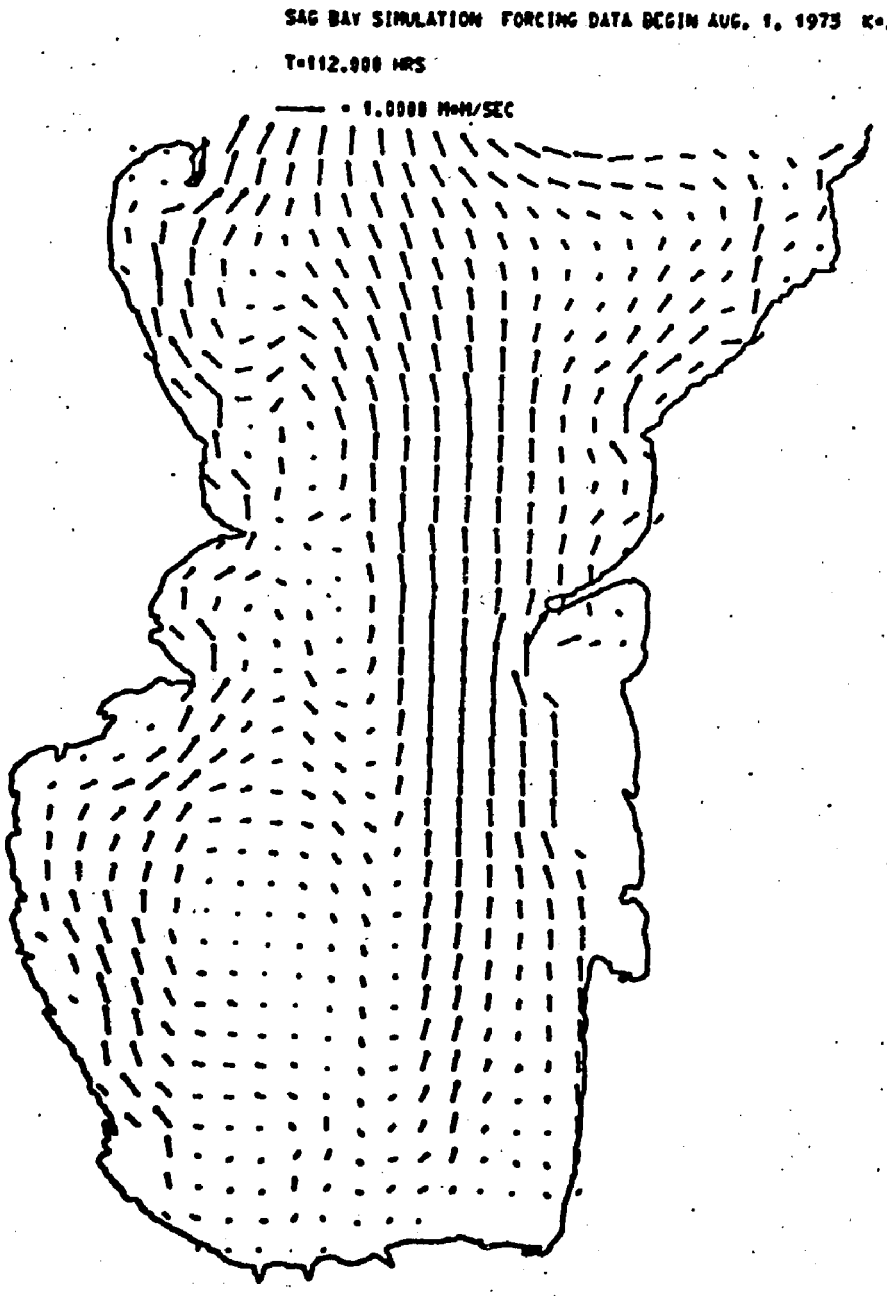


Figure 24. Circulation from realistic simulation. Friction parameter is .03 cm/sec. Figs. 23-25 show less than 10 percent differences in computed transport.

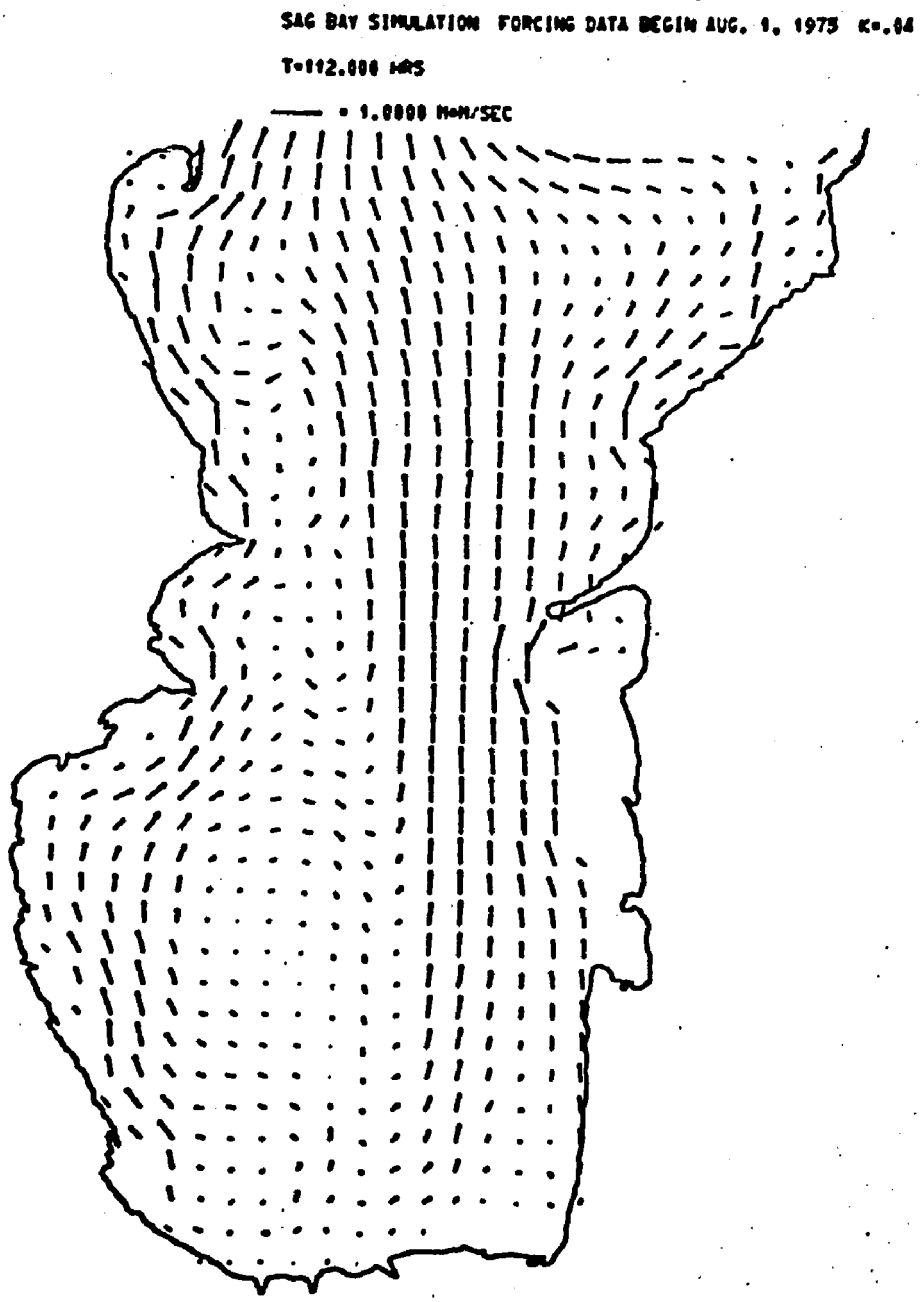


Figure 25. Circulation from realistic simulation. Friction parameter is .04 cm/sec (compare Figs. 23 and 24).

from rest and using the initial matter distribution. Thus, the second simulation just described has a duration of only 24 hours at the 204th hour of forcing data. From Figures 26 and 28 it is clear that radically different initial conditions for the flow field were obliterated in less than one day. This is an important fact since initial conditions for the flow problem are rather imprecisely known. The concentration field has a much longer "memory". In fact, Figures 27 and 29 show that the matter distribution may change very slowly during periods of weak forcing.

In a test similar to the above it was of interest to determine whether computed variables might tend to a different solution if started from perturbed initial conditions. In this regard Figures 30 and 31 show the flow and concentration patterns, respectively, which were obtained after the model had been run 360 hr subject to forcing beginning 1 August 1973. To obtain perturbed initial conditions the solution at $t = 180$ hr for the computer run to which Figures 30 and 31 belong was modified as follows: all variables at all grid points were changed in a random manner by as much as 10 percent of their originally computed values. Figures 32 and 33 represent the graphics of the fields of unknowns at $t = 360$ hr which were obtained by using these randomized initial conditions. It does not appear that the outputs in these two cases tend toward different solutions.

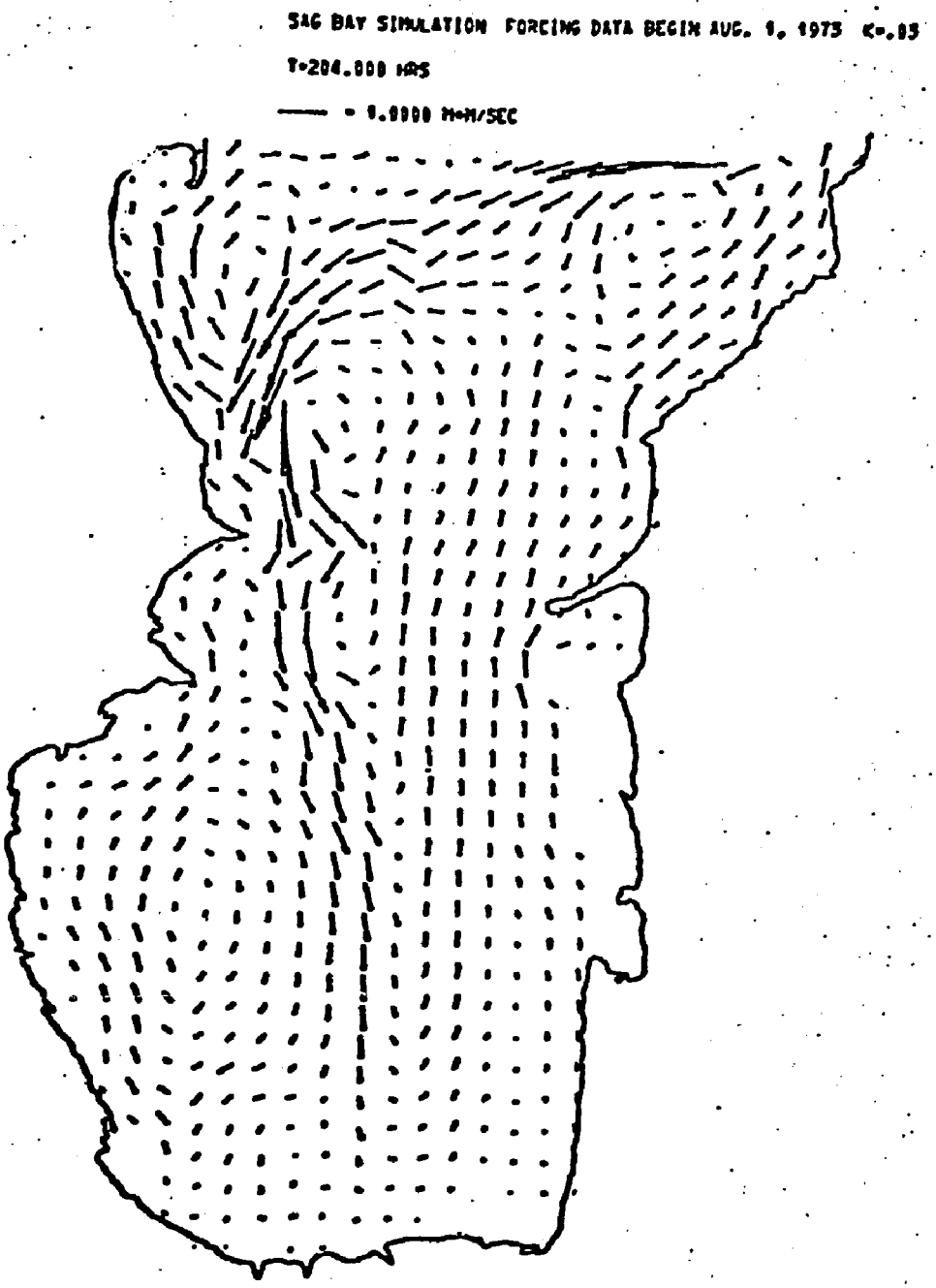


Figure 26. Circulation from realistic simulation, 204 hr after starting from rest (compare Fig. 28).

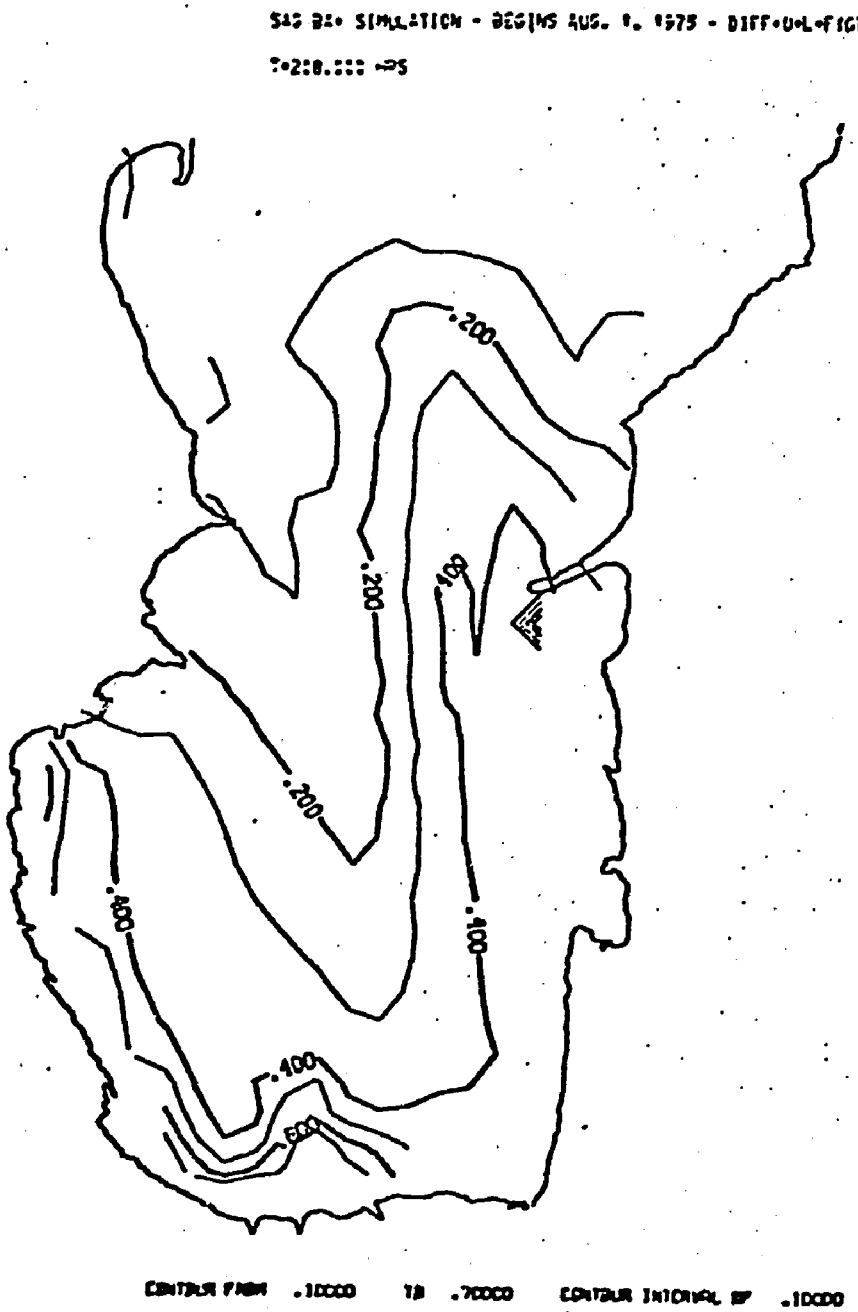


Figure 27. Chlorinity contours from realistic simulation, 208 hr after starting from rest (Compare Fig. 29).

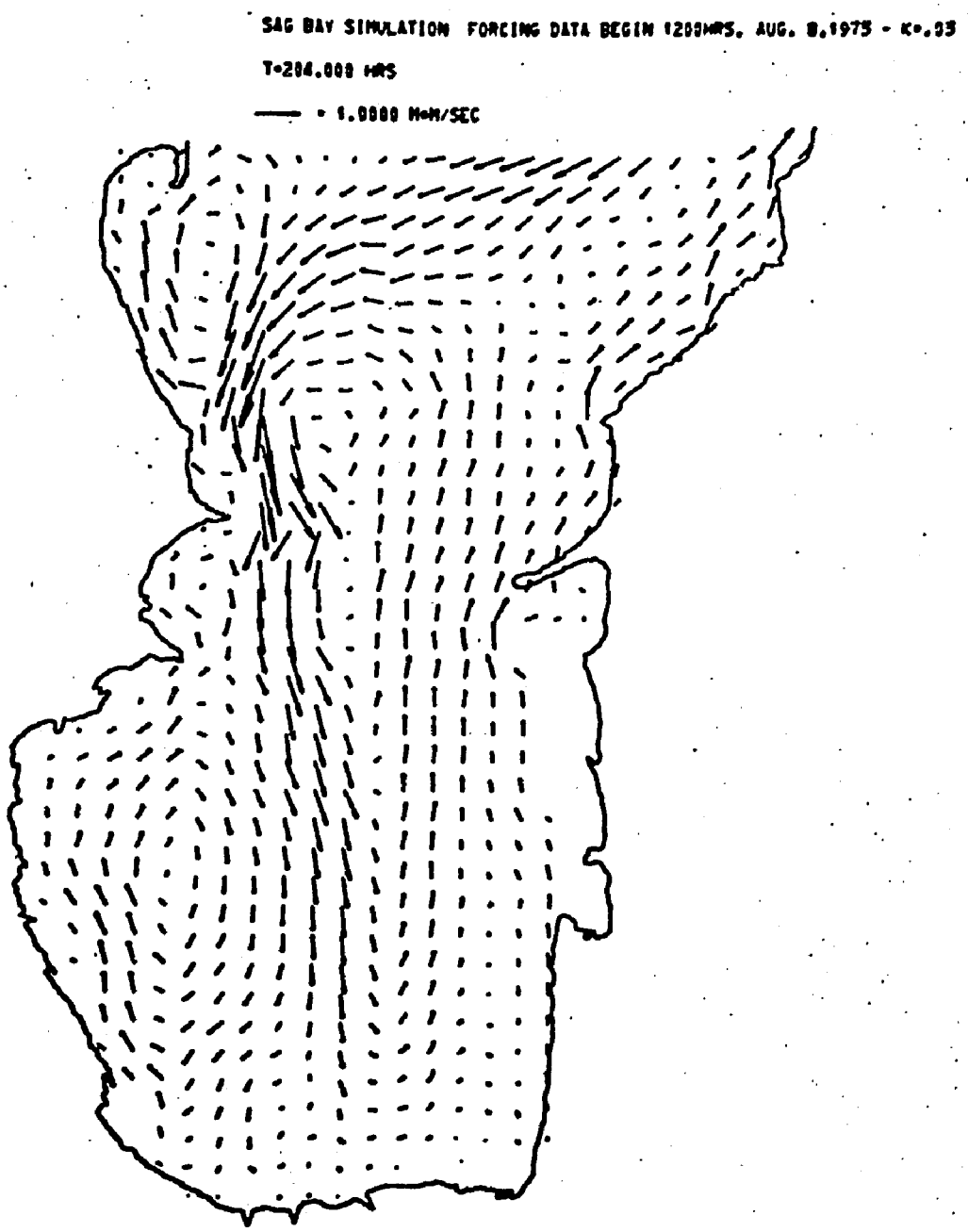


Figure 28. Circulation from realistic simulation, 24 hr after starting from rest with the 180th hr of forcing data. Different initial condition obliterated in less than 24 hr(compare Fig. 26).

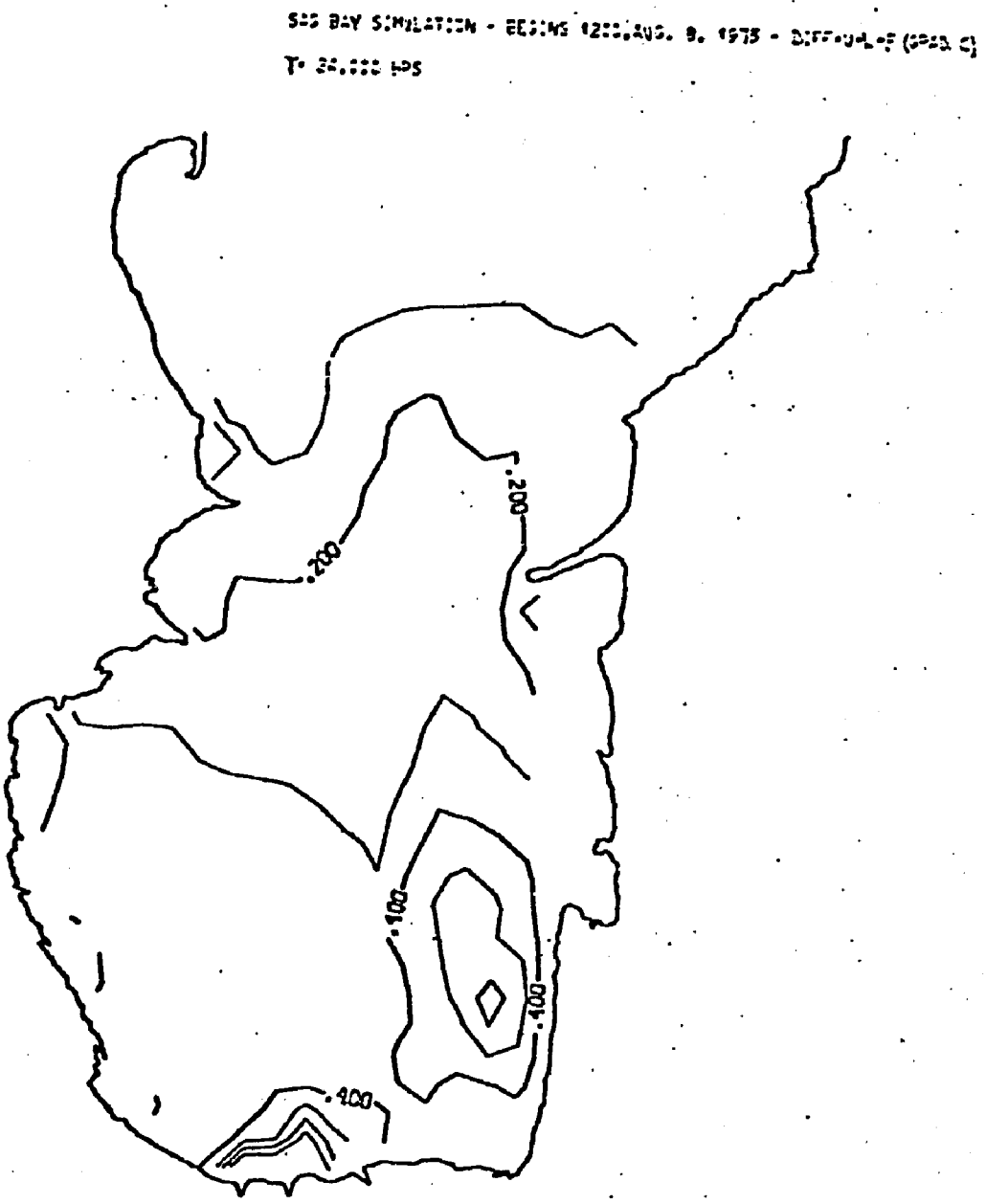


Figure 29. Chlorinity contours from realistic simulation, 24 hr after starting from rest with initial matter distribution at 180th hr of forcing data. Effects of initial conditions are retained (compare Figure 27.)

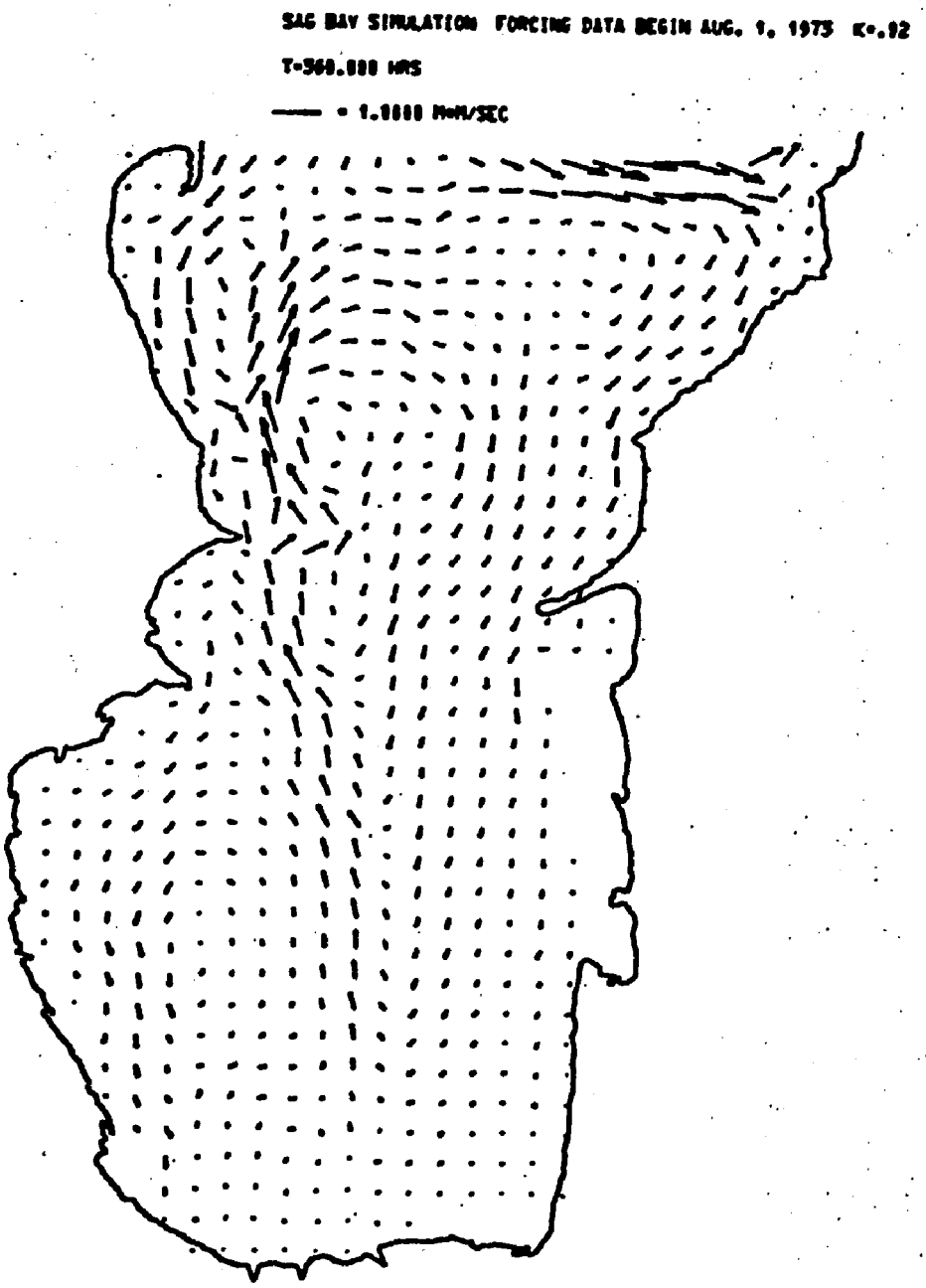


Figure 30. Circulation from realistic simulation after 300 hr. (compare Fig. 32).



Figure 31. Chlorinity contours from realistic simulation after 300 hr (compare Fig. 33).

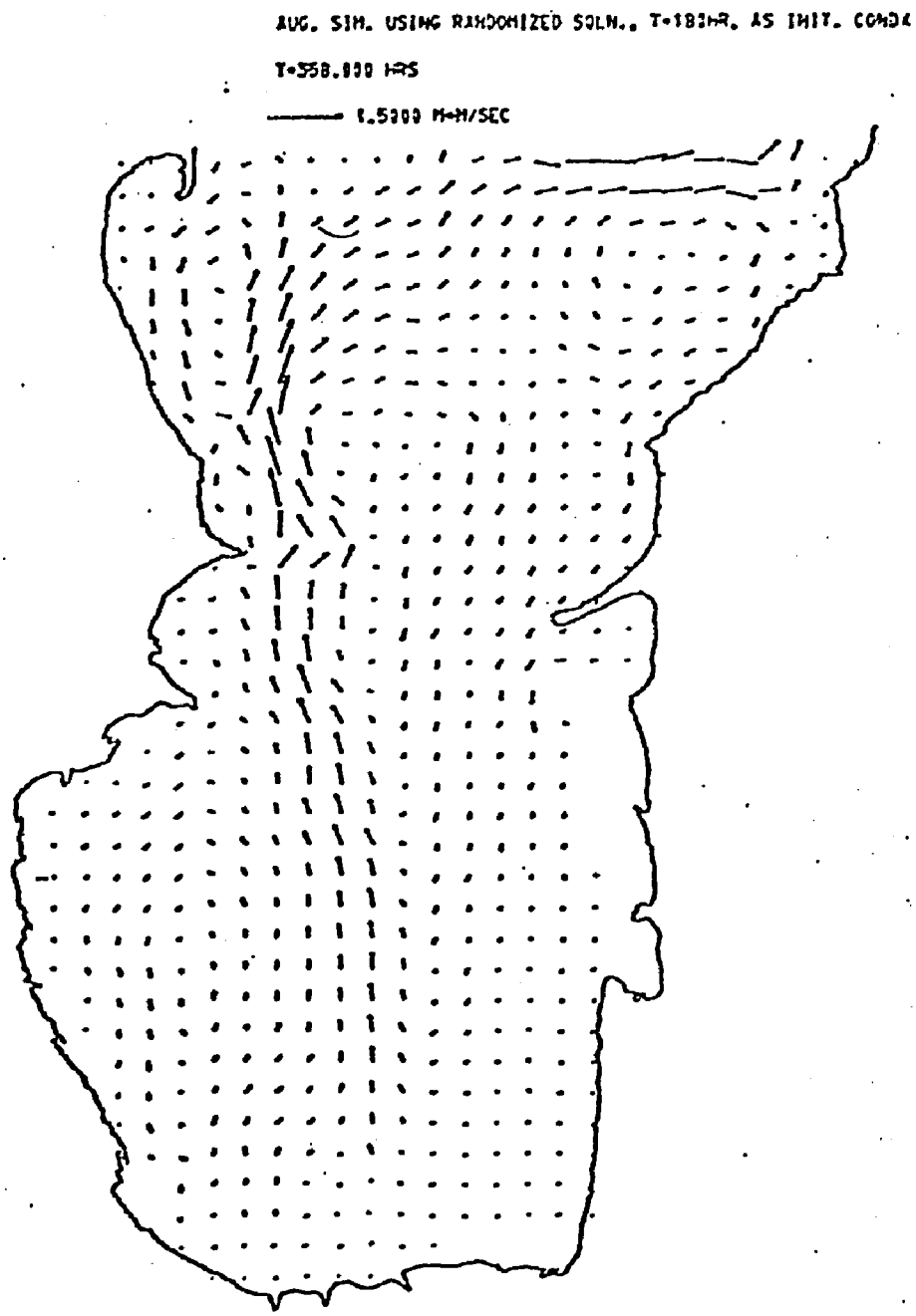


Figure 32. Circulation from realistic simulation after 300 hr, starting with randomized initial conditions at 180 hr. Results did not tend toward different solution than shown in Fig. 30.



Figure 33. Chlorinity contours from realistic simulation after 360 hr, starting with randomized initial conditions at 180 hr. Results did not tend toward different solution than that shown in Fig. 31.

E. Effects of diffusion coefficients

The sensitivity of the concentration solution to the magnitude of the diffusion coefficients was studied carefully. Figure 34 shows the results of a simulation out to 96 hr using constant diffusion $D_x = D_y = 10^4 cm^2/sec$. The solution obviously suffered a catastrophic degradation. Careful comparison with the contemporary flow fields showed that wherever there was an anomalously high concentration, one of two conditions existed: 1) there was a sharp concentration gradient near a boundary in the upstream direction from the local flow pattern; 2) there was approximately a 180° reversal in flow direction across the point of interest. Further, careful study of the computer output showed that the concentration solution exhibited "wiggles" upstream from nearly any point where either of the above conditions is met. The occurrence of numerical "wiggles" is by no means an unknown phenomenon, but such numerical artifacts not germane to the problem must be controlled.

Essentially, a given matter distribution coupled with transport direction can result in an "upstream discontinuity". The Fourier decomposition of this jump has short wave components which cannot be resolved by the grid network. They become aggregated into waves with only a few computational points per wavelength, resulting in a slowly propagating disturbance which underestimates the



Figure 34. Chlorinity contours from steady forcing, diffusion coefficients = 10^4 cm^2/sec. Catastrophic effects of behavioral errors shown by existence of areas of anomalously high concentration.

effects of diffusion. This effect has been noted and discussed by Leendertse (1970) regarding the introduction of source points within the computational field. Wiggles have also been analyzed by Roache (1972) in regards to differencing methods at outflow boundaries. In this research the reversals of the flow direction across a given point are a necessary consequence of the finite difference method. Such reversals give rise to a third way in which "wiggles" can arise.

Spatial oscillations in the solutions can be studied in a semi-quantitative manner by considering the advection-diffusion equation in one dimension:

$$\frac{\partial Hc}{\partial t} + \frac{\partial}{\partial x}(cu) - \frac{\partial}{\partial x}(HD_x\frac{\partial c}{\partial x}) = 0 \qquad (5.1)$$

Over the long term it is likely that $\partial c/\partial t \simeq 0$ at least in some region of the domain during some time interval. Further, suppose H and D_x are constants since a localization of the problem is being considered, then (5.1) becomes

$$\frac{\partial}{\partial x}(cu) - HD_x\frac{\partial^2 c}{\partial x^2} = 0 \qquad (5.2)$$

The following spatial differencing for (5.2) is chosen:

$$1/2\Delta x\ [u_{j+1/2}(c_{j+1} + c_j) - u_{j-1/2}(c_j + c_{j-1})] \qquad (5.3)$$

$$- HD_x/\Delta x^2[c_{j+1} - 2c_j + c_{j-1}] = 0$$

(The same results are obtained if simple centered-differencing is used on a network in which u and c are defined at

all grid points.) There are two cases to consider.

First, suppose that the flow opposes itself at adjacent grid points; then $u_{j+1/2} = -Ku_{j-1/2}$, where K is a positive constant. Define $C_{j+1}/C_{j-1} = A_{j+1}$ and $C_j/C_{j-1} = A_j$. Then (5.3) can be written

$$(2/R_c - 1)A_{j+1} = (K - 2/R_c) + 4A_j/R_c + (1 + K)A_j \qquad (5.4)$$

where $R_c = u\Delta x/HD_x$ is a non-dimensional parameter completely analagous to the cell Reynolds' number discussed by Roache (1972). In this work the parameter R_c compares the inertial effects (based on the lattice spacing) to the diffusive effects. If $R_c<2$, no difficulties occur since A_{j+1} simply increases to compensate for the increase in A_j. If $R_c>2$ the quantity multiplying A_{j+1} is negative and A_{j+1} must be negative to satisfy the finite difference equation. The second derivative at the next point is somewhat reduced and a wiggle pattern feeds forward. (The direction of propagation of the distrubance appears to depend on the direction of sweep through the computational network.) The problem becomes singular if $R_c=2$ in the sense that the difference equation violates the monotonicity and boundedness properties of the continuum equation if $R_c>2$.

For the second case suppose that the flow is given locally by $u_{j+1/2} = Ku_{j-1/2}$, $K>0$. Then (5.3) can be written

$$(2/R_c - 1)A_{j+1} = (4/R_c + 1 - K)A_j - (2/R_c + K) \qquad (5.5)$$

As stated in the previous paragraph, $R_c<2$ causes no difficulty. If $R_c>2$ substitution of reasonable values for A_j and K into (5.5) indicates that A_{j+1} may or may not be required to assume negative values. Thus, there are solutions which admit to wiggles and solutions which exhibit reasonable numerical behavior. This case explains how introduction of source functions within the computational field can lead to wiggles as noted by Leendertse (1970).

In this work diffusion coefficients were represented as D = UL/H (Chapter III, section D). Thus

$$R_c = U^{n+1/2}\Delta x/[H(U^n/H)L] \leq 2$$

implies that $\Delta X \leq 2L$ (since $U^{n+1/2} \approx U^n$) or a wiggle pattern is practically unavoidable.

The spurious occurrence of these numerical wiggles was suppressed completely when the eddy diffusion coefficients were elevated to $5(10^5)cm^2/sec$, as is depicted in Figure 35. Note that the product of the Kolmogoroff length scale based upon twice the grid spacing (Chapter III) and a fluid speed of 10 cm/sec is approximately $5(10^5)cm^2/sec$. As was shown above this diffusion value is just sufficient to quell disturbances which arise from the network's inability to resolve phenomena having spatial scales less than twice the lattice spacing.

Alternate methods exist which suppress such numerical wiggles, besides blatant and widespread increase

of diffusive properties. For example, the saving features of upwind differencing have been used by meteorologists for many years. In fact behavioral errors represented by wiggles in the solution which arise near outflow boundaries can be remedied by upwind differencing or by use of the gradient boundary condition $\partial c/\partial x = 0$ (Roache, 1972). However, in the problem at hand behavioral errors arose within the computational field, which made it impractical to switch to an upwind differencing technique. Therefore, artificial diffusion was introduced. In such a procedure by Lax and Wendroff (see Richtmeyer and Morton (1962)) the artificial term is chosen so that additional diffusion is obtained only when adjacent concentrations are widely different. In particular the diffusion coefficients become

$$D_{x\,j+1/2,k} = U_{j+1/2,k} L/H_{U\,j+1/2,k} \left[1 + \frac{(c_{j+1,k}-c_{j,k})^2}{(c_{j+1,k}+c_{j,k})^2} k_d\right]$$

and similarly for $D_{y_{j,k+1/2}}$, where k_d is a constant established through numerical experiment. Representative improvements are shown in Figure 36, which may be compared with Figures 34 and 35.

F. Long term simulations

The necessary procedures to produce a realistic, long-term simulation have been presented. The results of runs extending over periods of the order of one month can now be discussed. Figures 37 through 50 pertain to a simulation beginning 1 August 1973, using all of the

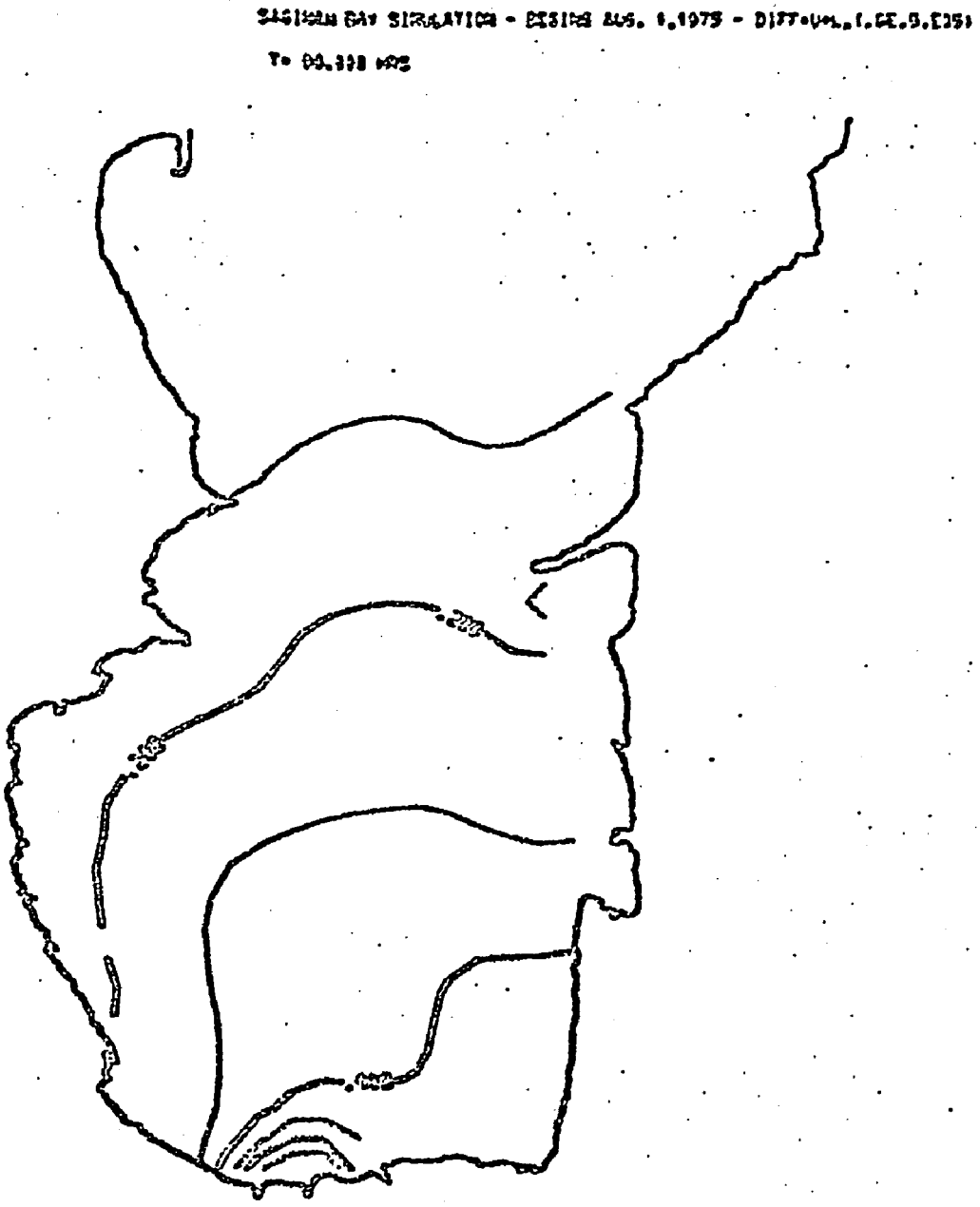


Figure 35. Chlorinity contours from realistic simulation, diffusion coefficients = $5(10^2)$ cm^2/sec. Behavioral errors are non-existent (compare Figure 34) but system is overly diffusive.

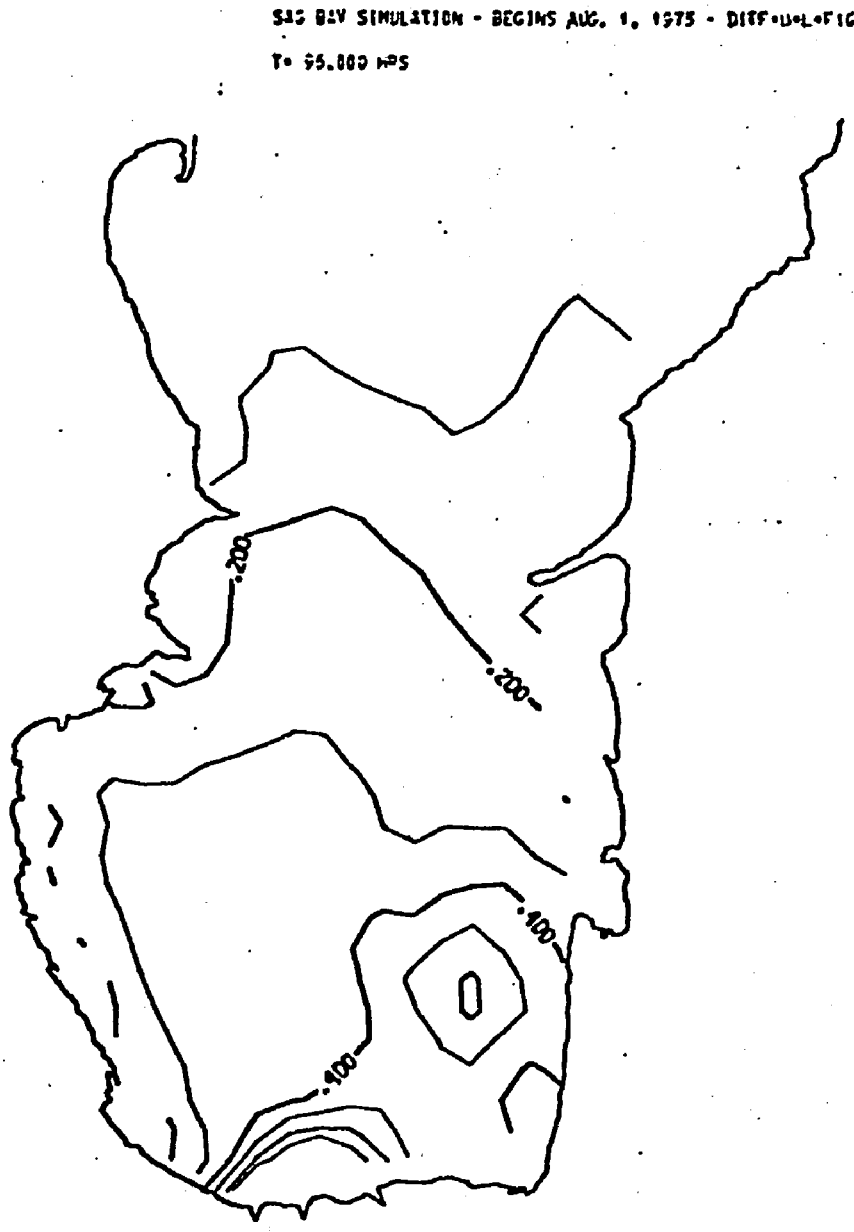


Figure 36. Chlorinity contours from realistic simulation. Artificial diffusion increases diffusion coefficients only where gradients of concentration are large (compare Figures 34-35).

techniques outlined in the previous chapters, and indeed those in the preceeding paragraphs. Many interesting things about Sgainaw Bay, and perhaps certain other shallow water estuaries can be learned from these results. It is evident that radically different circulation patterns can supplant one another in relatively short periods of time, viz., 8 hr or less. The chlorinity distribution evolves on a much longer time scale, but may be sensibly related to the wind conditions of the previous 24 hr. Figures 51 and 52 represent the wind conditions prior to and contemporary with a particularly interesting occurrence in the bay. This occurrence, shown in Figure 40 is a spectacular release from a transverse "set-up", produced by a strong northwesterly wind of several hours duration, as seen in the wind graphs. This would appear to elucidate a significant mechanism for coastal inundation other than direct run-up on the downwind shore. Some features of the observed circulation have been more or less confirmed by previous observational work. The connecting channel between the inner and outer bays serves as a release valve to effect conservation of mass when large amounts of water leave or enter the bay. There is seldom much activity lakeward of the northwest corner of the bay, where, unfortunately, a water intake now exists. The general gyral motion of the bay has been partially inferred by Beeton et. al. (1967), and recent measurements by NOAA confirm the role of the connecting

channel. As seen in all of these latter figures, the magnitudes of the transport are far greater than those caused by steady winds (Figures 17-20). Formulation of the wind stress according to a square law means that significant energy is pumped into the system through peaks in the external forcing having surreptitiously short duration. Measurements of current speed(NOAA) suggest this is correct. The chlorinity distribution responds to the predominantly southwesterly winds by moving lakeward along the southern shore, although the contour lines obviously reflect significant influxes of matter through the connecting channel as has been described above. The transport fields can be arithmetically averaged in time to give mean transport data appropriate for specific periods of time. Figures 53 and 54 are average transport plots over two-week intervals. The day to day winds for these intervals were quite different. The mean circulation of the bay did not change as much as was expected. The boundary current along the southern shore has been observed by investigators from Consumers Power Co. and from NOAA. The mean gyral pattern evident in the latter figures may account for the existence of the shoreline cusps known as Sand Point and Lookout Point (private communication, Erwin Seibel). The average transport fields are also currently being used by other investigators (Canale, 1975) to develop ecosystem models of the bay.

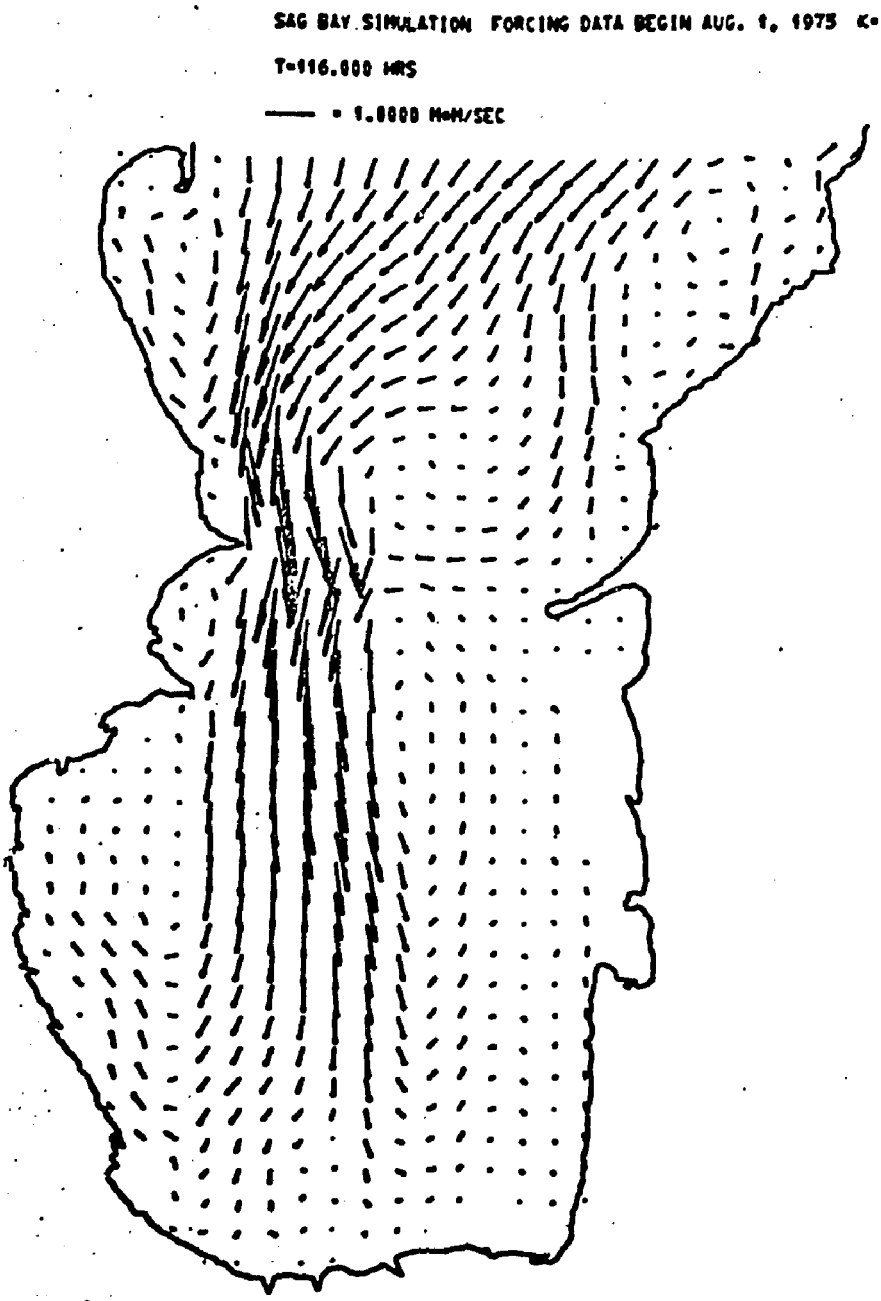


Figure 37. Circulation from realistic simulation. Predominant southwesterly wind produces pattern similar to that seen in Figure 17. Inner bay shows similarity to "Talweg" (compare Figure 2).

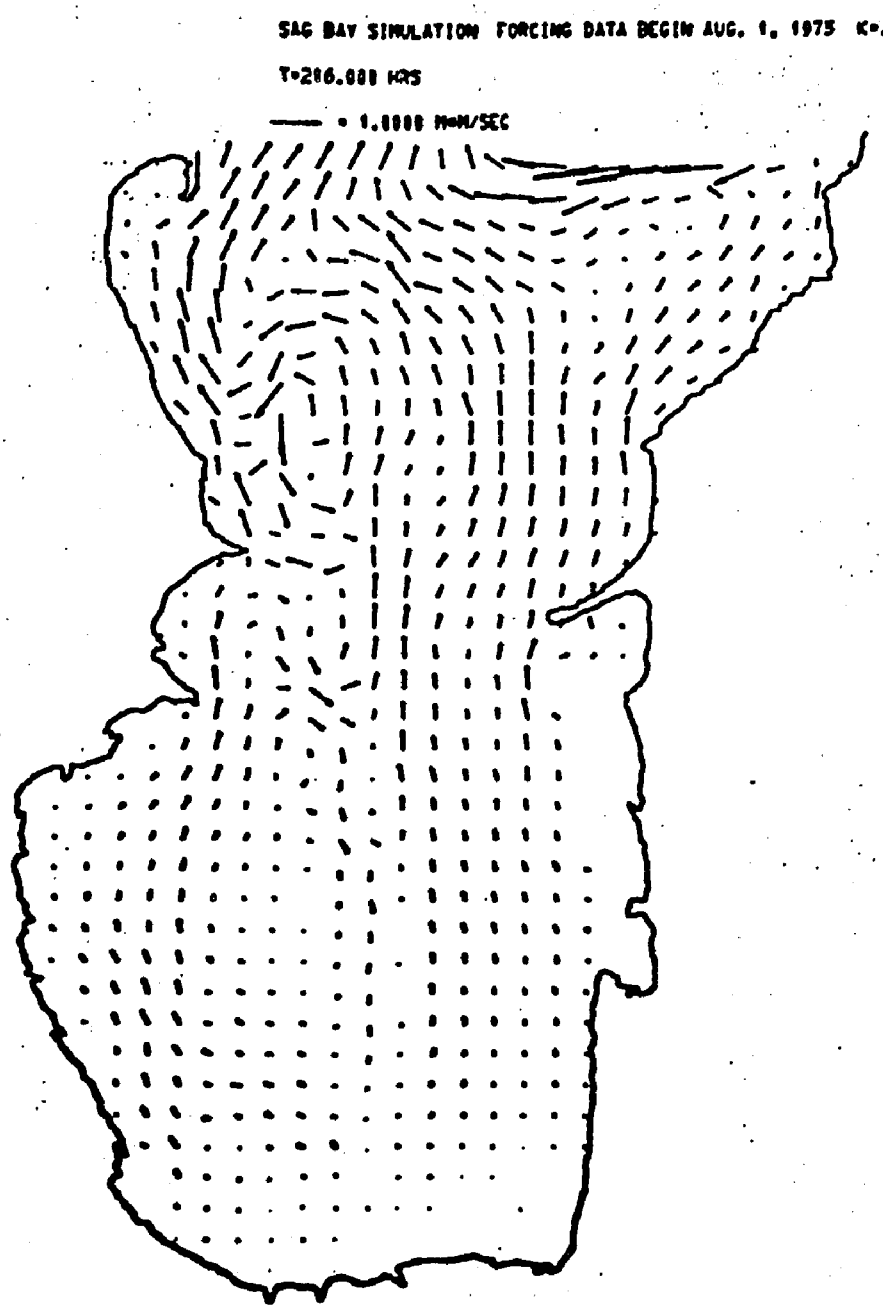


Figure 38.

Figure 38. Circulation from realistic simulation. Organized flow in channel region breaks down as wind direction changes.

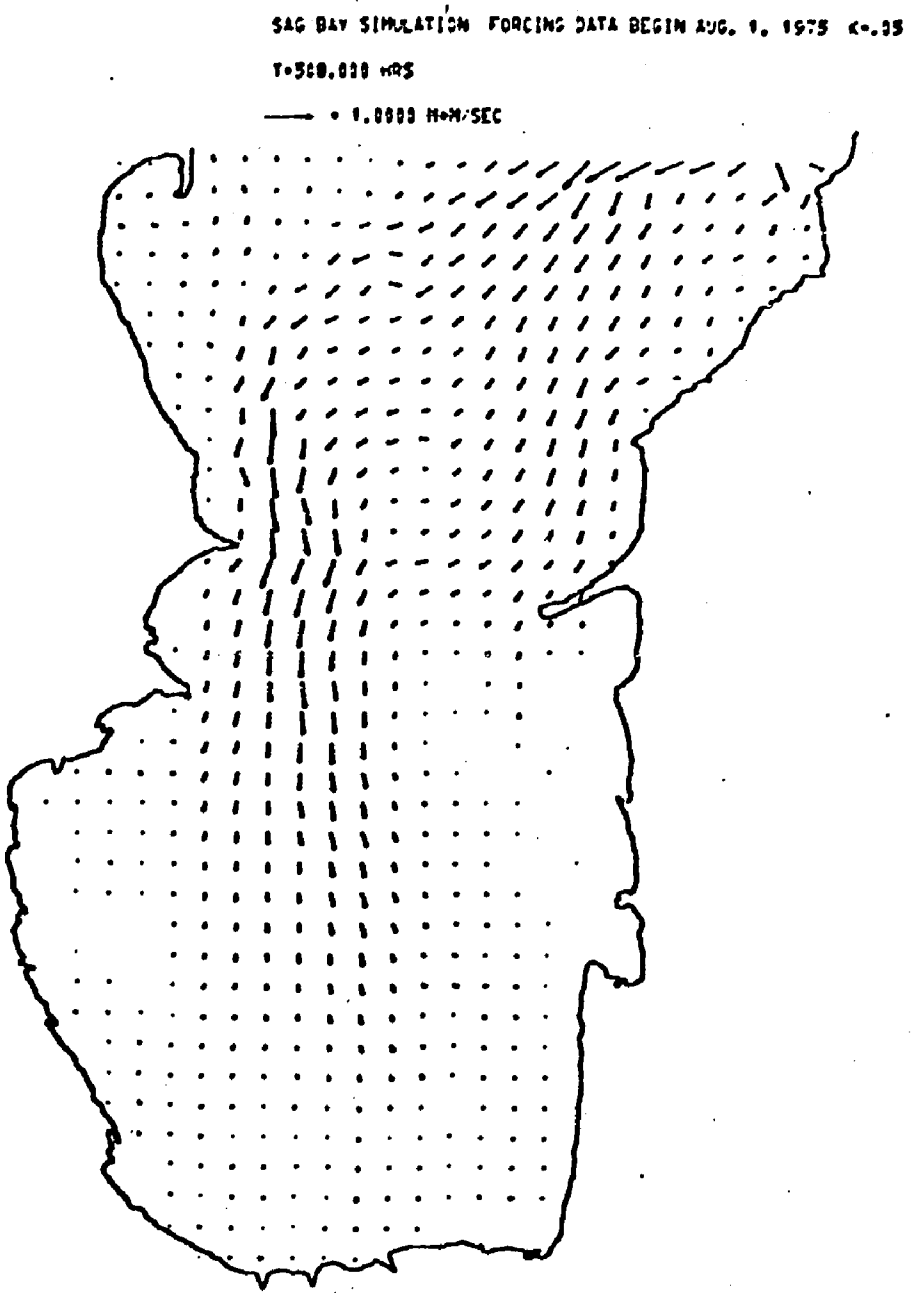


Figure 39. Circulation from realistic simulation. Magnitudes of transports become small after only a few hours when forcing is weak.

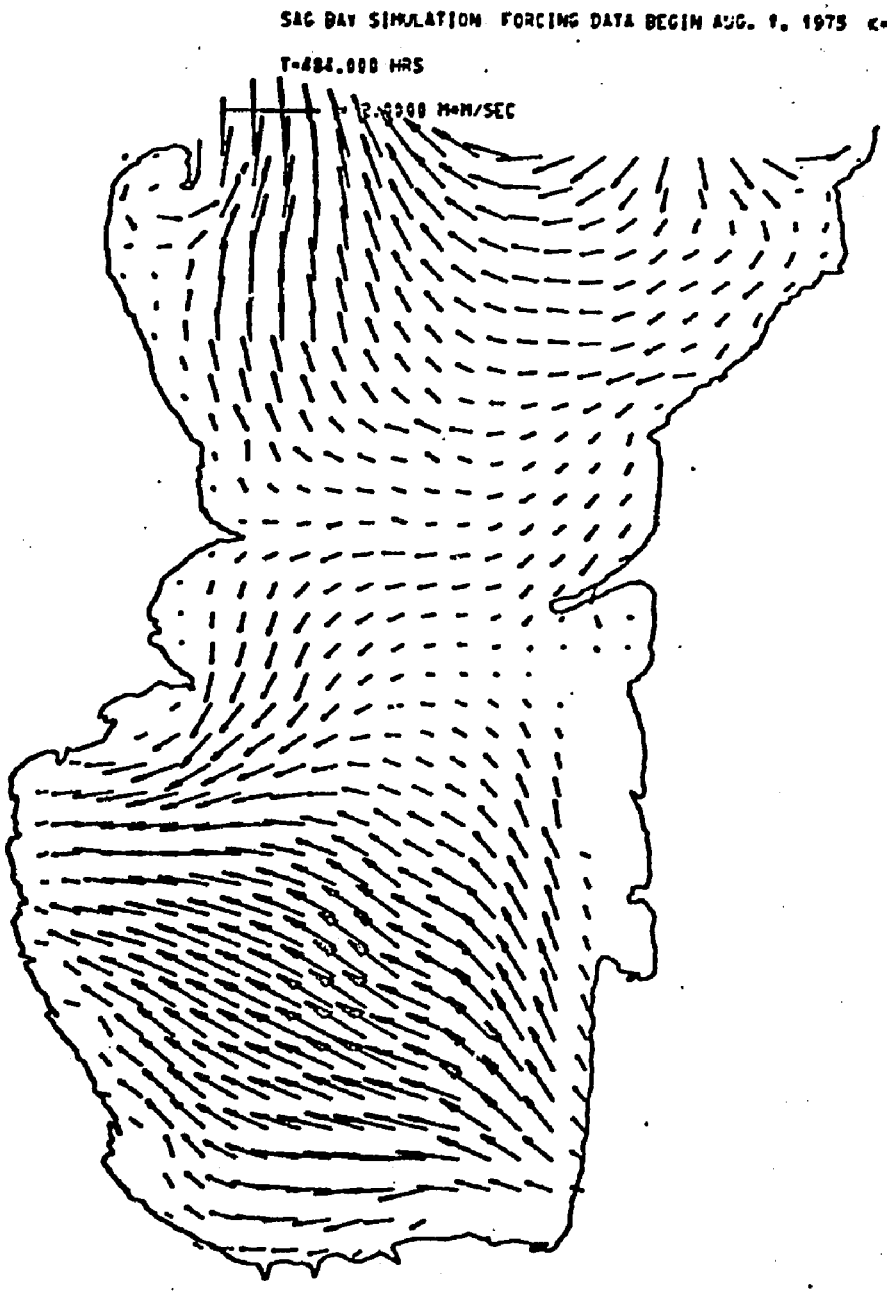


Figure 40. Circulation from realistic simulation. Release from transverse set-up is shown following abatement of strong northwesterly wind.

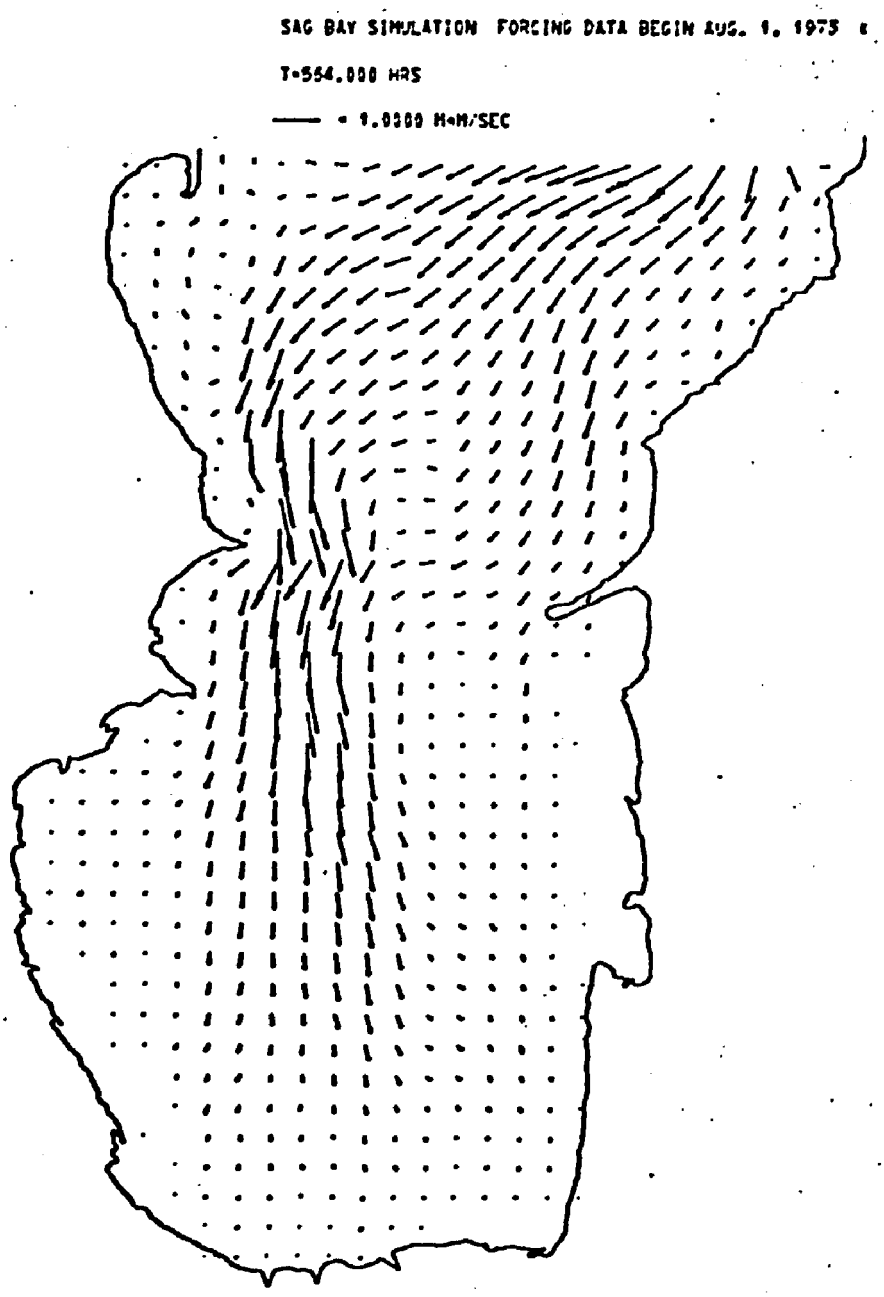


Figure 41. Circulation from realistic simulation. Flow in channel region is downwind (sout until significant inflow has occurred.



Figure 42. Circulation from realistic simulation. Pattern resulting from strong west-southwest winds starts to break down after wind subsides.

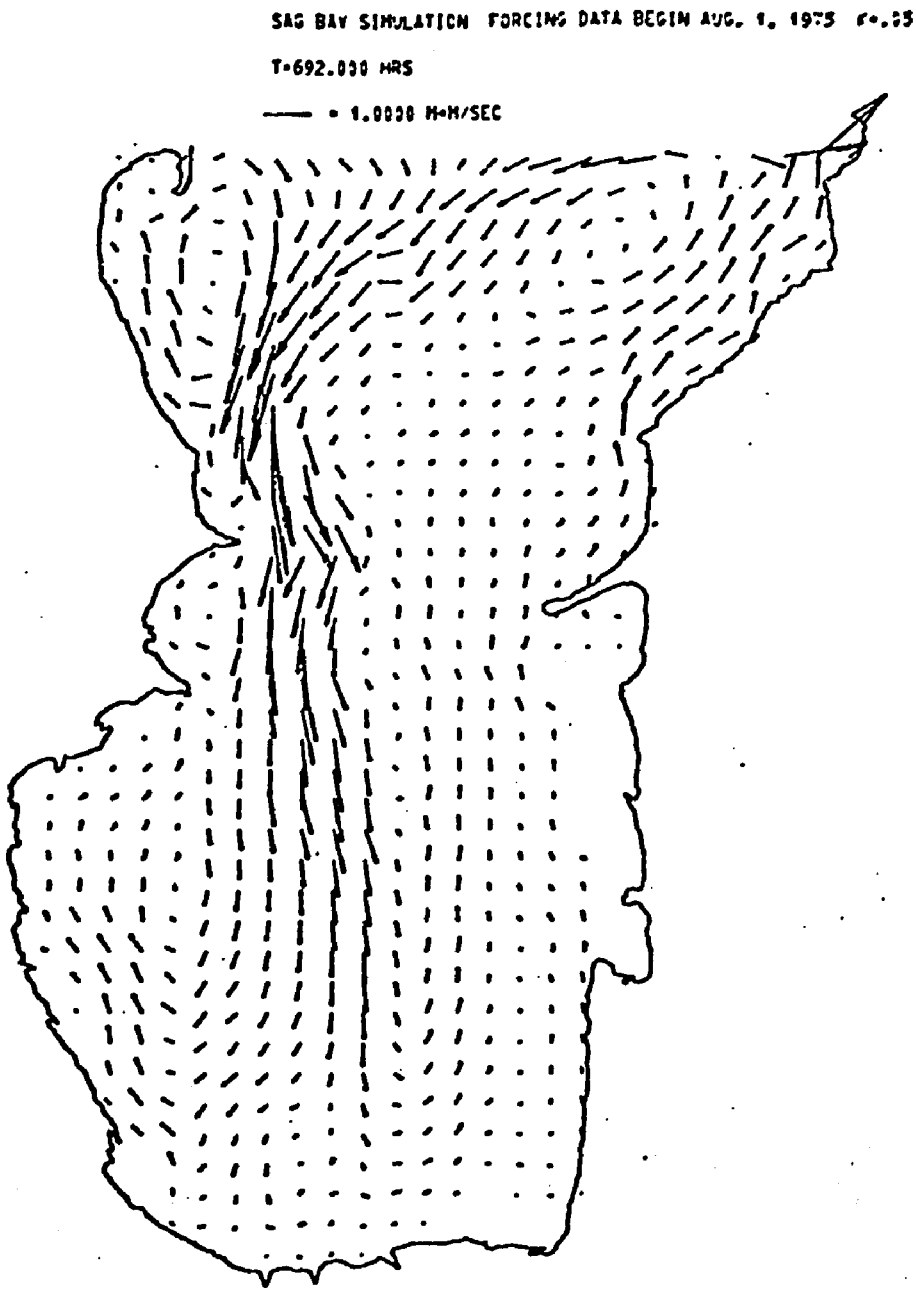


Figure 43. Circulation from realistic simulation. Flow regime typifies response to predominant southwest wind.

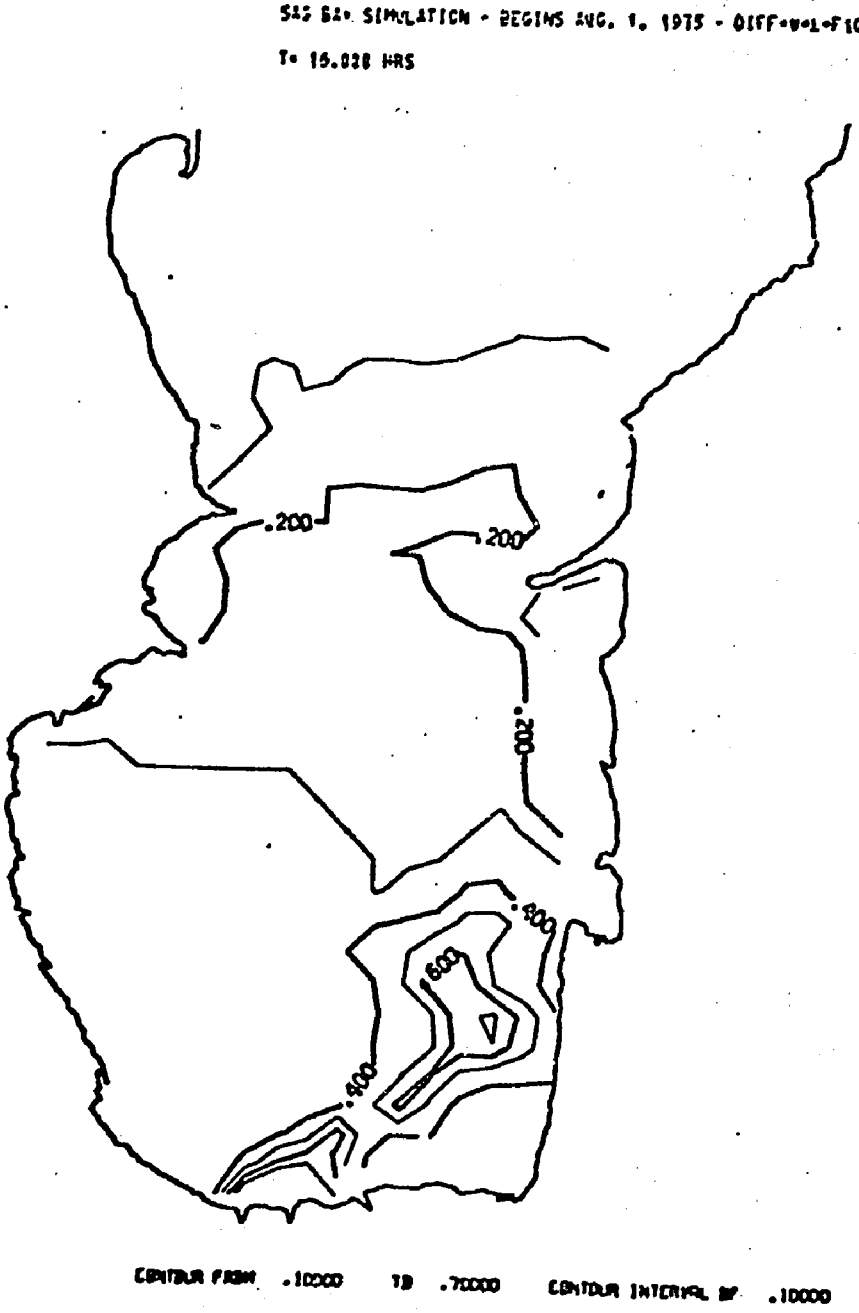


Figure 44. Chlorinity contours from realistic simulation. Pattern evolves on time scale an order of magnitude greater than flow. Distribution shown is essentially initial state.



Figure 45. Chlorinity contours from realistic simulation. Pattern changes slowly during times of weak forcing.

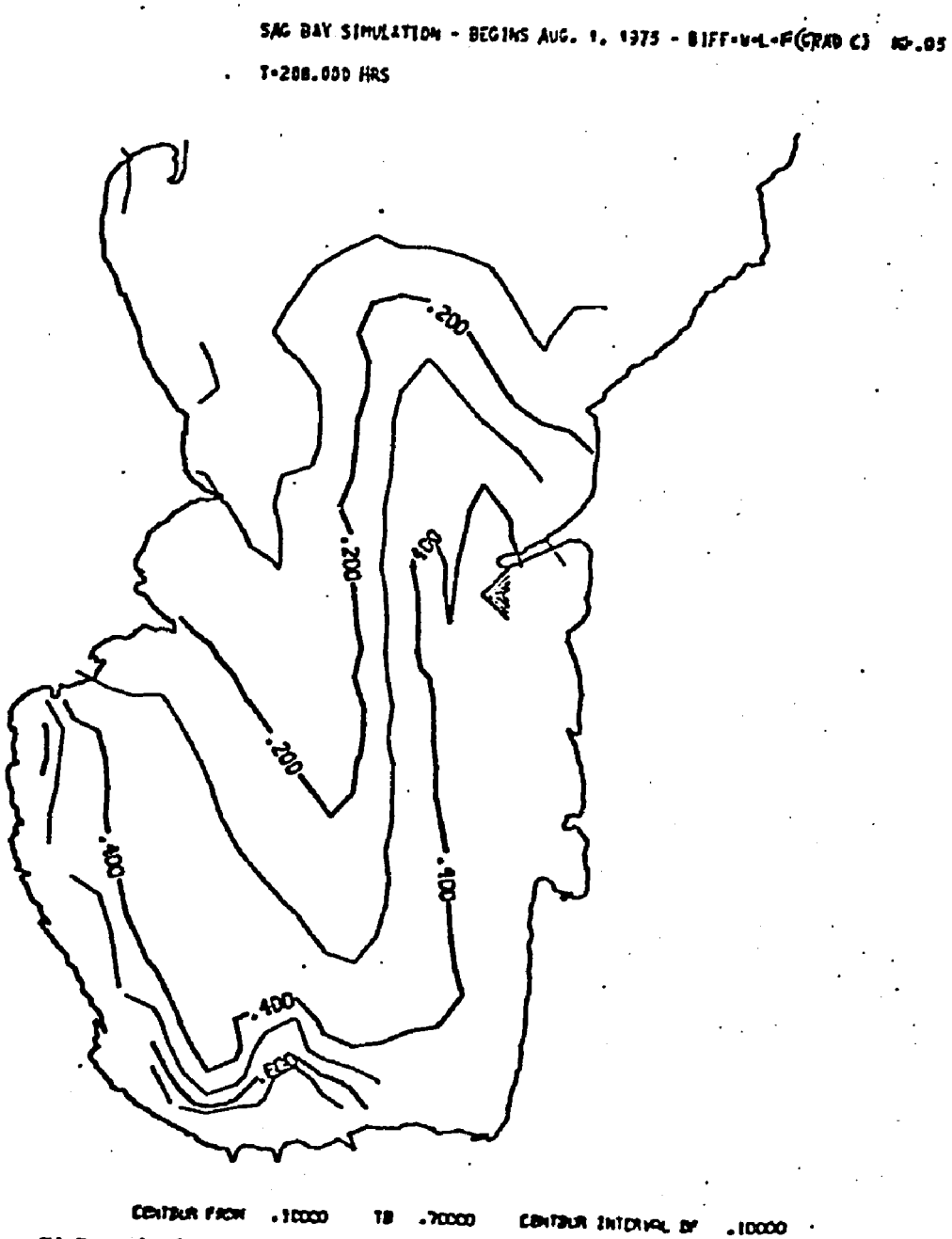


Figure 46. Chlorinity contours from realistic simulation. Distribution is seen to respond to advection induced by predominant flow pattern resulting from southwest wind.

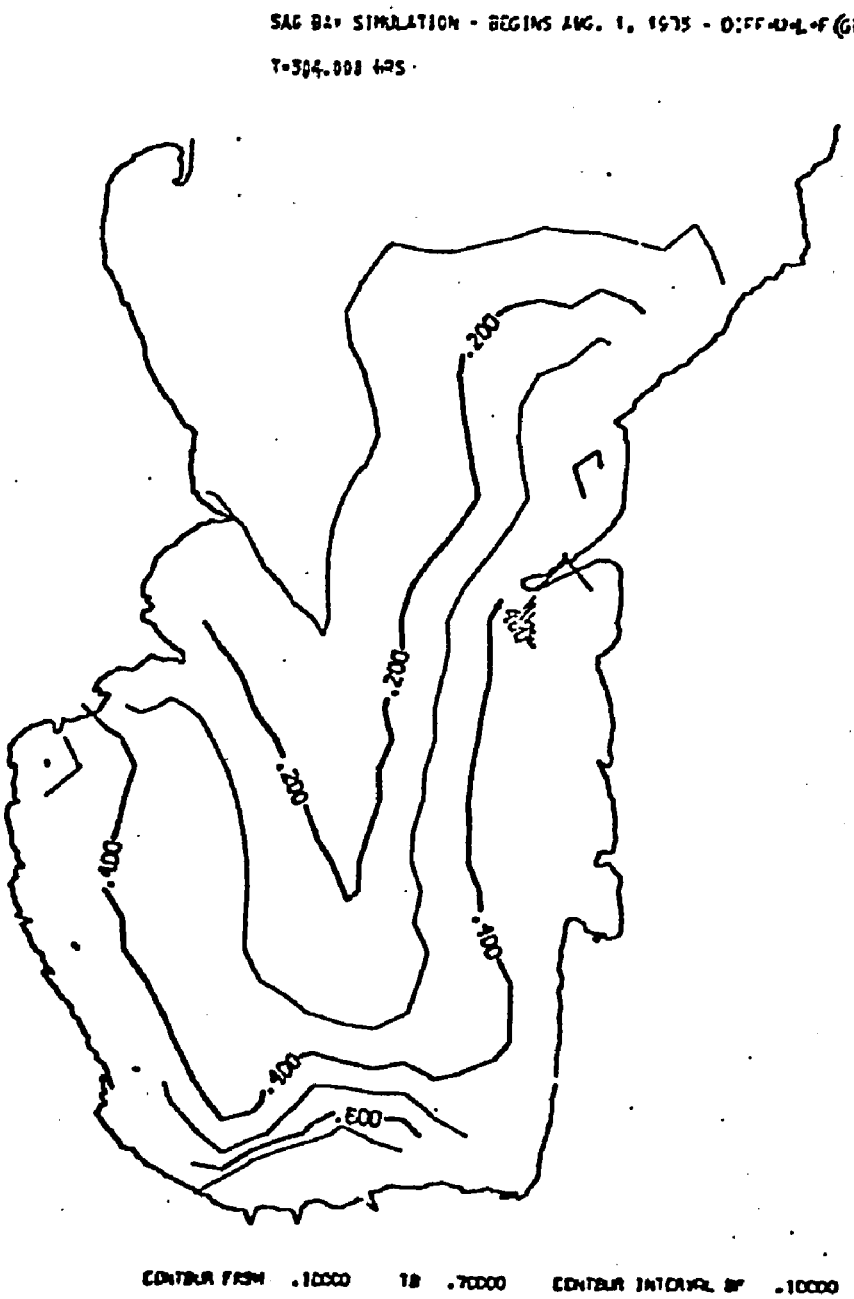


Figure 47. Chlorinity contours from realistic simulation. Activity is greater in outer bay than inner bay during periods when forcing is weak. Pattern is modified accordingly (compare Figure 46).

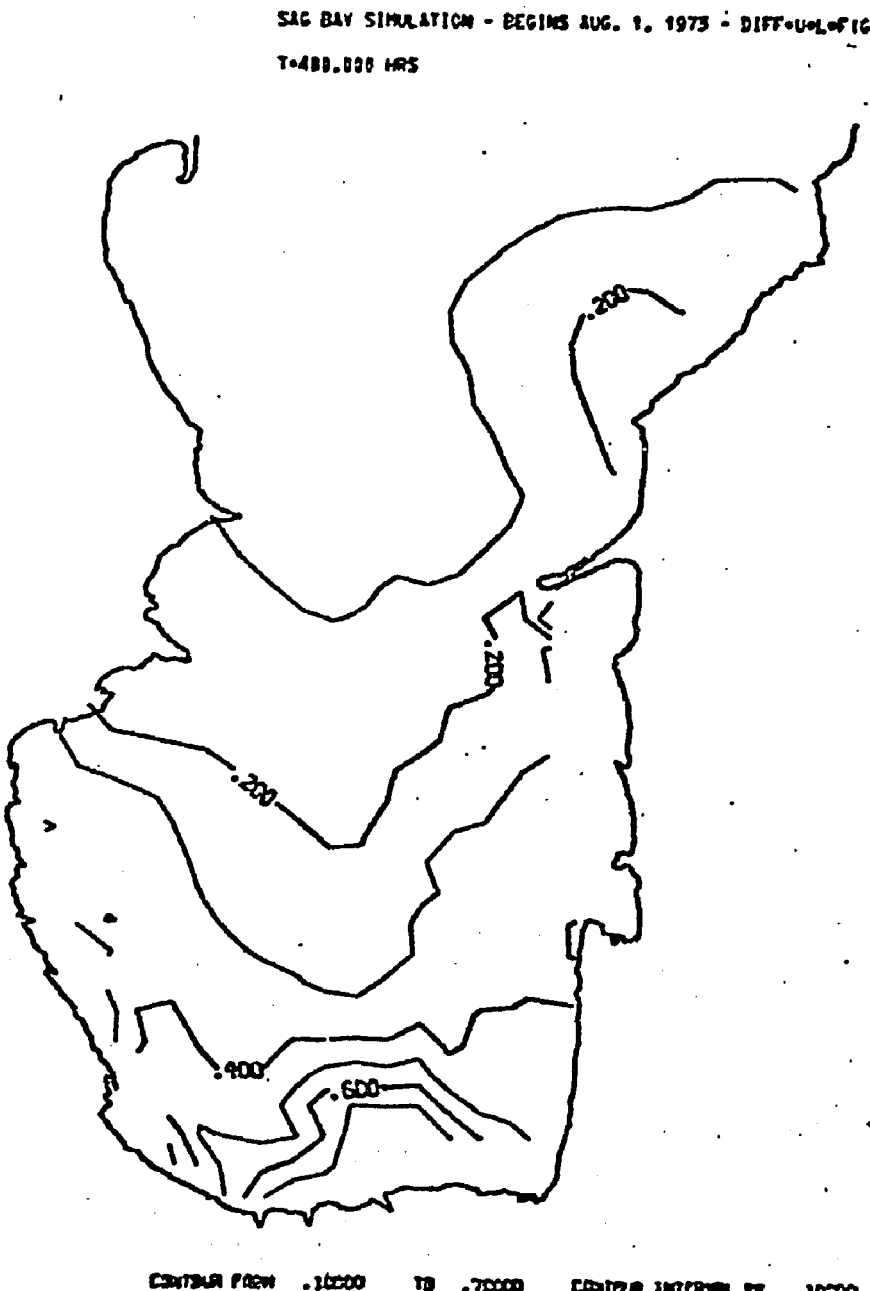


Figure 48. Chlorinity contours from realistic simulation. Time-dependent behavior is difficult to anticipate. Concentration in shoal regions changes significantly (compare Figure 46).

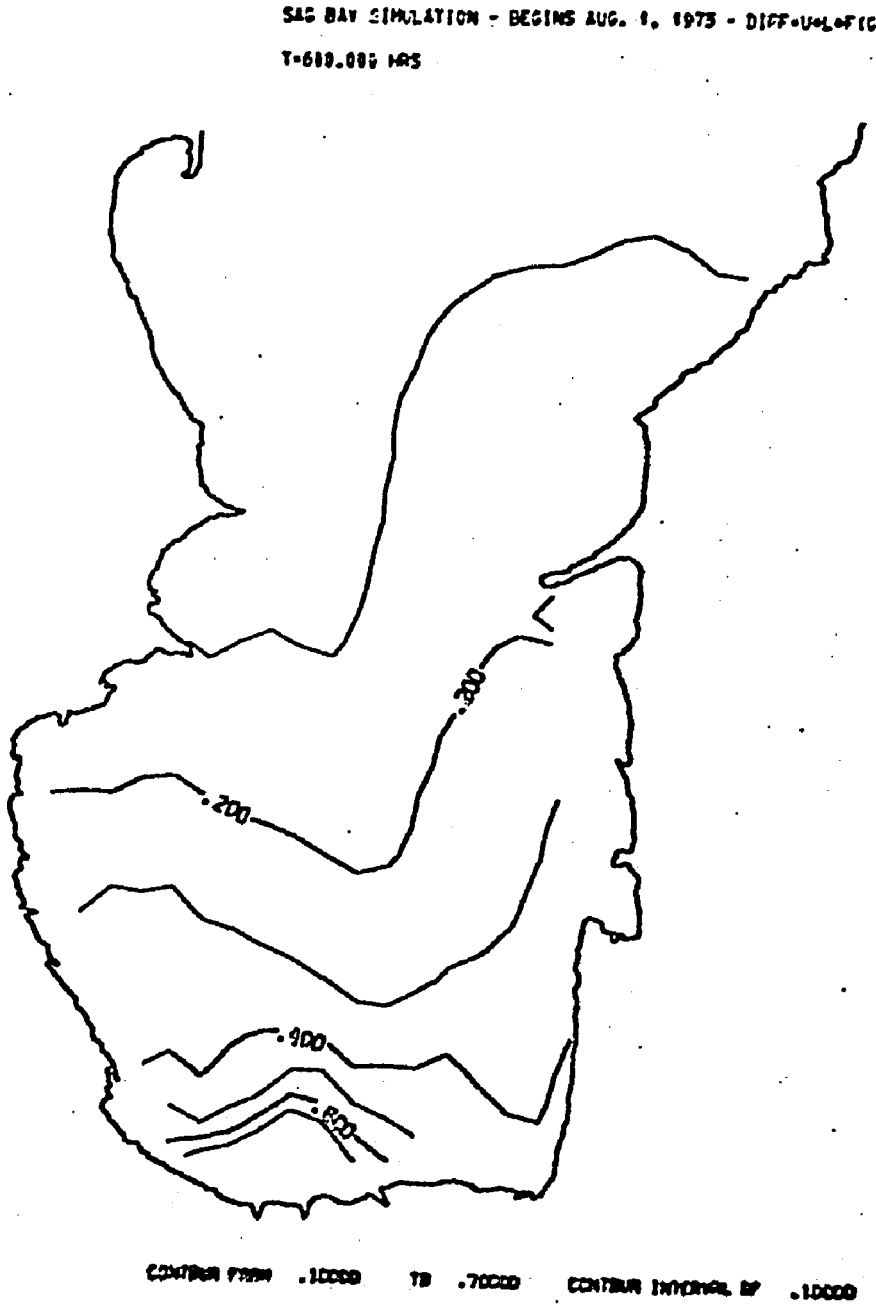


Figure 49. Chlorinity contours from realistic simulation. Bay freshens due to large influx of water under northwesterly wind.

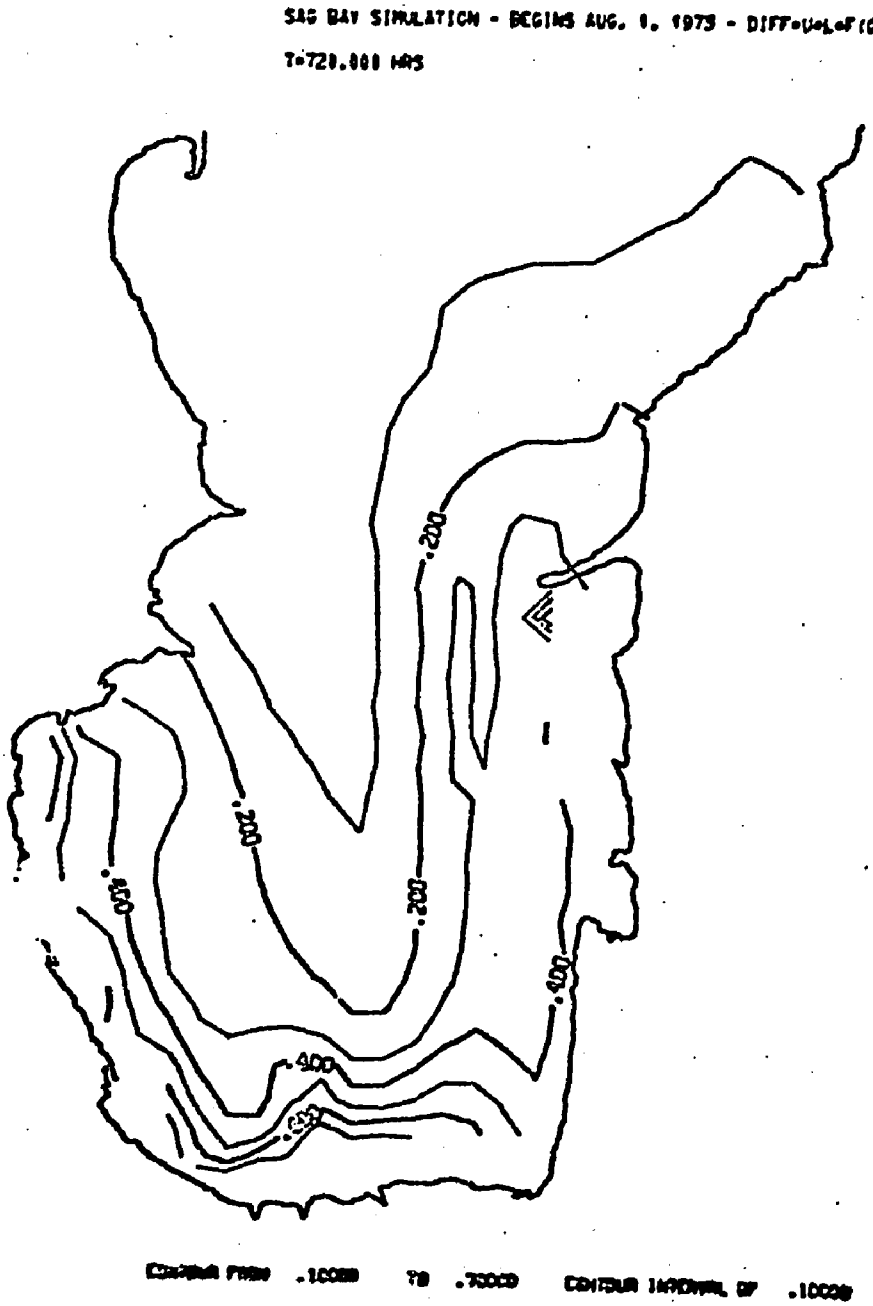


Figure 50. Chlorinity contours from realistic simulation. Strong southwest wind causes pattern to creep lakeward along the southern shore.

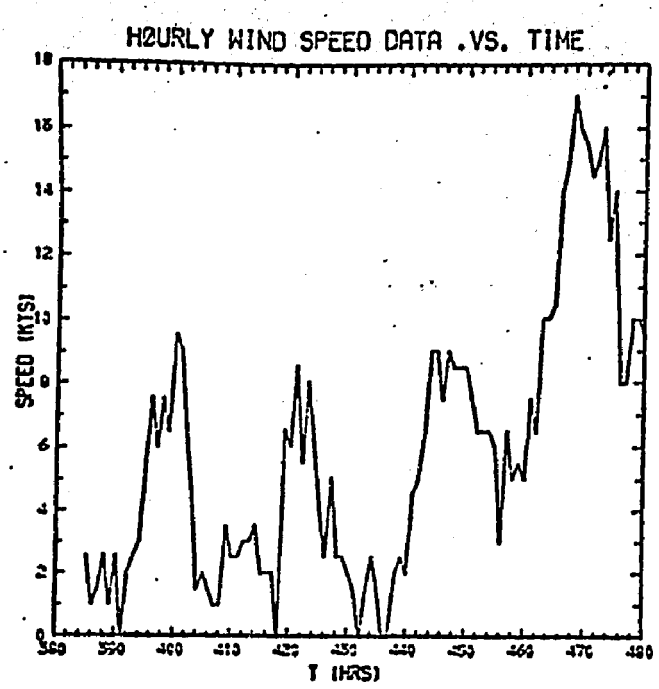


Figure 51. Representative wind speed data used as external forcing for model, beginning 1 August 1973. Strong northwesterly wind is shown which produced conditions for release from set-up seen in Figure 40.

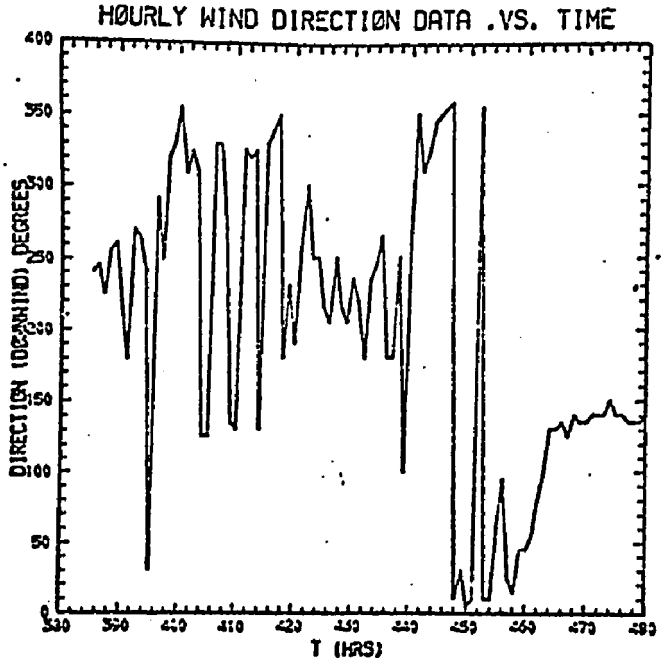


Figure 52. Representative wind direction data used as external forcing for model, beginning 1 August 1973.

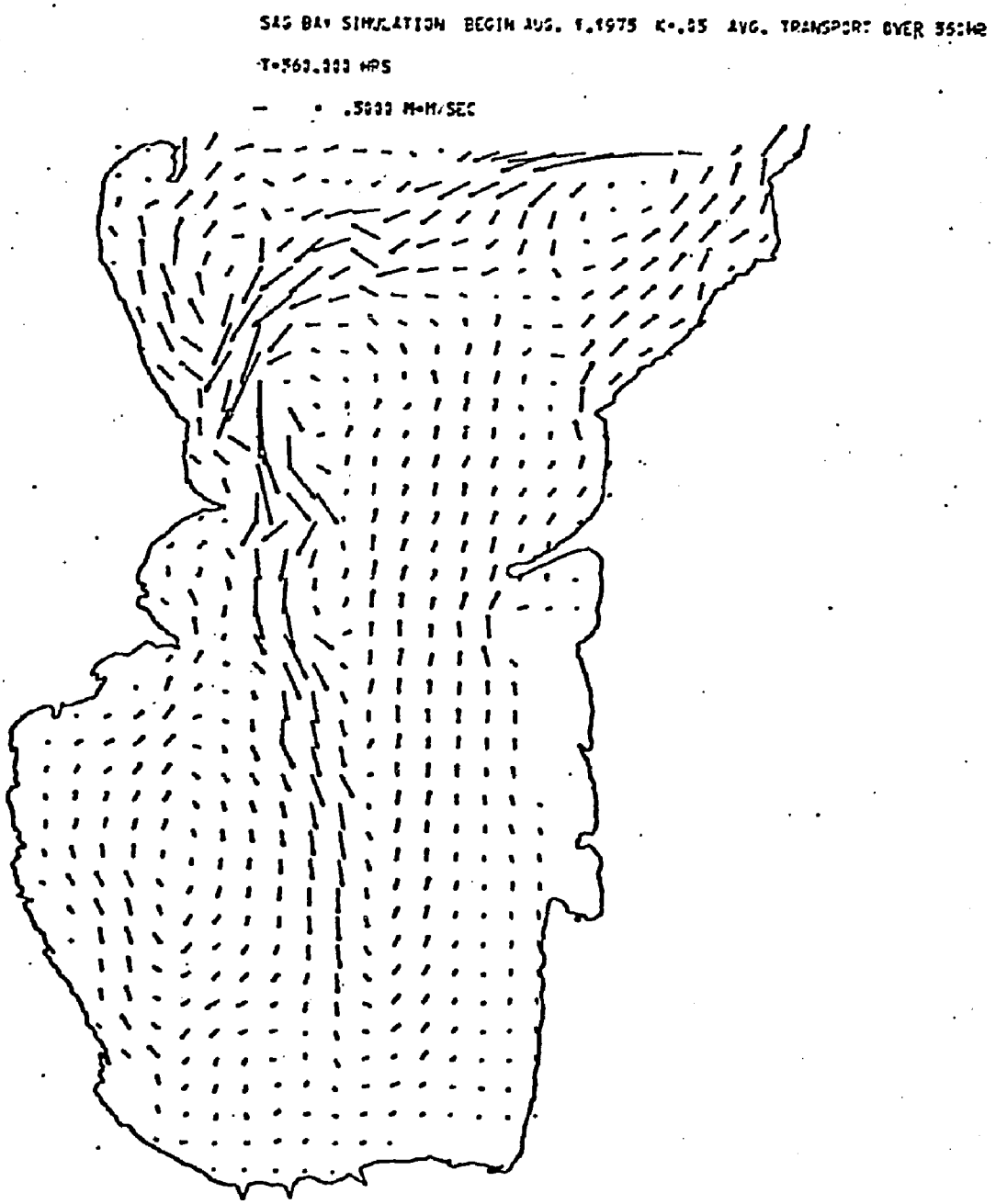


Figure 53. Average circulation over two week period from realistic simulation. Gyral patterns may have produced shoreline cusps.

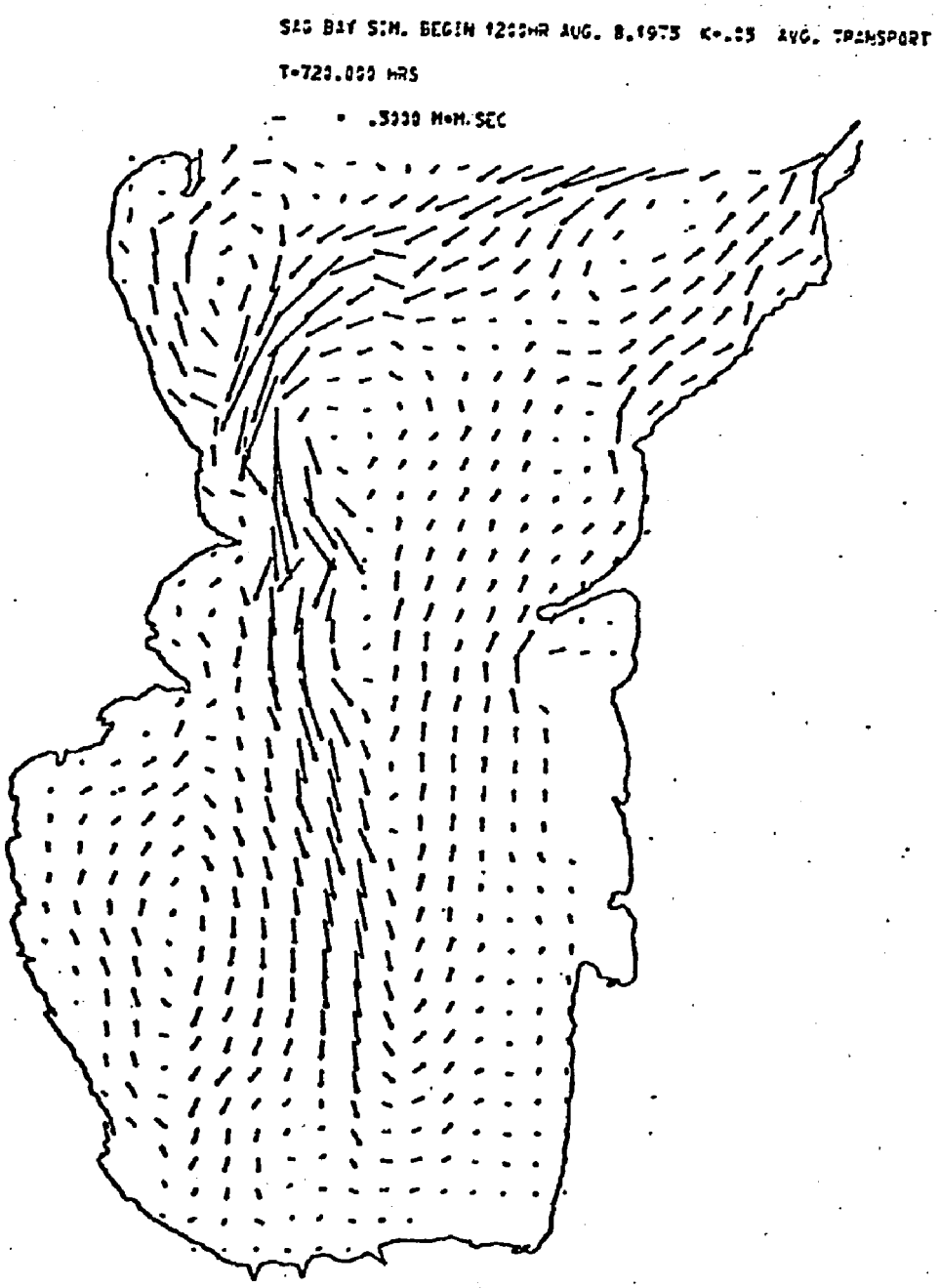


Figure 54. Average circulation over two week period from realistic simulation. Day to day wind quite different during this period than that represented by Figure 53, but patterns are similar. Figures 53-54 show similarities to Figure 17 (southwest wind forcing).

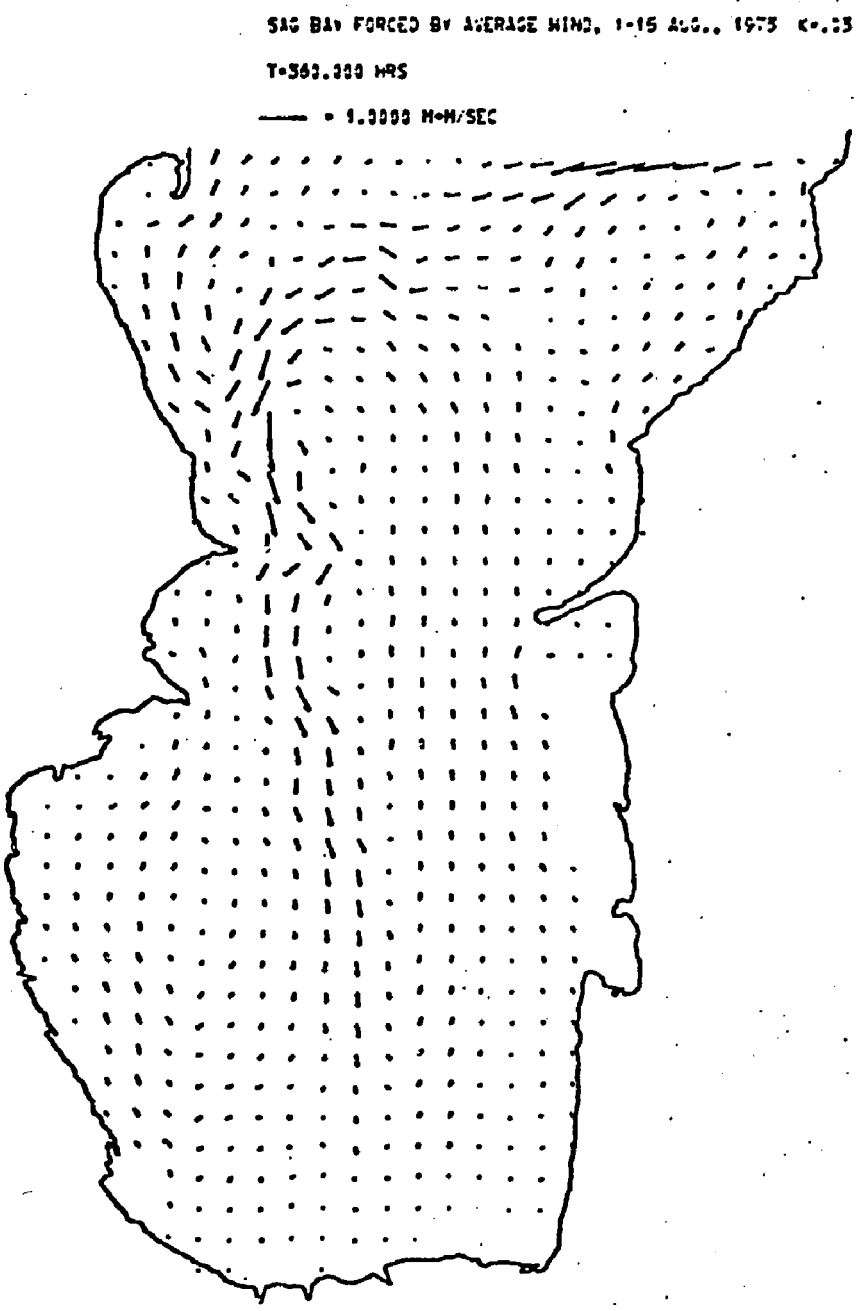


Figure 55. Quasi-steady-state circulation produced by mean wind, 1-15 August, 1973 (compare Figures 17 and 53).

The quasi-steady-state response to the time-averaged wind (1 August - 15 August, 1973) is shown in Figure 55. This graph can be compared with Figure 53 (the time-averaged response to the time-dependent wind, 1 August - 15 August, 1973). The steady state circulation is seen to be slightly less energetic than the time-averaged circulation. The magnitudes of transports caused by the average wind were usually less than those which arose during realistic simulations (see Figures 37-50).

The time dependent behavior of the concentration distribution is difficult to anticipate, even though the evolution of the distribution corresponds to some extent with advection induced by the mean forcing. Figure 46 shows that 208 hr after the beginning of the simulation the concentration in the region of the water intake mentioned above reaches a value significantly higher than existed in the initial matter distribtuion or than exists at later times in the simulation. Thus, detailed features of physical processes are revealed by the time dependent solution which do not appear in average conditions, even for the concentration problem.

Tabulated values of selected U,V,ζ, and C arrays are presented in Tables 3-10. Tables 3-6 give values for the U and V arithmetic mean arrays which are plotted in Figure 54. Tables 7-10 give values for the ζ and C arrays 60 hr after the beginning of the simulation depicted by Figures 37-50.

ARITHMETIC MEAN ARRAY, U COMP., COLS. 2-14

0.000	0.000	0.000	0.000	0.000	0.000	0.000	0.000	0.000	0.000	0.000	0.000	0.000
0.000	0.000	0.000	0.000	0.000	0.000	0.000	0.000	0.000	0.000	0.000	0.000	0.000
0.000	0.000	0.000	0.000	0.000	-.095	.003	.005	.029	-.009	.027	.026	.026
0.000	0.000	-.033	.005	-.040	-.128	-.018	.030	.006	.011	.034	.076	.067
0.000	0.000	-.062	.004	-.149	-.074	.029	.038	.021	.079	.077	.065	.125
0.000	0.000	-.099	-.111	-.109	-.050	.051	.174	.119	.133	.099	.063	.092
0.000	0.000	-.023	-.199	-.177	-.044	.105	.233	.157	.246	.134	-.135	.148
0.000	0.000	0.000	-.210	-.219	-.030	.218	.351	.264	.160	.084	-.016	.033
0.000	0.000	0.000	-.153	-.177	-.158	.390	.437	.254	.082	.046	-.038	.005
0.000	0.000	0.000	-.071	-.227	-.051	.347	.555	.215	.026	.024	-.044	-.011
0.000	0.000	0.000	0.000	-.199	-.024	.380	.611	.055	.019	.023	-.027	-.085
0.000	0.000	0.000	0.000	0.000	-.104	.252	.643	.117	-.005	-.005	-.052	-.041
0.000	0.000	0.000	0.000	0.000	-.130	.323	.398	.349	-.001	-.051	-.067	-.039
0.000	0.000	0.000	0.000	0.000	-.120	.022	.669	.286	.057	-.075	-.042	-.051
0.000	0.000	0.000	0.000	0.000	0.000	-.081	.408	.369	.171	-.028	-.059	-.060
0.000	0.000	0.000	0.000	0.000	0.000	-.049	.283	.169	.400	.046	-.092	-.068
0.000	0.000	0.000	0.000	0.000	-.054	.110	.286	.271	.241	-.022	-.091	-.083
0.000	0.000	0.000	0.000	-.068	-.027	.114	.347	.331	.174	-.007	-.134	-.096
0.000	0.000	0.000	0.000	-.074	-.059	.147	.354	.347	.147	-.034	-.127	-.113
0.000	0.000	0.000	0.000	0.000	-.095	.122	.261	.434	.129	-.013	-.112	-.109
0.000	0.000	0.000	0.000	0.000	-.069	.083	.164	.379	.210	.035	-.068	-.123
0.000	0.000	0.000	0.000	-.063	-.003	.062	.130	.315	.277	.123	-.101	-.114
0.000	0.000	0.000	-.035	-.109	.024	.079	.127	.280	.297	.120	-.062	-.105
0.000	-.021	-.036	-.062	-.079	.043	.090	.172	.236	.252	.198	-.043	-.116
-.039	-.051	-.037	-.075	-.063	.081	.103	.137	.195	.314	.230	-.026	-.093
-.061	-.067	-.057	-.070	-.054	.078	.115	.131	.176	.272	.239	.062	-.097
-.060	-.078	-.077	-.077	-.064	.100	.120	.137	.169	.250	.267	.078	-.098
-.074	-.082	-.082	-.086	-.036	.089	.134	.132	.166	.225	.257	.114	-.091
-.043	-.094	-.101	-.104	-.011	.091	.132	.132	.154	.193	.257	.121	-.068
0.000	-.067	-.096	-.104	-.046	.104	.115	.126	.152	.187	.244	.120	-.075
0.000	-.016	-.106	-.116	-.044	.125	.093	.115	.128	.178	.230	.114	-.071
0.000	0.000	-.099	-.091	-.040	.115	.085	.110	.108	.142	.211	.099	-.071
0.000	0.000	-.078	-.095	.028	.050	.109	.103	.093	.112	.175	.064	-.054
0.000	0.000	-.058	-.081	-.001	.120	.103	.067	.053	.103	.104	.061	-.048
0.000	0.000	0.000	-.091	-.017	.118	.099	.070	.046	.017	.111	.002	-.018
0.000	0.000	0.000	0.000	-.081	.081	.096	.099	.032	-.050	.081	.013	-.027
0.000	0.000	0.000	0.000	-.045	.054	.077	.074	-.019	.005	.014	-.002	-.023
0.000	0.000	0.000	0.000	-.031	.027	.063	.051	-.036	-.018	.018	-.020	-.016
0.000	0.000	0.000	0.000	0.000	.009	.009	-.002	.010	-.029	-.011	0.000	0.000
0.000	0.000	0.000	0.000	0.000	0.000	0.000	0.000	0.000	0.000	0.000	0.000	0.000

↑ Lakeward (34° magnetic)

Table 3. Arithmetic mean transport (U component) in m^2/sec, columns 2-14, for the period 16-31 August 1973. (+U is toward 214 magnetic.)

ARITHMETIC MEAN ARRAY, U COMP., COLS. 15-27

0.000	0.000	0.000	0.000	0.000	0.000	0.000	0.000	0.000	0.000	0.000	0.000	0.000	0.000
0.000	0.000	0.000	0.000	0.000	0.000	0.000	0.000	0.000	0.000	0.000	0.000	0.000	0.000
.013	.040	.079	.062	.126	.098	.204	.129	.132	.108	-.023	-.440	-.195	
.032	.156	.122	.115	.215	.157	.087	.003	-.018	-.095	-.235	-.254	0.000	
.142	.122	.125	.123	.114	.081	.012	.005	-.112	-.123	-.162	-.206	0.000	
.089	.090	.101	.128	.100	.044	-.019	-.081	-.136	-.142	-.126	-.113	0.000	
.065	.050	.068	.096	.086	-.021	-.076	-.089	-.145	-.193	-.072	0.000	0.000	
.033	.020	.053	.007	.028	-.032	-.092	-.100	-.122	-.171	0.000	0.000	0.000	
-.002	-.005	-.021	.020	.002	-.062	-.098	-.098	-.079	-.102	0.000	0.000	0.000	
-.027	-.039	-.072	.008	.010	-.099	-.118	-.094	-.047	0.000	0.000	0.000	0.000	
-.051	-.053	-.065	-.047	.022	-.118	-.151	0.000	0.000	0.000	0.000	0.000	0.000	
-.088	-.084	-.066	-.031	-.006	-.213	0.000	0.000	0.000	0.000	0.000	0.000	0.000	
-.079	-.071	-.061	.002	-.049	-.178	0.000	0.000	0.000	0.000	0.000	0.000	0.000	
-.070	-.066	-.063	-.015	-.017	-.107	-.069	0.000	0.000	0.000	0.000	0.000	0.000	
-.080	-.073	-.031	-.036	-.043	-.081	-.043	0.000	0.000	0.000	0.000	0.000	0.000	
-.071	-.071	-.063	-.049	-.059	-.067	0.000	0.000	0.000	0.000	0.000	0.000	0.000	
-.072	-.070	-.099	-.047	-.085	0.000	0.000	0.000	0.000	0.000	0.000	0.000	0.000	
-.082	-.072	-.106	-.053	-.055	0.000	0.000	0.000	0.000	0.000	0.000	0.000	0.000	
-.054	-.111	-.104	-.045	-.024	-.024	0.000	0.000	0.000	0.000	0.000	0.000	0.000	
-.091	-.129	-.174	0.000	0.000	0.000	0.000	0.000	0.000	0.000	0.000	0.000	0.000	
-.090	-.108	-.192	0.000	0.000	0.000	0.000	0.000	0.000	0.000	0.000	0.000	0.000	
-.095	-.089	-.104	-.081	0.000	0.000	0.000	0.000	0.000	0.000	0.000	0.000	0.000	
-.099	-.093	-.080	-.088	0.000	0.000	0.000	0.000	0.000	0.000	0.000	0.000	0.000	
-.096	-.095	-.077	-.076	0.000	0.000	0.000	0.000	0.000	0.000	0.000	0.000	0.000	
-.096	-.087	-.066	-.068	0.000	0.000	0.000	0.000	0.000	0.000	0.000	0.000	0.000	
-.097	-.077	-.054	-.069	0.000	0.000	0.000	0.000	0.000	0.000	0.000	0.000	0.000	
-.093	-.046	-.049	-.042	-.028	0.000	0.000	0.000	0.000	0.000	0.000	0.000	0.000	
-.082	-.043	-.028	-.035	-.043	0.000	0.000	0.000	0.000	0.000	0.000	0.000	0.000	
-.083	-.045	-.005	-.030	-.060	0.000	0.000	0.000	0.000	0.000	0.000	0.000	0.000	
-.080	-.037	-.006	-.036	-.042	0.000	0.000	0.000	0.000	0.000	0.000	0.000	0.000	
-.080	-.026	-.011	-.021	-.056	0.000	0.000	0.000	0.000	0.000	0.000	0.000	0.000	
-.067	-.027	.007	-.043	-.044	0.000	0.000	0.000	0.000	0.000	0.000	0.000	0.000	
-.062	-.016	.011	-.044	-.041	0.000	0.000	0.000	0.000	0.000	0.000	0.000	0.000	
-.049	-.017	.007	-.022	-.043	0.000	0.000	0.000	0.000	0.000	0.000	0.000	0.000	
-.050	-.019	.024	-.007	-.042	0.000	0.000	0.000	0.000	0.000	0.000	0.000	0.000	
-.044	.000	.004	.017	-.038	0.000	0.000	0.000	0.000	0.000	0.000	0.000	0.000	
-.022	-.008	.015	.018	-.026	0.000	0.000	0.000	0.000	0.000	0.000	0.000	0.000	
0.000	0.000	0.000	0.000	0.000	0.000	0.000	0.000	0.000	0.000	0.000	0.000	0.000	
0.000	0.000	0.000	0.000	0.000	0.000	0.000	0.000	0.000	0.000	0.000	0.000	0.000	
0.000	0.000	0.000	0.000	0.000	0.000	0.000	0.000	0.000	0.000	0.000	0.000	0.000	

↑ Lakeward (34° magnetic)

Table 4. Arithmetic mean transport (U component) in m^2/sec, columns 15-27, for the period 16-31 August 1973. (+U is toward 214 magnetic.)

ARITHMETIC MEAN ARRAY, V COMP., COLS. 2-14

0.000	0.000	0.000	0.000	0.000	0.000	0.000	0.000	0.000	0.000	0.000	0.000	0.000	0.000
0.000	0.000	0.000	0.000	0.000	0.000	0.000	0.000	0.000	0.000	0.000	0.000	0.000	0.000
0.000	0.000	0.000	.030	.022	.059	.101	.121	.038	.060	.042	.035	-.013	
0.000	0.000	0.000	.026	.025	.131	.075	.023	.028	.013	-.057	-.100	-.093	
0.000	0.000	0.000	.034	.146	.103	.078	.053	-.033	-.132	-.187	-.215	-.208	
0.000	0.000	0.000	-.079	.007	.073	.066	.010	-.110	-.150	-.264	-.299	-.102	
0.000	0.000	0.000	-.023	-.015	.025	.003	-.105	-.164	-.272	-.186	-.135	-.254	
0.000	0.000	0.000	0.000	-.059	-.103	.025	-.149	-.256	-.255	-.177	-.139	-.116	
0.000	0.000	0.000	0.000	-.084	-.035	-.143	-.101	-.199	-.153	-.093	-.069	-.062	
0.000	0.000	0.000	0.000	-.074	-.112	-.141	-.174	-.230	-.069	-.063	-.060	-.074	
0.000	0.000	0.000	0.000	0.000	-.190	-.111	.017	-.015	-.077	-.051	-.022	.006	
0.000	0.000	0.000	0.000	0.000	0.000	.026	-.043	.201	-.030	-.031	.028	.045	
0.000	0.000	0.000	0.000	0.000	0.000	-.010	.292	.023	.087	.031	.047	.025	
0.000	0.000	0.000	0.000	0.000	0.000	-.118	-.014	.248	.166	.055	.010	.029	
0.000	0.000	0.000	0.000	0.000	0.000	0.000	-.031	.096	.296	.068	-.005	.029	
0.000	0.000	0.000	0.000	0.000	0.000	.057	-.099	-.101	-.201	-.040	.028	.025	
0.000	0.000	0.000	0.000	0.000	.073	.050	.050	-.009	-.057	.001	-.014	.029	
0.000	0.000	0.000	0.000	0.000	.011	.046	.016	.001	-.013	.016	.043	.037	
0.000	0.000	0.000	0.000	0.000	-.069	-.029	-.001	.103	.018	.046	.027	.013	
0.000	0.000	0.000	0.000	0.000	0.000	-.024	.017	.117	.174	.086	.038	-.006	
0.000	0.000	0.000	0.000	0.000	.085	.022	.046	.082	.149	.083	-.003	.032	
0.000	0.000	0.000	0.000	.037	.064	.040	.024	.029	.065	.046	.051	.013	
0.000	0.000	.025	.065	.095	.067	.050	.041	-.003	.041	.087	.009	-.009	
0.000	.042	.075	.080	.095	.081	.044	.033	.059	.110	.050	.049	.033	
0.000	.026	.046	.070	.068	.061	.066	.054	.060	.081	.123	.085	-.002	
0.000	.005	.022	.046	.056	.068	.046	.041	.035	.042	.065	.037	.022	
0.000	.022	.033	.042	.053	.025	.036	.022	.026	.029	.053	.063	.027	
0.000	-.022	-.012	.013	.034	.010	.009	.010	.010	.021	.046	.045	.035	
0.000	-.031	-.040	-.039	-.037	.000	-.013	.003	.007	.008	.019	.031	.031	
0.000	0.000	-.043	-.029	-.014	-.015	-.037	-.015	-.005	.018	.026	.038	.043	
0.000	0.000	-.005	-.017	-.042	-.046	-.036	-.030	-.026	-.007	.028	.045	.058	
0.000	0.000	0.000	-.011	-.007	-.076	-.013	-.039	-.034	-.021	.008	.042	.076	
0.000	0.000	0.000	-.020	-.035	-.068	-.080	-.076	-.042	-.005	.002	.070	.071	
0.000	0.000	0.000	-.058	-.050	-.037	-.037	-.037	-.043	-.038	.045	.035	.091	
0.000	0.000	0.000	0.000	-.092	-.031	.003	.002	-.030	-.020	.043	.069	.054	
0.000	0.000	0.000	0.000	0.000	-.040	-.018	-.004	.015	.062	.001	.062	.073	
0.000	0.000	0.000	0.000	0.000	-.020	.003	.012	.030	.041	.058	.048	.060	
0.000	0.000	0.000	0.000	0.000	-.036	-.024	.024	.071	.020	.024	.047	.022	
0.000	0.000	0.000	0.000	0.000	0.000	.004	.008	.015	.035	.016	0.000	0.000	
0.000	0.000	0.000	0.000	0.000	0.000	0.000	0.000	0.000	0.000	0.000	0.000	0.000	

↑ Lakeward (34° magnetic)

Table 5. Arithmetic mean transport (V component) in m^2/sec, columns 2-14, for the period 16-31 August 1973. (+V is toward 124 magnetic.)

ARITHMETIC MEAN ARRAY, V COMP., COLS. 15-27

0.000	0.000	0.000	0.000	0.000	0.000	0.000	0.000	0.000	0.000	0.000	0.000	0.000
0.000	0.000	0.000	0.000	0.000	0.000	0.000	0.000	0.000	0.000	0.000	0.000	0.000
-.054	-.071	-.186	-.228	-.279	-.368	-.425	-.398	-.192	-.031	.172	.383	.196
-.150	-.261	-.227	-.231	-.240	-.140	-.065	.009	.006	.037	.124	.050	0.000
-.173	-.121	-.091	-.067	-.072	-.059	-.023	.008	.094	.116	.133	.095	0.000
-.158	-.135	-.094	-.061	-.028	-.014	.051	.107	.114	.122	.172	.116	0.000
-.138	-.104	-.073	-.067	.023	.083	.095	.111	.121	.097	.074	0.000	0.000
-.087	-.050	-.024	.061	.049	.076	.108	.114	.112	.070	0.000	0.000	0.000
-.045	-.018	.018	.071	.085	.078	.117	.138	.134	.102	0.000	0.000	0.000
.004	.030	.046	.042	.098	.068	.108	.141	.048	0.000	0.000	0.000	0.000
-.036	.004	.038	.040	.026	.056	.152	0.000	0.000	0.000	0.000	0.000	0.000
.047	.040	.030	.026	-.007	.036	0.000	0.000	0.000	0.000	0.000	0.000	0.000
.039	.031	.026	.027	.043	.009	-.065	0.000	0.000	0.000	0.000	0.000	0.000
.039	.048	.055	.021	.040	.062	.031	0.000	0.000	0.000	0.000	0.000	0.000
.036	.026	.021	.049	.057	.067	.047	0.000	0.000	0.000	0.000	0.000	0.000
.040	.037	.031	.062	.054	.073	0.000	0.000	0.000	0.000	0.000	0.000	0.000
.040	.046	.043	.043	.041	0.000	0.000	0.000	0.000	0.000	0.000	0.000	0.000
.052	.020	.055	.047	.032	-.009	0.000	0.000	0.000	0.000	0.000	0.000	0.000
.009	.044	.058	.124	.073	.038	0.000	0.000	0.000	0.000	0.000	0.000	0.000
.009	.007	-.015	0.000	0.000	0.000	0.000	0.000	0.000	0.000	0.000	0.000	0.000
.024	.028	.009	-.000	0.000	0.000	0.000	0.000	0.000	0.000	0.000	0.000	0.000
.004	.008	.014	-.008	0.000	0.000	0.000	0.000	0.000	0.000	0.000	0.000	0.000
.004	.003	.009	.009	0.000	0.000	0.000	0.000	0.000	0.000	0.000	0.000	0.000
.010	.012	.009	.002	0.000	0.000	0.000	0.000	0.000	0.000	0.000	0.000	0.000
.004	.008	.002	-.006	0.000	0.000	0.000	0.000	0.000	0.000	0.000	0.000	0.000
.023	.020	-.008	-.008	-.031	0.000	0.000	0.000	0.000	0.000	0.000	0.000	0.000
.019	.009	.007	-.012	-.017	0.000	0.000	0.000	0.000	0.000	0.000	0.000	0.000
.014	.013	.013	-.010	-.016	0.000	0.000	0.000	0.000	0.000	0.000	0.000	0.000
.036	.031	.020	.018	.021	0.000	0.000	0.000	0.000	0.000	0.000	0.000	0.000
.036	.032	.017	.017	-.005	0.000	0.000	0.000	0.000	0.000	0.000	0.000	0.000
.056	.039	.034	.008	.022	0.000	0.000	0.000	0.000	0.000	0.000	0.000	0.000
.056	.048	.031	.021	.013	0.000	0.000	0.000	0.000	0.000	0.000	0.000	0.000
.061	.043	.039	.035	.006	0.000	0.000	0.000	0.000	0.000	0.000	0.000	0.000
.058	.054	.050	.027	.007	0.000	0.000	0.000	0.000	0.000	0.000	0.000	0.000
.060	.049	.026	.040	.010	0.000	0.000	0.000	0.000	0.000	0.000	0.000	0.000
.064	.038	.041	.026	.018	0.000	0.000	0.000	0.000	0.000	0.000	0.000	0.000
.048	.022	.010	.020	.032	0.000	0.000	0.000	0.000	0.000	0.000	0.000	0.000
0.000	0.000	0.000	0.000	0.000	0.000	0.000	0.000	0.000	0.000	0.000	0.000	0.000
0.000	0.000	0.000	0.000	0.000	0.000	0.000	0.000	0.000	0.000	0.000	0.000	0.000
0.000	0.000	0.000	0.000	0.000	0.000	0.000	0.000	0.000	0.000	0.000	0.000	0.000
0.000	0.000	0.000	0.000	0.000	0.000	0.000	0.000	0.000	0.000	0.000	0.000	0.000

↑ Lakeward (34° magnetic)

Table 6. Arithmetic mean transport (V component) in m^2/sec, columns 15-27, for the period 16-31 August 1973. (+V is toward 124 magnetic.)

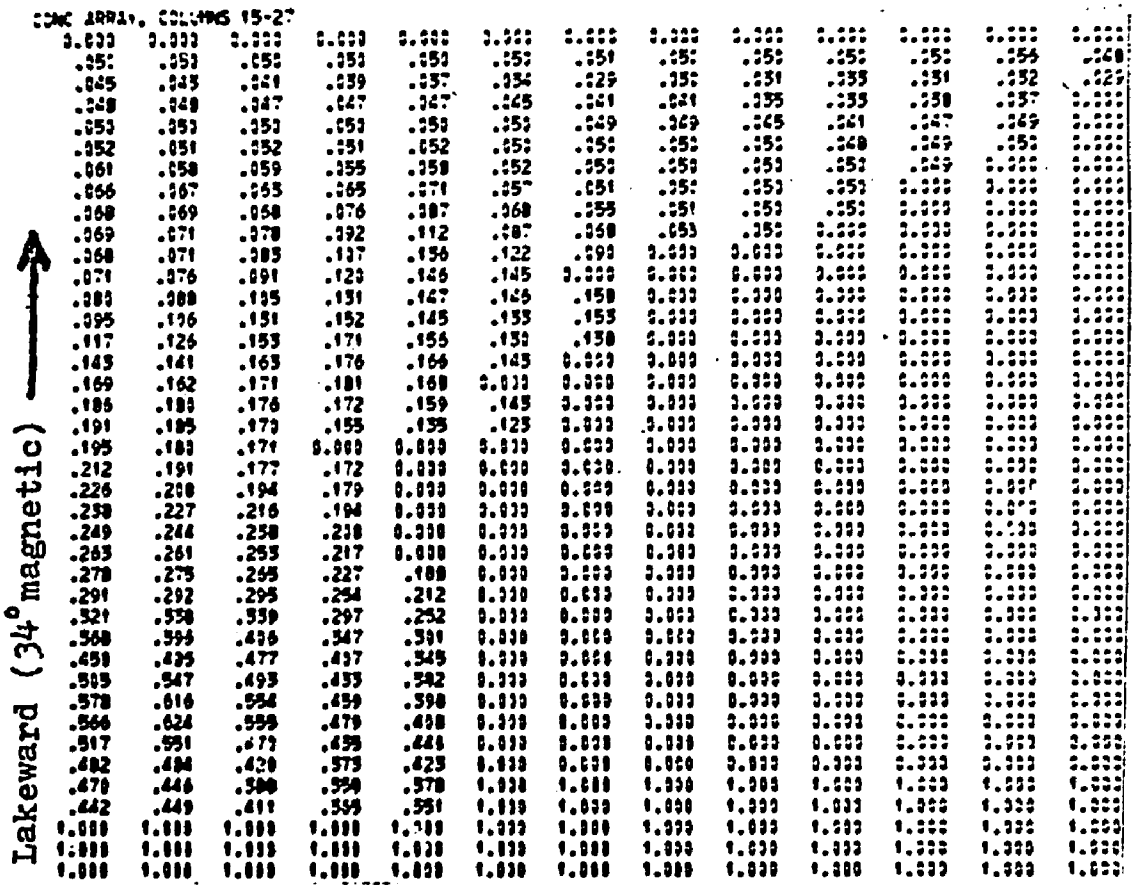


Table 7. Surface height (ζ) in m for t = 60 hr, columns 2-14, from simulation which began 1 August 1973.

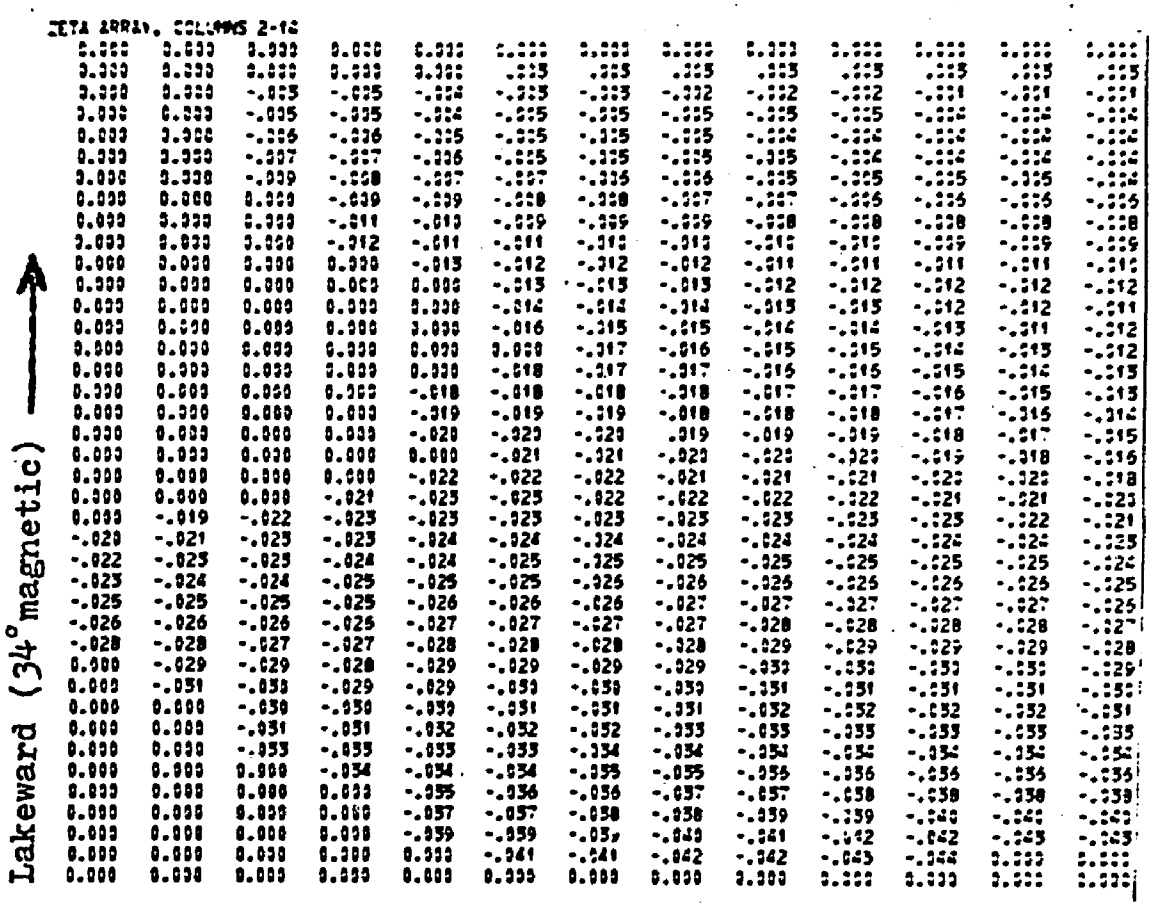


Table 8. Surface height (ζ) in m for t = 60 hr, columns 15-27, from simulation which began 1 August 1973.

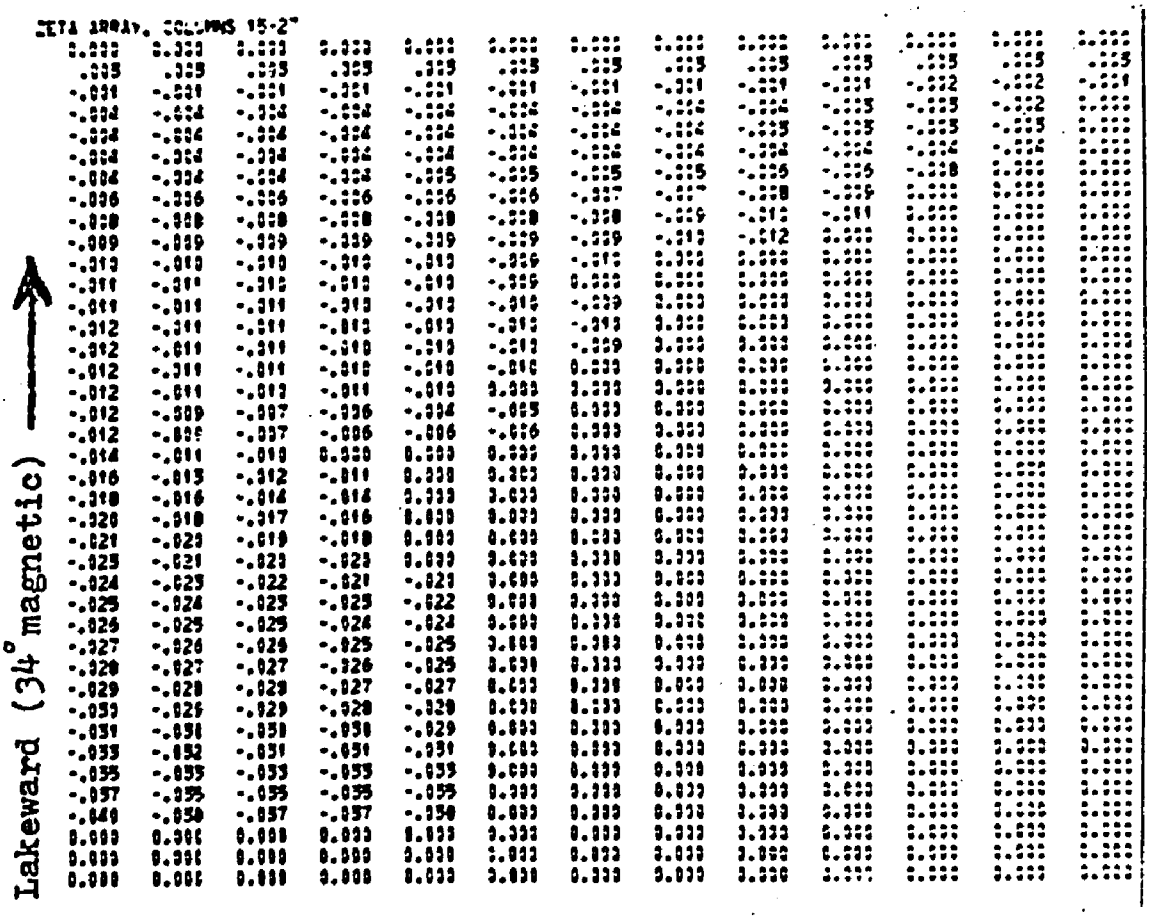


Table 9. Chlorine concentration in ppm/100 for t = 60 hr, columns 2-14, from simulation which began 1 August 1973.

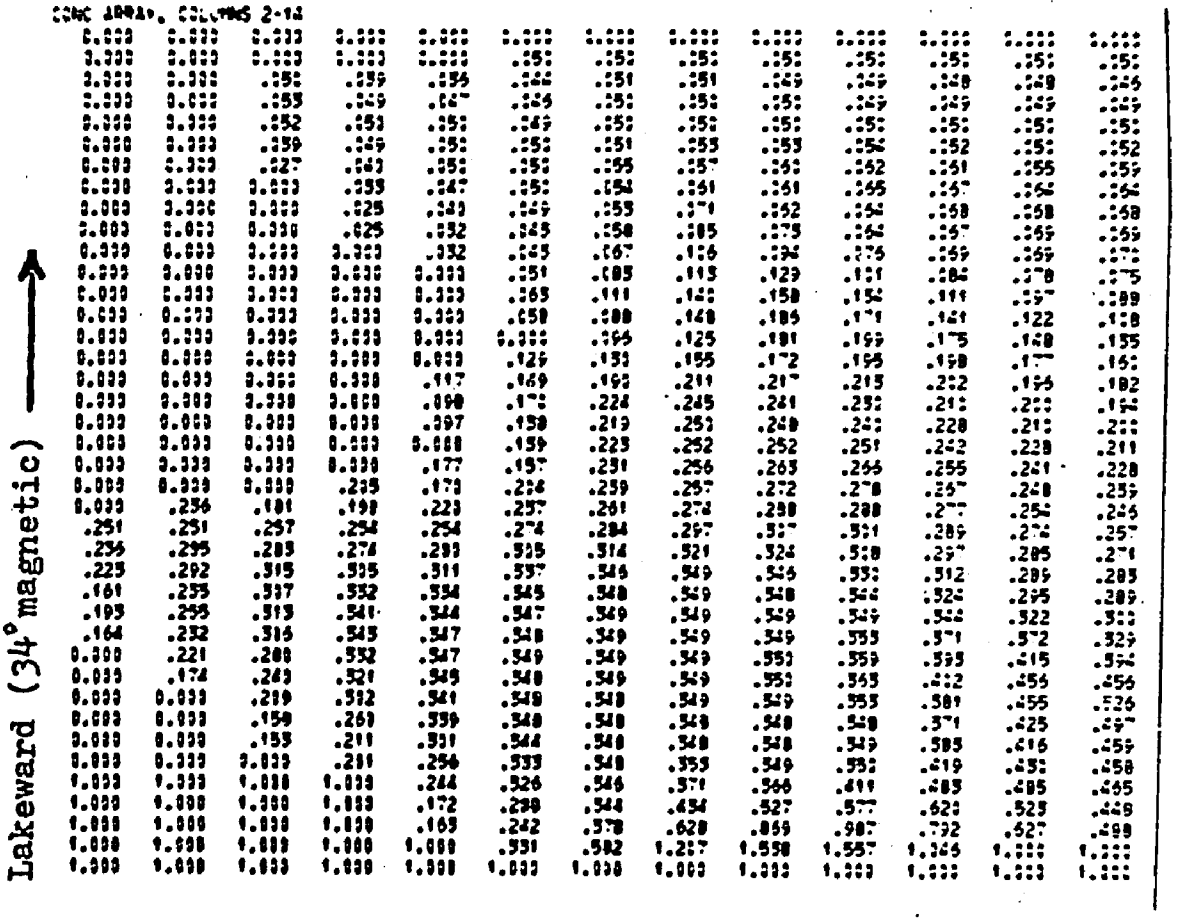


Table 10. Chlorine concentration in ppm/100 for t = 60 hr, columns 15-27, from simulation which began 1 August 1973.

Each matrix of values has 40 rows and 28 columns. The odd numbered tables contain columns 2-14 and the even numbered tables contain columns 15-27.

Many additional simulations have been made, and representative figures appear in Appendix C. Detailed wind histories are also reproduced to allow comparison with the model's response.

VI. Concluding remarks

Circulation and advection-diffusion processes in Saginaw Bay have been studied through numerical integration of the governing continuum equations. The following conclusions can be made based upon this work: 1) motions having periods of less than two hours are strongly damped in the inner bay; 2) the motion of the bay is clearly influenced by seiching of Lake Huron, and the periods of frequently observed modes having the greatest amplitudes are 3.3 hr and 1.8 hr; 3) radically different circulation patterns can supplant one another in 8 hr or less; 4) chlorinity distributions evolve on a time scale at least an order of magnitude greater than flow patterns; 5) transverse seiching of the bay appears to be a significant mechanism for coastal inundation; 6) corroborative observational results show that the numerical model explains anomalously high chlorine concentrations which arise in certain portions of the bay under given forcing conditions; 7) the flow patterns show strong orographic effects which are difficult to anticipate

a priori; 8) the time dependent solutions reveal important and interesting occurrences which are not seen in time-averaged results; 9) the difference equations show no instabilities or indications that the problems are ill-posed; 10) behavioral errors which result from the combination of the complexity of the flow patterns and the differencing parameters have been suppressed through the use of artificial diffusion; 11) usage of the ADI technique results in at least a 75 percent savings in computer time compared to a purely explicit type of integration procedure; 12) the ADI technique appears to be an excellent method of solution for barotropic problems.

In the near future observational results will be available which will allow further comparison of the numerically predicted dynamics with the bay's actual behavior. This can eventually lead to a much more complete understanding of the bay's motion than could the numerical or observational results alone. Through man's proclivity to doubt the machine, and with the aid of the purists among us, who continually focus their attention upon the most fundamental roots of man's knowledge, numerical modeling has arisen as a viable tool, which provides an invaluable method of assisting mankind in the study of his environment.

Appendix A

STABILITY ANALYSIS FOR FLOW EQUATIONS

In Chapter IV the von Neumann stability analysis for linear equations was described. In this appendix the method is applied in detail to the transport equations as represented by the difference formulations (4.4), (4.5), (4.7), (4.8) in Chapter IV. Substitution of the solution $\bar{U}(x,y,t) = \bar{U}^n e^{i(\sigma_1 j\Delta x + \sigma_2 k\Delta y)}$ leads to the following matrix representation of the difference scheme:

$$\begin{bmatrix} 1 & 0 & -i\alpha gH \\ 0 & 1 & 0 \\ -i\alpha & 0 & 1 \end{bmatrix}^{-1} \begin{bmatrix} 1 & 0 & 0 \\ 0 & 1 & i\gamma gH \\ 0 & i\alpha & 1 \end{bmatrix} \bar{U}^{n+1} \qquad (A.1)$$

$$= \begin{bmatrix} 1 & 0 & i\alpha gH \\ 0 & 1 & 0 \\ i\alpha & 0 & 1 \end{bmatrix}^{-1} \begin{bmatrix} 1 & 0 & 0 \\ 0 & 1 & -i\alpha gH \\ 0 & -i\gamma & 1 \end{bmatrix} \bar{U}^n$$

where $\alpha = \frac{\Delta t}{\Delta x} \sin \sigma_1 \frac{\Delta x}{2}$ and $\gamma = \frac{\Delta t}{\Delta y} \sin \sigma_2 \frac{\Delta y}{2}$. The eigenvalues of the scheme's amplification matrix, $\lambda_i = e^{i\beta n\Delta t}$, can now be found from the determinant

$$\left| \begin{bmatrix} 1 & 0 & -i\alpha gH \\ 0 & 1+\alpha^2 gH & 0 \\ -i\alpha & 0 & 1 \end{bmatrix} \begin{bmatrix} 1 & 0 & 0 \\ 0 & 1 & 0 \\ 0 & -i\gamma & 1 \end{bmatrix} - \lambda \begin{bmatrix} 1 & 0 & i\alpha gH \\ 0 & 1+\alpha^2 gH & 0 \\ i\alpha & 0 & 1 \end{bmatrix} \begin{bmatrix} 1 & 0 & 0 \\ 0 & 1 & i\gamma gH \\ 0 & +i\gamma & 1 \end{bmatrix} \right| = 0 \qquad (A.2)$$

The characteristic equation is

$$\lambda^3 - \left[\frac{3+2\gamma^2 gH-\alpha^2 gH}{(1+\alpha^2 gH)(1+\gamma^2 gH)}\right]\lambda^2 - \left[\frac{\alpha^2 gH}{(1+\alpha^2 gH} - \frac{\gamma^2 gH+3}{(1+\alpha^2 gH)(1+\gamma^2 gH}\right]\lambda$$

$$- \frac{1}{(1+\alpha^2 gH)} = 0$$

Since solving the resulting cubic is a formidable task, a method will be used which shows that the eigenvalues are less than 1, but does not find them precisely. Following Leendertse (1967) consider the cubic $f(\lambda)$ with real coefficients which is obtained from the amplification matrix. This equation can be written

$$f(\lambda) = \lambda^3 + a_1\lambda^2 + a_2\lambda + a_3 \qquad (A.3)$$

If the substitution $\lambda = 1/u$ is made, then A.3 becomes

$$1 + a_1u + a_2u^2 + a_3u^3 = 0 \qquad (A.4)$$

The latter equation may be further transformed, using $u = (1-V)/(1+V)$. The result is

$$(1 - a_1 + a_2 - a_3)V^3 + (3 - a_1 - a_2 + 3a_3)V^2$$
$$+ (3 + a_1 - a_2 - 3a_3)V + (1 + a_1 + a_2 + a_3) = 0 \qquad (A.5)$$

If an inverse root of A.3 is a complex number, $u_1 = a+ib$, then

$$V = \frac{1 - a^2 - b^2 - 2ib}{1 + a^2 + b^2 + 2a}$$

Thus, it may be concluded that if $|u_1| > 1$, $(|\lambda_1| < 1)$, then the corresponding root V_1 is in the negative half plane. Defining the coefficients

$$A_0 = (1 - a_1 + a_2 - a_3)$$
$$A_1 = (3 - a_1 - a_2 + 3a_3)$$

$$A_2 = (3 + a_1 - a_2 - 3a_3)$$
$$A_3 = (1 + a_1 + a_2 + a_3)$$

the roots of A.5 have negative real parts if the following Routh-Hurwitz criteria are satisfied, (Kaplan, 1962):

$A_0>0$, $A_1>0$, and $\Delta_2=A_1A_2-A_3A_0>0$

Now, let $\alpha^2gh = A$ and $\gamma^2gh = B$. The quantities A and B are always positive. The Routh-Hurwitz determinants become,

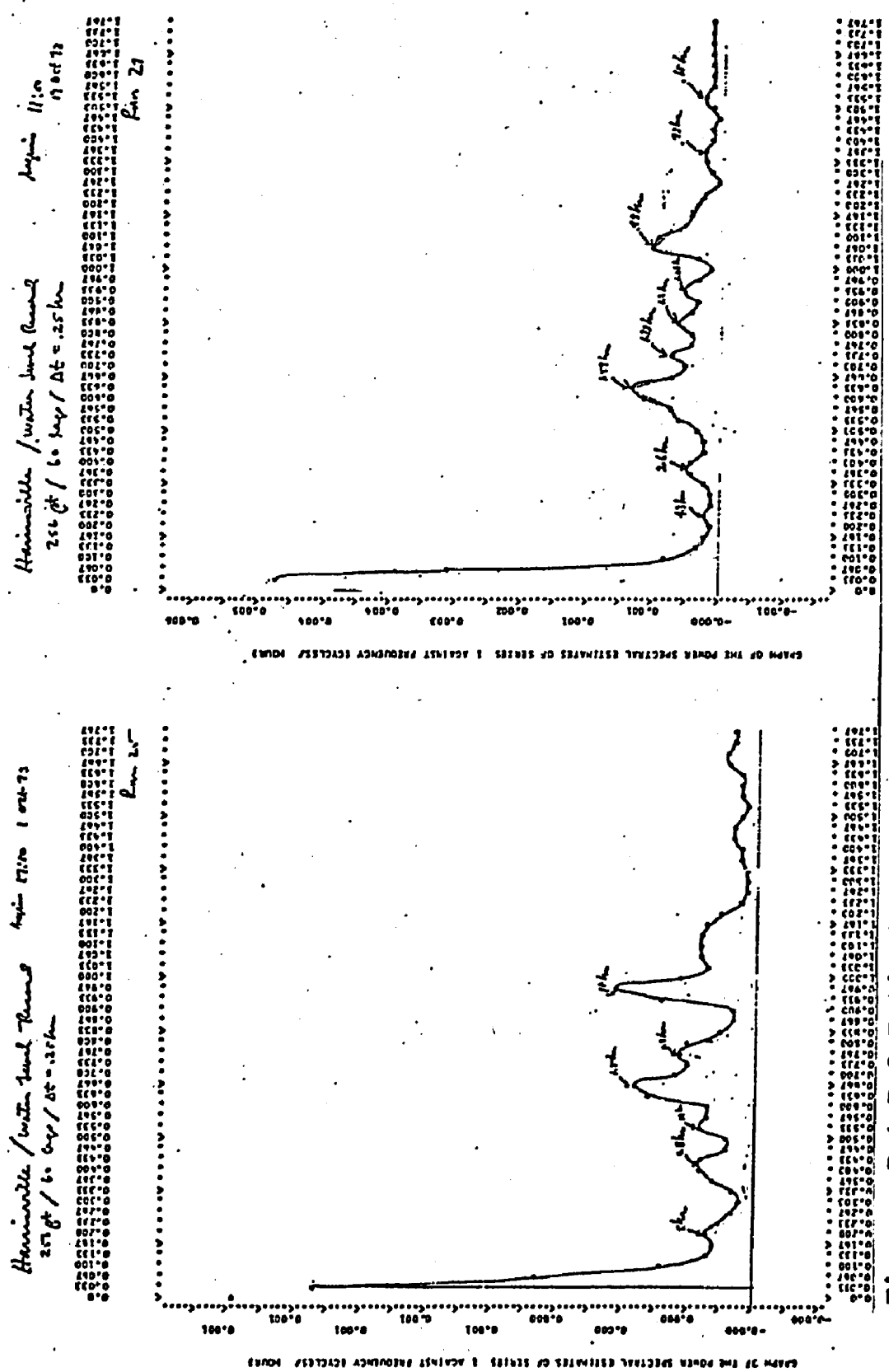
$$A_0 = 2 + 2B$$
$$A_1 = 4B + 2AB$$
$$\Delta_2 = 6 + 8B + A = 2B^2$$

which are all clearly positive. The von Neumann analysis thus indicates that the difference scheme is stable as written.

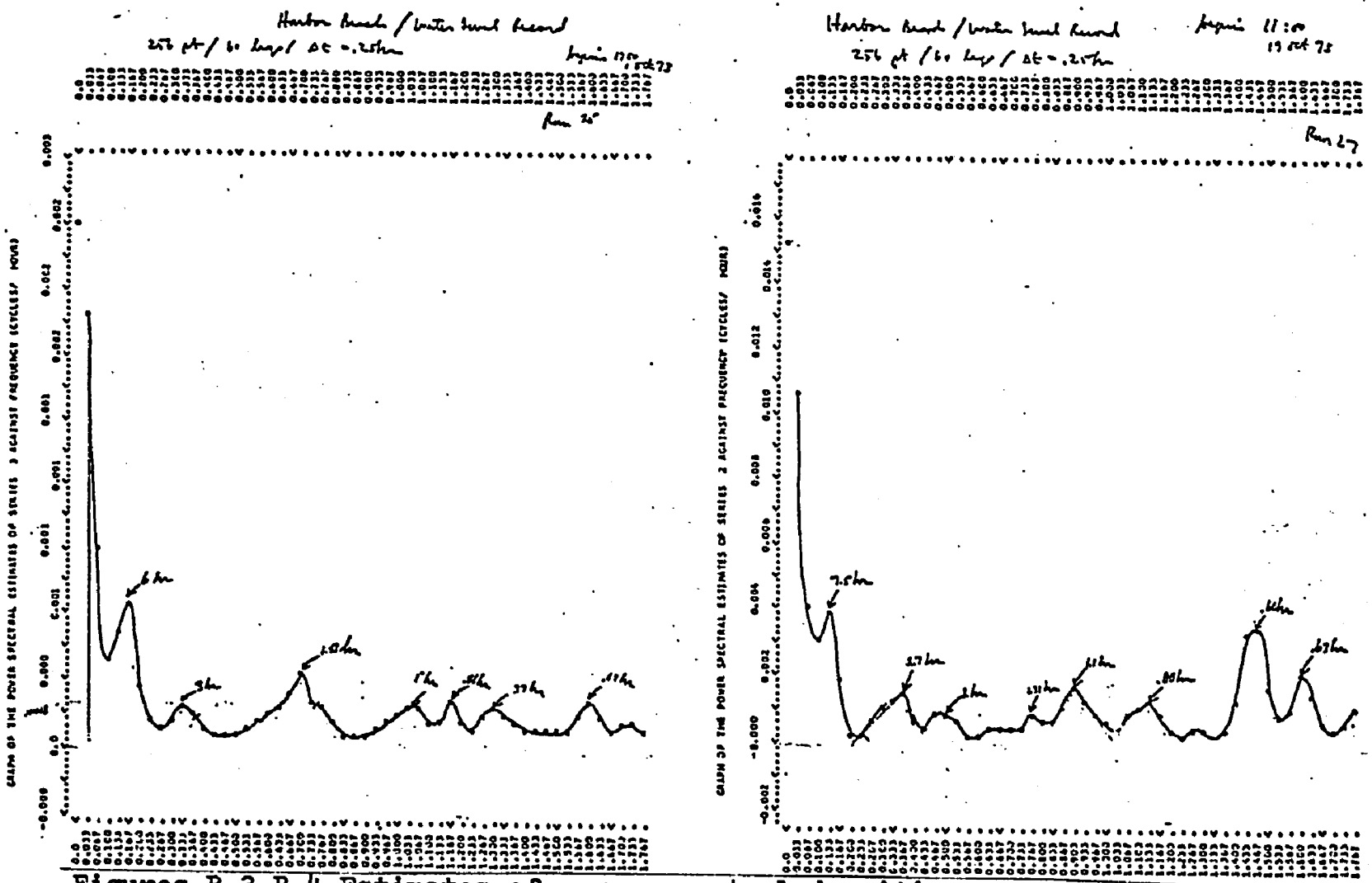
Appendix B

GRAPHICAL PRESENTATION OF ADDITIONAL SPECTRAL RESULTS

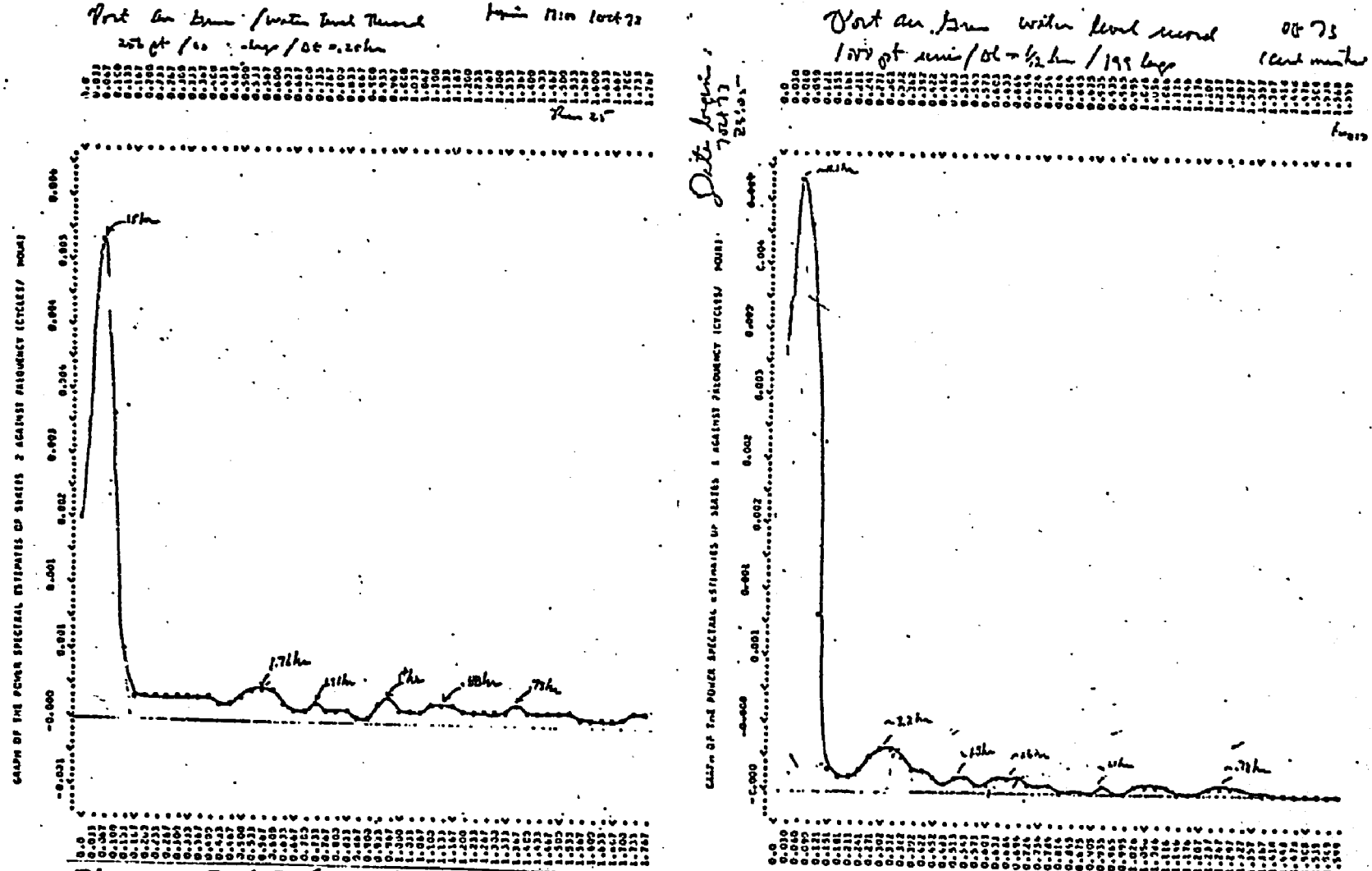
This appendix contains additional results of the spectral analyses performed as part of this research to determine the nature of seiche forcing of Saginaw Bay by Lake Huron. All power spectra are for a time series of length 64 hr, and used 60 lags, unless otherwise indicated. The units of the ordinate for the spectra are FT^2HR, and the abscissa is given in HR, unless otherwise indicated.



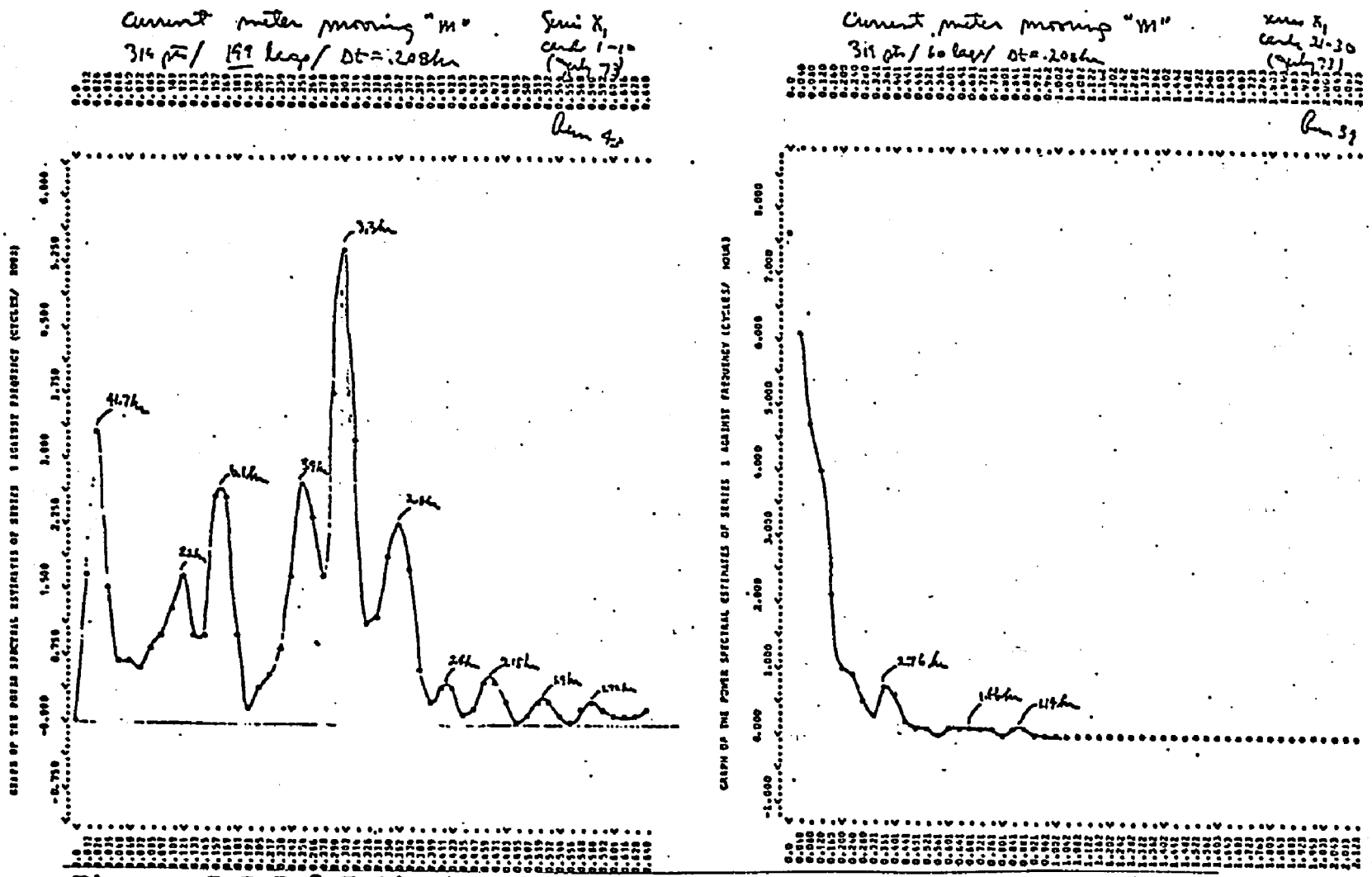
Figures B.1-B.2 Estimates of power spectral densities near Harrisville; periods of dominant motions are 2.6 hr, 1.6 hr, and 1.0 hr.



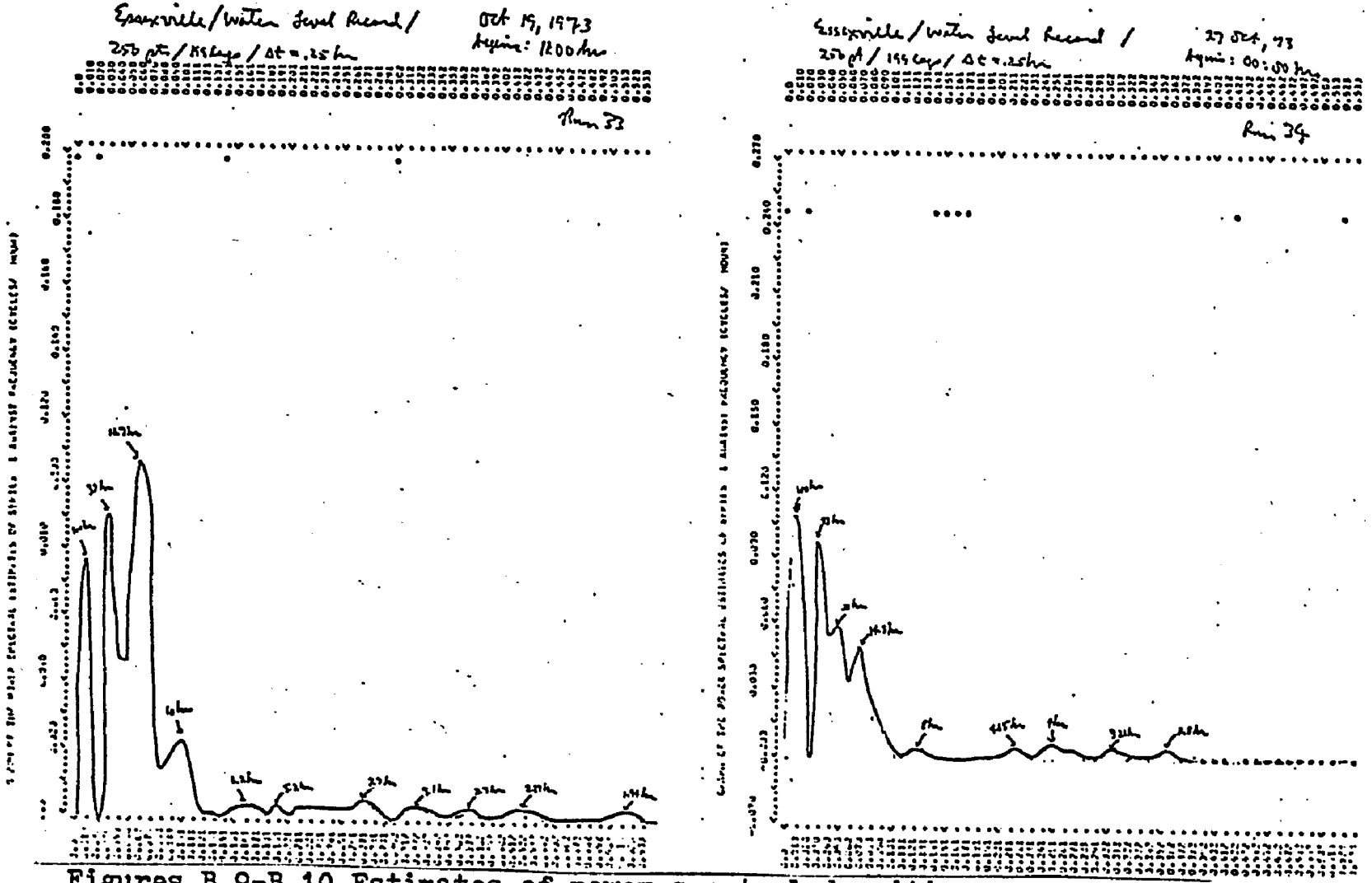
Figures B.3-B.4 Estimates of power spectral densities near Harbor Beach; periods of dominant motions are 6.0 hr, 3.0 hr, 1.6 hr, and 1.0 hr.



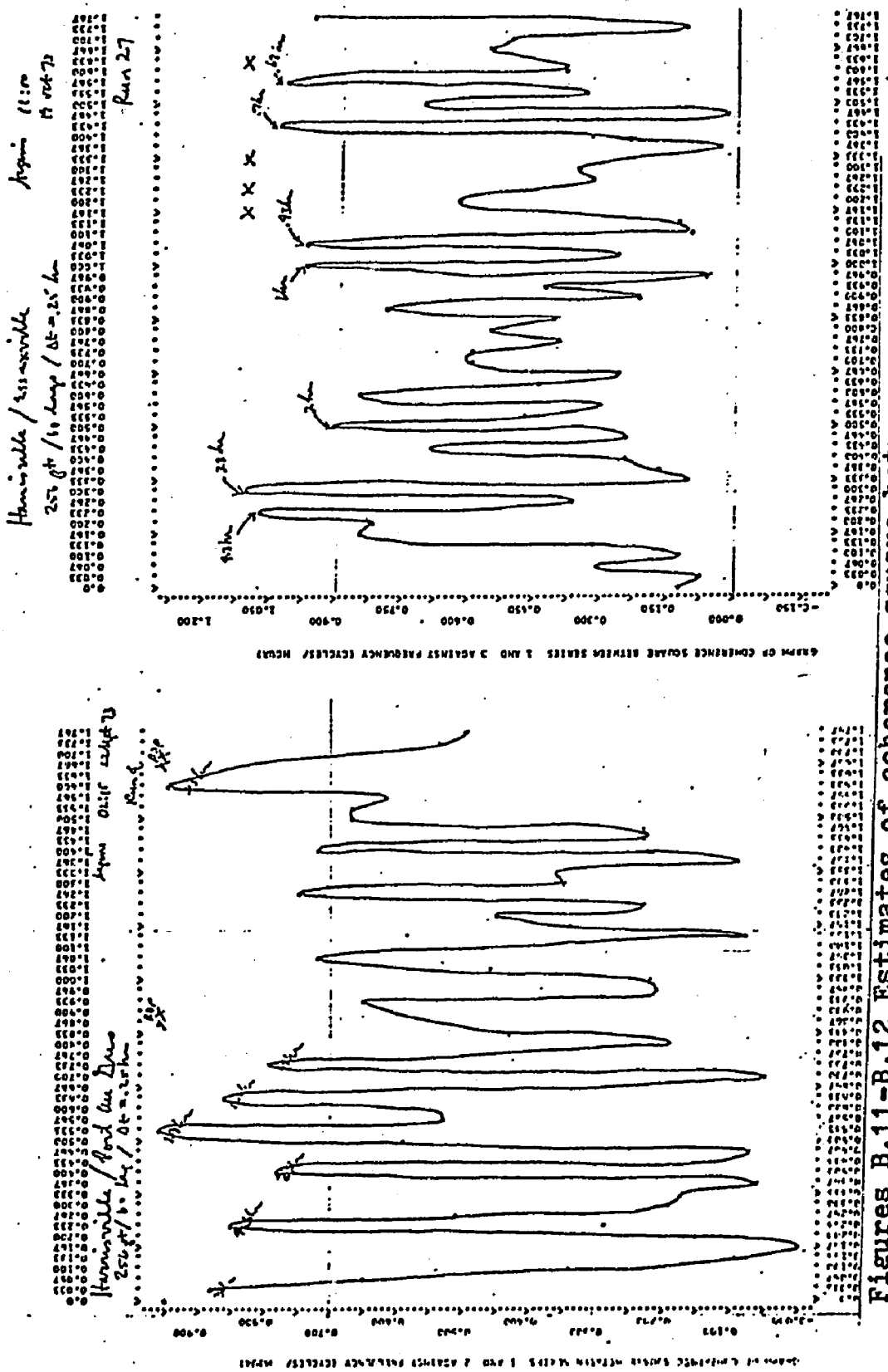
Figures B.5-B.6 Estimates of power spectral densities near Port AuGres; periods of dominant motions are 3.2 hr and 1.8 hr.



Figures B.7-B.8 Estimates of power spectral densities near Point Lookout (from current meter record); ordinate has units $cm^2/sec^2 hr$; periods of dominant motions are 3.3 hr and 2.8 hr.



Figures B.9-B.10 Estimates of power spectral densities near Essexville; many oscillatory modes are present; 10 hr and 3.3 hr are 1st and 2nd longitudinal modes of bay.

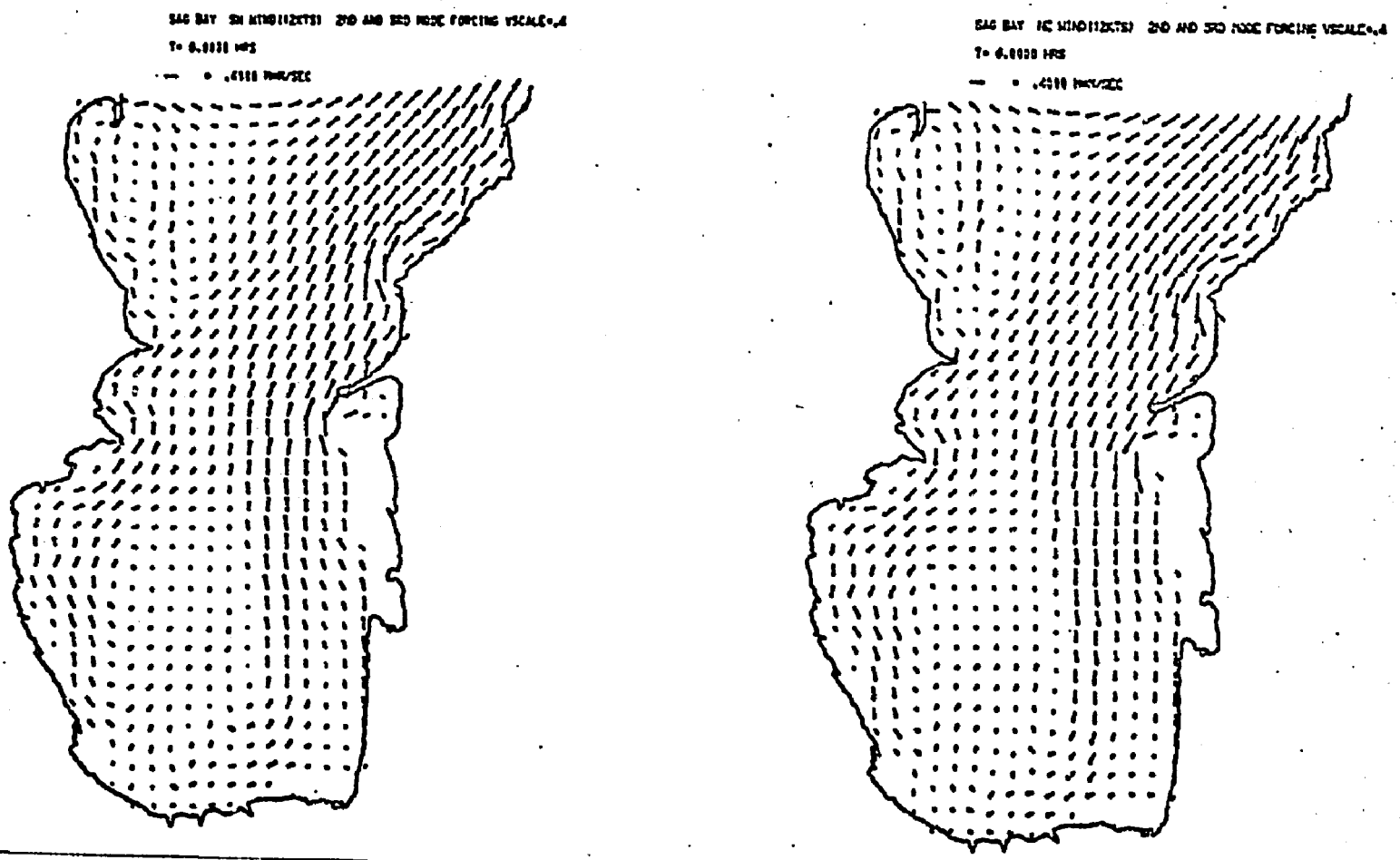


Figures B.11-B.12 Estimates of coherence square between Harrisville-Port AuGres (left) and Harrisville-Essexville (right); periods of motions having highest coherencies are 4.3 hr, 3.3 hr, 2.2 hr, and 1.6 hr.

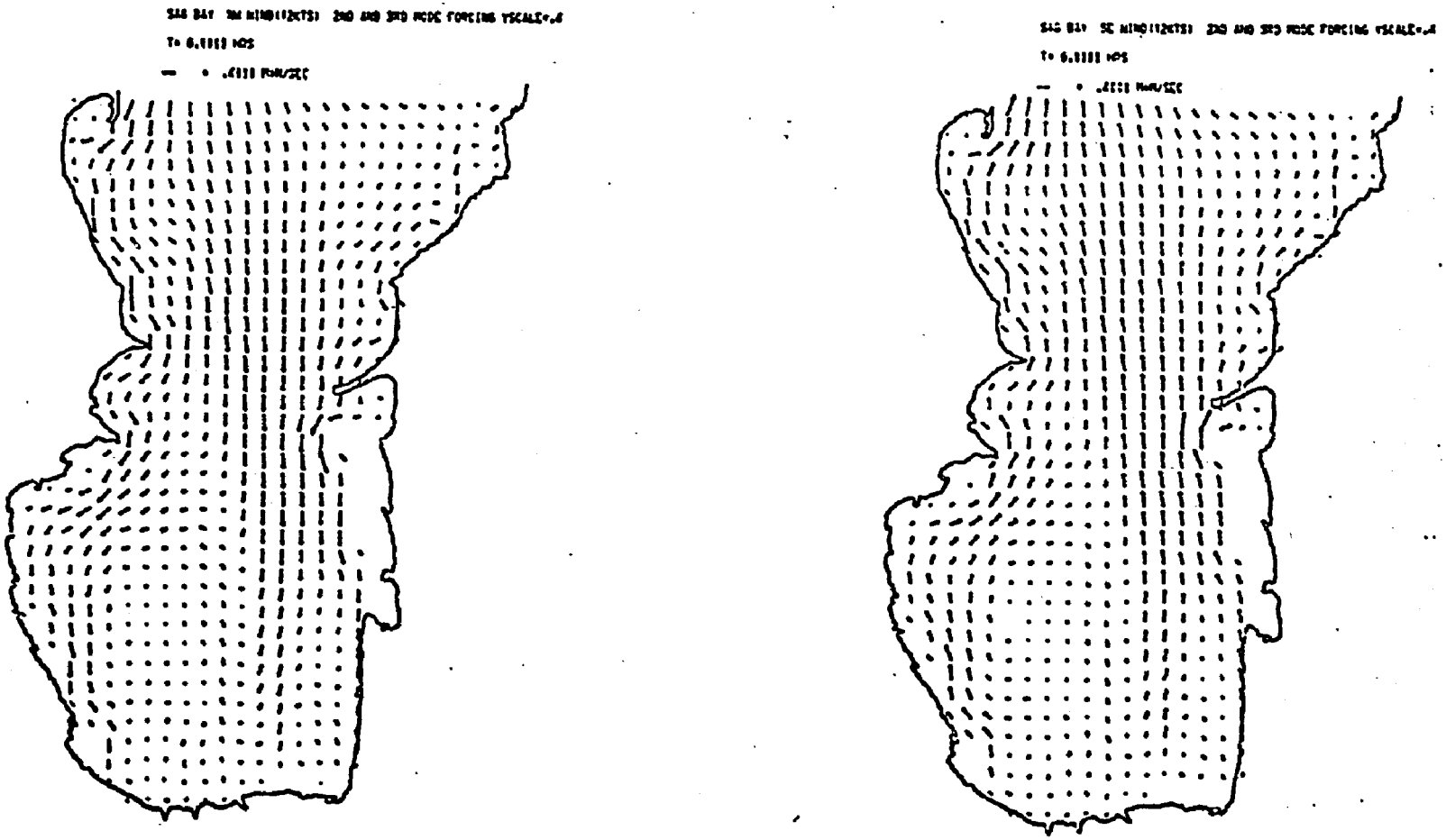
Appendix C

GRAPHICAL PRESENTATION OF FURTHER NUMERICAL SIMULATIONS

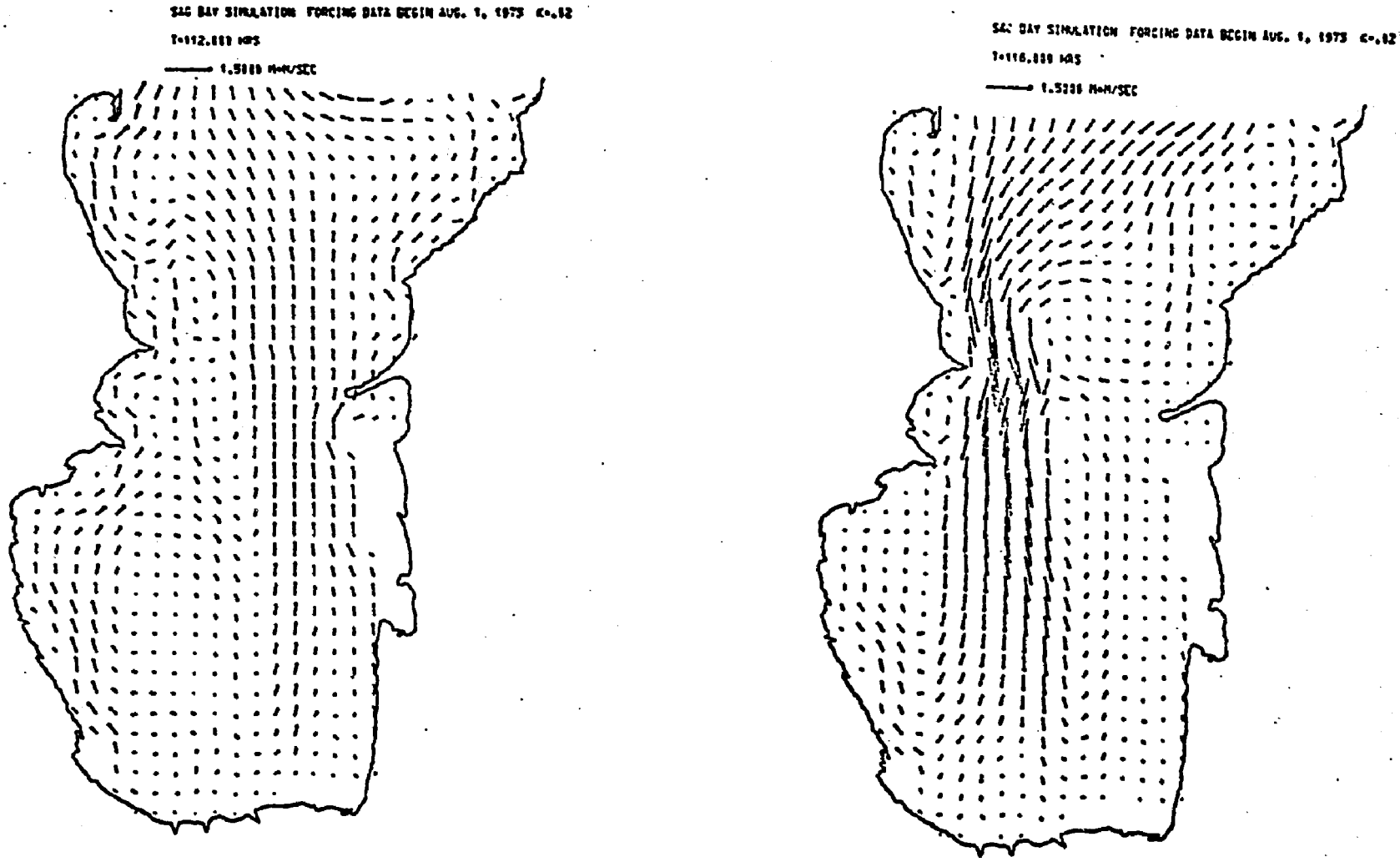
This appendix contains additional results of computer simulation of physical processes in Saginaw Bay. Both transport plots and concentration contour plots are presented, the conditions being largely self-explanatory due to the annotations accompanying each graph. Averaged hourly wind data for the month of August, 1973, is also presented. This information is included for two reasons. First, it is supportive of many conclusions stated within the preceeding text. Second, it is the author's desire to consolidate some of the results of this study owing to the likelihood of future reference.



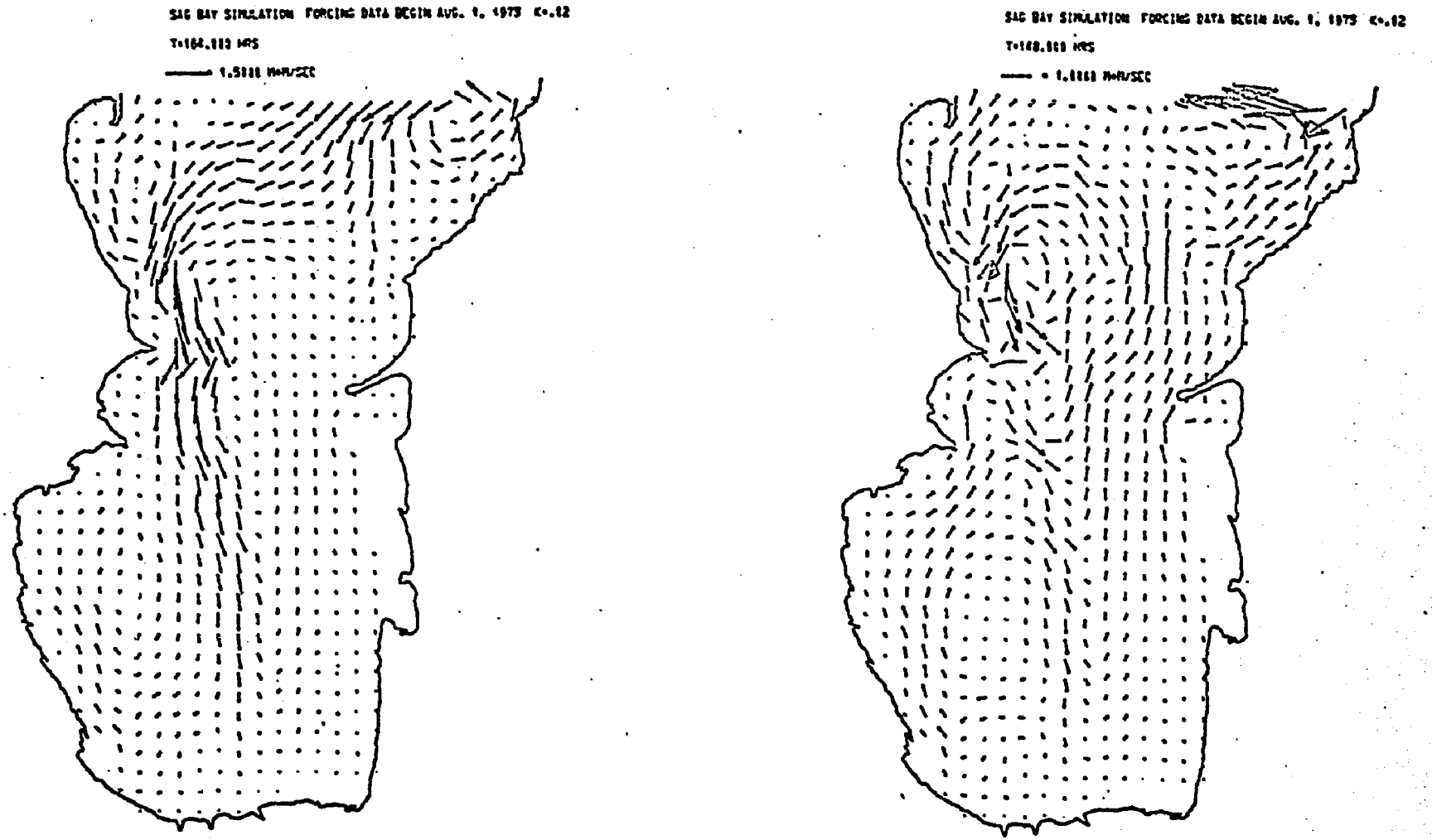
Figures C.1-C.2 Responses to southwest wind (left) and northeast wind (right). Wind speed was 12 kt and weak boundary forcing at 3.3 hr and 2.0 hr was applied.



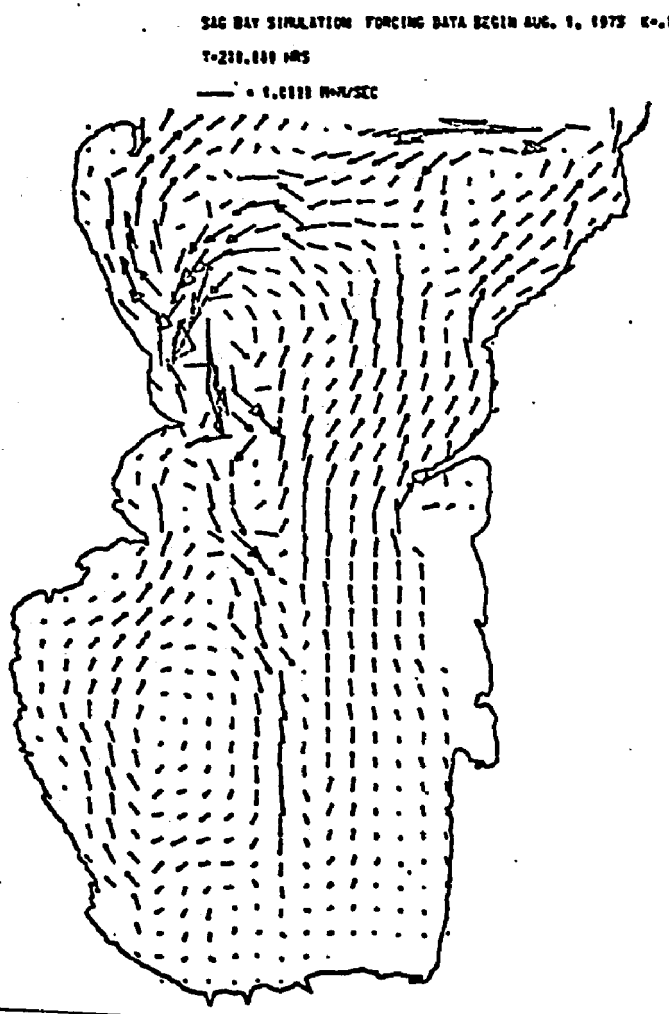
Figures C.3-C.4 Responses to northwest wind (left) and southeast wind (right). Wind speed was 12 kt and weak boundary forcing at 3.3 hr and 2.0 hr was applied.

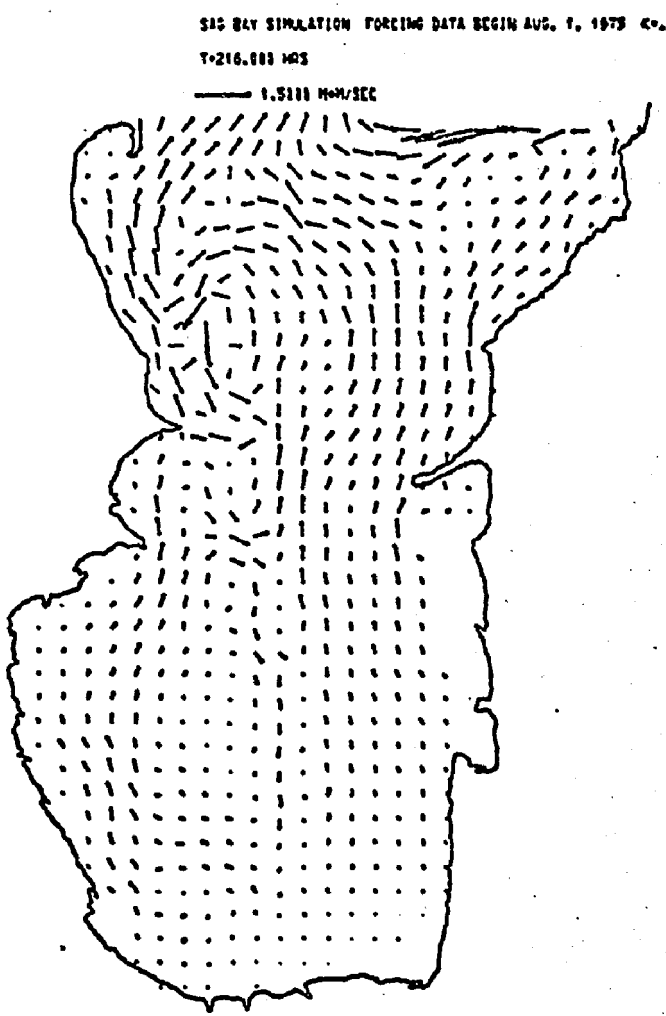


Figures C.5-C.6 Circulations from realistic simulation. Pattern can change significantly in only 4 hr.

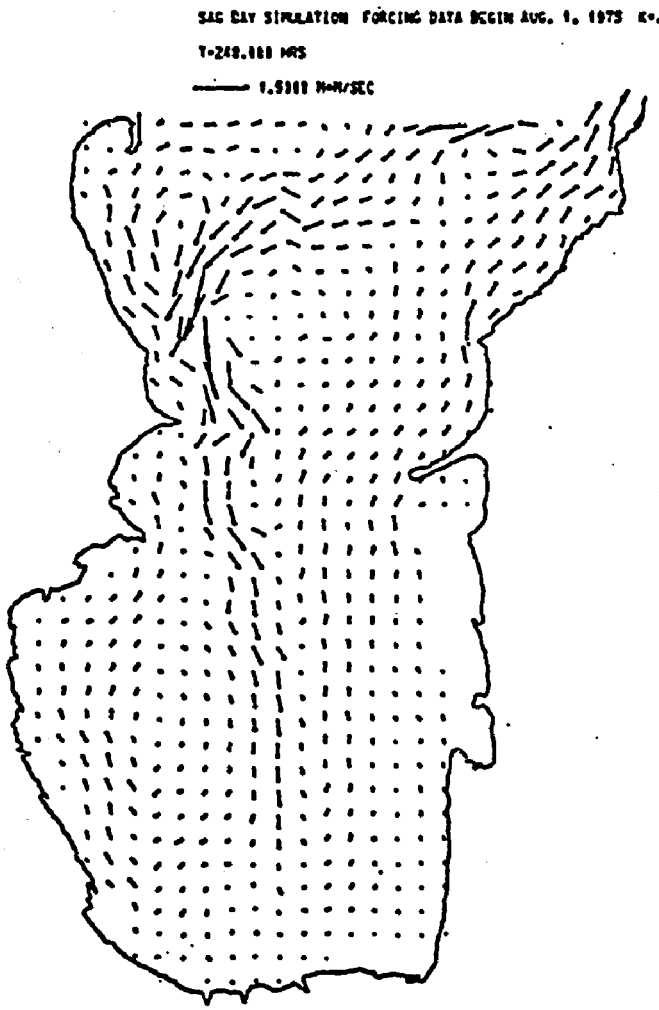


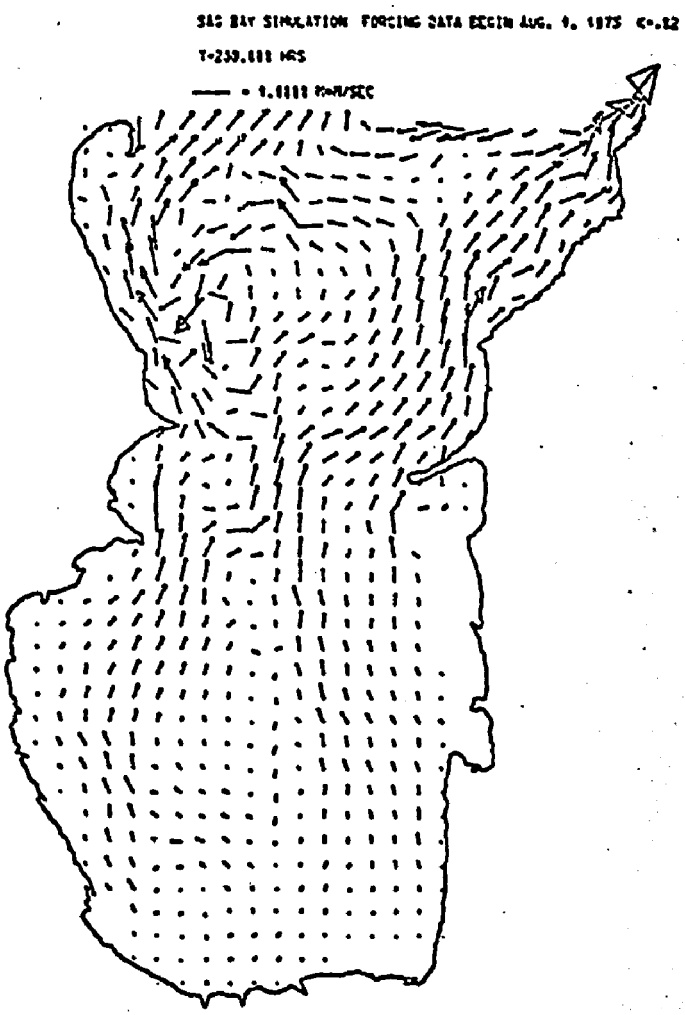
Figures C.7-C.8 Circulations from realistic simulation. Organized flow in channel region (left) sometimes breaks into several sub-gyral patterns (right).



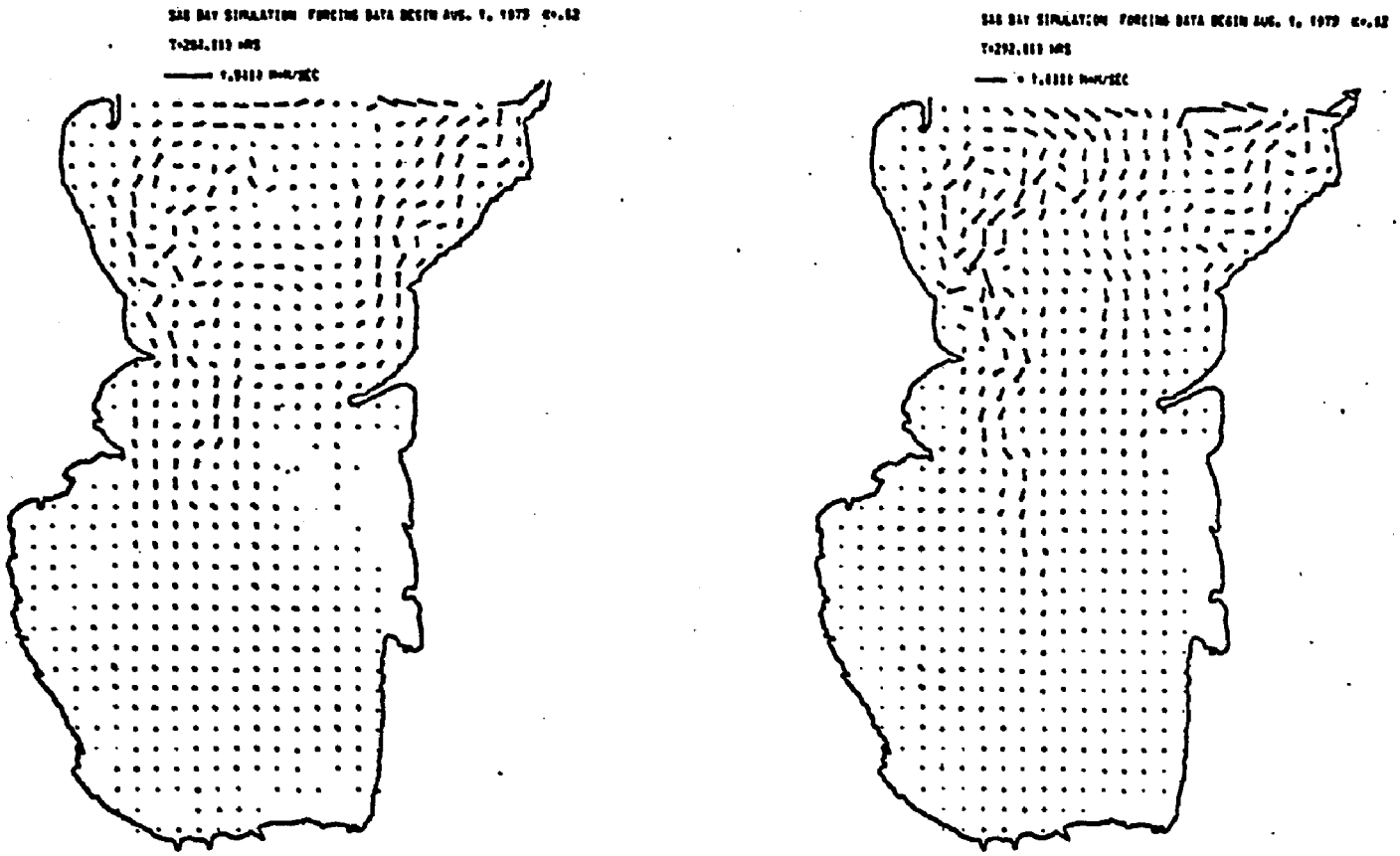


Figures C.9-C.10 Circulations from realistic simulation. Complex patterns often arise when wind subsides after system has developed strong flow regime.

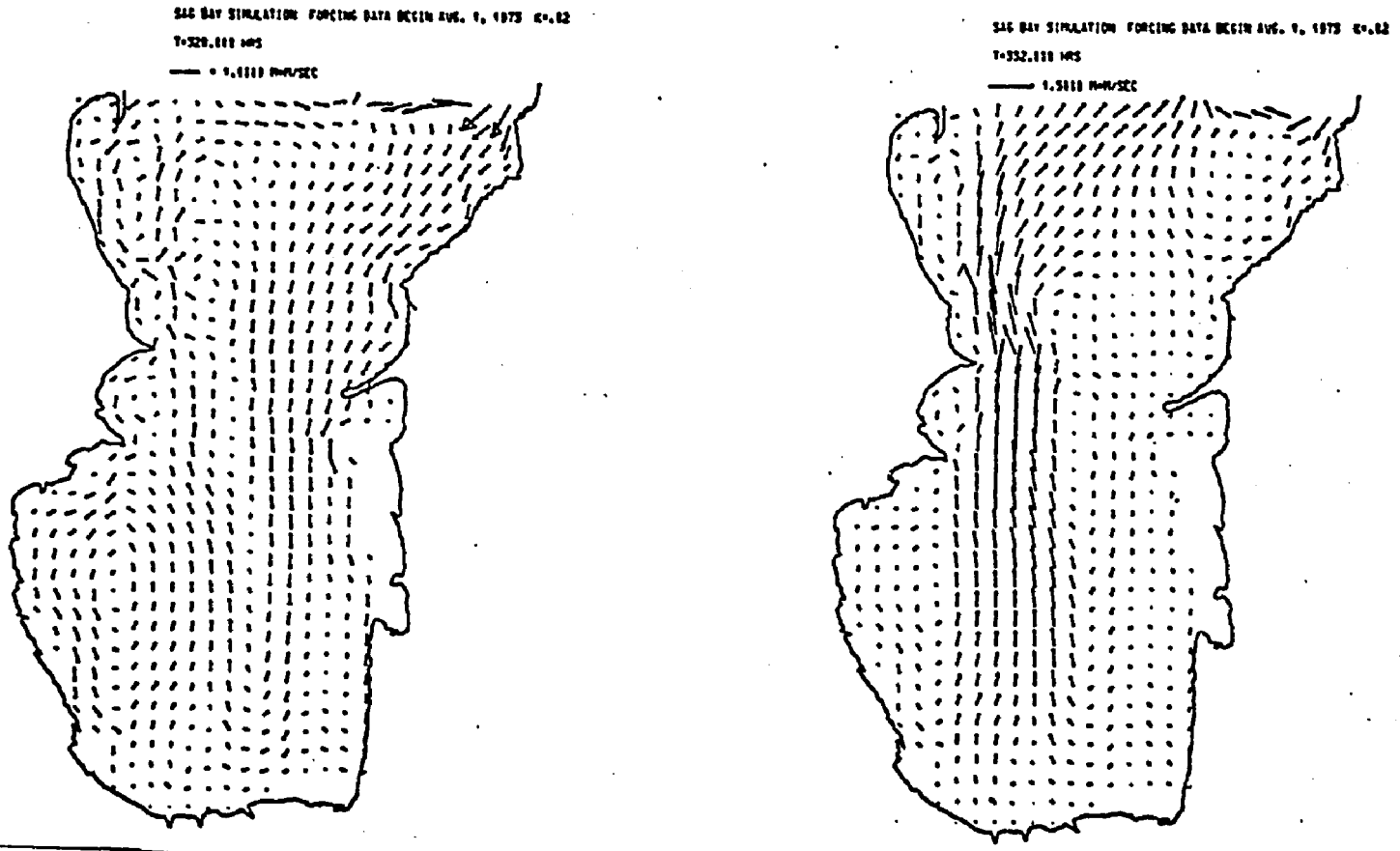




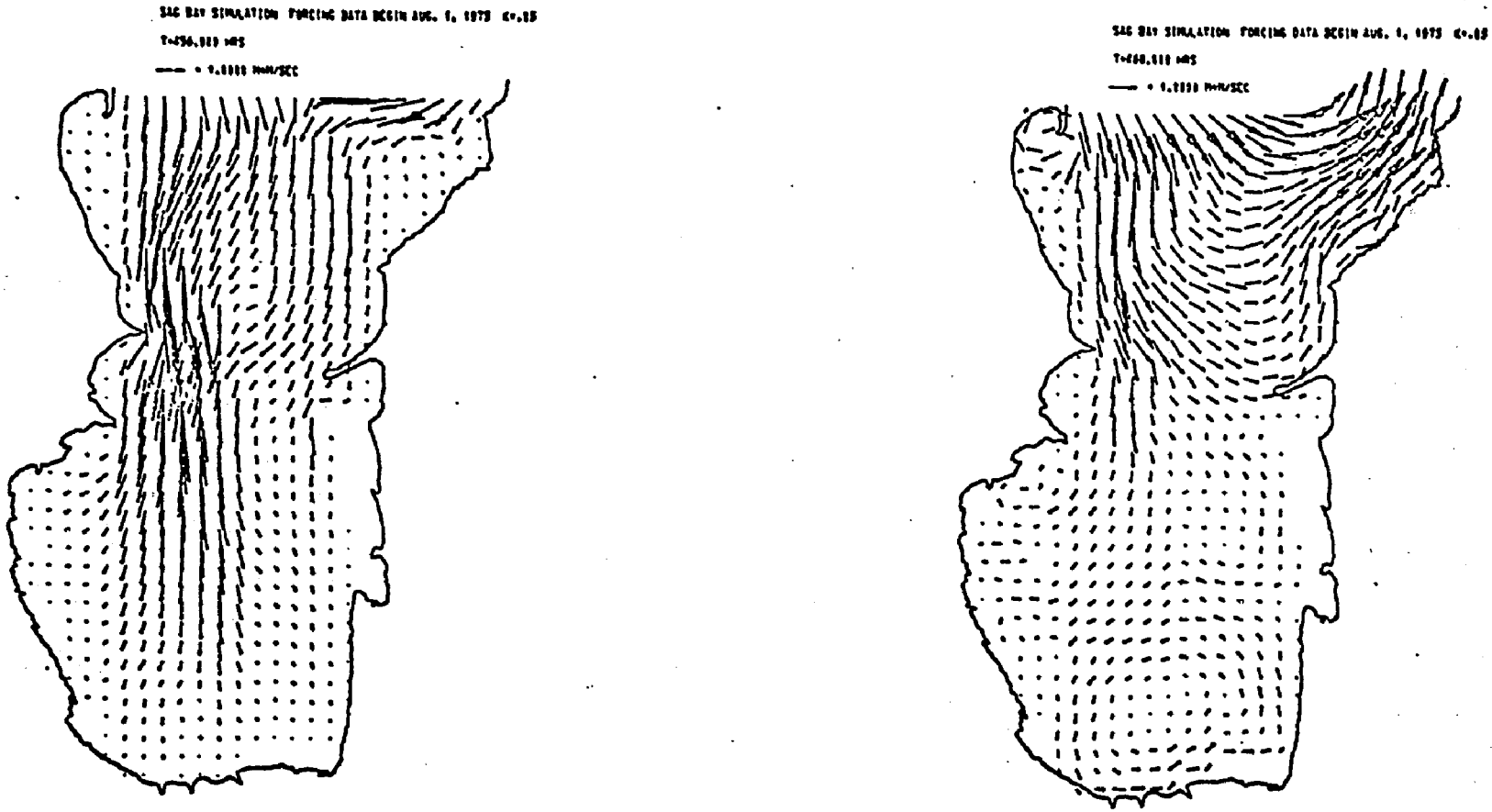
Figures C.11-C.12 Circulations from realistic simulation. Figure on left shows a commomly occurring pattern, figure on right shows complex behavior during outflow conditions.



Figures C.13-C.14 Circulations from realistic simulation. The bay often returns to nearly quiescent conditions after the wind abates.

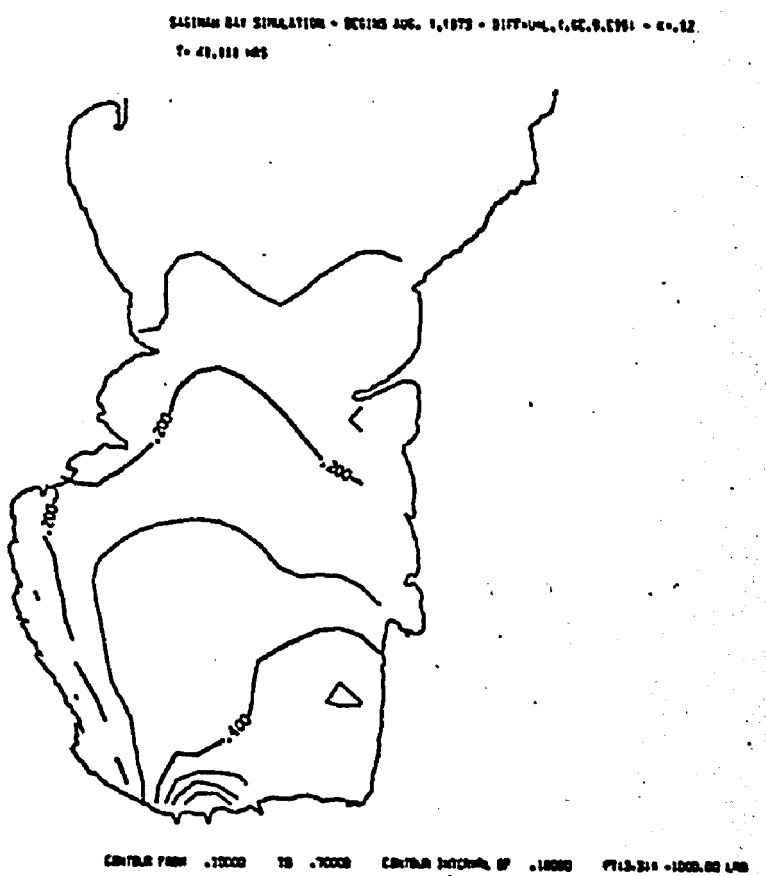


Figures C.15-C.16 Circulations from realistic simulation. Developed pattern caused by northerly wind (left) changes rapidly as subsidence of wind allows release from longitudinal set-up (right).

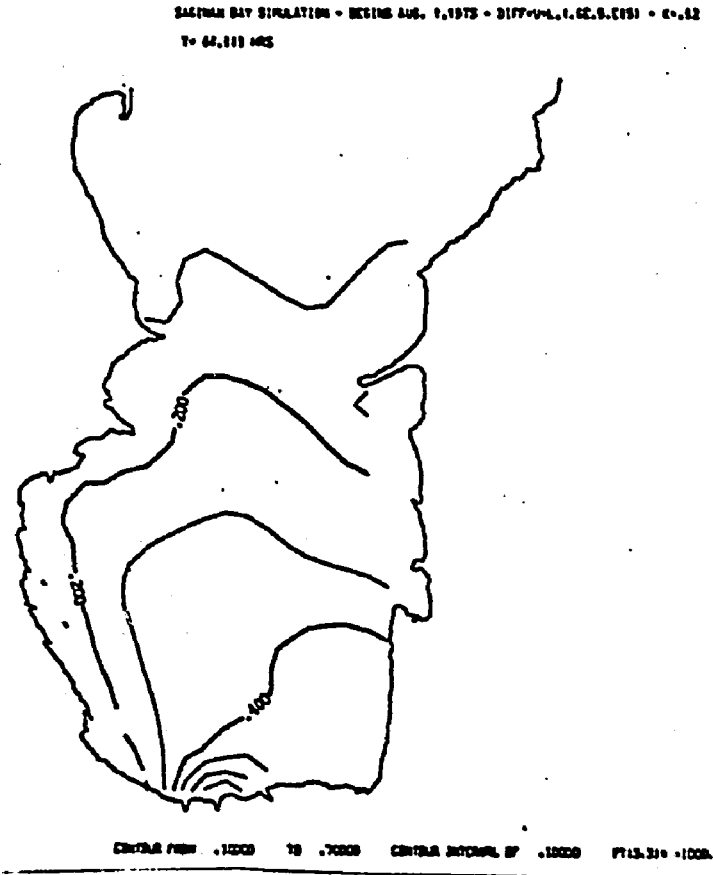


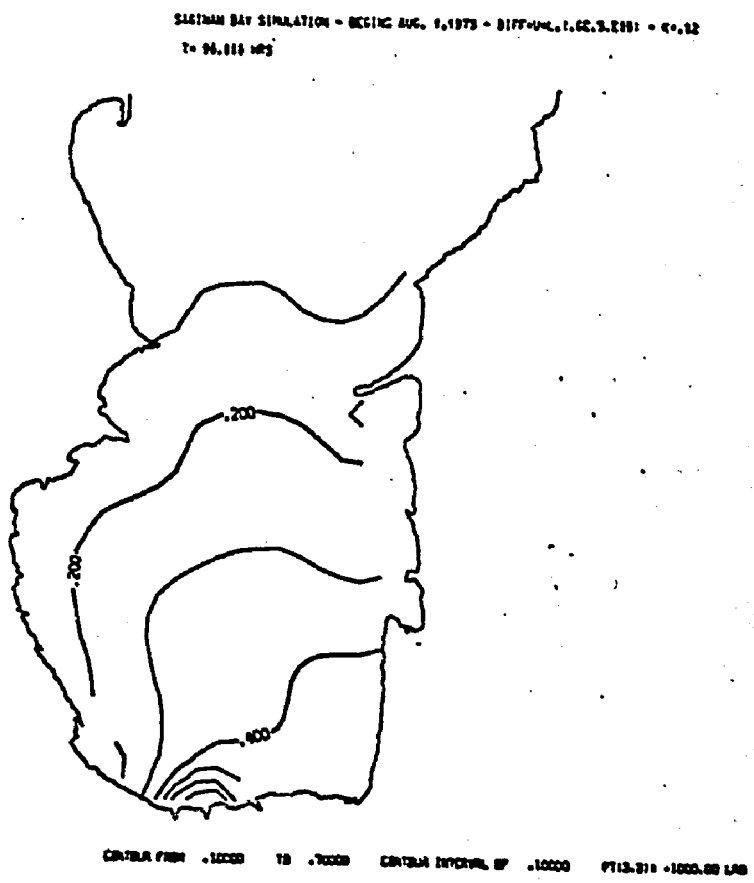
Figures C.17-C.18 Circulations from realistic simulation. Strong inflow (left) is followed by development of longitudinal set-up as wind direction becomes northerly (right).





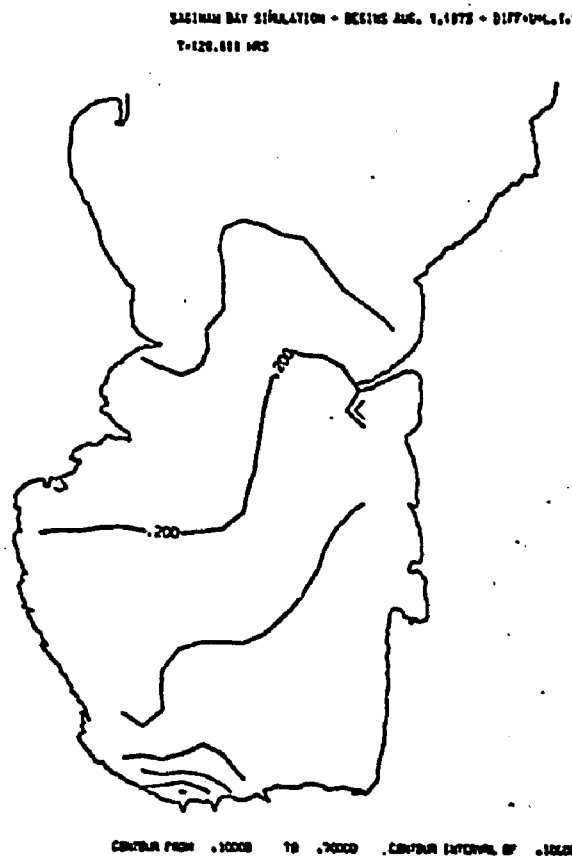
Figures C.19-C.20 Chlorinity contours from realistic simulation. Strong gradients in the initial matter distribution (left) disappear quickly in overly diffusive system (right).



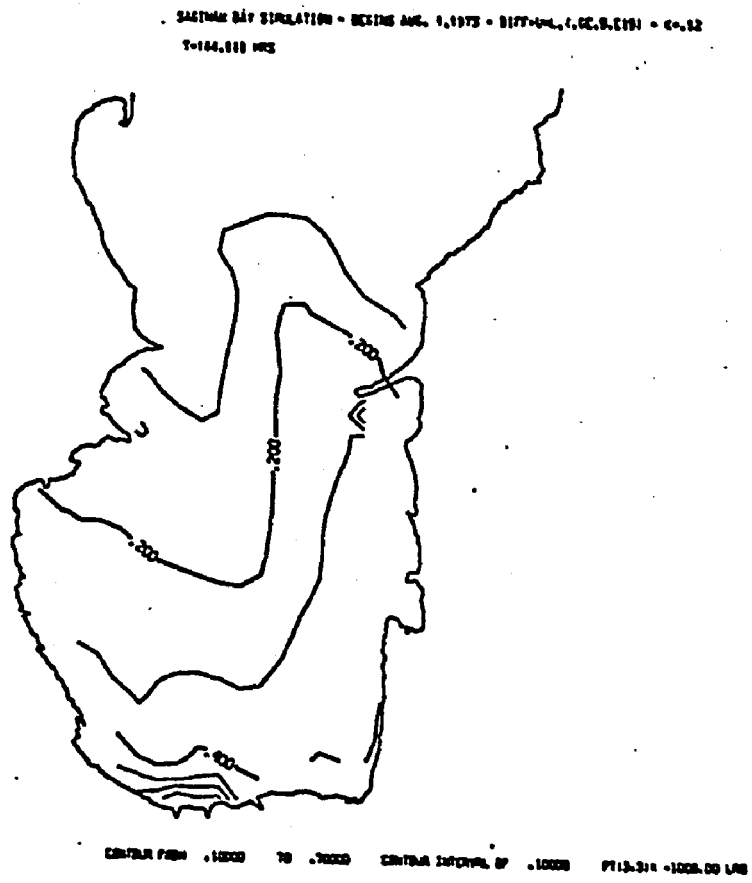


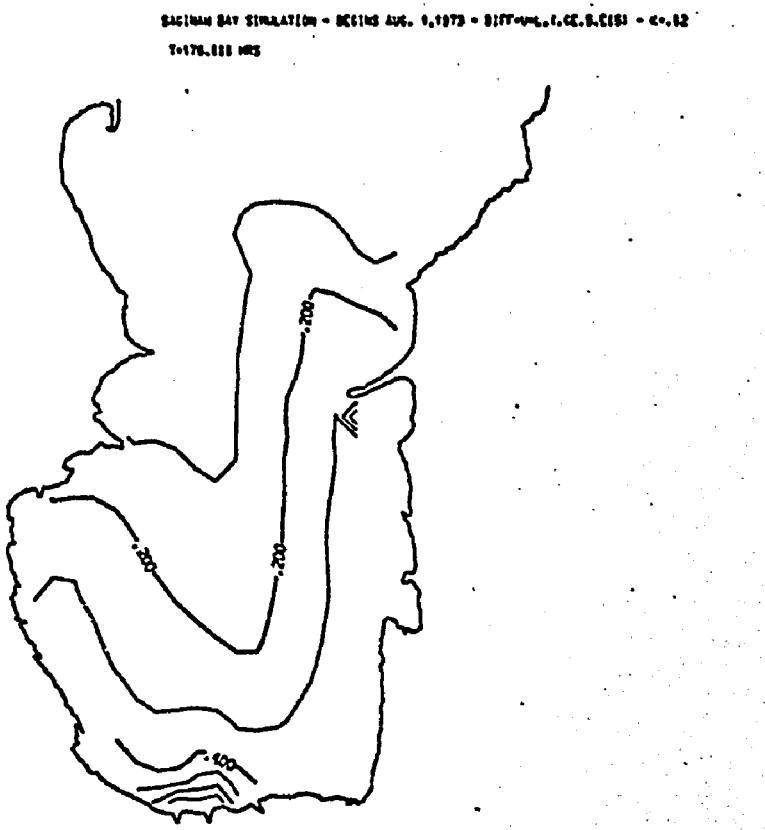
Figures C.21-C.22 Chlorinity contours from realistic simulation. Weak circulation during this period causes pattern to change slowly.



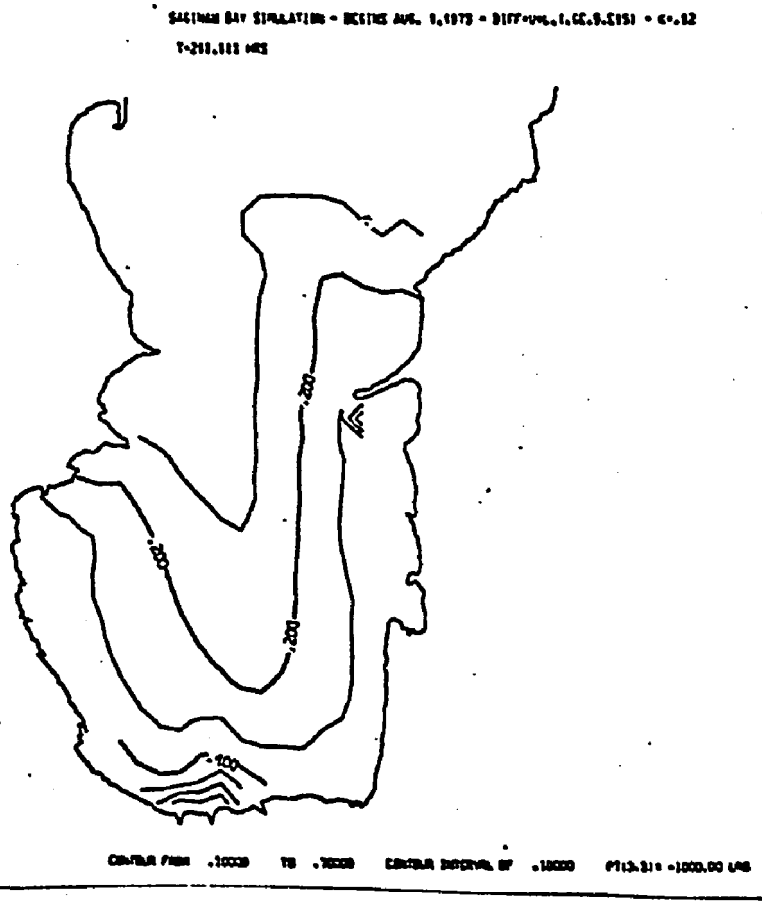


Figures C.23-C.24 Chlorinity contours from realistic simulation. Inflow in channel region due to predominant southwesterly winds freshens bay along its northwest shore.



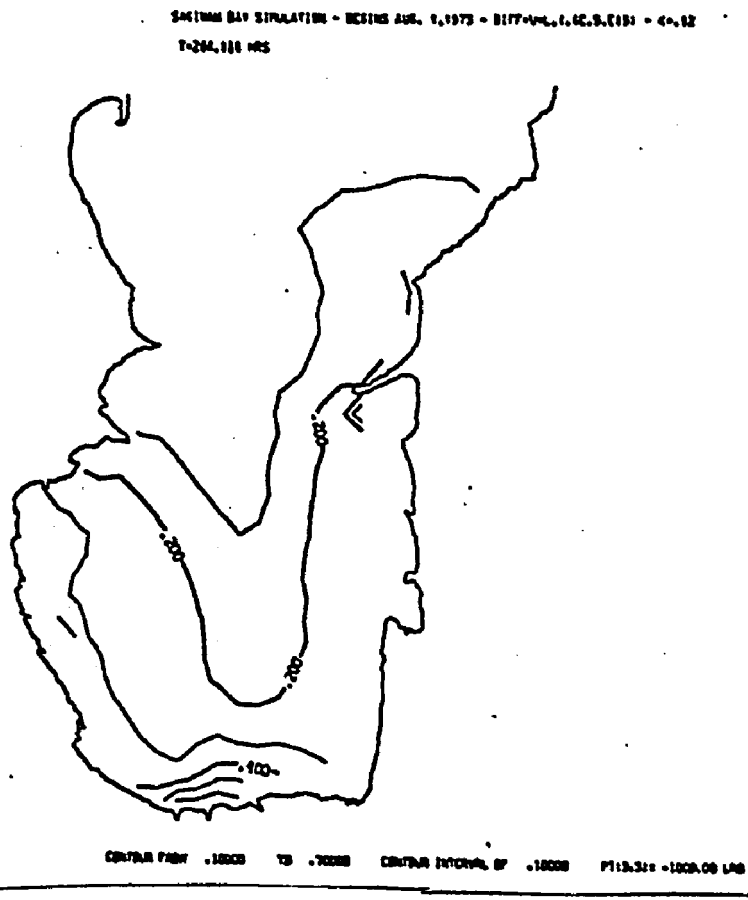


Figures C.25-C.26 Chlorinity contours from realistic simulation. Boundary current arising under predominant southwesterly wind causes fluid with higher concentration to move lakeward along southeast shore of bay.



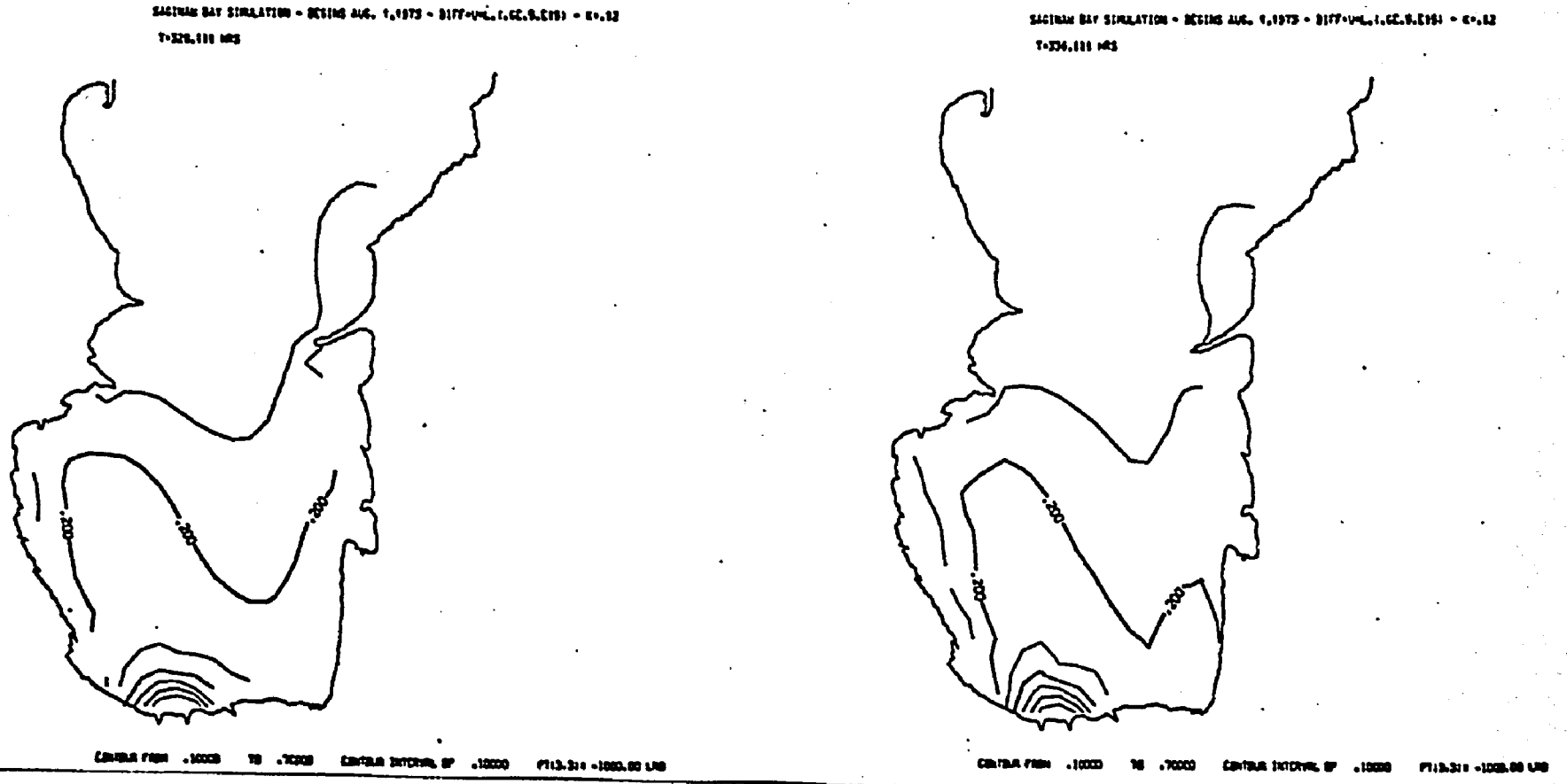


Figures C.27-C.28 Chlorinity contours from realistic simulation. Effects of strong inflow through channel connecting inner and outer bays is evident.

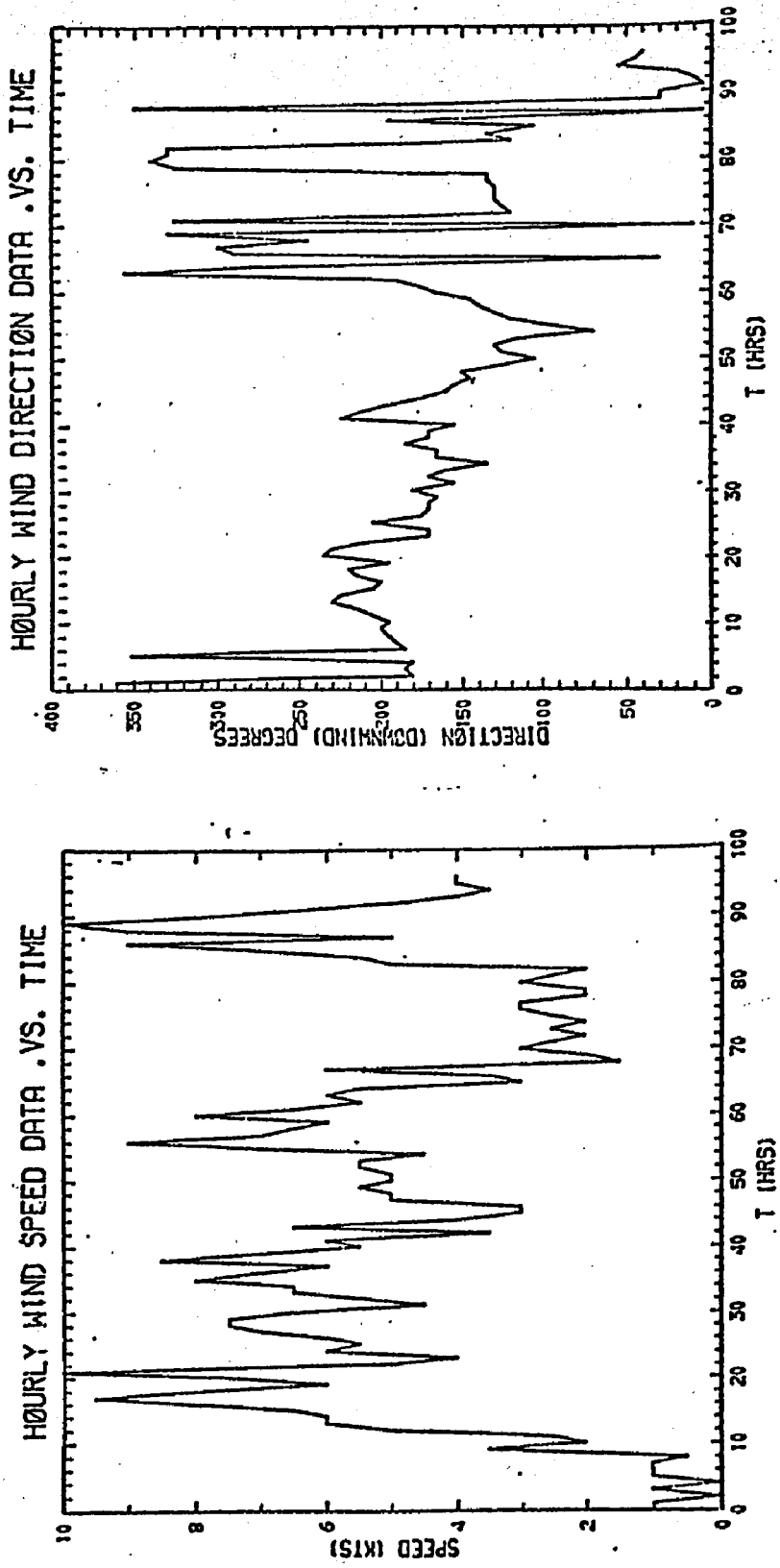




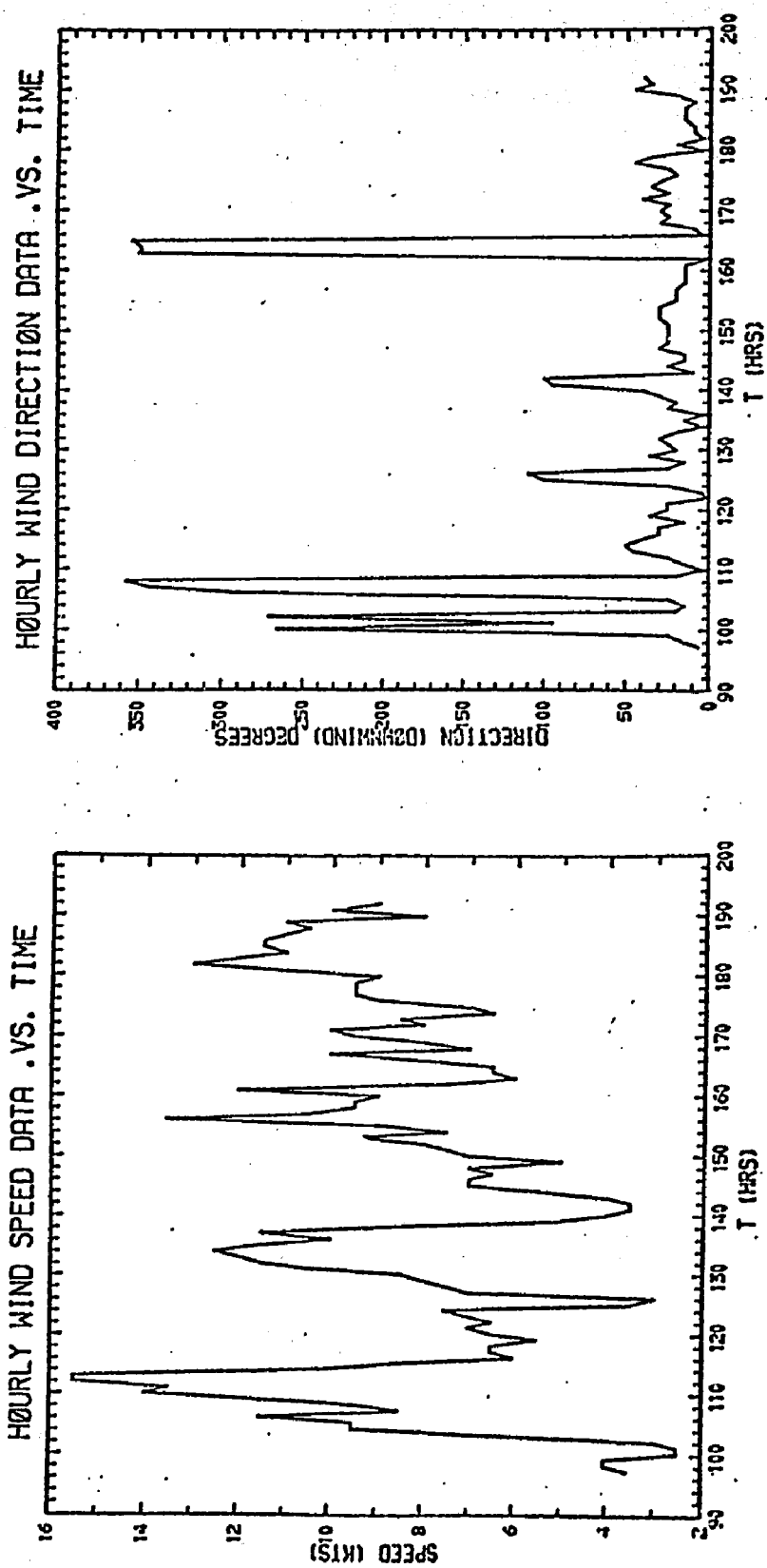
Figures C.29-C.30 Chlorinity contours from realistic simulation. Effects of diffusion coefficients which are too large are shown. Concentration gradients are being severely reduced.



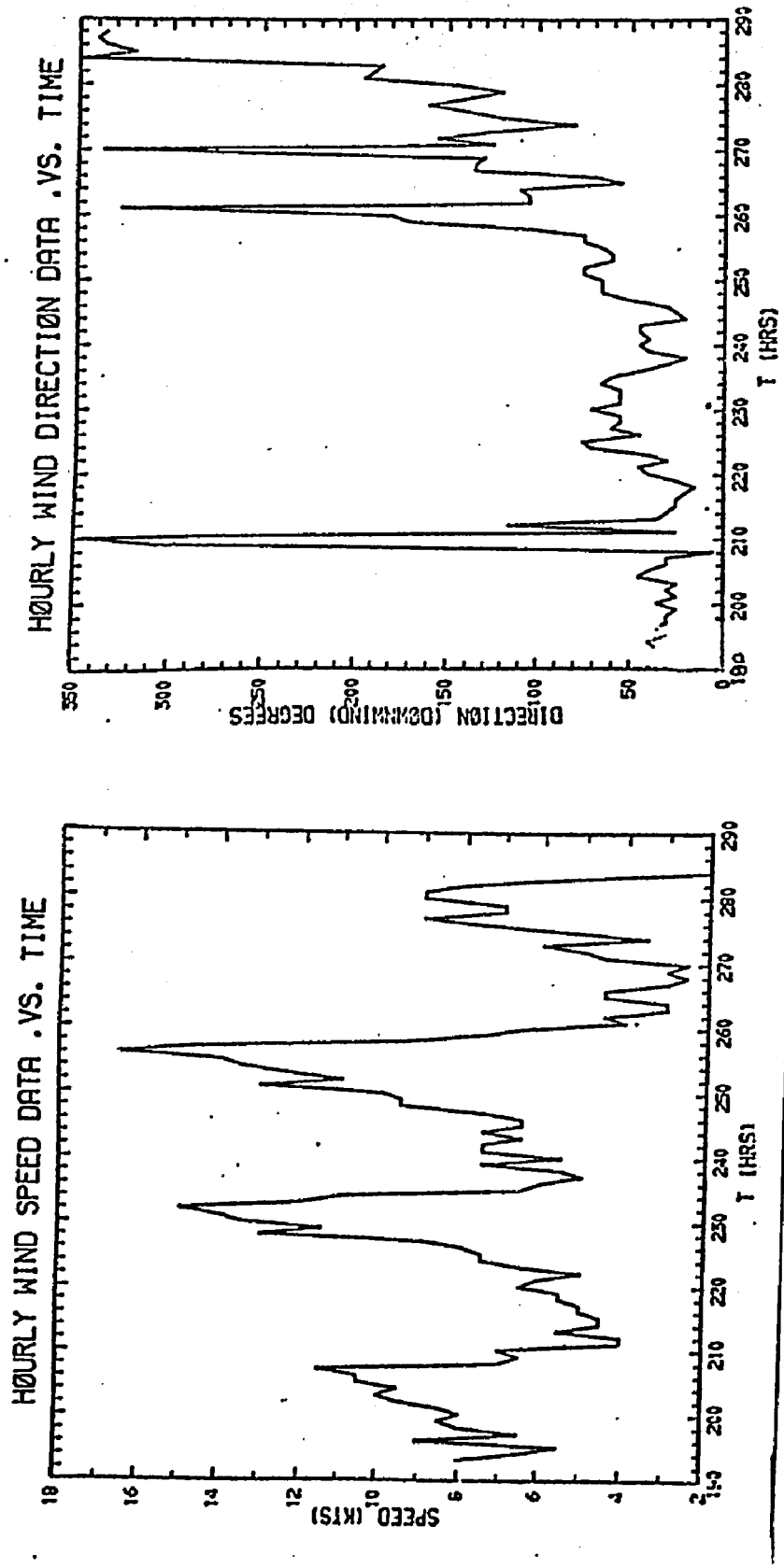
Figures C.31-C.32 Chlorinity contours from realistic simulation. Entire bay freshens shortly after the onset of strong northerly wind.



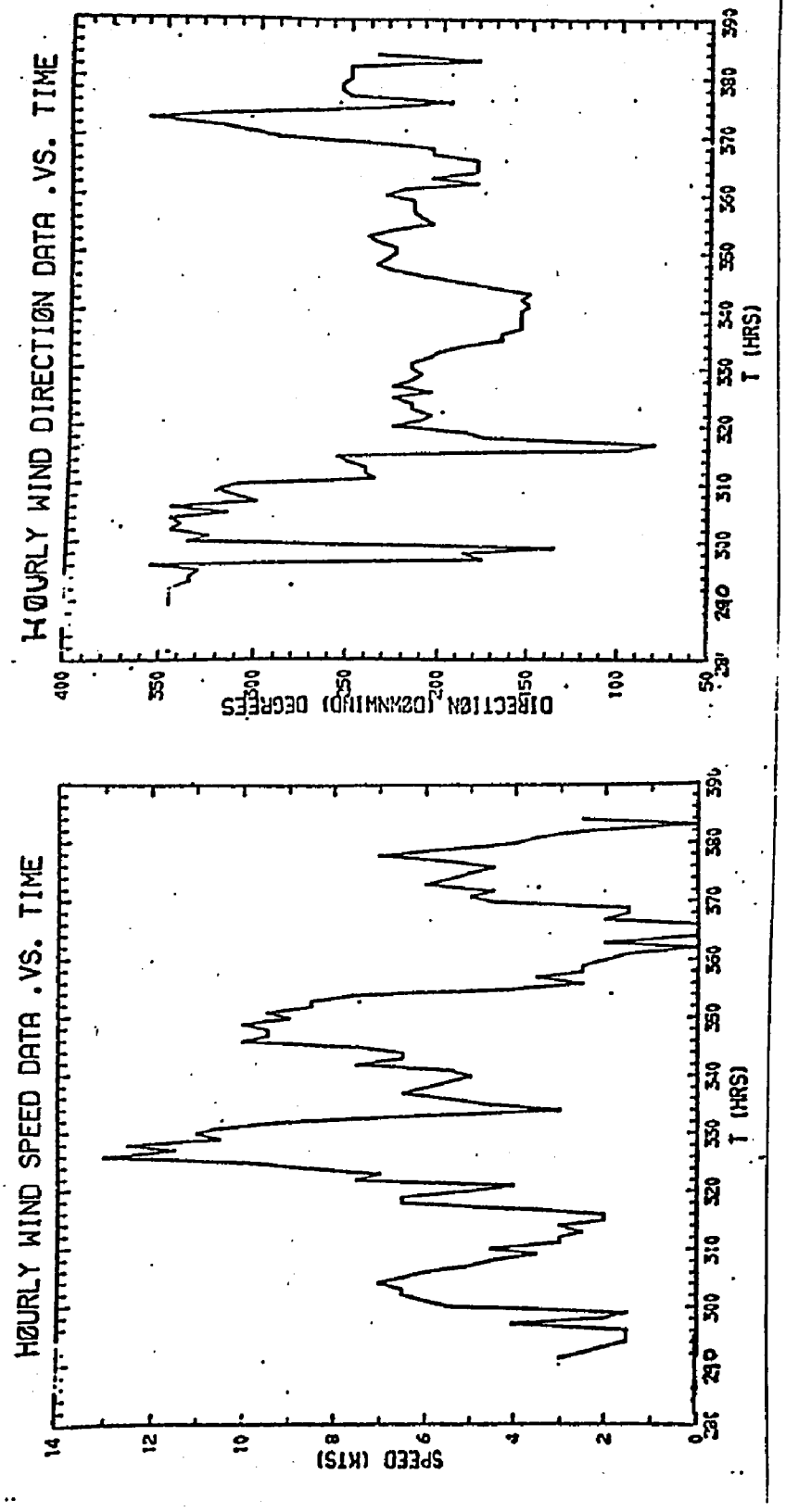
Figures C.33-C.34 Averaged hourly wind data used to generate external forcing. Data begins 1 August 1973.



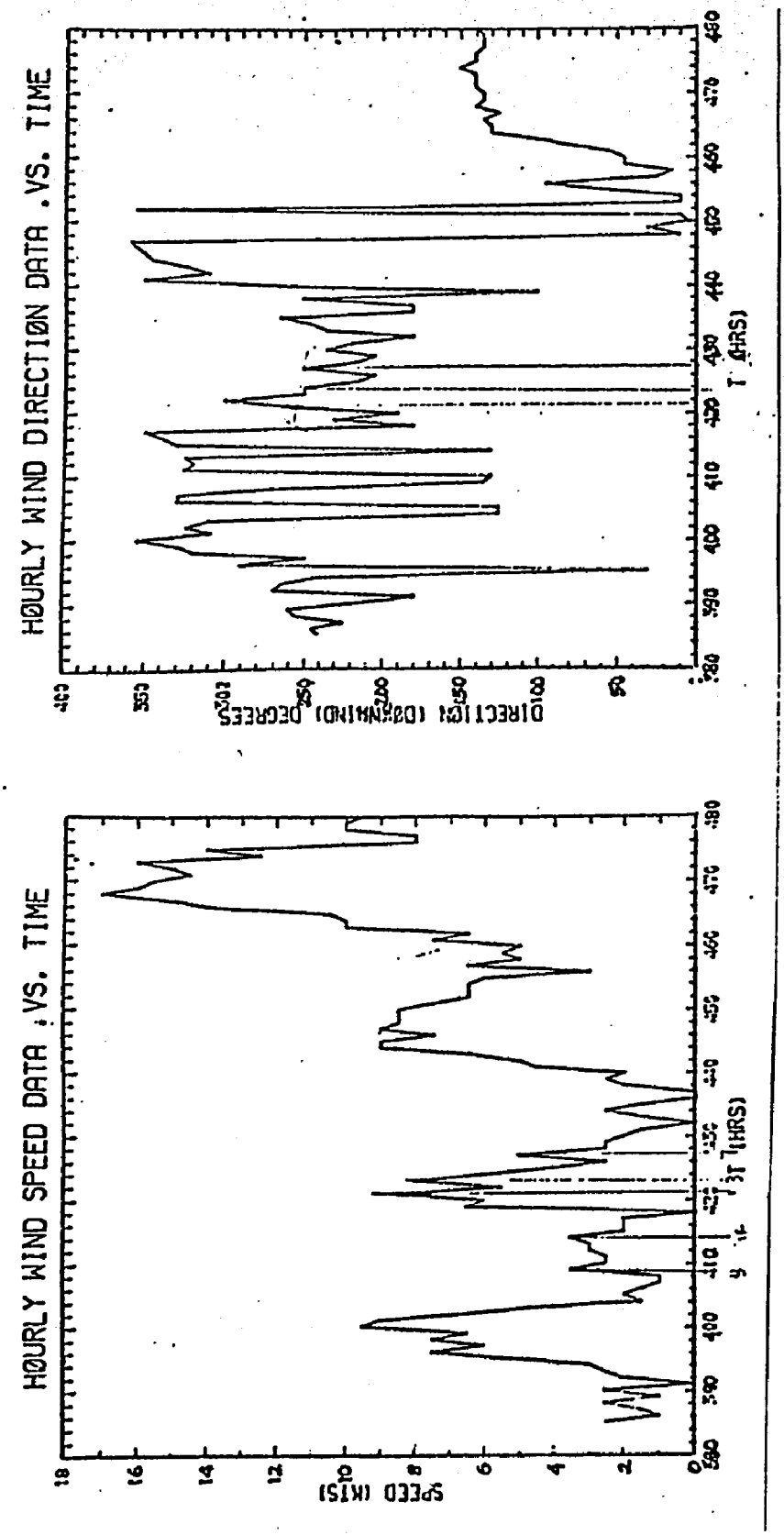
Figures C.35-C.36 Averaged hourly wind data used to generate external forcing. Data begins 1 August 1973.



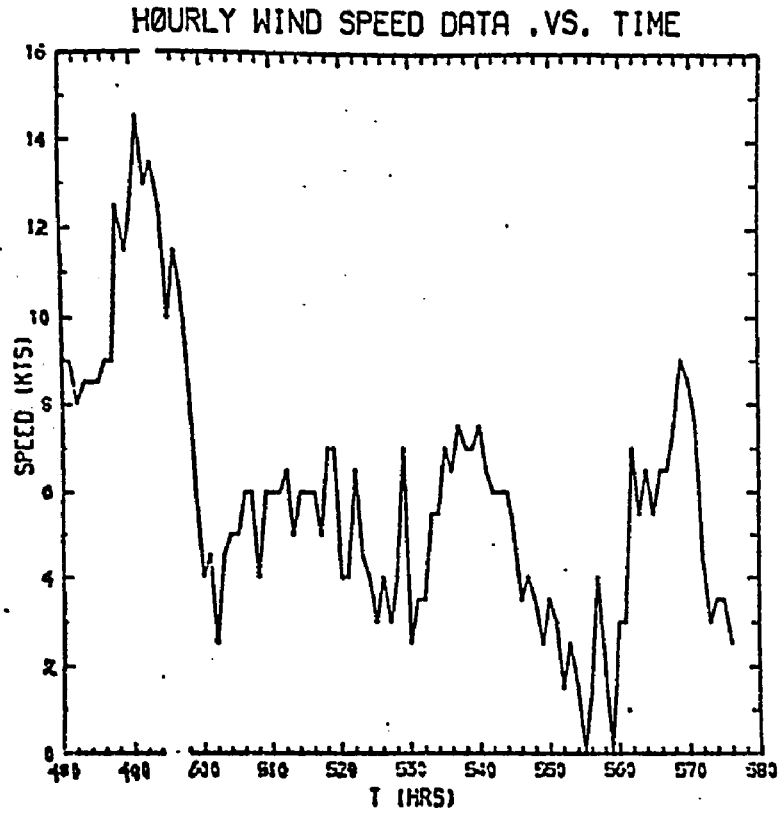
Figures C.37-C.38 Averaged hourly wind data used to generate external forcing. Data begins 1 August 1973.

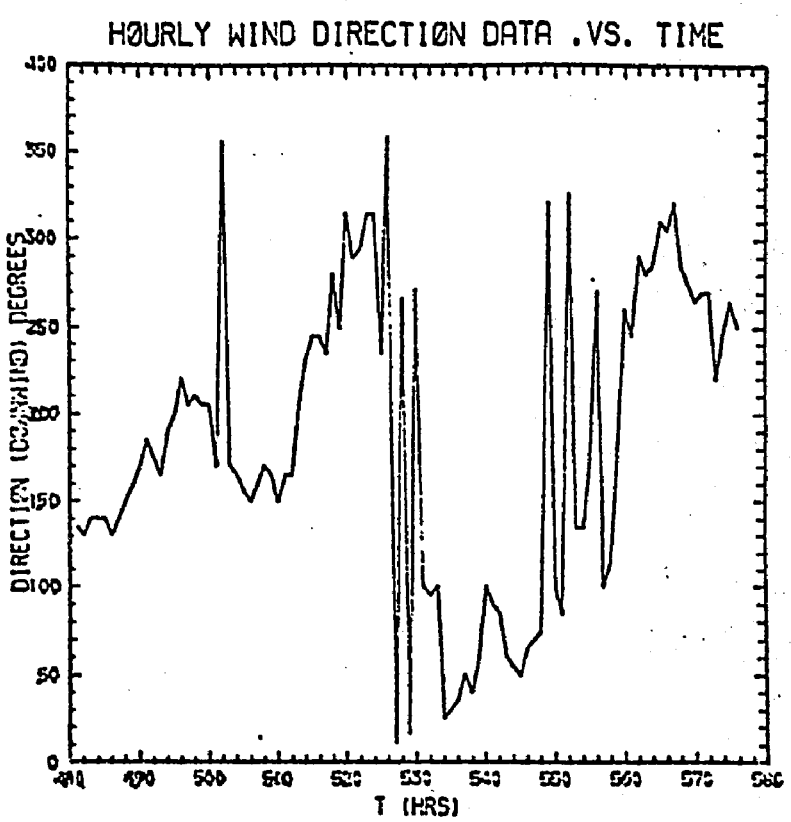


Figures C.39-C.40 Averaged hourly wind data used to generate external forcing. Data begins 1 August 1973.

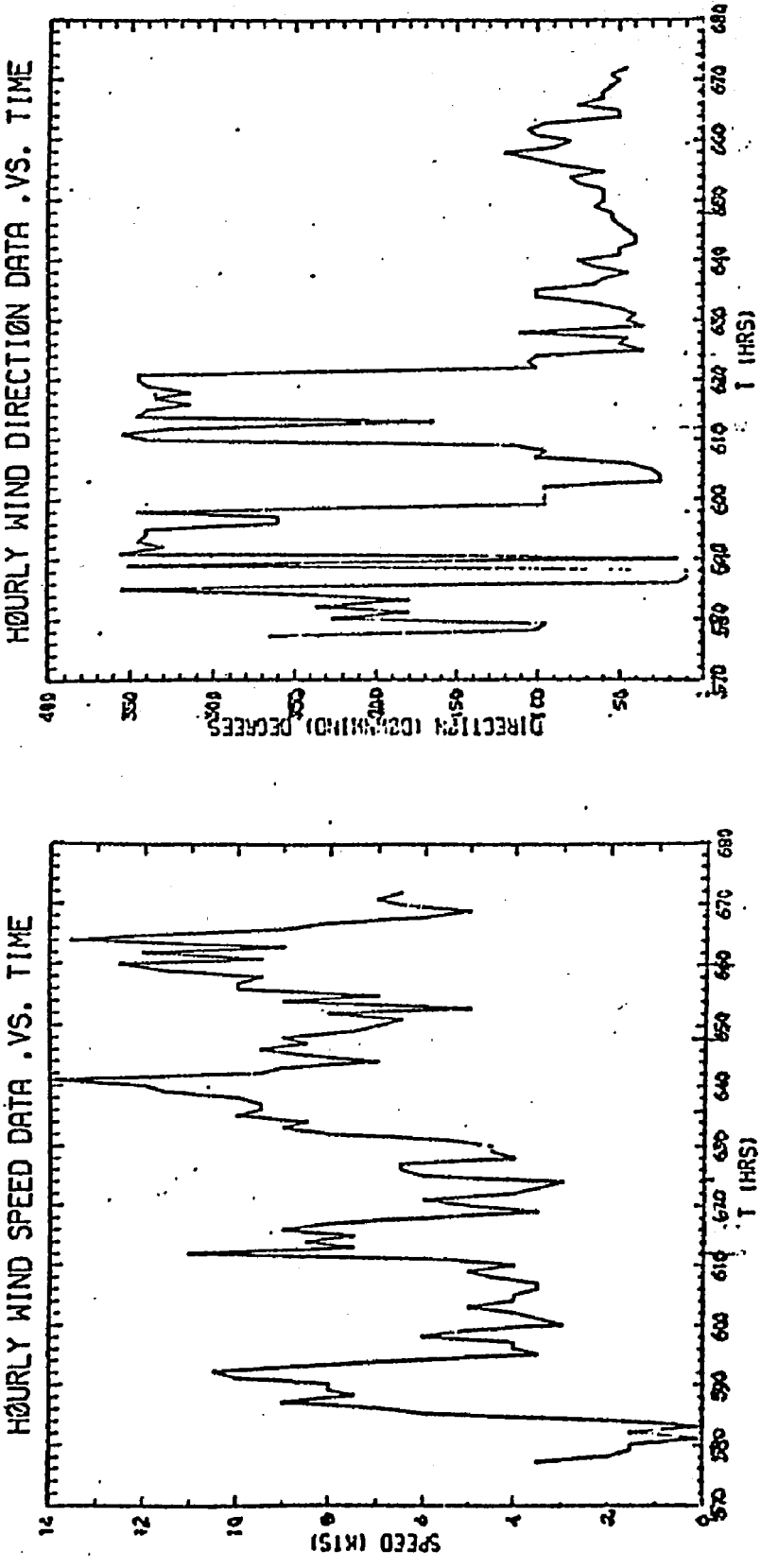


Figures C.41-C.42 Averaged hourly wind data used to generate external forcing. Data begins 1 August 1973.

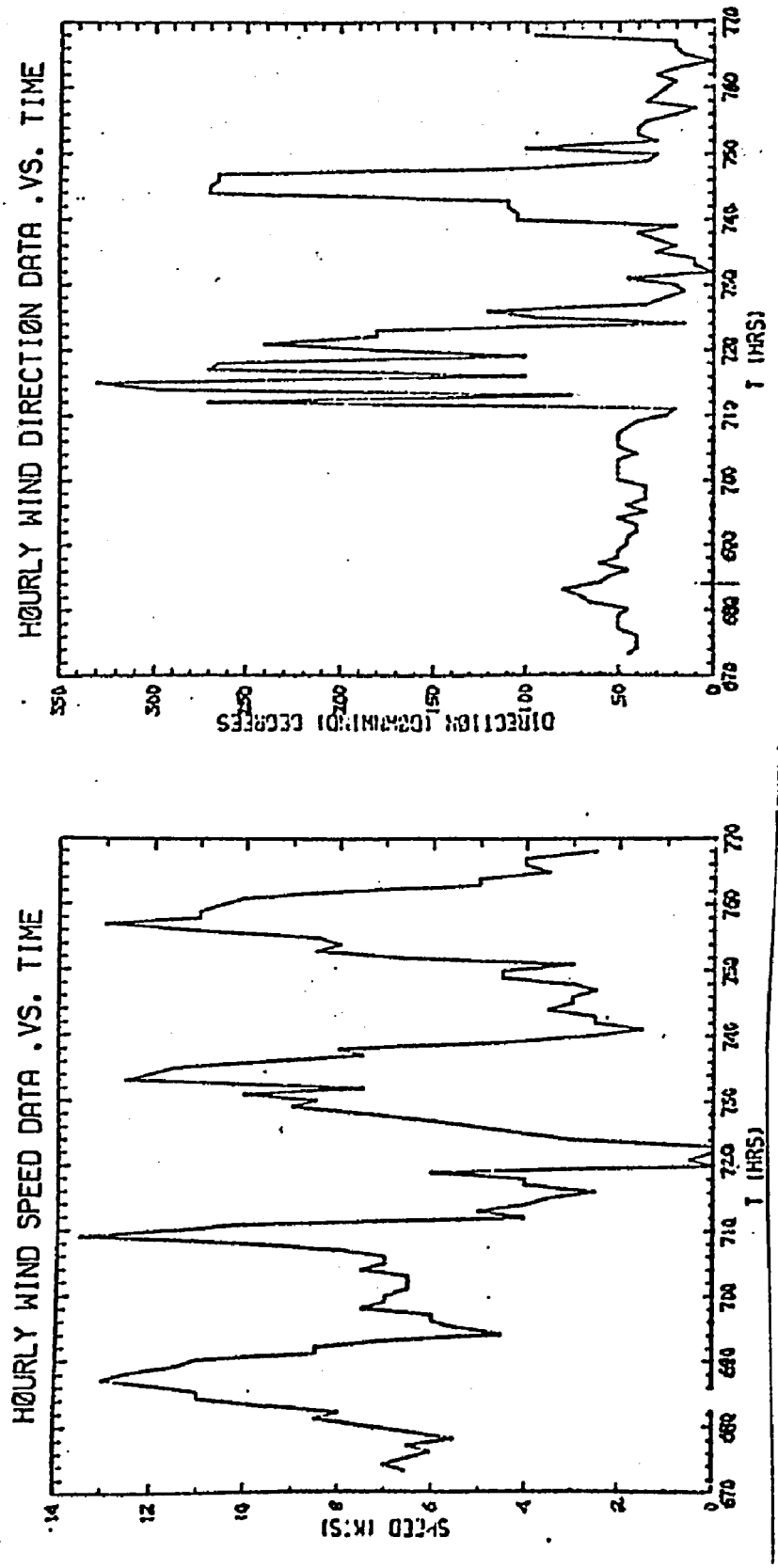




Figures C.43-C.44 Averaged hourly wind data used to generate external forcing. Data begin 1 August 1973.



Figures C.45-C.46 Averaged hourly wind data used to generate external forcing. Data begin 1 August 1973.



Figures C.47-C.48 Averaged hourly wind data used to generate external forcing, Data begin 1 August 1973.

REFERENCES

Ahrnsbrak, W.F. and R.M. Ragotzkie, 1970: Mixing processes in Green Bay. Proc. 13th Conf. Great Lakes Res., 880-890.

Beeton, A.M., S.H. Smith, and F.H. Hooper, 1967: Physical Limnology of Saginaw Bay, Lake Huron. Great Lakes Fishery Commission, technical report no. 12.

Bendat, J.S. and A.C. Piersol, 1966: Measurement and analysis of random data. John Wiley and Sons, New York.

Blackman, R.B., and J.W. Tukey, 1958: The measurement of power spectra. Dover Publications, New York.

Bowden, K.F., 1953: Note on wind drift in a channel in the presence of tidal currents. Proc. Roy. Soc., 219, 426-446.

Bryan, K. and M.D. Cox, 1967: A numerical investigation of the general oceanic circulation. Tellus, 19, 54-80.

_____, 1968a: A nonlinear model of an ocean driven by wind and differential heating: Part I. Description of the three-dimensional velocity and density fields. Jour. Atmos. Sci., 25, 945-967.

_____, 1968b: A nonlinear model of an ocean driven by wind and differential heating: Part II. An analysis of the heat, vorticity, and energy balance. Jour. Atmos. Sci., 25, 968-978.

_____, S. Manabe, and M.J. Spelman, 1975: A global ocean-atmosphere climate model: Part II. The oceanic circulation. Jour. Phys. Oceanogr., 5, 30-46.

Canale, R., 1975: A model for phosphorus in Saginaw Bay. Eighteenth Proc. Great Lakes Res. (abstract).

Charney, J.G., R. Fjorfort, and J. von Neumann, 1950: Numerical integration of the barotropic vorticity equation. Tellus, 4, 237-254.

Courant, R., and D. Hilbert, 1953: Methods of mathematical physics, vol. 1 1962: Partial differential equations, vol. 2. Interscience, New York.

Crowley, W.P., 1968: A global numerical ocean model: Part I. Jour. Comp. Phys., 3, 111-147.

Csanady, G.T., 1963: Turbulence and diffusion in the Great Lakes Pub. no. 11, Great Lakes Research Division, The University of Mich.

Csanady, G.T., 1973: Wind induced barotropic motions in long lakes. J. Phys. Oceanogr., 3, 429-438.

Davidson, K.L., 1970: An investigation of the influence of water waves on the adjacent air flow. Ph.D. thesis, Dept. of Meteorology and Oceanography, The University of Mich.

Davies, H.C., 1973: On the initial -boundary value problem of some geophysical fluid flows. Jour. Comp. Phys., 13, 398-422.

Deacon, E.L. and E.K. Webb, 1960: "Dependence of drag on atmospheric stability" in The Sea, vol. I, ed. by M.N. Hill, Interscience, New York.

Defant, F., 1953: Theorie der seiches des Michigansees und ihre Abwandlung durch Wirkung der Corioliskraft. Archiv. Met. Geophys. Bioklimatol., Wien, A, 6, 218-241.

Douglas, J., Jr ., 1955: On the numerical integration of $\partial^2 u/\partial x^2 + \partial^2 y/\partial y^2 = \partial u/\partial t$ by implicit methods. Jour. Soc. Indus. Appl. Math., 3, 1, 42-65.

_____, 1957: A note on the alternating direction implicit method for the numerical solution of heat flow problems. Proc. Am. Math. Soc., 8, 409-412.

Elvius, T., A. Sundstrom, 1973: Computationally efficient schemes and boundary conditions for a fine-mesh barotropic model based on the shallow-water equations. Tellus, 25, 2, 132-156.

Enochson, L.D. and R.K. Otnes, 1968: Programming and analysis for digital time series data. The shock and vibration information center, United States Department of Defense, Navy publication and printing service office.

Fischer, G., 1959: Ein numerisches Verfahren zur Errechnung von Windstau und Gezeiten in Randmeeren. Tellus, 11, 60-76.

Garabedian, P.R., 1964: Partial differential equations. John Wiley and Sons, New York.

Gedney, R.T. and W. Lick, 1970: Numerical calculations of the steady-state, wind-driven currents in Lake Erie. Proc. 13th Conf. Great Lakes Res., 829-838.

_____, 1971: Numerical calculations of the wind-driven currents in Lake Erie and comparison with measurements. Proc. 14th Conf. Great Lakes Res., 454-466.

Groen, P. and G.W. Groves, 1960: "Surges" in The Sea. vol. I, ed. by M.N. Hill, Interscience, New York, 611-646.

Hamblin, P.F., 1971: An investigation of horizontal diffusion in Lake Ontario. Proc. 14th Conf. Great Lakes Res., 570-577.

Hansen, W., 1956: Theorie zur Errechnung des Wasserstands und der Strongungen in Randeeren nebat Anwendungen. Tellus, 8, 287-300.

_____, 1962: "Tides" in The Sea, vol. I, ed. by M.N. Hill, Interscience, New York, 764-801.

Harris, D.L. and C.P. Jelasnianski, 1964: Some problems involved in the numerical solution of tidal hydraulics equations. Monthly Weather Rev., 92, 409-422.

Ippen, A.T., 1966: Estuary and coastline hydrodynamics. McGraw-Hill, New York.

Kaplan, W., 1952: Advanced calculus. Addison-Wesley, Mass.

_____, 1962: Operational methods for linear systems. Addison-Wesley, Mass.

Kreiss, H. and J. Oliger, 1973: Methods for the approximate solution of time dependent problems. GARP, pub. no. 10, World Meteorological Organization.

Kuskova, T.V., 1968: Difference method for calculating the flow of a viscous incompressible fluid. Sb. Rabot Vyshisl, Tsentra Most. Un-ta, 7, 16-27.

Lamb, H., 1932: Hydrodynamics, 6th edition. Cambridge University Press, New York.

Lee, K.K. and J.A. Liggett, 1970: Computation for circulation in stratified lakes. Jour. of the Hydraulics Div., Proc. ASCE, 96, no. HY10, 2089-2115.

Leendertse, J.J., 1967: Aspects of a computational model for long-period water wave propagation. Memorandum RM-5294-PR. Rand Corp., Santa Monica, California.

_____, 1970: A water-quality simulation model for well-mixed estuaries and coastal seas: vol. I, principles of computation. Memorandum RM-6230-RC, Rand Corp., Santa Monica, California.

Miyazaki, M., T. Ueno, and S. Unoki, 1962: Theoretical investigations of typhoon surges along the Japanese Coast (II). The Oceanographical Mag., 13, 103-117.

Monahan, E.C., 1974: unpublished observational data on Saginaw Bay. The University of Mich.

Mortimer, C.H., 1965: Spectra of long surface gravity waves and tides in Lake Michigan and at Green Bay, Wisconsin, Publ. no. 13, Great Lakes Research Division, The University of Mich., 304-325.

Murthy, C.R., 1970: An experimental study of horizontal diffusion in Lake Ontario. Proc. 13th Conf. Great Lakes Res., 477-489.

Murty, T. and D.B. Rao, 1970: Wind-generated circulations in Lakes Erie, Huron, Michigan, and Superior. Proc. 13th Conf. Great Lakes Res., 927-941.

Neumann, G. and W.J. Pierson, 1966: Principles of physical oceanography, Prentice-Hall, Englewood Cliffs, New Jersey.

Ogata, A. and R. Banks, 1961: A solution of the differential equation of longitudinal dispersion in porous medium. Prof. Paper no. 411-A, U.S. Geological Survey, Washington, D.C., 1961.

Pao, Y.H. and R.J. Daugherty, 1969: Time-dependent viscous incompressible flow past a finite flat plate. Boeing Scientific Research Laboratories, D1-82-0822, January.

Peaceman, D.W. and H.H. Rachford, 1955: The numerical solution of parobolic and elliptic differential equations. Jour. Soc. Indus. Appl. Math., 3, 1, 28-41.

Platzman, G.W., 1958: A numerical calculation of the surge of June 26, 1954 on Lake Michigan. Geophysica (Helsinki) 6, 3-4.

_____ and D.B. Rao, 1964: "The free oscillations of Lake Erie" in Studies in Oceanography, ed. by K. Yoshida, University of Tokyo Press, 359-382.

Proudman, J., 1953: Physical oceanography. Metheun, London.

Richards, T.L., H. Dragert, and D.R. McIntyre, 1966: Influence of atmospheric stability and over-water fetch on winds over the lower Great Lakes. Monthly Weather Rev., 94, 7, 448-453.

Richtmeyer, R.D. and K.W. Morton, 1967: Difference Methods for initial value problems, 2nd edition. Interscience, New York.

Roache, P.J., 1972: Computational Fluid Dynamics. Hermosa Publishers, Alburquerque, New Mexico.

Rockwell, D.C., 1966: Theoretical free oscillations of the Great Lakes. Publ. no. 15, Great Lakes Research Division, The University of Mich.

Seibel, E., 1974: Personal communications. Great Lakes Research Division, The University of Mich.

Simons, T.J., 1971a: Development of three-dimensional models of the Great Lakes. Internal report, Canada Center for Inland Waters, Burlington, Ontario.

_____, 1971b: Development of numerical models of Lake Ontario. Proc. of 14th Conf. Great Lakes Res., 644-669.

_____, 1972: Development of numerical models of Lake Ontario, Part II. Proc. of 15th Conf. Great Lakes Res.

_____ and D.E. Jordan, 1972: Computed water circulation of Lake Ontario for observed winds from 20 April to 14 May 1971. Internal report, Canada Center for Inland Waters, Burlington, Ontario.

Smith, E.B., 1972: Wind driven and seiche forced water motion in Grand Traverse Bay, Michigan. Ph.D. thesis, The University of Mich.

Sundstrom, A., 1973: On the well-posedness of the shallow-water equations. Report DM-9, Institute of Meteorology, Stockholm.

Taylor, G.I., 1954: Dispersion of matter in turbulent flow through a pipe. Proc. Roy. Soc., London, A, 223.

Veronis, G., 1966: Wind-driven ocean circulation, Part II, numerical solutions of the non-linear problem. Deep-Sea Research, 13, 31-55.

Welander, P., 1966: A two-layer frictional model of wind-driven motion in a rectangular basin. Tellus, 18, 54-62.

Wurtele, M.G., J. Paegle, and A. Sielicki, 1971: The use of open boundary conditions with the storm-surge equations. Monthly Weather Rev., 99, 6, 537-544.